[AMERICAN JOURNAL OF SCIENCE, VOL. 274, DECEMBER, 1974, P. 1089-1198]

American Journal of Science

DECEMBER 1974

THEORETICAL PREDICTION OF THE THERMODYNAMIC BEHAVIOR OF AQUEOUS ELECTROLYTES AT HIGH PRESSURES AND TEMPERATURES: I. SUMMARY OF THE THERMODYNAMIC/ELECTROSTATIC PROPERTIES OF THE SOLVENT

HAROLD C. HELGESON and DAVID H. KIRKHAM

Department of Geology and Geophysics, University of California, Berkeley, California 94720

ABSTRACT. Thermodynamic/electrostatic properties of H_2O at high pressures and temperatures were calculated from regression equations representing dielectric constant data reported by Oshry (ms), Owen and others (1961), and Heger (ms) for temperatures and pressures from 0° to 550°C and 0.001 to 5 kb together with finite difference derivatives computed from specific volumes given by Burnham, Holloway, and Davis (1969b) for 20° to 900°C and 1 to 10 kb. Corresponding properties below a kilobar were computed with the aid of the equation of state developed by Keenan and others (1969), which describes the thermodynamic behavior of H_2O in close accord with the tolerances of the International Skeleton Tables of 1963. The results of the calculations are given in equations, tables, and diagrams depicting isotherms, isobars, and isopleths of specific volume, entropy, enthalpy, internal energy, Helmholtz and Gibbs free energies, fugacity, and heat capacity, together with the dielectric constant, coefficients of isobaric thermal expansion and isothermal compressibility, the Born (1920) free energy function, and their partial derivatives. Perturbation of the thermodynamic/electrostatic behavior of H_2O by the critical phenomenon leads to significant differences in the dependence of its properties on temperature, pressure, and density above and below ~ 400°C and ~ 1 to 2 kb. The calculations permit prediction of the consequences of these differences on the chemical interaction of minerals and aqueous electrolyte solutions in geochemical processes.

INTRODUCTION

Recent advances in solution chemistry, thermodynamics, and computer technology make it possible to describe quantitatively equilibrium and mass transfer among minerals and aqueous electrolytes in geochemical processes involving large numbers of components, phases, and chemical species at both high and low temperatures and pressures. The present series of communications is intended to provide a comprehensive set of equations and data to facilitate such calculations.

Theoretical and experimental studies of hydrothermal systems over the past 50 years leave little doubt that mineral solubilities and the chemical and thermodynamic behavior of solute species in aqueous electrolytes are controlled to a large extent by the thermodynamic/electrostatic properties of the solvent, which change dramatically with increasing temperature and pressure. The equations, tables, and diagrams presented below constitute an internally consistent summary of these properties, based on critical evaluation and regression of density and dielectric constant data reported in the literature for temperatures and

pressures from 0° to 900°C and 0.001 to 10 kb. These conditions bracket those found in the Earth from its surface to a lithostatic depth of ~ 35 km, which is equivalent in pressure to a hydrostatic depth of ~ 100 km. The temperature span ranges from the stability fields of ice I and VI to the low-pressure melting temperatures of hydrous silicate rocks.

The thermodynamic properties of H_2O have long been of interest to engineers responsible for power generation and in recent decades to geologists concerned with geochemical and geophysical processes at high temperatures and pressures. As a consequence, a plethora of steam tables and other compilations has appeared through the years, most of which cater to engineers and are too restricted in the scope of pressures, temperatures, and/or the properties considered to be generally applicable in science. Many of the compilations are based on conventions and expressed in units that are inconvenient in a geochemical context, some are insufficiently detailed, and none includes all properties of interest in solution chemistry. Among the more important of these is the dielectric constant and its partial derivatives with respect to pressure and temperature. The latter variables can be used in conjunction with expansibilities, compressibilities, and other thermodynamic properties of H_2O to compute electrostatic parameters in the Debye-Hückel theory, evaluate Born charging equations, and formulate algorithms and equations of state for predicting and correlating the thermodynamic properties of aqueous electrolytes at high pressures and temperatures.

REVIEW OF PREVIOUS WORK

A multitude of experimental and theoretical studies of the thermodynamic properties of steam, water, and ice has accumulated in the century and a half since Carnot (1824) published his famous memoir on the power of heat, but only in the last 50 years have systematic and coordinated efforts been made to compile accurate data of high precision in a comprehensive and organized program of research. Following the appearance of the International Critical Tables in 1928, the First International Conference on the Properties of Steam was organized to establish tolerances and compile a set of skeleton tables listing accepted values for the thermodynamic properties of H_2O. The skeleton tables compiled at this conference provided the basis for the ASME steam tables of 1930 (Keenan, 1930). Two years later, Mollier's (1932) tables and diagrams appeared almost simultaneously with those of Knoblauch and others (1932). At the Third International Conference on the Properties of Steam in 1934, agreement was reached on a revised and expanded set of skeleton tables and tolerances for temperatures $\leq$ 550°C and pressures $\leq$ 300 bars. Shortly thereafter, Keenan and Keyes (1936) produced the first comprehensive set of steam tables for temperatures and pressures from 0° to 871°C and 0 to 380 bars. The latter tables, which proved to be highly reliable and widely used, were based on a critical review of the literature and an equation of state derived from precise pressure–volume–temperature measurements from 0° to 460°C and 0 to 350 atm (Smith and Keyes,

1934; Keyes, Smith, and Gerry, 1936). These data, together with many others, were reported in Dorsey's (1940) exhaustive review and compilation of the properties of H_2O, which has been complemented recently by extensive critiques of the physical chemistry of water (Horne, 1969, 1972; Franks, 1972).

International conferences on the properties of steam have been held intermittently since 1934, but it was not until the sixth conference in 1963 that agreement was reached on a revised and enlarged set of skeleton tables extending from 0° to 800°C and from 0 to 1 kb. The advent of high-speed computers and the skeleton tables compiled at the third and sixth international conferences on the properties of steam generated a myriad of regression and interpolation formulas, equations of state, and steam tables, which have appeared in steady succession since World War II (for example, Callendar and Egerton, 1944, 1958; Schall, 1950; Dzung and Rohrbach, 1955; Vukalovich, 1958; Vukalovich and others, 1959; Nowak and Grosh, 1961; Bain, 1964; Juza, Kmoníček, and Šifner, 1966; Meyer and others, 1967; Schmidt, 1969; Papetti and Fujisaki, 1971, Barker and Henderson, 1972; Sengers and Greer, 1972). In recent years efforts have been made to extend the level of precision of pressure–volume–temperature measurements (for example, Owen, White, and Smith, 1956; Kell, 1967; Kell and Whalley, 1965; Kell, McLaurin, and Whalley, 1968; Millero, Curry, and Drost-Hansen, 1969; Rowe and Chou, 1970; Grindley and Lind, 1971; Gildseth, Habenschuss, and Spedding, 1972; Greene, Beachey, and Milne, 1972; Millero, Knox, and Emmet, 1972; Wang and Millero, 1973; Fine and Millero, 1973), and in 1965 the International Formulation Committee reached agreement on the form of the equations to be used by the International Conference on the Properties of Steam for computer representation of the skeleton tables (Internat. Formulation Comm., 1967, 1968).

Measurements of the specific volume of H_2O at high pressures and low temperatures have been carried out since the turn of the century (for example, Amagat, 1893; Bridgeman, 1913, 1931, 1935; Adams, 1931), but it was not until Kennedy (1950) applied modern technology to check and extend early reconnaissance measurements (Tamman and Rühenbeck, 1932; Goranson, 1938) that reliable data became available for pressures above a kilobar at high temperatures. Since then, numerous experimental and theoretical studies of the density of H_2O at high pressures and temperatures have appeared (for example, Kennedy, 1957; Kennedy, Knight, and Holser, 1958; Holser and Kennedy, 1958, 1959; Howard, 1961; Maier and Franck, 1966; Walsh and Rice, 1957; Rice and Walsh, 1957; Al'tshuler, Bakanova, and Trunin, 1958; Sharp, 1962; Köster and Franck, 1969; Grindley and Lind, 1971), but none has been as systematic and comprehensive as that reported by Burnham, Holloway, and Davis (1969a, and b). Repeated calculations of the fugacity and other properties of H_2O at high temperatures and pressures have been made from these various data (for example, Holser, 1954; Pistorius and Sharp, 1960, 1961; Anderson, 1964, 1967; Burnham, Holloway, and Davis, 1969b; Haas,

1970; Holloway, Eggler, and Davis, 1971), most of which are in general (but not always close) agreement with one another.

In the same year that Burnham, Holloway and Davis' data became available, Keenan and others (1969) published an independent set of steam tables for the thermodynamic properties of H_2O to 1300°C and 1 kb based on critical evaluation of precise experimental data reported in the literature and a remarkably versatile "fundamental" equation for the Helmholtz free energy (relative to zero entropy of H_2O_{liquid} at the triple point) as a function of temperature and density. Also in the same year, Heger (ms) reported his measurements of the dielectric constant of H_2O at high temperatures and pressures. All three of these outstanding contributions have been of inestimable value to the present study.

The electrostatic properties of H_2O have received extensive experimental and theoretical attention through the years, particularly at low temperatures and pressures (for example, Wyman, 1930; Åkerlöf, 1932; Wyman and Ingalls, 1938; Kirkwood, 1939; Dorsey, 1940; Oster and Kirkwood, 1943; Malmberg and Maryott, 1956; Cole, 1960; Hasted, 1961, 1972; Vidulich and Kay, 1962; Vidulich, Evans, and Kay, 1967; Kay, Vidulich, and Pribadi, 1969). The dielectric constant of saturated water from 100°C to the critical temperature was measured by Oshry (ms; Åkerlöf and Oshry, 1950), and Fogo, Benson, and Copeland (1954) published values for steam from 377° to 395°C at densities from 0.1 to 0.5 g cm^{-3}. In recent years, measurements of the dielectric constant at high pressures and low temperatures (for example, Kyropoulos, 1926; Lees, ms; Harris, Haycock, and Alder, 1953; Scaife, 1955; Owen and others, 1961) have been extended to high temperatures (Gier and Young, 1963; Heger, ms). Although considerable discrepancy exists among these various sets of data, they afford close estimates of the electrostatic behavior of H_2O in the supercritical region (Franck, 1956; Quist and Marshall, 1965; Franck, 1969; Jansoone and Franck, 1972). These estimates have been used in conjunction with viscosity and conductance measurements to compute activity product constants of H_2O, which are now available to 1000°C and 120 kb (David and Hamann, 1959, 1960; Franck, 1961; Dudziak and Franck, 1966; Holzapfel and Franck, 1966; Quist, 1970; Fisher and Barnes, 1972; Whitfield, 1972; Millero, Hoff, and Kahn, 1972). A number of the thermodynamic, transport, and electrostatic properties of H_2O at both low and high pressures and temperatures have been reviewed recently by Franck (1969), Kell (1972), and Tödheide (1972).

The outstanding progress made in the last decade toward documenting and expanding the state of knowledge concerning the thermodynamic/electrostatic behavior of H_2O at high pressures and temperatures will no doubt be considered in depth at the 1974 International Conference on the Properties of Steam. Hopefully, the members of that conference will expand the scope of the steam tables to include all properties of interest in solution chemistry, geology, and other scientific disciplines concerned with H_2O at high pressures and temperatures.

CONVENTIONS, UNITS, AND NOTATION

The standard state for H_2O adopted in this study is one of unit fugacity (f) of the *hypothetical* perfect gas at 1 bar and any specified temperature. Accordingly, the compressibility factor (z) and the fugacity coefficient (χ) of H_2O approach unity as $P \rightarrow 0$, and the activity (a) and fugacity of H_2O are equal at all pressures and temperatures. Because the fugacities and fugacity coefficients reported below for both the liquid and gas phase regions are based on the standard state properties of steam (that is, those of the hypothetical perfect gas at 1 bar), the activities of H_2O_{liquid} and H_2O_{gas} are equal at saturation. At 1 bar and temperatures below 100°C, the fugacity coefficient of H_2O corresponds to that of metastable steam, which becomes increasingly nonideal as temperature decreases. However, as temperature increases to ~ 600°C at 1 bar, $\chi \rightarrow 1$ as H_2O approaches ideality.

Owing to the critical phenomenon, no single standard state is equally convenient for simultaneous consideration of the liquid, gas, and supercritical phases of H_2O. Although designation of separate standard states for H_2O_{liquid} and H_2O_{gas} leads to dual activities and fugacities in the supercritical region, such a distinction is nevertheless advantageous in many geochemical calculations. For example, the standard state described above facilitates quantitative interpretation of univariant equilibria in the supercritical region, but solubility calculations can be simplified by adopting a standard state convention which is unrestricted with respect to both pressure and temperature. Under these circumstances, $a = 1$ and $f = f^\circ$ at all pressures and temperatures.

The standard state for H_2O most commonly encountered in solution chemistry specifies unit activity of the pure liquid at 1 bar. Activities of H_2O_{liquid} consistent with this standard state can be computed from the apparent molal Gibbs free energies of formation (ΔG) given (and defined below for 1 bar and temperatures < 100°C by first designating the corresponding fugacity reported for 1 bar as f°, which requires the activity of H_2O_{liquid} to be unity at 1 bar. The activity of H_2O_{liquid} at a higher pressure can then be computed from $\ln a = (\Delta G - \Delta G^\circ)/RT$ with ΔG equal to the apparent standard molal Gibbs free energy of formation of H_2O_{liquid} at unit pressure; that is, the values of ΔG reported below for 1 bar and temperatures < 100°C. In certain cases, it may be advantageous to specify unit activity of H_2O at 1 bar and any temperature, which requires ΔG° to be equal to $\Delta G_{1\ bar}$ at all temperatures. Similarly, it may be convenient in solubility studies to adopt a standard state convention which requires the activity of H_2O_{liquid} to be unity at all saturation pressures and temperatures. Under these conditions, $\Delta G^\circ_{H_2O,\ liquid}$ equals the values of ΔG for steam-saturated liquid H_2O. Values of ΔG° for the various standard states can be taken from table 29 or computed from equations presented below. Any liquid standard state is related to the

gas standard state adopted in this study by RT ln $(a_{H_2O,\ gas}/a_{H_2O,\ liquid}) = (\Delta G^\circ_{H_2O,\ liquid} - \Delta G^\circ_{H_2O,\ gas})$ at saturation.

The symbol P is used in this communication to designate pressure in preference to its lower case equivalent, which is commonly employed in gas chemistry to designate pressure in a one component system. All temperatures are thermodynamic (that is, the units are consistent with the celsius scale of temperature rather than the international practical temperature scale) expressed in degrees kelvin (°K) or degrees centigrade (°C) and designated by T and t, respectively. The symbols T_r and P_r refer to a reference temperature and pressure of 298.15°K and 1 bar. Similarly, T_{tr} and P_{tr} stand for the triple point temperature and pressure (273.16°K and 0.006113 bars). The subscript *triple* appended to a symbol indicates that it pertains to liquid H_2O at the triple point. Other subscripts include *c* or *critical* to refer to the critical point (374.136°C and 220.88 bars), *sat* to designate saturated liquid along the vapor pressure curve, and P, T, P_r, T_r, P_{tr}, and T_{tr} to designate particular pressures and temperatures. The superscript ° denotes standard state properties of H_2O for the convention adopted above. All other standard states discussed below are designated by the superscript ° to preclude confusion.

The values of entropy (S) and heat capacity (C_P or C_V) given in the tables and diagrams below are expressed in thermochemical calories (4.184 calories joule^{-1}) per mole per degree Kelvin (therm cal mole^{-1} (°K)$^{-1}$ or cal mole^{-1} (°K)$^{-1}$). Similarly, enthalpy (H) internal energy (E), and Gibbs (G) and Helmholtz (A) free energies are expressed in cal mole^{-1} or kilocalories per mole (kcal mole^{-1}), which can be converted to joules per mole (j mole^{-1}), joules per gram (j g^{-1}), international calories per mole (int cal mole^{-1}), or int cal g^{-1} with the aid of table 1. Volume (V) is expressed in cm^3 mole^{-1} or cm^3 g^{-1}, which can also be converted to other units by applying conversion factors in table 1. Density (ρ) is given in g cm^{-3}, and the coefficients of isobaric thermal expansion (α) and isothermal compressibility (β) in (°K)$^{-1}$ and bar^{-1}, respectively. The derivatives of α, β, and ε (the dielectric constant, which is dimensionless) are also expressed in reciprocal degrees kelvin and reciprocal bars to appropriate powers. Fugacity (f) is given in bars or kilobars. The fugacity coefficient (χ) is dimensionless ($\chi = f/P$), as is the compressibility factor ($z = PV/RT$) and activity ($a = f/f^\circ$). All molal properties given in the tables are referred to a molecular weight of H_2O equal to 18.0153 g mole^{-1} consistent with the 1961 table of relative atomic weights based on $^{12}C = 12$ exactly. Values of the gas constant (R) with various dimensions are given in table 1 to facilitate thermodynamic calculations in alternate units.

All values shown in parentheses in the tables or represented by dashed lines in the figures given below represent interpolated, extrapolated, or otherwise more uncertain values. The number of decimal digits specified in the tables does not necessarily imply an absolute level of numerical uncertainty, which is discussed in the text accompanying the tables. In certain cases, relative uncertainties can be assessed from the

TABLE 1

Conversion factors and values of the gas constant (R) in various units[a]

	cm^3 g^{-1}	cm^3 mole^{-1}	j g^{-1} bar^{-1}	j mole^{-1} bar^{-1}	therm cal g^{-1} bar^{-1}	therm cal mole^{-1} bar^{-1}	int cal g^{-1} bar^{-1}	int cal mole^{-1} bar^{-1}
1 cm^3 g^{-1} =	1	18.0153	0.1	1.80153	0.023901	0.430584	0.023885	0.430295
1 cm^3 mole^{-1} =	0.05551	1	0.005551	0.1	0.001327	0.023901	0.001326	0.023885
1 j g^{-1} bar^{-1} =	10	180.1477						
1 j mole^{-1} bar^{-1} =	0.55508	10						
1 therm cal g^{-1} bar^{-1} =	41.8393	735.579						
1 therm cal mole^{-1} bar^{-1} =	2.32243	41.8393						
1 int cal g^{-1} bar^{-1} =	41.86728	754.148						
1 int cal mole^{-1} bar^{-1} =	2.32399	41.8673						

	j g^{-1}	j mole^{-1}	therm cal g^{-1}	therm cal mole^{-1}	int cal g^{-1}	int cal mole^{-1}
1 j g^{-1} =	1	18.0153	0.23901	4.30584	0.23885	4.30295
1 j mole^{-1} =	0.05551	1	0.01327	0.23901	0.01326	0.23885
1 therm cal g^{-1} =	4.1840	75.3760	1	18.0153	1.00067	18.02737
1 therm cal mole^{-1} =	0.23225	4.1840	0.05551	1	0.05555	1.00067
1 int cal g^{-1} =	4.1868	75.4265	0.99933	18.00323	1	18.0153
1 int cal mole^{-1} =	0.23240	4.1868	0.05547	0.99933	0.05551	1

R	units	R	units	R	units
0.46151	j g^{-1} (°K)$^{-1}$	0.110306	therm cal g^{-1}(°K)$^{-1}$	0.110232	int cal g^{-1}(°K)$^{-1}$
8.31424	j mole^{-1}(°K)$^{-1}$	1.98719	therm cal mole^{-1}(°K)$^{-1}$	1.98586	int cal mole^{-1}(°K)$^{-1}$

R	units
4.6151	cm^3 bar g^{-1} (°K)$^{-1}$
83.14241	cm^3 bar mole^{-1}(°K)$^{-1}$

[a] The molal units shown in the table are referred to a molecular mass of H_2O equal to 18.0153 g mole^{-1}, which is consistent with the 1961 table of relative atomic weights based on $^{12}C = 12$ exactly.

tables by noting differences in the number of decimals given for high and low temperatures and pressures. The labels *sat* or *saturation* refer to steam-saturated liquid H_2O.

Most steam tables published in the last 15 years, as well as the recent compilation by Burnham, Holloway, and Davis (1969b), are predicated on $S_{triple} = G_{triple} = 0$, which is the convention adopted by the 5th International Conference on the Properties of Steam. The values of H and S reported in steam tables are thus actually $H - H_{triple}$ and $S - S_{triple}$. Although the steam table convention facilitates engineering studies, it is not particularly convenient for geochemical calculations because the stipulation that $S_{triple} = G_{triple} = 0$ conflicts with standard state conventions used to compute and tabulate thermodynamic properties of minerals and gases in other widely used compilations (for example, Latimer, 1952; Wagman and others, 1965, 1966, 1968, 1969; Wagman and others, 1971; Parker, Wagman, and Evans, 1971; Stull and Prophet, 1971; Robie and Waldbaum, 1968). Entropies and enthalpies of H_2O based on the steam table convention can be converted to other reference systems simply by adding values of S_{triple} and H_{triple} consistent with the desired convention to the respective values of S and H reported in the steam tables. Similarly, because densities and volumes reported in steam tables are absolute values, internal energies based on other conventions can be computed directly from steam table data by specifying E_{triple} and evaluating

$$E - E_{triple} = H - H_{triple} + PV - P_{tr} V_{triple} \tag{1}$$

In contrast, calculation of corresponding Gibbs or Helmholtz free energies from values of H and S reported in steam tables requires specification of S_{triple} as well as G_{triple} or A_{triple} consistent with the desired convention. The extent to which the free energies of H_2O change with temperature depends on the magnitude of the entropy at the reference temperature and pressure, which can be demonstrated by writing

$$G - G_{triple} = H - H_{triple} - TS + T_{tr} S_{triple} \tag{2}$$

and

$$\begin{aligned} A - A_{triple} &= E - E_{triple} - TS + T_{tr} S_{triple} \\ &= G - G_{triple} - PV + P_{tr} V_{triple} \end{aligned} \tag{3}$$

which are not equivalent to

$$G = H - TS \tag{4}$$

and

$$A = E - TS \tag{5}$$

unless

$$S_{triple} = 0.$$

To facilitate geochemical calculations, the enthalpies, internal energies, and Gibbs and Helmholtz free energies of H_2O given in the tables and diagrams below are expressed as apparent molal enthalpies, internal energies, and Gibbs and Helmholtz free energies of formation from the

elements (ΔH, ΔE, ΔG, and ΔA) consistent with their standard molal counterparts at 298.15°K and 1 bar; that is,[1]

$$\begin{aligned} \Delta H &\equiv \Delta H^\bullet_f + (H - H_{P_r,T_r}) \\ &= \Delta H^\bullet_f + (H - H_{triple}) - (H_{P_r,T_r} - H_{triple}) \end{aligned} \tag{6}$$

$$\begin{aligned} \Delta E &= \Delta E^\bullet_f + (E - E_{P_r,T_r}) \\ &= \Delta E^\bullet_f + (E - E_{triple}) - (E_{P_r,T_r} - E_{triple}) \end{aligned} \tag{7}$$

$$\begin{aligned} \Delta G &= \Delta G^\bullet_f + (G - G_{P_r,T_r}) \\ &= \Delta G^\bullet_f + (G - G_{triple}) - (G_{P_r,T_r} - G_{triple}) \end{aligned} \tag{8}$$

and

$$\begin{aligned} \Delta A &= \Delta A^\bullet_f + (A - A_{P_r,T_r}) \\ &= \Delta A^\bullet_f + (A - A_{triple}) - (A_{P_r,T_r} - A_{triple}) \end{aligned} \tag{9}$$

where $\Delta H^\bullet_f$, $\Delta E^\bullet_f$, $\Delta G^\bullet_f$, and $\Delta A^\bullet_f$ refer to the standard molal enthalpy, internal energy, Gibbs free energy, and enthalpy of formation of liquid H_2O from its elements in their stable form at 298.15°K (T_r) and one bar (P_r). The superscript $^\bullet$ is used in equations (6) through (9) rather than $^\circ$ to distinguish the standard state properties given by Wagman and others (1968) for liquid H_2O from those of the gas standard state adopted in this study. The values of $\Delta H^\bullet_f$ and $\Delta G^\bullet_f$ employed below are given in table 2 together with corresponding values of $\Delta E^\bullet_f$ and $\Delta A^\bullet_f$ computed from

$$\Delta E^\bullet_f = \Delta H^\bullet_f - P_r \Delta V^\bullet_f \tag{10}$$

and

$$\Delta A^\bullet_f = \Delta G^\bullet_f - P_r \Delta V^\bullet_f \tag{11}$$

using $V^\circ_{O_2} = V^\circ_{H_2} = V_{ideal\ gas} = 24{,}465$ cm^3 mole^{-1}. The entropies and heat capacities reported below are third law molal properties consistent with

$$\begin{aligned} S &= -\left(\frac{\partial \Delta G}{\partial T}\right)_P = -\left(\frac{\partial \Delta A}{\partial T}\right)_V = S^\bullet + (S - S_{P_r,T_r}) \\ &= S^\bullet + (S - S_{triple}) - (S_{P_r,T_r} - S_{triple}) \end{aligned} \tag{12}$$

and

$$C_P = \left(\frac{\partial \Delta H}{\partial T}\right)_P = T\left(\frac{\partial S}{\partial T}\right)_P. \tag{13}$$

where $S^\bullet$ represents the standard molal third law entropy of liquid H_2O at 298.15°K and one bar given by Wagman and others (1968).

Conversion of the apparent molal enthalpies, internal energies, and free energies as well as the third law molal entropies given below to corresponding values based on the steam table convention can be made with

[1] Use of the word apparent in referring to ΔH, ΔE, ΔG, and ΔA was suggested by Benson (1968) to preclude confusion with corresponding properties of formation from the elements at high pressures and temperatures such as those tabulated by Robie and Waldbaum (1968). The latter properties include provision for changes in the thermodynamic properties of the elements with increasing pressure and temperature, which cause in thermal reactions.

The values shown for pressures ≤ a kilobar were computed from the Helmholtz function derived by Keenan and others (1969), which can be written as

$$\psi = \psi_o + RT(\ln \rho + \rho Q) \tag{14}$$

where

$$\psi_o = \left(\sum_{i=1}^{6} C_i/\tau^{i-1} \right) + C_7 \ln T + C_8 \ln (T/\tau) \tag{15}$$

and

$$Q = (\tau - \tau_c) \sum_{j=1}^{7} (\tau - \tau_{aj})^{j-2} \left(\sum_{i=1}^{8} A_{ij} (\rho - \rho_{aj})^{i-1} + e^{-4.8\rho} \sum_{i=9}^{10} A_{ij} \rho^{i-9} \right) \tag{16}$$

where ρ refers to the density of H_2O in g cm^{-3}, T denotes temperature in °K, R stands for the gas constant in joules g^{-1} (°K)$^{-1}$ (table 1), $\tau = 1000/T$, $\tau_c = 1000/T_{critical} = 1.544912$, $\tau_{aj} = \tau_c$ for $j = i$ and 2.5 for $j > 1$, $\rho_{aj} = 0.634$ for $j = 1$ and 1.0 for $j > 1$, C_i and A_{ij} represent arrays of coefficients given in table 4, and

$$\psi = A - A_{triple} + S_{triple}(T - T_{tr}) \tag{17}$$

where A is the Helmholtz free energy in joules g^{-1} of H_2O at the temperature and pressure of interest, A_{triple} refers to the Helmholtz free energy in joules g^{-1} of liquid H_2O at the triple point (273.16°K and 0.006113 bars), and S_{triple} stands for the third law entropy in joules g^{-1} (°K)$^{-1}$ of the liquid at the triple point. It follows from equations (14), (17), and the relation

$$dA = -SdT - PdV = -SdT + \frac{P}{\rho^2} d\rho \tag{18}$$

that

$$P = -\left(\frac{\partial A}{\partial V}\right)_T = \rho^2 \left(\frac{\partial A}{\partial \rho}\right)_T = \rho^2 \left(\frac{\partial \psi}{\partial \rho}\right)_T = \rho RT \left(1 + \rho Q + \rho^2 \left(\frac{\partial Q}{\partial \rho}\right)_T\right) \tag{19}$$

where P refers to pressure in bars, V is the specific volume of H_2O in cm^3 g^{-1}, and $(\partial Q/\partial \rho)_T$ corresponds to the partial derivative of equation (16) with respect to density at constant temperature (eq A-22 in the app).

Equation (19) represents experimental pressure–volume–temperature data for H_2O to 0.1 percent or better from 0° to 800°C and 0° to 1 kb, but at temperatures below 220°C the uncertainty is 0.01 percent (Keenan

the aid of the properties of liquid H_2O given in table 2 for the triple point and 298.15°K and 1 bar. Corresponding values of heat capacity and volume are also given in table 2 along with the respective differences in the thermodynamic properties of liquid H_2O caused by increasing temperature and pressure from T_{tr} and P_{tr} to T_r and P_r.

VOLUME

The volume of H_2O in cm^3 mole^{-1} is given in table 3 and plotted in figures 1 and 2 for temperatures and pressures to 900°C and 10 kb.

TABLE 2

Thermodynamic properties of liquid H_2O at the triple point and corresponding values of the properties at 298.15°K (T_r) and 1 bar (P_r) consistent with the standard state for liquid H_2O adopted by Wagman and others (1968) and the definitions represented by equations (6) through (9), (12), and (13)[a]

Property	j g^{-1}	therm cal mole^{-1}	Property	j g^{-1} (°K)$^{-1}$	therm cal mole^{-1} (°K)$^{-1}$
ΔH_f°	-15,866	-68,315[b]	ΔA_f°	-12,962	-55,812[c]
$H_{P_r,T_r} - H_{triple}$	104.89[d]	451.63	$A_{P_r,T_r} - A_{triple}$	-92.28[e,g]	-397.32
ΔH_{triple}	-15,971	-68,767	ΔA_{triple}	-12,870	-55,415
ΔE_f°	-15,662	-67,436[c]	ΔG_f°	-13,165	-56,687[b]
$E_{P_r,T_r} - E_{triple}$	104.79[e,h]	451.20	$G_{P_r,T_r} - G_{triple}$	-92.18[e,f]	-396.89
ΔE_{triple}	-15,766	-67,887	ΔG_{triple}	-13,073	-56,290
S°	3.8808[k]	16.71[b,m]	V°	0.100296[d,i,k]	0.43186[j]
$S_{P_r,T_r} - S_{triple}$	0.3664[d,k]	1.5776[m]	$V_{P_r,T_r} - V_{triple}$	0.00028[e,i]	0.00119[j]
S_{triple}	3.5144[k]	15.132[m]	V_{triple}	0.10002[d,i]	0.43067[j]
C_P°	4.183[d,k]	18.01[m]	C_V°	4.141[d,k]	17.83[m]

[a] ΔH_{triple}, ΔE_{triple}, ΔA_{triple}, and ΔG_{triple} correspond, respectively, to the standard enthalpy, internal energy, and Helmholtz and Gibbs free energies of formation of one mole of liquid H_2O from its elements in their stable form at 298.15°K and one bar (ΔH_f°, ΔE_f°, ΔA_f°, and ΔG_f°) plus the change in the respective properties of liquid H_2O ($H_{P_r,T_r} - H_{triple}$, $E_{P_r,T_r} - E_{triple}$, $A_{P_r,T_r} - A_{triple}$, and $G_{P_r,T_r} - G_{triple}$) caused by decreasing the temperature and pressure to 273.16°K and 0.006113 bars at the triple point (eqs 6 through 9). S_{triple} represents the molal third law entropy of liquid H_2O at the triple point computed from equation (12) and the values of S° and $S_{P_r,T_r} - S_{triple}$ given above. [b] Wagman and others (1968). [c] computed from equations (10) and (11). [d] Keenan and others (1969) and Schmidt (1969). [e] calculated from data given in the sources referenced in footnote d. [f] Equation (2). [g] Equation (3). [h] Equation (1). [i] j g^{-1} bar^{-1}. [j] therm cal mole^{-1} bar^{-1}. [k] Kell (1967). [l] j gm^{-1} (°K)$^{-1}$. [m] therm cal mole^{-1} (°K)$^{-1}$.

TABLE 5

Coefficients for the statement of equation (21) applicable to region 1 in figure 3 (for which $r = 1$ and $i = 9$) computed from those given by Burnham, Holloway, and Davis (1969b)

$$a_{ij} = \hat{a}_{ij} \times 10^{a^*_{ij}}$$

$\hat{a}_{ij}$

i \ j	0	1	2	3	4	5	6	7	8	9
0	-3.8106590	1.0564665	-7.6454683	7.0956600	1.0454935	-4.4887845	9.0586480	-9.8313225	5.5147402	-1.2547995
1	6.6431473	-4.2654409	8.2193439	-4.6017503	1.5484386	-3.0809442	3.4462611	-1.9805288	4.5366798	
2	-8.9413365	8.9222030	1.9719748	-4.8796036	1.9017140	-2.7155343	1.5518783	-2.9266747		
3	9.2076993	4.3805877	3.1779963	-1.4111684	1.9087901	-3.3016835	-2.0239777			
4	-4.7887922	-6.1891487	1.9043321	-1.1153384	-1.2650068	6.0544695				
5	1.3798565	-1.3233046	-1.4943777	2.5569347	-3.4096098					
6	-1.9886789	2.3912344	-7.5721292	-6.0823080						
7	1.5064451	-1.2791592	5.7844948							
8	-6.0211303	1.7501650								
9	1.0682110									

a^*_{ij}

i \ j	0	1	2	3	4	5	6	7	8	9
0	1	0	-5	-10	-11	-15	-19	-23	-27	-31
1	-1	-4	-7	-10	-13	-17	-21	-25	-30	
2	-3	-7	-10	-13	-16	-20	-24	-29		
3	-5	-9	-13	-15	-19	-24	-28			
4	-7	-12	-14	-18	-22	-27				
5	-9	-13	-17	-21	-26					
6	-12	-16	-21	-25						
7	-15	-19	-24							
8	-19	-23								
9	-22									

TABLE 6

Coefficients for the statement of equation (21) applicable to region 2 in figure 3 (for which $r = -1$ and $i = 8$) computed from those given by Burnham, Holloway, and Davis (1969b)

$$a_{ij} = \hat{a}_{ij} \times 10^{a^*_{ij}}$$

$\hat{a}_{ij}$

i \ j	0	1	2	3	4	5	6	7	8
0	6.2333394	2.7662646	-1.0740139	2.5322920	-4.8726693	6.4561026	-5.4093771	2.5488337	-5.1020454
1	-1.8696559	-1.0455591	2.0433223	1.9631668	-5.9663826	6.7298320	-3.6953264	7.9719676	
2	1.0560104	3.9214358	-1.0866710	5.1510625	-3.3120122	1.4945128	-2.3568834		
3	-3.0872023	-5.4077159	1.7653195	-2.2745747	1.4365051	-1.6687313			
4	4.7066592	2.8059817	-1.9666573	1.3446174	2.8271453				
5	-3.5684092	2.7903289	1.1733349	-6.4912023					
6	4.5184280	-4.1996643	-2.7133198						
7	1.0665197	1.5583195							
8	-4.8594177								

a^*_{ij}

i \ j	0	1	2	3	4	5	6	7	8
0	3	0	-5	-10	-13	-21	-24	-27	-29
1	-1	-4	-9	-12	-15	-18	-21	-23	
2	-3	-7	-7	-9	-12	-15	-17		
3	-5	-9	-12	-14	-8	-11			
4	-7	-12	-14	-18	-9				
5	-9	-13	-17	-21					
6	-12	-16	-21						
7	-15	-19							
8	-19								

TABLE 3

Molal volume (V) in cm³ mole⁻¹ computed from equations (19) through (21)—see figures 1, 2, and 4

t (°C)	PRESSURE, KB											
	SAT	0.5	1	2	3	4	5	6	7	8	9	10
25	18.0681	17.6886	17.3547	16.84	16.41	16.05	15.72	15.45	15.22	15.01	14.79	14.61
50	18.2340	17.8610	17.5303	17.02	16.59	16.23	15.91	15.62	15.39	15.17	14.97	14.79
75	18.4820	18.0933	17.7526	17.22	16.18	16.42	16.09	15.80	15.55	15.34	15.13	14.96
100	18.7991	18.3778	18.0161	17.44	16.98	16.61	16.28	15.98	15.73	15.50	15.30	15.11
125	19.1851	18.7147	18.3211	17.70	17.21	16.82	16.48	16.17	15.91	15.67	15.46	15.27
150	19.6455	19.1075	18.6697	18.00	17.46	17.04	16.69	16.37	16.09	15.85	15.63	15.42
175	20.1901	19.5606	19.0638	18.33	17.73	17.28	16.91	16.57	16.28	16.03	15.79	15.58
200	20.8344	20.0907	19.5054	18.69	18.03	17.53	17.13	16.78	16.48	16.21	15.97	15.74
225	21.6039	20.6782	19.9976	19.08	18.34	17.80	17.37	17.00	16.68	16.40	16.14	15.90
250	22.5416	21.3703	20.5457	19.50	18.68	18.08	17.62	17.23	16.89	16.59	16.32	16.07
275	23.7224	22.1850	21.1593	19.95	19.05	18.38	17.88	17.46	17.10	16.79	16.51	16.25
300	25.2958	23.1669	21.8528	20.43	19.43	18.69	18.14	17.70	17.32	16.99	16.72	16.42
325	27.5307	24.3871	22.6469	20.95	19.83	19.02	18.43	17.95	17.54	17.20	16.89	16.60
350	31.3508	25.9614	23.5689	21.51	20.26	19.37	18.72	18.20	17.77	17.41	17.09	16.77
375		28.0920	24.6535	22.12	20.71	19.73	19.02	18.47	18.01	17.62	17.27	16.95
400		31.1324	25.9406	22.79	21.19	20.11	19.34	18.75	18.26	17.84	17.47	17.13
425		36.1590	27.4745	23.52	21.70	20.51	19.67	19.03	18.51	19.07	17.67	17.31
450		44.7894	29.3033	24.31	22.24	20.93	20.02	19.33	18.77	18.30	17.89	17.49
475		57.1878	31.4791	25.18	22.81	21.36	20.37	19.63	19.04	18.53	18.09	17.63
500		70.1236	34.0536	26.13	23.41	21.82	20.74	19.95	19.31	18.77	18.30	17.86
525		81.8168	37.0572	27.15	24.05	22.29	21.12	20.27	19.59	19.02	18.52	18.05
550		92.2038	40.4681	28.25	24.71	22.77	21.52	20.60	19.87	19.27	18.73	18.24
575		101.5571	44.1991	29.43	25.40	23.28	21.52	20.94	20.17	19.52	18.96	18.43
600		110.1153	48.1255	30.67	26.13	23.79	22.33	21.28	20.46	19.78	19.18	18.63
625		118.0515	52.1293	31.98	26.89	24.33	22.75	21.64	20.76	20.04	19.41	18.84
650		125.4694	56.1235	33.35	27.67	24.88	23.18	22.00	21.07	20.31	19.65	19.04
675		132.5197	60.0537	34.77	28.48	25.44	23.63	22.36	21.38	20.58	19.89	19.25
700		139.2110	63.8902	36.24	29.31	26.02	24.08	22.74	21.70	20.85	20.13	19.47
725		145.6166	67.6192	37.74	30.16	26.62	24.54	23.12	22.02	21.13	20.37	19.69
750		151.7790	71.2367	39.26	31.04	27.23	25.01	23.50	22.35	21.41	20.62	19.91
775		157.7331	74.7445	40.81	31.94	27.85	25.49	23.90	22.68	21.70	20.87	20.13
800		163.5079	78.1479	42.36	32.86	28.49	25.98	24.30	23.02	21.53	21.12	20.35
825		169.1279	81.4536	43.92	33.80	29.14	26.47	24.70	23.36	22.28	21.37	20.57
850		174.6139	84.6695	45.48	34.75	29.79	26.97	25.10	23.71	22.58	21.63	20.80
875		179.9838	87.8033	47.03	35.71	30.44	27.46	25.51	24.06	22.89	21.90	21.02
900		185.2535	90.8630	48.57	36.66	31.09	27.94	25.91	24.41	23.20	22.18	21.26

TABLE 4

A_{ij}, C_i, and F_i coefficients for equations (15), (16), and (20) after Keenan and others (1969)

i \ j	1	2	3	4	5	6	7
1	29.492937	-5.1985860	6.8335354	-0.1564104	-6.3972405	-3.9661401	-0.69648554
2	-132.13917	7.7779182	-26.149751	-0.72546108	26.409282	15.453061	2.7407416
3	274.64632	-33.301902	65.326396	-9.2734289	-47.740374	-29.142470	-5.1028070
4	-360.93828	-16.254622	-26.181978	4.3125840	56.323130	29.568796	3.9636085
5	342.18431	-177.31074	0	0	0	0	0
6	-244.50042	127.48742	0	0	0	0	0
7	155.18535	137.46153	0	0	0	0	0
8	5.9728487	155.97836	0	0	0	0	0
9	-410.30848	337.31180	-137.46618	6.7874983	136.87317	79.847970	13.041253
10	-416.05860	-209.88866	-733.96848	10.401717	645.81880	399.17570	71.531353

C_1 = 1857.065	C_5 = -20.5516	F_1 = -741.9242	F_5 = 0.1094098
C_2 = 3229.12	C_6 = 4.85233	F_2 = -29.72100	F_6 = 0.439993
C_3 = -419.465	C_7 = 46.0	F_3 = -11.55286	F_7 = 0.2520658
C_4 = 36.6649	C_8 = -1011.249	F_4 = -0.8685635	F_8 = 0.05218684

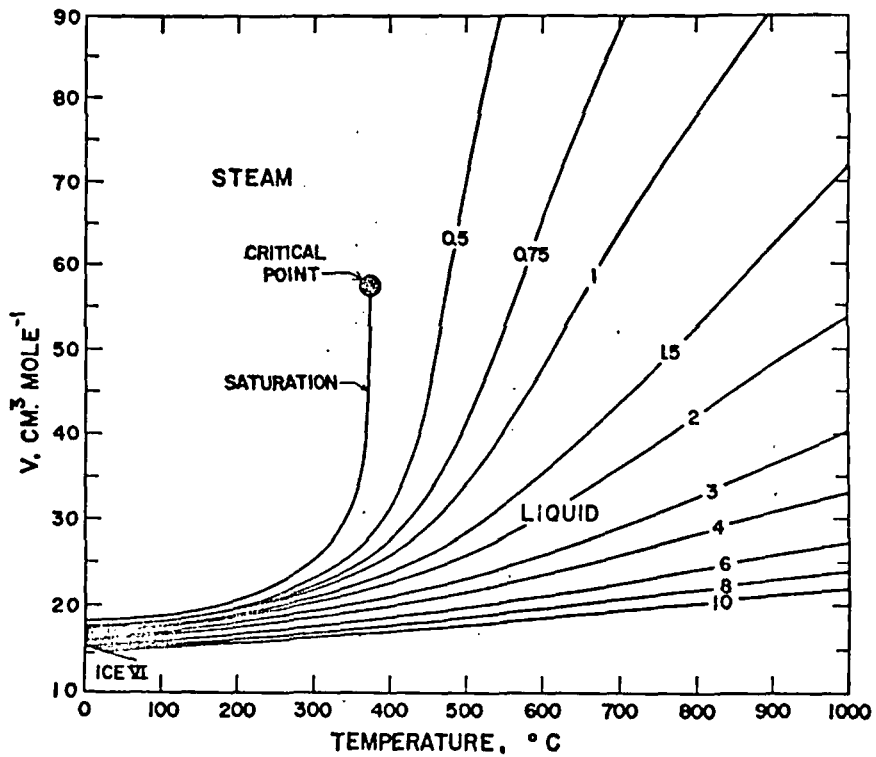

Fig. 1. Molal volume (table 3) as a function of temperature at constant pressure (labeled in kb) computed from equations (19) through (21) and the coefficients in tables 4 through 6.

and others, 1969) which is comparable to that reported by Kell and Whalley (1965) and Fine and Millero (1973). Even more accurate representation (to within 0.008 percent) of the saturation curve is afforded by

$$P_{sat} = P_c \exp\left(10^{-5}\tau(t_c - t) \sum_{i=1}^{8} F_i\,(0.65 - 0.01t)^{i-1} \right) \qquad (20)$$

where P_{sat} stands for saturation pressure, $P_c = P_{critical} = 220.88$ bars, τ is again 1000/T (where T is in °K), t represents temperature in °C, $t_c = t_{critical} = 374.136$°C, and F_i refers to an array of coefficients in table 4 (Keenan and others, 1969).

Equations (19) and (20) were used together with iterative computer techniques to calculate the molal volumes shown in table 3 and figures 1 and 2 for pressures ≤ a kilobar. The volumes shown for pressures above a kilobar were computed from a modification of the regression poly-

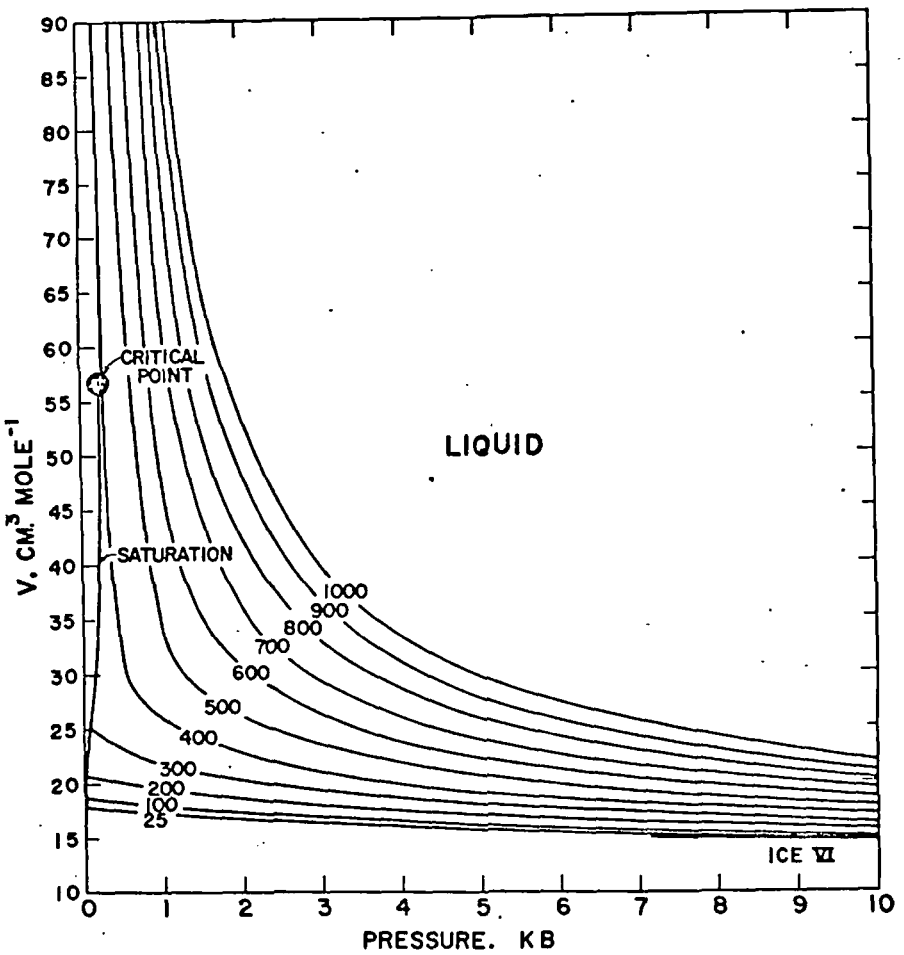

Fig. 2. Molal volume (table 3) as a function of pressure at constant temperature (labeled in °C) computed from equations (19) through (21) and the coefficients in tables 4 through 6.

nomial employed by Burnham, Holloway, and Davis (1969b), which can be written as

$$V = \sum_{i=0}^{\hat{i}} \sum_{j=0}^{\hat{i}-i} a_{ij}\, t^i\, P^{j-1} \qquad (21)$$

where V is again the specific volume of H_2O in $cm^3\ g^{-1}$, P stands for pressure in bars, t refers to temperature in °C, τ is a switch constant equal to 1 or −1 (see below), and a_{ij} refers to the arrays of fit coefficients in tables 5 and 6. Owing to the critical phenomenon and the extrapolation procedure employed in computing volumes beyond the upper pressure-

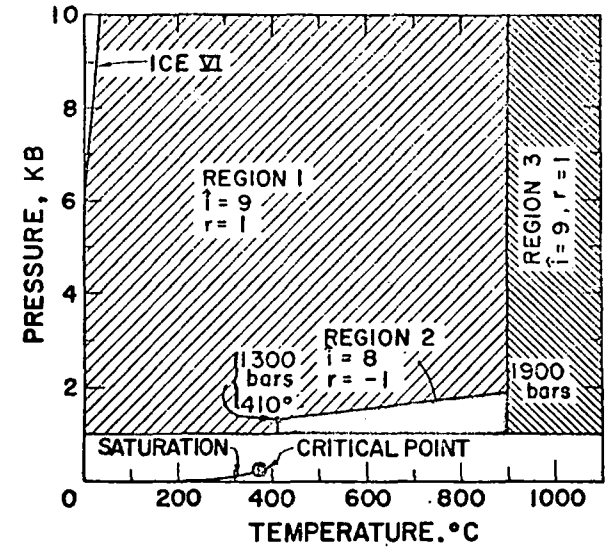

Fig. 3. Regions of pressure and temperature represented by alternate statements of equation (21) with the values of $\hat{\imath}$ and r shown above (Burnham, Holloway, and Davis, 1969).

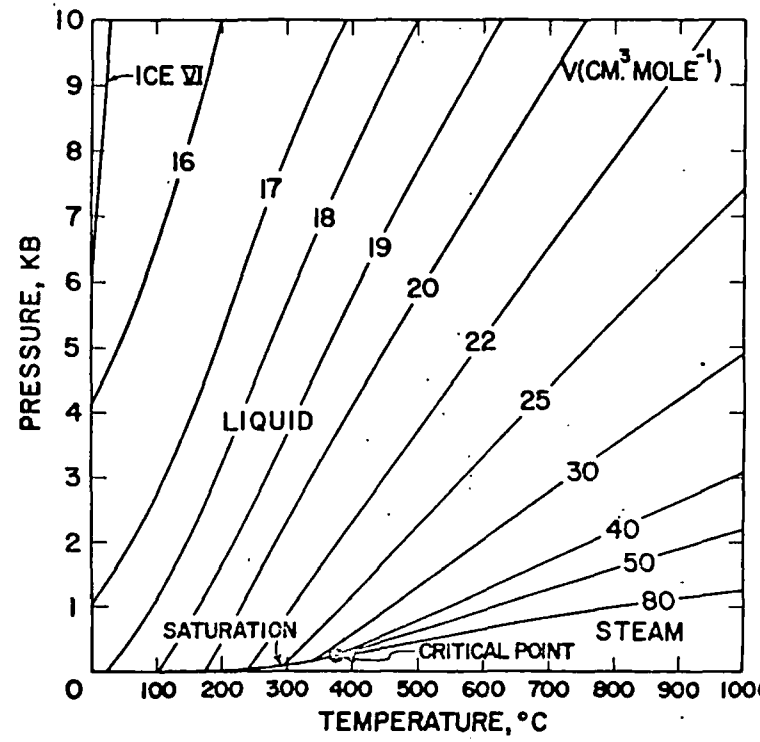

Fig. 4. Isochores (labeled in cm³ mole⁻¹) as a function of pressure and temperature (table 3 and figs. 1 and 2).

temperature limits of their measurements (8400 bars and 900°C), Burnham, Holloway, and Davis (1969b) used separate statements of equation (21) to represent the specific volume of H_2O in different pressure-temperature regions. These regions (numbered 1, 2, and 3) and the values of $\hat{\imath}$ and r in the statement of equation (21) appropriate to each are shown in figure 3. The a_{ij} coefficients for regions 1 and 2 are given in tables 5 and 6, respectively, but the corresponding coefficients for region 3 were omitted from this communication because they are based entirely on extrapolation of measurements at lower temperatures.

Specific volumes computed from equation (21) are reported to be within 0.3 percent of the measured volumes (Burnham, Holloway, and Davis, 1969b), but more recent measurements indicate that the uncertainty at high pressures and temperatures may be as high as ± 0.6 percent (C. W. Burnham, personal commun.). Comparison of specific volumes computed from equation (21) with those reported by Grindley and Lind (1971) for temperatures from 25° to 150°C reveals discrepancies ranging from 0.2 percent or less at 2 kb to 0.6 percent or less at 8 kb. The values given by Grindley and Lind are consistently lower than those computed from equation (21). Similarly, the specific volumes reported by Burnham, Holloway, and Davis (1969b) at high pressures and temperatures are slightly lower than those measured recently (C. W. Burnham and V. Wall, personal commun.), but at temperatures below 150°C, the latter measurements are in close agreement with those reported by Grindley and Lind (V. Wall, personal commun.). It thus appears that a slight (≤ 0.6 percent) but systematic error is inherent in densities computed from equation (21) and the coefficients in tables 5 and 6. The possible effect of this error on the calculations presented below is included in the overall uncertainties assigned to the results of the calculations.

It can be seen in figures 1 and 2 that the volume of H_2O forms a hyperbolic surface in pressure–volume–temperature space. However, at 10 kb the volume of H_2O increases only of the order of 7 cm³ mole^{-1} as temperature increases from 30° to 1000°C, which is approximately twice the increase associated with decreasing pressure from 10 kb to 1 bar at ~ 30°C. Note in figure 4 that the isochores for water take on a slight sigmoid shape as temperature decreases, and their curvature increases as they approach the melting curves of the ice polymorphs.

COMPRESSIBILITY AND THERMAL EXPANSION

The coefficient of isothermal compressibility (β) of H_2O can be computed for pressures ≤ a kilobar by differentiating equation (19) with respect to density at constant temperature. The resulting expression appears as

$$\beta^{-1} = \rho\left(\frac{\partial P}{\partial \rho}\right)_T = P + \rho^2 RT\left(Q + 3\rho\left(\frac{\partial Q}{\partial \rho}\right)_T + \rho^2\left(\frac{\partial^2 Q}{\partial \rho^2}\right)_T\right) \qquad (22)$$

$$+\frac{1}{\rho^2}\left(\frac{\partial\left(\frac{\partial\left(\frac{\partial Q}{\partial\rho}\right)_T}{\partial T}\right)_\rho}{\partial T}\right)_P - 2\rho^2\alpha\left(\frac{\partial\left(\frac{\partial Q}{\partial\rho}\right)_T}{\partial T}\right)_\rho\Bigg) \quad (27)$$

where $(\partial Q/\partial T)_\rho$, $(\partial(\partial Q/\partial T)_\rho/\partial T)_P$, $(\partial(\partial Q/\partial\rho)_T/\partial T)_\rho$, and $(\partial(\partial(\partial Q/\partial\rho)_T/\partial T)_\rho/\partial T)_P$ represent additional partial derivatives of equation (16) given in the appendix (eqs A-43, A-45, A-46, and A-47). Equations (19), (20), (22), and (25) were used to compute the values of α and β for pressures $\leq$ a kilobar in tables 7 and 8, which are represented by the curves in figures 5 through 8.

TABLE 7

Coefficient of isobaric thermal expansion (α) in $(°K)^{-1} \times 10^5$ computed from equations (25), (33), and (39) and the values of V in table 3—see figures 5, 6, and 16

t	PRESSURE, KB								
(°C)	SAT	0.5	1	2	3	4	5	6	7
25	25.53	30.99	34.30	38.4	40.6	42.3	43.4	43.9	44.2
50	46.24	45.80	45.76	44.5	44.6	44.8	44.7	44.5	44.3
75	61.39	57.21	54.79	50.4	48.8	47.7	46.7	45.8	45.0
100	74.86	67.55	63.03	56.1	52.9	50.6	48.8	47.2	46.0
125	88.36	77.84	71.27	61.6	56.7	53.5	50.9	48.7	47.0
150	102.71	88.36	79.51	67.0	60.4	56.1	52.8	50.1	48.0
175	118.70	99.24	87.61	72.4	63.9	58.5	54.5	51.4	48.8
200	137.62	110.87	95.60	77.8	67.2	60.7	56.1	52.4	49.6
225	161.75	124.03	103.80	83.1	70.4	62.7	57.4	53.3	50.1
250	195.13	139.93	112.71	88.3	73.5	64.6	58.6	54.1	50.6
275	245.37	160.30	123.00	93.5	76.5	66.4	59.8	54.8	51.0
300	329.48	187.56	135.41	98.7	79.4	68.2	60.9	55.5	51.4
325	499.05	225.16	150.64	103.9	82.4	70.0	62.0	56.2	51.8
350	1038.30	278.55	169.21	109.4	85.5	71.9	63.2	57.0	52.2
375		358.22	191.25	115.3	88.6	73.8	64.5	57.9	52.8
400		488.47	216.32	121.5	91.8	75.8	65.9	58.8	53.4
425		715.91	243.57	128.0	95.1	77.9	67.3	59.8	54.0
450		973.36	272.09	134.9	98.4	79.9	68.7	60.8	54.7
475		923.47	300.82	141.9	101.5	81.8	70.0	61.8	55.4
500		707.36	327.40	148.9	104.3	83.4	71.1	62.6	55.9
525		537.73	347.20	156.7	107.2	85.7			
550		426.21	354.86	161.6	109.8	87.0			
575		351.40	348.44	165.3	111.9	88.0			
600		298.71	331.01	167.7	113.5	88.8	(74.8)	(65.6)	(58.2)
625		259.87	307.74	168.8	114.6	89.3			
650		230.18	282.87	168.5	115.2	89.6			
675		206.79	258.89	167.1	115.2	89.7			
700		187.93	236.91	164.5	114.8	89.7	(75.3)	(66.1)	(58.4)
725		172.44	217.29	161.1	114.2	89.7			
750		159.52	200.01	157.0	113.3	89.8			
775		148.61	184.87	152.5	112.4	89.8			
800		139.29	171.64	147.6	111.4	89.9	(76.1)	(67.7)	(60.2)
825		131.26	160.06						
850		124.28	149.92						
875		118.18	141.02						
900		112.80	133.17						

which can in turn be differentiated to give

$$\left(\frac{\partial\beta}{\partial P}\right)_T = \beta^2\left(2\beta P - 3 - \rho^3\beta RT\left(4\left(\frac{\partial Q}{\partial\rho}\right)_T + 5\rho\left(\frac{\partial^2 Q}{\partial\rho^2}\right)_T + \rho^2\left(\frac{\partial^3 Q}{\partial\rho^3}\right)_T\right)\right) \quad (23)$$

and

$$\left(\frac{\partial\beta}{\partial T}\right)_P = -\left(\frac{\partial\alpha}{\partial P}\right)_T = (1-\beta P)\left(2\alpha\beta - \frac{\beta}{T}\right) - \beta^2\rho^2 RT\left(\left(\frac{\partial Q}{\partial T}\right)_P + 3\rho\left(\frac{\partial\left(\frac{\partial Q}{\partial\rho}\right)_T}{\partial T}\right)_P - 3\rho\alpha\left(\frac{\partial Q}{\partial\rho}\right)_T + \rho^2\left(\frac{\partial\left(\frac{\partial^2 Q}{\partial\rho^2}\right)_T}{\partial T}\right)_P - 2\rho^2\alpha\left(\frac{\partial^2 Q}{\partial\rho^2}\right)_T\right) \quad (24)$$

where $(\partial Q/\partial T)_P$, $(\partial Q/\partial\rho)_T$, $(\partial^2 Q/\partial\rho^2)_T$, $(\partial^3 Q/\partial\rho^3)_T$, $(\partial(\partial Q/\partial\rho)_T/\partial T)_P$, and $(\partial(\partial^2 Q/\partial\rho^2)_T/\partial T)_P$ correspond to partial derivatives of equation (16) given in the appendix (eqs A-8, A-22, A-23, A-24, A-35, and A-39), and α represents the coefficient of isobaric thermal expansion, which can be computed for pressures $\leq$ a kilobar from

$$\alpha = -\frac{1}{\rho}\left(\frac{\partial\rho}{\partial T}\right)_P = \frac{\beta P}{T} + \rho RT\beta\left(\rho\left(\frac{\partial Q}{\partial T}\right)_\rho + \rho^2\left(\frac{\partial\left(\frac{\partial Q}{\partial\rho}\right)_T}{\partial T}\right)_\rho\right) \quad (25)$$

Equation (25) is the result of combining the partial derivative of equation (19) with respect to temperature at constant density with the identity,

$$\left(\frac{\partial P}{\partial T}\right)_\rho = \frac{\alpha}{\beta}, \quad (26)$$

which leads to

$$\left(\frac{\partial\alpha}{\partial T}\right)_P = \frac{\alpha}{\beta}\left(\frac{\partial\beta}{\partial T}\right)_P - \frac{2\beta P}{T^2} + \frac{\alpha}{T}(1-\alpha T+\beta P) + \rho RT\beta\left(\rho\left(\frac{\partial\left(\frac{\partial Q}{\partial T}\right)_\rho}{\partial T}\right)_P - \rho\alpha\left(\frac{\partial Q}{\partial T}\right)_\rho +$$

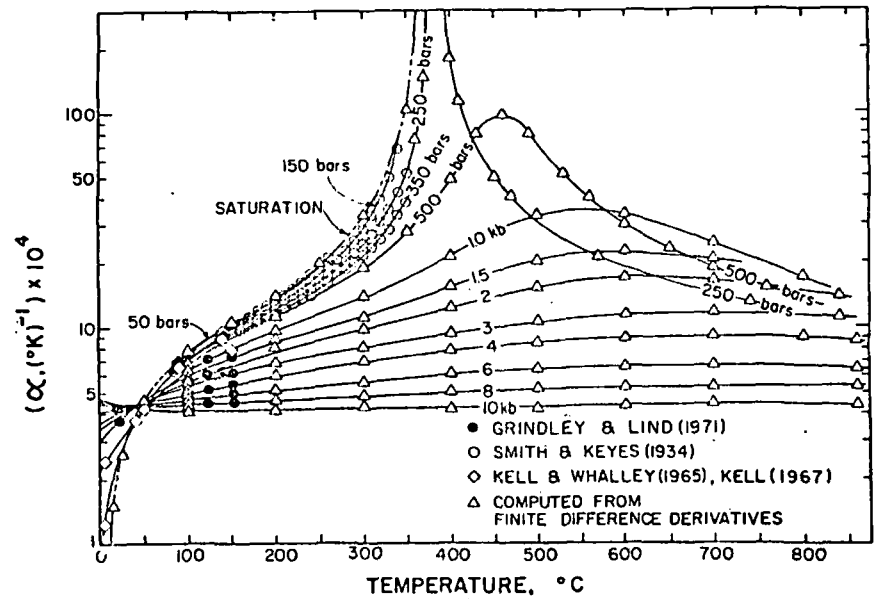

Fig. 5. *Coefficient of isobaric thermal expansion* (table 7) as a *function of temperature* at constant pressure (labeled in bars and kb) computed from equations (19) through (21), (25), (33), and (39) and coefficients in tables 4, 5, 6, 9, and 10 (curves). The symbols represent values taken from the literature or computed from finite difference derivatives of specific volumes given by Schmidt (1969), Burnham, Holloway, and Davis (1969b), and Keenan and others (1969).

Because equation (19) so closely represents the dependence of density on pressure and temperature below a kilobar (Keenan and others, 1969), minimal uncertainties attend calculation of β, $(\partial\beta/\partial P)_T$, $(\partial\beta/\partial T)_P$, α, and $(\partial\alpha/\partial T)_P$ for pressures $\leqq$ a kilobar from equations (22) through (25) and (27). It can be seen in figures 5 through 8 that the calculated values of α and β are in close agreement with corresponding coefficients of isothermal compressibility and isobaric thermal expansion reported in the literature. Values of β computed from equation (22) for temperatures from 25° to 100°C and pressures from 1 to 1000 bars are within 1 percent or less of those derived from sound velocity data by Fine and Millero (1973), except for pressures at or near a kilobar where the difference is 4 percent or less. Similar comparison of expansibilities computed from equation (25) with those reported by Fine and Millero (1973) yields corresponding differences of 1 percent and 2 percent, respectively. The expansibilities and compressibilities given by Fine and Millero are within ~ 1 percent or less of those reported by Kell and Whalley (1965). It can also be seen in figures 5 through 8 that the values of α and β computed from equations (22) and (25) are in close agreement with corresponding values calculated from finite differences in specific volume $((\Delta V/\Delta T)_P/V$ and $(-\Delta V/\Delta P)_T/V)$. As shown below, equations (23), (24), and (27) afford similar agreement with their finite difference counterparts

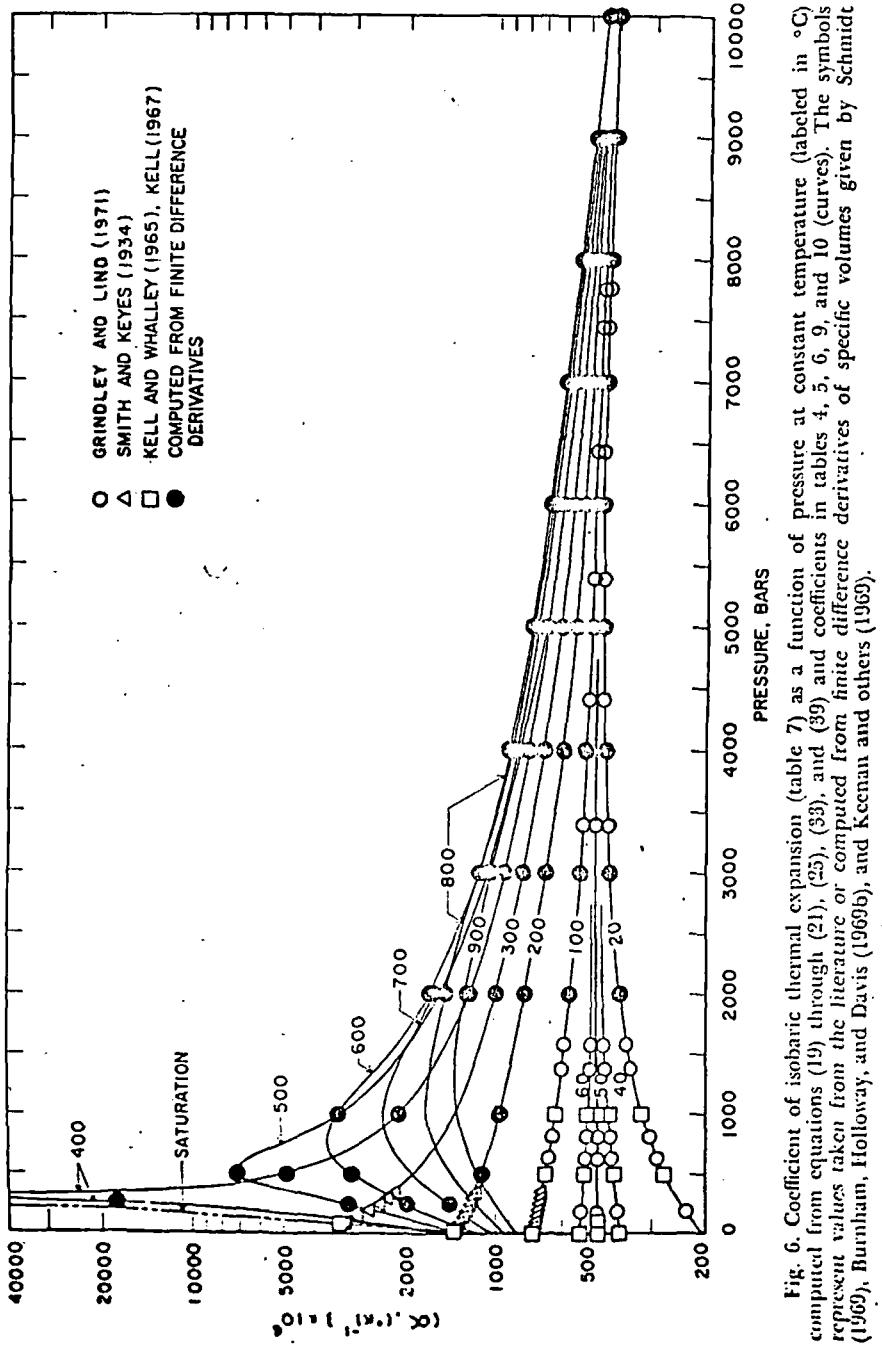

Fig. 6. Coefficient of isobaric thermal expansion (table 7) as a function of pressure at constant temperature (labeled in °C) computed from equations (19) through (21), (25), (33), and (39) and coefficients in tables 4, 5, 6, 9, and 10 (curves). The symbols represent values taken from the literature or computed from finite difference derivatives of specific volumes given by Schmidt (1969), Burnham, Holloway, and Davis (1969b), and Keenan and others (1969).

$((\Delta((-\Delta V/\Delta P)_T/V)/\Delta P)_T$, $(\Delta((-\Delta V/\Delta P)_T/V)/\Delta T)_P$, and $(\Delta((\Delta V/\Delta T)_P/V)/\Delta T)_P$).

In principle, the compressibility and thermal expansion of H_2O at pressures above a kilobar can be computed from the isothermal and isobaric partial derivatives of equation (21), which can be written as

$$\left(\frac{\partial V}{\partial P}\right)_T = -V\beta = \sum_{i=0}^{i}\sum_{j=0}^{i-i} (rj-1)\, a_{ij}\, t^i\, P^{rj-2} \qquad (28)$$

and

$$\left(\frac{\partial V}{\partial T}\right)_P = V\alpha = \sum_{i=0}^{i}\sum_{j=0}^{i-i} i a_{ij}\, t^{i-1}\, P^{rj-1} \qquad (29)$$

TABLE 8

Coefficient of isothermal compressibility (β) in $bar^{-1} \times 10^6$ computed from equations (22), (32), and (38) and the values of V in table 3—see figures 7, 8, and 17[a]

t	PRESSURE, KB									
(°C)	SAT	0.5	1	2	3	4	5	6	7	8
25	45.60	39.91	36.57	30.0	25.3	21.6	18.8	16.7	15.2	14.1
50	44.36	38.95	36.07	29.8	25.1	21.6	18.8	16.7	15.2	14.1
75	45.89	39.86	36.44	30.0	25.2	21.7	18.9	16.8	15.3	14.2
100	49.50	42.11	37.70	30.8	25.6	22.0	19.2	17.1	15.5	14.4
125	55.12	45.60	39.82	32.0	26.4	22.6	19.7	17.5	15.9	14.6
150	63.09	50.41	42.83	34.0	27.5	23.3	20.3	18.0	16.3	15.0
175	74.24	56.82	46.82	36.6	29.0	24.3	21.0	18.6	16.8	15.4
200	90.09	65.35	52.02	39.7	30.9	25.5	21.9	19.3	17.3	15.8
225	113.48	76.87	58.73	43.6	33.1	27.0	23.0	20.1	18.0	16.4
250	149.96	92.75	67.45	48.1	35.7	28.6	24.1	21.0	18.7	17.0
275	211.54	115.26	78.84	53.3	38.6	30.4	25.4	22.0	19.5	17.7
300	329.06	148.27	93.85	59.3	41.9	32.5	26.9	23.1	20.4	18.4
325	607.65	198.70	113.72	66.3	45.6	34.8	28.5	24.3	21.4	19.2
350	1698.85	280.16	140.04	74.3	49.8	37.3	30.2	25.6	22.5	20.1
375		423.17	174.66	83.6	54.3	40.0	32.1	27.1	23.6	21.1
400		707.68	219.66	94.3	59.3	42.9	34.1	28.6	24.8	22.1
425		1349.14	277.43	106.7	64.8	46.1	36.2	30.2	26.1	23.2
450		2525.76	350.85	120.9	70.7	49.4	38.5	31.9	27.5	24.4
475		3289.09	442.71	137.1	77.1	53.0	40.9	33.7	29.0	25.6
500		3266.80	553.11	155.4	84.0	56.7	43.4	35.6	30.5	26.9
525		3043.18	674.90							
550		2839.08	792.51	189.8	99.9	67.7	48.6	39.9	(33.3)	(29.2)
575		2680.23	889.54							
600		2558.34	958.68	230.0	116.5	76.3	54.0	43.8	(36.5)	(31.9)
625		2463.48	1002.28							
650		2388.27	1026.73	269.1	133.9	85.5	59.5	47.8	(39.7)	(34.5)
675		2327.61	1038.30							
700		2277.93	1041.66	305.5	151.2	94.7	65.1	51.8	(43.0)	(37.2)
725		2236.74	1040.01							
750		2202.21	1035.45	337.3	167.3	103.8	70.5	55.7	(46.1)	(40.0)
775		2173.01	1029.28							
800		2148.12	1022.36	363.7	181.6	112.6	75.8	59.5	(49.3)	(43.0)
825		2126.74	1015.20							
850		2108.27	1008.12							
875		2092.22	1001.31							
900		2078.18	994.87							

[a]Values given for temperatures and pressures above 500°C and 6 kb are based on graphic interpolation (see text).

However, evaluation of equations (28) and (29) with the fit coefficients in tables 5 and 6 (which were derived from those obtained by Burnham, Holloway, and Davis, 1969b) from regression of their experimental specific volume measurements with equation 21) yields partial derivatives that differ significantly from corresponding finite difference derivatives $((\Delta V/\Delta P)_T$ and $(\Delta V/\Delta T)_P)$ computed directly from the smoothed specific volumes generated by the regression polynomial. Equations (28) and (29) and the coefficients in tables 5 and 6 also yield values of $(\partial V/\partial P)_T$ and $(\partial V/\partial T)_P$ between 1 and 2 kb which are inconsistent with those computed from equations (22) and (25) for pressures ≤ a kilobar. Regression of the experimental data with equation (21) apparently led to an overfit of the specific volume measurements in certain parts of the regions depicted in figure 3, and an underfit in others. Linear regression of asymptotic surfaces may lead to errors in derivatives caused by overfitting which are not manifest in the fits of the integral function. In this case the fit coefficients for equation (21) in tables 5 and 6 yield specific volumes to within 0.6 percent of the measured values (see above), but uncertainties in the partial derivatives generated by equations (28) and (29) are as much as two or more orders of magnitude greater at the boundaries of the fit regions.

The coefficients of isothermal compressibility and isobaric thermal expansion of H_2O exhibit dramatic saddle-shaped pressure-temperature configurations with "pommels" at the critical point, where $-(\partial V/\partial P)_T = (\partial V/\partial T)_P = \alpha = \beta = \infty$. To overcome difficulties inherent in achieving accurate algebraic representation of these complicated surfaces with analytic derivatives of specific volume regression polynomials, finite difference derivatives were first computed from specific volumes generated by equation (21) at closely spaced intervals from 0.001 to 10 kb and 20° to 900°C. The computed values of V were used in preference to the experimental measurements to minimize the effect of experimental uncertainty on the finite difference derivatives. The spacing of the intervals was determined by the requirement that the percent change in specific volume be substantially greater than the percent uncertainty in the specific volumes but small enough to yield close approximations of the true derivatives at the midpoints of the intervals. After sorting to eliminate obvious aberrations caused by asymmetry in a number of the finite differences, the values of both $(\Delta V/\Delta P)_T$ and $(\Delta V/\Delta T)_P$ (or corresponding values of α and β computed from the finite difference derivatives) were regressed simultaneously with appropriate derivative polynomials generated from a single integral equation. In an effort to identify the best algebraic expression for this purpose, various polynomials were used to regress the finite difference values as a function of pressure and temperature or density and temperature, but none fit all the values adequately over the entire pressure-temperature range represented by regions 1 and 2 in figure 3. The best fit for the combined regions was obtained by in-

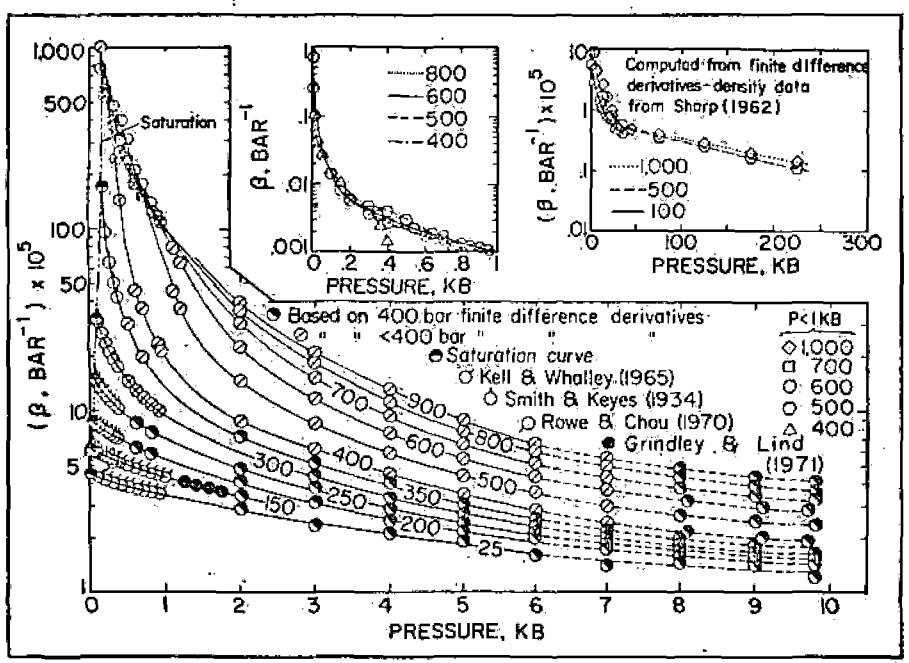

Fig. 8. Coefficient of isothermal compressibility (table 8) as a function of pressure at constant temperature (labeled in °C) computed from equations (19) through (22), (32), and (38) and coefficients in tables 4, 5, 6, 9, and 10 (solid curves). The symbols represent values taken from the literature or computed from finite difference derivatives of specific volumes given by Schmidt (1969), Burnham, Holloway, and Davis (1969b), and Keenan and others (1969). The dashed curves are based on smooth graphic interpolation of the finite difference β values.

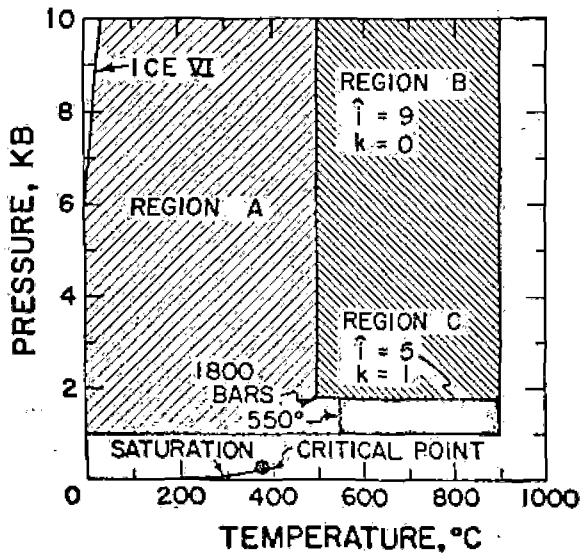

Fig. 9. Regions of pressure and temperature represented by equations (32) through (37) for region A and alternate statements of equations (38) through (43) for regions B and C.

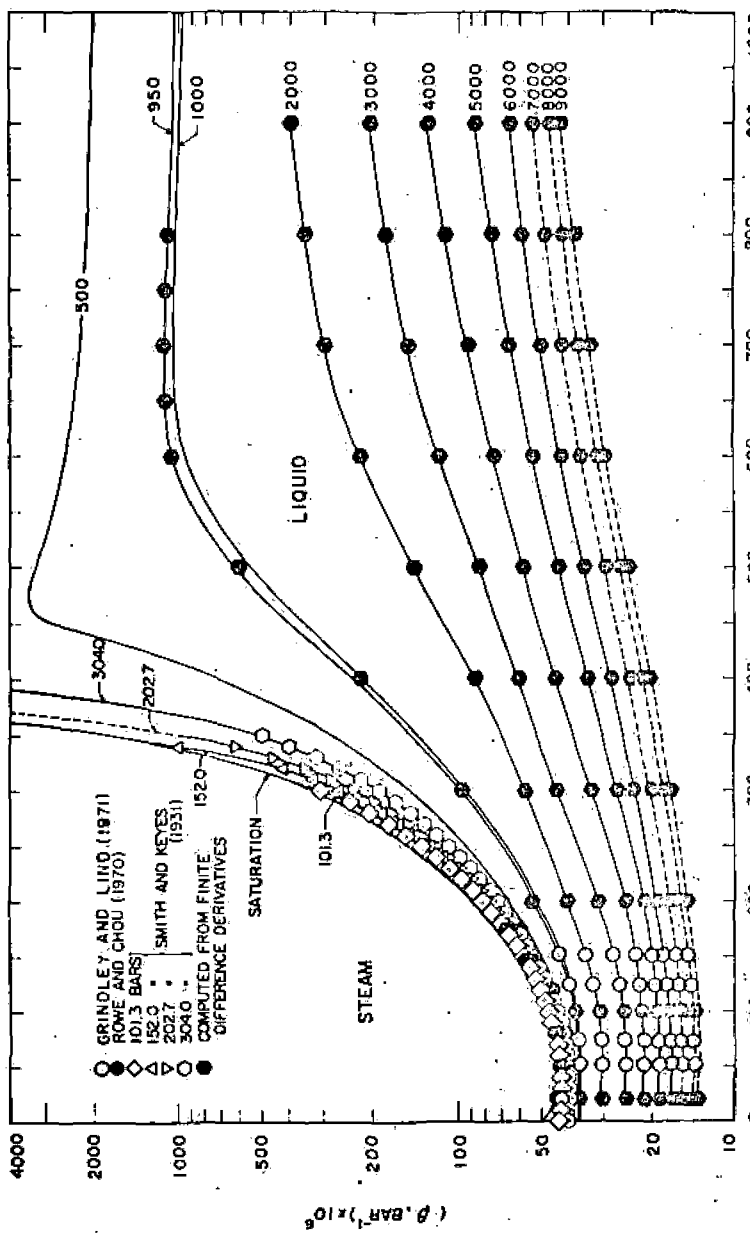

Fig. 7. Coefficient of isothermal compressibility (table 8) as a function of temperature at constant pressure (labeled in bars) computed from equations (19) through (22), (32), and (38) and coefficients in tables 4, 5, 6, 9, and 10 (solid curves). The symbols represent values taken from the literature or computed from finite difference derivatives of specific volumes given by Schmidt (1969), Burnham, Holloway, and Davis (1969b), and Keenan and others (1969). The dashed curves are based on smooth graphic interpolation of the finite difference β values.

dependent nonlinear regression of the finite difference α and β values with exponential functions of the form

$$\beta = \exp\left(\sum_{i=0}^{3}\sum_{j=0}^{7-i} b_{ij}\, T^i\, P^j\right) \tag{30}$$

and

$$\alpha = \exp\left(\sum_{i=0}^{3}\sum_{j=0}^{7-i} c_{ij}\, T^i\, P^j\right) \tag{31}$$

which for the most part rendered residuals in α of less than 1 percent and residuals in β of less than 5 percent. However, at pressures < 1500 bars the residuals increased and reached 10 to 15 percent at the low-pressure boundary of the fit region. The failure of these functions at pressures from 1000 to 1500 bars together with unacceptable discrepancies in the cross derivatives and correspondingly large uncertainties in $(\partial\beta/\partial P)_T$ and $(\partial\alpha/\partial T)_P$ computed from the partial derivatives of equations (30) and (31) forced rejection of these expressions as adequate representatives of α and β.

Further numerical analysis with other functions of temperature and density led to the decision to subdivide the region of pressure and temperature in a fashion similar to that chosen by Burnham, Holloway, and Davis (1969b) for specific volume (fig. 3). Comparative overlapping regression of $(\Delta V/\Delta P)_T$ and $(\Delta V/\Delta T)_P$ in alternate subdivisions with and without including data for pressures $\leq$ a kilobar indicated that all the finite difference derivatives and corresponding values of α and β could be represented with adequate accuracy by separate polynomials describing these variables in the three regions of pressure-temperature space labeled A, B, and C in figure 9. The best fits in region A were obtained with

$$\beta^{-1} = \sum_{j=0}^{5}\sum_{i=0}^{8-j} j\, B_{ij}\, T^i\, \rho^j \tag{32}$$

and

$$\alpha = \beta \sum_{j=0}^{5}\sum_{i=0}^{8-j} i\, B_{ij}\, T^{i-1}\, \rho^j \tag{33}$$

which are consistent with

$$P = \sum_{j=0}^{5}\sum_{i=0}^{8-j} B_{ij}\, T^i\, \rho^j \tag{34}$$

where B_{ij} stands for the coefficients given in table 9 for region A in figure 9. Differentiating equation (32) with respect to pressure at constant temperature leads to

$$\left(\frac{\partial\beta}{\partial P}\right)_T = -\beta^3 \sum_{j=0}^{5}\sum_{i=0}^{8-j} j^2 B_{ij}\, T^i\, \rho^j \tag{35}$$

and the corresponding partial derivative with respect to temperature at constant pressure can be written as

$$\left(\frac{\partial\beta}{\partial T}\right)_P = -\left(\frac{\partial\alpha}{\partial P}\right)_T = -\beta^2 \sum_{j=0}^{5}\sum_{i=0}^{8-j} j\, B_{ij}\,(i T^{i-1}\, \rho^j - j T^i\, \rho^j \alpha) \tag{36}$$

TABLE 9

Coefficients for equations (32) and (33) in region A of figure 9

$\underline{B}_{ij} = \hat{\underline{B}}_{ij} \times 10^{\underline{B^*}_{ij}}$

$\hat{\underline{B}}_{ij}$

i \ j	0	1	2	3	4	5
0	0.	5.541654961	-5.647694994	1.391084523	9.314051406	-4.224085781
1	2.001619452	-6.480330829	7.804635059	-4.149778955	8.284235229	-3.173272705
2	-8.445248783	2.599081364	-2.997059355	1.567146158	-3.437390375	1.864672542
3	1.849203613	-5.126544377	5.215914752	-2.327295430	4.123082012	-1.650956925
4	-2.344156348	5.544129599	-4.597168845	1.520379055	-1.562138539	
5	1.782166279	-3.321663469	1.982307354	-3.619181443		
6	-8.063473576	1.021229414	-3.272068272			
7	2.064415341	-1.237172220				
8	-2.498805152					

$\underline{B^*}_{ij}$

i \ j	0	1	2	3	4	5
0	0	6	6	6	5	5
1	4	4	4	4	3	1
2	1	2	2	2	1	0
3	-1	-1	-1	-1	-2	-3
4	-4	-4	-4	-4	-5	
5	-7	-7	-7	-8		
6	-11	-10	-11			
7	-14	-14				
8	-18					

The coefficients in equations (32) through (37) for region A in figure 9 (table 9) and those in table 10 for alternate statements of equations (38) through (43) for regions B and C were obtained by simultaneous linear regression of $(-\Delta V/\Delta P)_T/V$ and $(\Delta V/\Delta T)_P/V$ with equations (32) and (33), and $(\Delta V/\Delta P)_T$ and $(\Delta V/\Delta T)_P$ with equations (38) and (39). The values of V employed in the calculations were computed from equation (21). The number of finite difference derivatives considered in the regression analysis of the regions varied from 100 to 300, depending on the region. The limits of the summation terms in equations (32) through (37) and (38) through (43) were defined by comparative regression of the finite difference data with polynomials of alternate degree in an effort to preclude overfit and insure partial derivatives consistent with their finite difference counterparts. Overlapping regression of the fit regions and incorporation of data for pressures below a kilobar in fitting regions A and C in figure 9 minimized inter-regional discontinuities in the computed values of α, β, and their partial derivatives as functions of temperature and pressure. In most cases the inter-regional discrepancies in α are less than 1 percent,

TABLE 10

Coefficients for equations (38) and (39) in regions B and C of figure 9 ($\hat{\imath} = 9$ and $k = 0$ for region B, and $\hat{\imath} = 5$ and $k = 1$ for region C)

$$\underset{ij}{p} = \underset{ij}{b} \cdot 10^{\underset{ij}{p^*}}$$

$\underset{ij}{b}$ for region B

i \ j	0	1	2	3	4
0	0.	-1.506919791	1.407973492	-7.507671325	2.471604532
1	-1.787555824	2.810937516	7.031625811	-5.954625622	2.223830468
2	4.503625642	-7.193775721	5.156729175	-1.997843646	4.202016232
3	1.986537032	-1.133016027	5.705056876	-1.410074499	1.247849426
4	-5.376132969	-1.172516191	3.305371107	3.521599490	-9.298307117
5	1.484589030	-3.463262360	-6.138922413	7.391640369	-1.171172934
6	-1.126373624	7.539081341	-1.272723651	-1.546134985	
7	-8.992177755	-4.538459618	1.368240982		
8	1.459740213	6.914686939			
9	-4.903210863				

i \ j	5	6	7	8	9
0	-5.205698231	7.023757340	-5.865013363	2.757432199	-5.572807869
1	-4.458179201	4.957412121	-2.879352329	6.815947672	
2	-4.702819663	2.617250953	-5.673263000		
3	-2.017582894	-1.207488032			
4	3.676616838				

$\hat{\underset{ij}{b}}$ for region C

i \ j	0	1	2	3
0	0.	4.668287584	-7.085868594	2.111356062
1	-7.041518381	2.955659758	2.779240901	-1.768464908
2	2.151504359	-1.525948185	4.132847534	9.211139144
3	-2.773357282	2.067817826	-2.526689074	-1.019479759
4	1.650048239	-1.137357755	1.051203720	
5	-3.731274546	2.162263875		

i \ j	4	5	6
0	7.9549338710	-4.642576017	6.177986362
1	3.383613741	-2.222308253	
2	-1.0825094726		

$\underset{ij}{p^*}$ for region B

i \ j	0	1	2	3	4	5	6	7	8	9
0	0	-3	-6	-10	-13	-17	-21	-25	-29	-34
1	-4	-8	-10	-13	-16	-20	-24	-28	-33	
2	-6	-9	-12	-15	-19	-23	-27	-32		
3	-8	-11	-15	-18	-22	-27	-31			
4	-11	-15	-18	-21	-26	-30				
5	-13	-17	-21	-25	-29					
6	-16	-20	-24	-28						
7	-20	-23	-27							
8	-23	-27								
9	-26									

$\underset{ij}{p^*}$ for region C

i \ j	0	1	2	3	4	5	6
0	0	-3	-5	-8	-12	-15	-19
1	-1	-4	-7	-10	-14	-18	
2	-3	-6	-10	-14	-17		
3	-6	-9	-13	-17			
4	-9	-12	-16				
5	-13	-16					

Similarly, the partial derivative of equation (33) with respect to temperature at constant pressure is given by

$$\left(\frac{\partial \alpha}{\partial T}\right)_P = \frac{\alpha}{\beta}\left(\frac{\partial \beta}{\partial T}\right)_P + \beta \sum_{j=0}^{5} \sum_{i=0}^{8-j} i\, B_{ij}\left((i-1)T^{i-2}\rho^j - jT^{i-1}\rho^j\alpha\right) \tag{37}$$

The finite difference derivatives in regions B and C of figure 9 can be represented closely by equations of the form

$$\left(\frac{\partial V}{\partial P}\right)_T = -\beta V = \sum_{i=0}^{\hat{\imath}} \sum_{j=0}^{\hat{\imath}+k-i} j\, D_{ij}\, T^i\, P^{j-1} \tag{38}$$

and

$$\left(\frac{\partial V}{\partial T}\right)_P = \alpha V = \sum_{i=0}^{\hat{\imath}} \sum_{j=0}^{\hat{\imath}+k-i} i\, D_{ij}\, T^{i-1}\, P^j \tag{39}$$

which are consistent with

$$V = \sum_{i=0}^{\hat{\imath}} \sum_{j=0}^{\hat{\imath}+k-i} D_{ij}\, T^i\, P^j \tag{40}$$

where D_{ij}, $\hat{\imath}$, and k refer to the arrays of fit coefficients and integer constants given in table 10 for regions B and C in figure 9. It follows from equation (38) that we can write

$$\left(\frac{\partial \beta}{\partial P}\right)_T = \beta^2 - \rho \sum_{i=0}^{\hat{\imath}} \sum_{j=0}^{\hat{\imath}+k-i} j(j-1) D_{ij}\, T^i\, P^{j-2} \tag{41}$$

and

$$\left(\frac{\partial \beta}{\partial T}\right)_P = -\left(\frac{\partial \alpha}{\partial P}\right)_T = -\alpha\beta - \rho \sum_{i=0}^{\hat{\imath}} \sum_{j=0}^{\hat{\imath}+k-i} ij D_{ij}\, T^{i-1}\, P^{j-1} \tag{42}$$

Similarly, the partial derivative of equation (39) with respect to temperature at constant pressure leads to

$$\left(\frac{\partial \alpha}{\partial T}\right)_P = -\alpha^2 + \rho \sum_{i=0}^{\hat{\imath}} \sum_{j=0}^{\hat{\imath}+k-i} i(i-1) D_{ij}\, T^{i-2}\, P^{j-1} \tag{43}$$

and those in β are less than 4 percent. However, corresponding discrepancies in the partial derivatives of α and β are generally larger (see below).

Equations (32) and (33) fit the finite difference values of α and β in region A of figure 9 to within 3 percent, except for three residuals less than 4 percent and four less than 8 percent. With the exception of two residuals less than 4 percent, equation (38) represents $(\Delta V/\Delta P)_T$ in region B of figure 9 to within 2 percent at pressures $\leq$ 6 kb. Above 6 kb in region B, the regression equation yields residuals in excess of minimal requirements for dependable partial differentiation. Most of the residuals above 6 kb in region B are of the order of 5 percent or less, seven are between 5 and 10 percent, and one is greater than 10 percent. Although these latter residuals are not excessive, their distribution is nonrandom, which precludes general application of equation (38) and the fit coefficients in table 10 for pressures above 6 kb in region B. The uncertainty in both α and β in region C is less than 4 percent, except four residuals in β which are less than 8 percent. Equation (39) reproduces the values of $(\Delta V/\Delta T)_P$ in both regions B and C to within 1 percent from 1 to 10 kb, with the exception of ten residuals which are less than 3 percent. Except as noted above and in the vicinity of the region boundaries, the residuals in all of the fits approximate random distributions. Values of α and β calculated from equations (32) and (33) for temperatures $\leq$ 150°C and pressures $>$ a kilobar are within 4 percent of those computed by Grindley and Lind (1971). The two sets of values diverge from one another with increasing pressure above $\sim$ 3 kb. At higher pressures, the values of α computed by Grindley and Lind are slightly lower and those of β slightly higher than the corresponding values computed in this study. Although equations (34) and (40) yield values of V in good accord with those generated by equation (21), the latter expression is more convenient to use and affords more accurate representation of the experimental specific volumes of H_2O reported by Burnham, Holloway, and Davis (1969a). Simultaneous regression of β^{-1}, α, and P with equations (32) through (34), and V, $(\Delta V/\Delta P)_T$ and $(\Delta V/\Delta T)_P$ with equations (38) through (40) rendered essentially the same results as those obtained without including P, V, and equations (34) and (40).

Values of α and β computed from equations (21), (32), (33), (38), and (39) for pressures greater than a kilobar in regions A, B, and C of figure 9 are given in tables 7 and 8 together with those calculated from equations (22) and (25) for pressures $\leq$ a kilobar. The close agreement of the computed values (solid curves) with their finite difference counterparts and those calculated by Grindley and Lind (1971) is apparent in figures 5 through 8, where α and β are plotted as functions of temperature and pressure. The coefficients for region A were used to compute the values for α and β at 500°C and pressures $>$ a kilobar. The dashed curves in figure 8 and the parenthetical values in table 8 above 500°C and 6 kb represent graphic extrapolations of the computed values below 6 kb, extended through the high-pressure finite difference β values. As indicated above, equation (38) and the fit coefficients in table 10 are not suitable

for accurate representation of β in this region of temperature-pressure space.

The dependence of β on pressure above 10 kb is depicted in the upper right inset diagram of figure 8, where finite difference values of β computed from specific volumes generated by Sharp (1962) from shock wave data are plotted for pressures to 225 kb at 500° and 1000°C. The curves in the upper right inset diagram of figure 8, like those for 600° to 900°C at pressures above 6 kb in figures 7 and 8, were not computed but represent smooth graphic interpolations of the finite difference values of β.

It can be seen in figure 5 that the logarithm of α exhibits a reverse sigmoid isobaric dependence on temperature at pressures and temperatures below $\sim$ 2 kb and the critical temperature; that is, as temperature increases at constant pressure from 0° to 374°C at low pressures, log α first increases to a decreasing degree and then to an increasing degree. At the critical point, α approaches infinity. For pressures greater than the critical pressure, the isobars in figure 5 exhibit extrema that dampen and shift progressively to higher temperatures with increasing pressure to $\sim$ 6 kb, above which the extrema disappear. At pressures from $\sim$ 2 to 5 kb, log α increases to a decreasing degree as temperature increases isobarically from 0° to $\sim$ 700°C, but at higher pressures the isobars exhibit minima below 100°C. At temperatures below $\sim$ 50°C, α increases as pressure increases isothermally, but between $\sim$ 50°C and the critical temperature α decreases with increasing pressure at constant temperature (fig. 6). The difference in the dependence of α on pressure above and below $\sim$ 50°C can be attributed to the effect of temperature on the structural order of liquid H_2O. At temperatures above the critical temperature, the isotherms in figure 6 exhibit extrema below $\sim$ 2 kb, which dampen and shift to higher pressures with increasing temperature.

In contrast to the behavior of α, β decreases monotonically as pressure increases isothermally at all temperatures (fig. 8), changing from $> 4 \times 10^{-5}$ bar^{-1} at 1 bar to $< 1 \times 10^{-6}$ bar^{-1} between 200 and 300 kb. Where the extrema in the isobaric temperature dependence of β dampen with increasing pressure and disappear above a kilobar (fig. 7), the extrema in the α isobars persist to much higher pressures (fig. 5). Nevertheless, the magnitude of the change in α and β is of the same order of magnitude for a temperature increase from 0° to 900°C at high pressures (figs. 5 and 7).

Partial derivatives of α and β calculated for pressures $\leq$ a kilobar from equations (23), (24), and (27) together with those for higher pressures computed from alternate statements of equations (35) through (37) and (41) through (43) for the various regions in figure 9 are given in tables 11 through 13 and plotted as curves in figures 10 through 15, where they can be compared with their finite difference counterparts (designated by the symbols). The values of V, α, and β required for the calculations were computed in the manner described above.

It can be seen in figures 10 through 13 that the calculated dependence of $(\partial\beta/\partial P)_T$ and $(\partial\alpha/\partial T)_P$ on temperature and pressure is in reasonably close agreement with that defined by the finite difference derivatives (figs. 10 through 13), which are uncertain to a comparable extent. The computed values of $(\partial\beta/\partial P)_T$ and $(\partial\alpha/\partial T)_P$ differ from their finite difference counterparts by less than ~ 10 to 20 percent, which corresponds to the maximum inter-regional discrepancy in the calculated values of $(\partial\beta/\partial P)_T$ at the boundary separating regions A and B in figure 9 above 4 kb (indicated by the zigzag segments of the 4.5 and 5.5 isobars in the inset diagram of fig. 10). For the most part, uncertainties in the values of $(\partial\beta/\partial P)_T$ and $(\partial\alpha/\partial T)_P$ computed for region A of figure 9 are of the order of 5 to 10 percent or less, which also corresponds to the uncertainty in the cross derivatives in all of the regions (figs. 14 and 15).

The configuration of the 850°C isotherm in the inset diagram of figure 13 is apparently the result of an overfit of α as a function of pres-

TABLE 11

Partial derivative of the coefficient of isothermal compressibility with respect to pressure at constant temperature in $bar^{-2} \times 10^9$ computed from equations (23), (35), and (41) and the values of V and β in tables 3 and 8—see figures 10 and 11

t	PRESSURE, KB									
(°C)	SAT	0.5	1	2	3	4	5	6	7	8
25	-15.66	-8.32	-5.48	-5.2	-4.5	-3.4	-2.4	-1.8	-1.3	-1.0
50	-15.17	-7.61	-4.33	-5.5	-4.4	-3.3	-2.4	-1.7	-1.3	-1.0
75	-16.66	-8.73	-5.38	-5.8	-4.4	-3.3	-2.4	-1.7	-1.3	-1.0
100	-20.20	-10.95	-7.23	-6.3	-4.6	-3.3	-2.4	-1.8	-1.4	-1.1
125	-26.18	-14.19	-9.58	-7.0	-4.8	-3.5	-2.5	-1.9	-1.4	-1.1
150	-35.71	-18.72	-12.49	-7.9	-5.3	-3.7	-2.7	-2.0	-1.5	-1.2
175	-51.18	-25.14	-16.17	-9.2	-5.9	-4.0	-2.8	-2.1	-1.6	-1.3
200	-77.56	-34.48	-20.99	-11.0	-6.6	-4.4	-3.1	-2.2	-1.7	-1.3
225	-126.08	-48.67	-27.52	-13.2	-7.6	-4.8	-3.4	-2.4	-1.8	-1.4
250	-225.07	-71.26	-36.64	-16.1	-8.8	-5.4	-3.7	-2.6	-2.0	-1.5
275	-458.96	-109.23	-49.69	-19.8	-10.2	-6.1	-4.0	-2.9	-2.1	-1.7
300	-1149.55	-177.26	-68.70	-24.3	-11.9	-6.8	-4.5	-3.1	-2.3	-1.8
325	-4157.99	-309.25	-96.73	-30.0	-14.0	-7.7	-4.9	-3.4	-2.5	-1.9
350	-36533.97	-593.80	-138.31	-37.1	-16.3	-8.7	-5.5	-3.7	-2.7	-2.1
375		-1301.64	-200.02	-46.0	-19.1	-9.9	-6.0	-4.1	-3.0	-2.2
400		-3408.99	-291.82	-57.0	-22.2	-11.1	-6.7	-4.5	-3.2	-2.4
425		-10301.90	-428.91	-70.7	-25.8	-12.5	-7.4	-4.9	-3.5	-2.6
450		-21635.72	-632.16	-87.5	-29.9	-14.0	-8.1	-5.3	-3.7	-2.8
475		-17449.07	-919.65	(-107.8)	(-34.6)	(-15.7)	(-8.9)	(-5.7)	(-4.0)	(-2.9)
500		-9634.83	-1281.11	(-131.9)	(-39.8)	(-17.5)	(-9.7)	(-6.2)	(-4.3)	(-3.1)
525		-6409.38	-1642.09							
550		-5247.95	-1868.38							
575		-4771.15	-1964.67							
600		-4540.93	-1913.62							
625		-4412.99	-1806.70							
650		-4333.65	-1690.38							
675		-4280.30	-1584.32							
700		-4242.27	-1494.07							
725		-4214.01	-1419.51							
750		-4192.36	-1358.69							
775		-4175.38	-1309.26							
800		-4161.80	-1269.07							
825		-4150.78	-1236.26							
850		-4141.68	-1209.35							
875		-4134.06	-1187.13							
900		-4127.57	-1168.66							

sure at temperatures ≧ 650°C, where the uncertainty in $(\partial\alpha/\partial T)_P$ is large. For this reason, values of $(\partial\alpha/\partial T)_P$ are not given in table 13 for temperatures > 500°C at pressures > a kilobar. The appearance of the isobars for 2, 5, and 10 kb in figure 12 also suggests overfit, but the similar configurations of the isobars for 1 and 2 kb imply that all the undulations in $(\partial\alpha/\partial T)_P$ as an isobaric function of temperature cannot be ascribed to

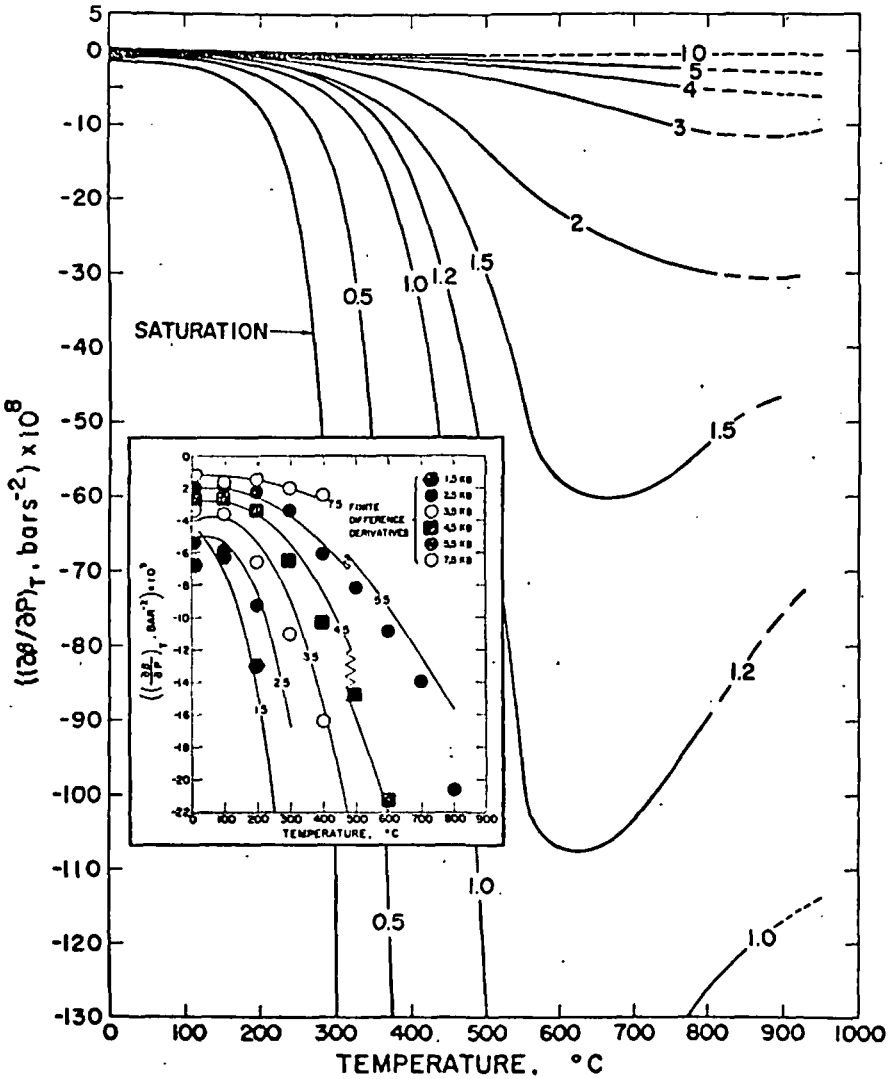

Fig. 10. Partial derivative of the coefficient of isothermal compressibility with respect to pressure at constant temperature (table 11) as a function of temperature at constant pressure (labeled in kb) computed from equations (19) through (23), (32), (35), (38), and (41) and coefficients in tables 4, 5, 6, 9, and 10 (curves). The symbols in the inset diagram represent finite difference derivatives calculated from the finite difference values of β plotted in figures 7 and 8.

regression vagaries. In contrast to the higher pressure isobars, the 1 kb curve was calculated from equation (27). Although no evidence of overfit is apparent in the computed curves of $(\partial\beta/\partial T)_P$ in figures 14 and 15, values of $(\partial\beta/\partial T)_P$ for temperatures $> 500°C$ at pressures > 1 kb have been omitted from table 12 because of the failure of equation (38) to represent adequately the finite difference values of β at high pressures and temperatures (see above). This observation, coupled with the interregional discrepancies in $(\partial\beta/\partial P)_T$ in figure 10, also required omission of values of $(\partial\beta/\partial P)_T$ from table 11 for temperatures $> 500°C$ at pressures $>$ a kilobar.

It can be seen in figure 11 that $(\partial\beta/\partial P)_T$ increases dramatically with increasing pressure at constant temperature. As pressure approaches 10 kb, $(\partial\beta/\partial P)_T \rightarrow (\partial^2\beta/\partial P^2)_T \rightarrow 0$ at all temperatures. Similarly, $(\partial\beta/\partial P)_T$ becomes a small negative number and $(\partial(\partial\beta/\partial P)_T/\partial T)_P \rightarrow 0$ as temperature decreases isobarically below $\sim 200°C$ at all pressures (fig. 10). The critical phenomenon causes $(\partial\beta/\partial P)_T$ to minimize with increasing tem-

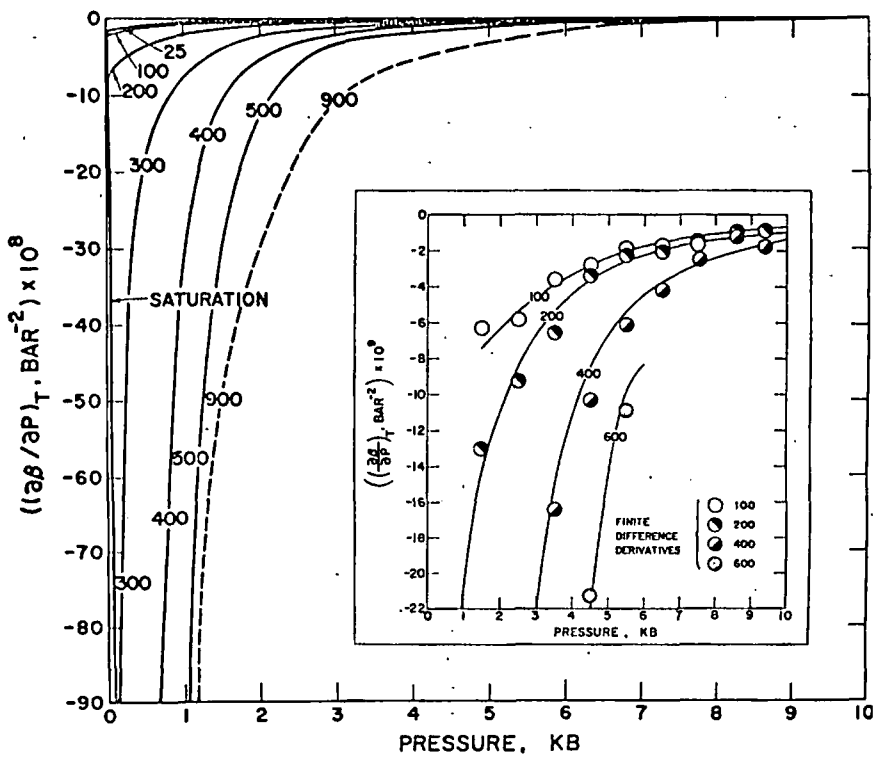

Fig. 11. Partial derivative of the coefficient of isothermal compressibility with respect to pressure at constant temperature (table 11) as a function of pressure at constant temperature (labeled in °C) computed from equations (19) through (23), (32), (35), and (41) and coefficients in tables 4, 5, 6, 9, and 10 (curves). The symbols in the inset diagram represent finite difference derivatives calculated from the finite difference values of β plotted in figures 7 and 8.

perature at constant pressure ≤ 3 kb, and the temperature corresponding to the minimum in the isobars increases with increasing pressure (fig. 10). Note in figures 14 and 15 that $(\partial\beta/\partial T)_P$ is small and negative at all pressures below $\sim 30°$ to 50°C but increases rapidly and maximizes with increasing temperature at constant pressure. At pressures $\leq$ a kilobar, further increase in temperature at constant pressure causes $(\partial\beta/\partial T)_P$ again to pass through zero and minimize at high temperatures. At higher pressures the high-temperature minimum disappears, as does the low-pressure extremum in the isothermal pressure dependence of $(\partial\beta/\partial T)_P$ as temperature decreases (fig. 16). In contrast, it can be seen in figure 12 that the isobaric maxima in $(\partial\alpha/\partial T)_P$ as a function of temperature at pressure ≤ 2 kb are complemented by minima at higher temperatures, all of which dampen and disappear at higher pressures where $(\partial^2\alpha/\partial T^2)_P$ becomes small. As pressure increases isothermally, $(\partial\alpha/\partial T)_P \rightarrow (\partial(\partial\alpha/$

TABLE 12

Partial derivative of the coefficient of isothermal compressibility with respect to temperature at constant pressure in bar^{-1} (°K)$^{-1}$ × 10^8 computed from equations (24), (36), and (42) and the values of V, α, and β in tables 3, 7, and 8—see figures 14 and 15

t	PRESSURE, KB									
(°C)	SAT	0.5	1	2	3	4	5	6	7	8
25	-12.38	-9.11	-3.75	-2.1	-2.2	-1.4	-0.8	-0.4	-0.2	-0.2
50	1.33	0.46	-0.29	0.2	-0.3	-0.1	0.1	0.2	0.3	0.2
75	10.53	6.48	3.26	2.2	1.4	1.1	1.0	0.8	0.7	0.6
100	18.44	11.49	6.77	4.2	2.8	2.1	1.7	1.4	1.2	1.0
125	27.00	16.47	10.22	6.2	4.1	3.0	2.4	1.9	1.5	1.3
150	37.95	22.18	13.91	8.3	5.3	3.9	3.0	2.4	1.9	1.6
175	53.72	29.45	18.21	10.6	6.6	4.7	3.6	2.8	2.3	1.9
200	78.49	39.39	23.55	13.2	7.9	5.5	4.1	3.2	2.6	2.1
225	120.67	53.64	30.48	16.0	9.3	6.3	4.6	3.6	2.9	2.4
250	199.64	74.87	39.68	19.1	10.7	7.0	5.1	4.0	3.2	2.6
275	368.11	107.72	52.08	22.6	12.1	7.8	5.6	4.3	3.5	2.9
300	808.94	160.75	68.82	26.3	13.7	8.6	6.1	4.7	3.8	3.1
325	2474.81	251.22	91.23	30.4	15.2	9.3	6.6	5.0	4.0	3.4
350	17421.98	419.05	120.56	34.9	16.9	10.1	7.1	5.4	4.3	3.6
375		772.55	157.77	40.0	18.5	10.9	7.6	5.8	4.6	3.9
400		1639.66	203.81	45.6	20.3	11.8	8.1	6.1	4.9	4.2
425		3741.13	260.33	52.0	22.2	12.6	8.6	6.5	5.2	4.4
450		4831.26	329.07	59.3	24.1	13.4	9.1	6.8	5.5	4.7
475		1076.18	406.24	(67.2)	(26.0)	(14.2)	(9.5)	(7.2)	(5.8)	(5.0)
500		-770.92	472.33	(75.8)	(27.9)	(14.9)	(9.9)	(7.5)	(6.1)	(5.2)
525		-900.62	491.07							
550		-723.48	438.04							
575		-554.18	333.40							
600		-427.69	221.75							
625		-336.07	131.55							
650		-268.95	68.35							
675		-218.72	27.26							
700		-180.33	1.73							
725		-150.40	-13.52							
750		-126.68	-22.16							
775		-107.60	-26.60							
800		-92.08	-28.43							
825		-79.33	-28.64							
850		-68.76	-27.87							
875		-59.95	-26.55							
900		-52.56	-24.93							

$\partial T)_P/\partial P)_T \rightarrow 0$ at all temperatures (fig. 13). Below ~ 500°C, $(\partial\alpha/\partial T)_P$ is positive, except at high pressures and low temperatures.

The effect of the critical phenomenon and low-temperature structural contributions to the expansibility and compressibility of H_2O are also apparent in figures 16 and 17, where isopleths of α and β are plotted as functions of pressure and temperature. It can be seen that $(\partial P/\partial T)_\alpha$ is negative at low temperatures for $\alpha < 4.3 \times 10^{-4}$ (°K)$^{-1}$, but at higher temperatures the isopleths curve around the "infinite peak" of the critical point in an elliptical pattern which widens progressively with increasing

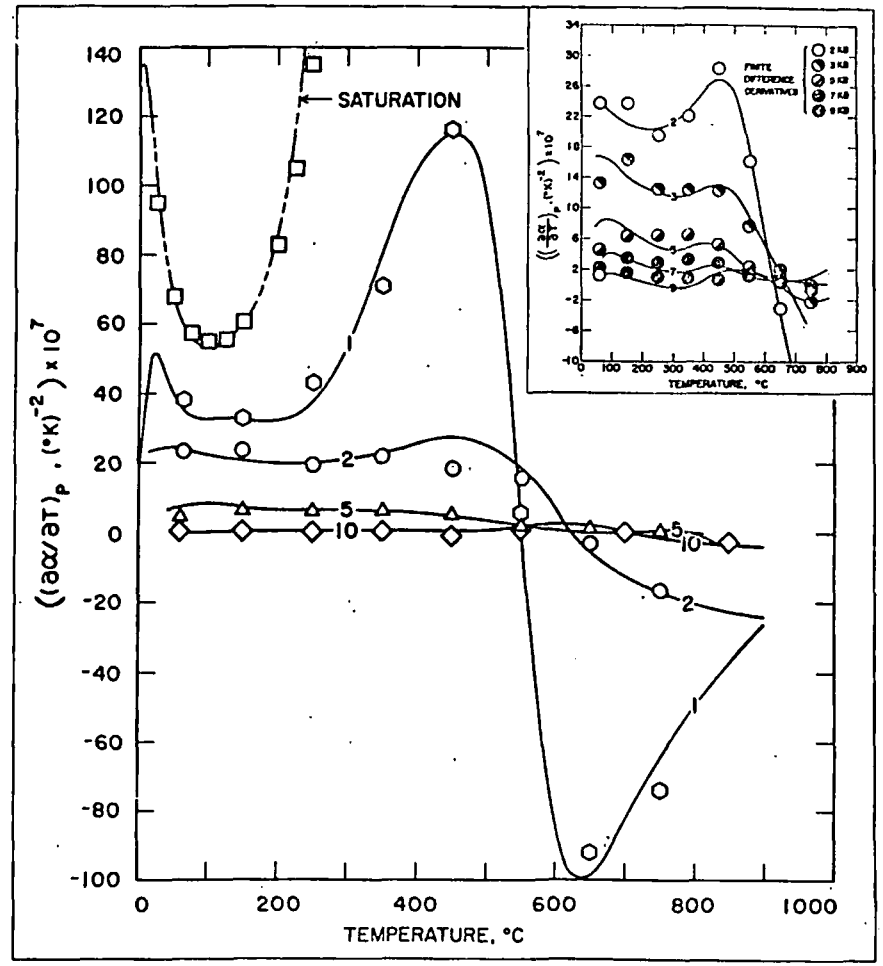

Fig. 12. Partial derivative of the coefficient of isobaric thermal expansion with respect to temperature at constant pressure (table 13) as a function of temperature at constant pressure (labeled in kb) computed from equations (19) through (21), (25), (27), (33), (37), (39), and (43) and coefficients in tables 4, 5, 6, 9, and 10 (curves). The symbols in the inset diagram represent finite difference derivatives calculated from the finite difference values of α plotted in figures 5 and 6.

pressure and temperature. At the critical point, $\alpha = \beta = (\partial\alpha/\partial T)_P = (\partial\beta/\partial P)_T = (\partial\beta/\partial T)_P = -(\partial\alpha/\partial P)_T = \infty$. However, as the thermodynamic behavior of H_2O approaches ideality with decreasing pressure, and $\alpha \rightarrow 1/T$, $\beta \rightarrow 1/P$. Hence, as $P \rightarrow 0$, $\beta \rightarrow (\partial\beta/\partial P)_T \rightarrow \infty$. As a consequence, the isopleths for $\beta \leq 10^{-3}$ bar^{-1} in figure 17 do not close around the infinite critical peak as the isopleths for α do in figure 16. Instead, the isopleths at high temperatures and low pressures in figure 17 coincide with isobaric contours along an infinite "cliff" at low pressures and high temperatures. The infinite critical peak is perched on the slope of the

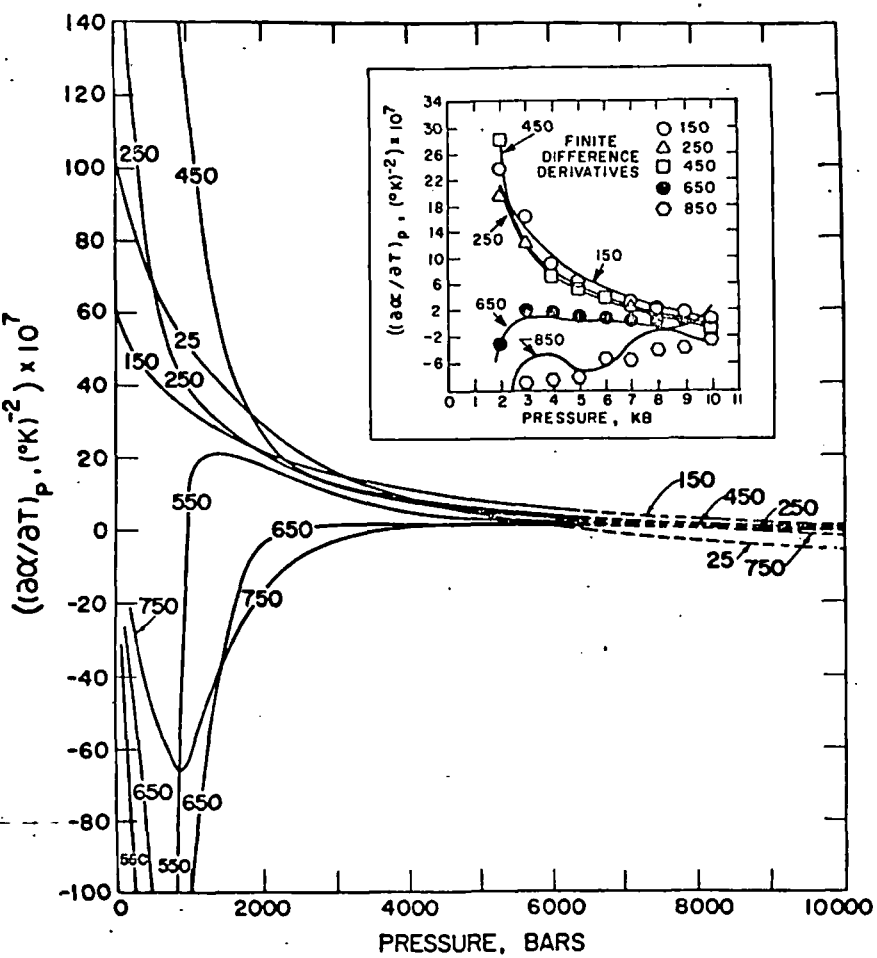

Fig. 13. Partial derivative of the coefficient of isobaric thermal expansion with respect to temperature at constant pressure (table 13) as a function of pressure at constant temperature (labeled in °C) computed from equations (19) through (21), (25), (27), (33), (37), (39), and (43) and coefficients in tables 4, 5, 6, 9, and 10 (curves). The symbols in the inset diagram represent finite difference derivatives calculated from the finite difference values of α plotted in figures 5 and 6.

cliff and separated from its summit by a minimum corresponding to $\beta > 10^{-3}$ bar^{-1}. As a consequence it fails to show up in figure 17.

The minimum in the isobaric temperature dependence of β at low temperatures (fig. 7) caused by structural ordering of the water dipoles results in corresponding minima in the isopleths for β below 100°C and ~ 2 kb in figure 17. No such minima occur in the case of α, but the latter variable becomes negative in the vicinity of the triple point, where β is positive and equal to its value at ~ 500°C and 5 kb. Increasing orientation of water dipoles with decreasing temperature thus has a dramatically different effect on α and β, and this difference persists to high pressures.

DIELECTRIC CONSTANT

Experimental values of the dielectric constant (ε) of H_2O are available at intervals ranging from a few degrees and bars along the satura-

TABLE 13

Partial derivative of the coefficient of isobaric thermal expansion with respect to temperature at constant pressure in $(°K)^{-2} \times 10^7$ computed from equations (27), (37), and (43) and the values of V and α in tables 3 and 7—see figures 12 and 13

t	PRESSURE, KB									
(°C)	SAT	0.5	1	2	3	4	5	6	7	8
25	101.96	69.82	51.56	24.1	15.4	8.7	3.9	0.6	-1.6	-3.4
50	68.17	50.48	39.88	24.2	16.8	11.2	7.0	4.0	1.9	0.2
75	55.57	42.42	33.64	23.4	16.7	12.0	8.3	5.6	3.6	2.0
100	53.29	40.93	32.79	22.4	16.1	11.8	8.6	6.1	4.2	2.8
125	55.46	41.54	33.05	21.6	15.3	11.2	8.2	5.9	4.2	2.8
150	60.54	42.65	32.73	20.9	14.4	10.4	7.6	5.5	3.8	2.5
175	69.80	44.66	32.08	20.5	13.5	9.6	6.9	4.8	3.3	2.1
200	86.69	48.93	32.11	20.3	12.8	8.7	6.1	4.2	2.7	1.6
225	117.28	57.15	33.81	20.3	12.1	8.0	5.4	3.6	2.2	1.1
250	173.68	71.19	37.93	20.5	11.7	7.5	4.9	3.2	1.8	0.8
275	285.40	93.38	44.90	20.8	11.4	7.1	4.6	2.9	1.6	0.6
300	547.08	126.95	54.83	21.3	11.4	7.0	4.5	2.8	1.6	0.5
325	1415.93	177.30	67.37	22.1	11.6	7.0	4.6	2.9	1.7	0.6
350	8078.16	256.26	81.34	23.0	11.9	7.3	4.8	3.2	1.9	0.8
375		396.13	94.69	24.1	12.2	7.5	5.1	3.4	2.1	1.1
400		680.35	105.24	25.2	12.5	7.7	5.3	3.7	2.4	1.3
425		1137.94	112.11	26.2	12.6	7.8	5.4	3.8	2.5	1.4
450		569.16	115.44	26.9	12.3	7.5	5.2	3.6	2.5	1.4
475		-775.34	112.92	(27.0)	(11.5)	(6.7)	(4.6)	(3.2)	(2.1)	(1.2)
500		-814.69	96.58	(26.0)	(9.9)	(5.5)	(3.6)	(2.4)	(1.5)	(0.7)
525		-547.52	57.91							
550		-360.14	1.93							
575		-247.84	-50.99							
600		-179.01	-84.80							
625		-134.70	-98.50							
650		-104.72	-98.82							
675		-83.55	-92.36							
700		-68.06	-83.26							
725		-56.38	-73.71							
750		-47.36	-64.69							
775		-40.24	-56.58							
800		-34.53	-49.46							
825		-29.88	-43.29							
850		-26.05	-37.97							
875		-22.87	-33.39							
900		-20.20	-29.45							

tion curve to intervals of 50°C and 250 bars above the critical point in the shaded pressure-temperature region of figure 18. Of the many low temperature data in the literature, the values of the dielectric constant given by Owen and others (1961) from 0° to 70°C and 0.001 to 1 kb appear to be most consistent with those measured by Oshry (ms) along the saturation curve and Heger (ms) at high pressures and temperatures. For this reason, the data of Owen and others (1961) were "accepted" in this study in preference to those of Malmberg and Maryott (1956) and others. The experimental data given by Oshry in his dissertation were used instead of the smooth values generated by Åkerlof and Oshry (1950) from Oshry's data because the latter paper contains several errors and inconsistencies.

Numerous attempts were made during the course of the present study to fit the data taken from Oshry (ms), Owen and others (1961), and Heger (ms) at close pressure-temperature intervals in the shaded region of figure 18 with the Kirkwood equation (Kirkwood, 1939; Oster and Kirkwood, 1943), which Kirkwood derived from an extension of Onsager's theory of dielectric polarization to compute dielectric constants of polar liquids. The Kirkwood equation can be written as

$$\varepsilon = \frac{1 + 9\Gamma + 2(2 + (1 + 9\Gamma)^2)^{1/2}}{4} \tag{44}$$

where

$$\Gamma = \frac{4\pi N° \rho}{3M_w}\left(\omega + \frac{10^{-36}\mu^2 g}{3kT}\right) \tag{45}$$

in which $\pi = 3.14159265$, N° stands for Avogadro's number (6.02252×10^{23} mole^{-1}), ρ again refers to the density of H_2O in g cm^{-3}, M_w designates the molecular weight of H_2O (18.0153 g mole^{-1}), k is Boltzman's constant (1.38054×10^{-16} erg (°K)$^{-1}$), ω represents the polarizability (1.58×10^{-24} cm^3 mole^{-1}) and μ the dipole moment of the H_2O molecule, T stands for temperature in °K, and g is the Kirkwood correlation factor (which provides for molecular orientation).

Franck's (1956) early estimates of the dielectric constant at high pressures and temperatures are based on graphic fits of the Kirkwood equation to data given by Wyman (1930), Wyman and Engalls (1938), Åkerlof and Oshry (1950), and Fogo, Benson, and Copeland (1954). Franck's graphic fits have since been superseded by regression calculations with the Kirkwood equation (Quist and Marshall, 1965).

Because the dependence of $\mu^2 g$ on temperature and pressure (or density) cannot be determined independently, $\mu^2 g$ must be represented by an empirical function of these variables to obtain fits of dielectric constant data with equation (39). In fitting equation (44) to the values of the dielectric constant given by Fogo, Benson, and Copeland (1954), Wyman and Ingalls (1938), Owen and others (1961), Lees (ms), Akerlof

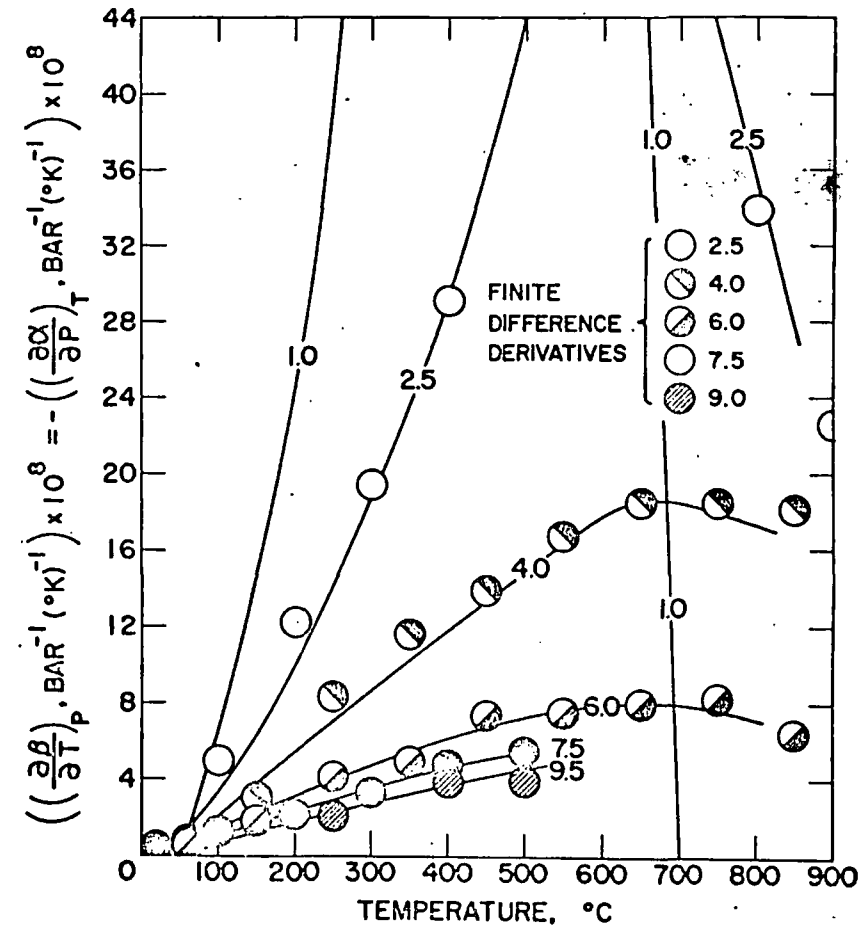

Fig. 14. Partial derivative of the coefficient of isothermal compressibility with respect to temperature at constant pressure (table 12) as a function of temperature at constant pressure (labeled in kb) computed from equations (19) through (22), (24), (25), (32), (33), (36), (38), (39), and (42) and coefficients in tables 4, 9, and 10 (curves). The symbols represent finite difference derivatives calculated from the finite difference values of α and β plotted in figures 5 through 8.

and Oshry (1950), and Gier and Young (1963)[2], Quist and Marshall (1965) represented $\mu^2 g$ with a power function of density and temperature of the form

$$\mu^2 g = 3.50 + \rho(\hat{A}_1 + \hat{A}_2\,\rho + \hat{A}_3\,\rho^2)\,f(T) \qquad (46)$$

where $\hat{A}_1$, $\hat{A}_2$, and $\hat{A}_3$ represent fit coefficents, and $f(T)$ stands for a density-independent power function of temperature. In trial and error re-

[2]All these data, which apply to pressures ranging up to ~ 12 kb at 50°C and below, 2 kb from 50° to 350°C, and a few hundred bars from 350° to 393°C, are not consistent with one another. Many of them have since been superseded by Heger's (ms) study, which is internally consistent.

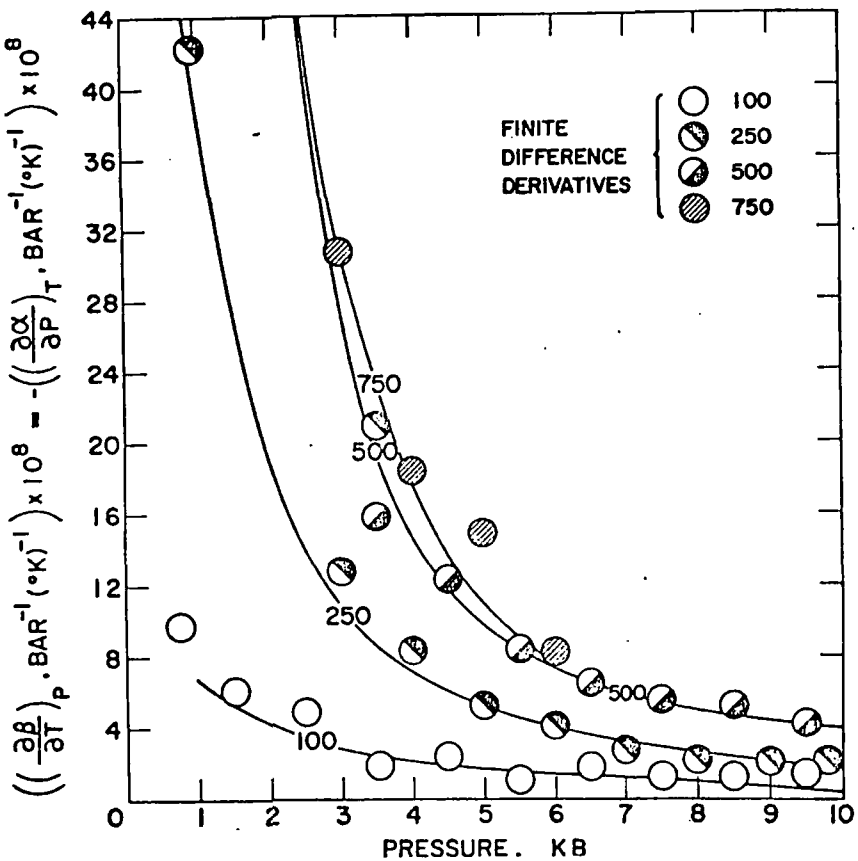

Fig. 15. Partial derivative of the coefficient of isothermal compressibility with respect to temperature at constant pressure (table 12) as a function of pressure at constant temperature (labeled in °C) computed from equations (19) through (22), (24), (25), (32), (33), (36), (38), (39), and (42) and coefficients in tables 4, 9, and 10 (curves). The symbols represent finite difference derivatives calculated from the finite difference values of α and β plotted in figures 5 through 8.

gression, Quist and Marshall permitted $f(T)$ to take any of three alternate forms ($f(T) = T^{-0.5}$, $f(T) = T^{-\hat{A}_4}$, or $f(T) = e^{-\hat{A}_4 T}$), each of which rendered equivalent fits of the data.

Regression of Heger's (ms) data in the present study with equations (44) through (46) using the alternate forms of $f(T)$ suggested by Quist and Marshall resulted in acceptable fits of the data at high temperatures and pressures, which is not surprising because Quist and Marshall's computed values of ϵ are in reasonable agreement with Heger's experimental data. However, as might be expected from Quist and Marshall's experience and the fact that alternate regression of Heger's data in the present study using different expressions for $f(T)$ failed to identify any one of the functions as better than another, composite fits of equations (44)

through (46) to all of the data reported by Owen and others (1961), Oshry (ms), and Heger (ms) resulted in relatively poor fits with nonrandom trends of residuals. The magnitude and distribution of the residuals introduced unacceptable uncertainties in the partial derivatives of the dielectric constant computed from the partial derivatives of equation (44). Repeated attempts to obtain close fits of both the high- and low-temperature data with the Kirkwood equation by representing $\mu^2 g$ with higher order power functions of density, with and without cross terms in density and temperature as well as modified alternate $f(T)$ functions, led to little improvement in the fits and eventually to the conclusion that (despite its theoretical origins) the Kirkwood equation is not suitable for comprehensive and accurate representation of the dielectric constant and its partial derivatives over the range of pressures and temperatures considered in this study.

In contrast to the Kirkwood equation, a simple fourth degree power function of temperature and density rendered close fits of all the experimental data as well as a random distribution of residuals over the entire shaded region of figure 18. This expression can be written as

$$\varepsilon = \sum_{i=0}^{4} \sum_{j=0}^{4-i} e_{ij} T^i \rho^j \qquad (47)$$

where e_{ij} stands for the array of fit coefficients given in table 14. Values of the dielectric constant computed from equation (47) and the values of V calculated above are given in table 15 and plotted as solid curves representing ε or ln ε in figures 19, 20, and 22 through 24, where they can be compared with the experimental values represented by the symbols.

Equation (47) fits the experimental data obtained by Oshry (ms), Owen and others (1961), and Heger (ms) to within 1 percent over most of the shaded region shown in figure 18. Only at the high temperature end of the saturation curve where Oshry's data exhibit excessive scatter (fig. 19) is the uncertainty greater, approaching 5 percent near the critical point where the dielectric constant is small. The maximum experimental uncertainty in the data ranges from < 0.1 percent for those of Owen and others to < 1 percent for the values of $\varepsilon > 10$ and < 3 percent for the values of $\varepsilon < 10$ given by Heger (ms). The maximum experimental uncertainty in Oshry's data for temperatures < 350°C is of the order of 1 to 2 percent.

It is apparent in figures 19, 20, and 22 through 24 that equation (47) not only affords accurate representation of the experimental data, but it also permits reasonable extrapolations of ε from 100° to 0°C at pressures

TABLE 14

Coefficients for equation (47)

$$\underline{e}_{ij} = \underline{\hat{e}}_{ij} \times 10^{\underline{e^*}_{ij}}$$

$\underline{\hat{e}}_{ij}$

j \ i	0	1	2	3	4
0	4.39109592	-2.33277456	4.61662109	-4.03643333	1.31604037
1	-2.18995148	1.00498361	-1.35650709	5.94046919	
2	1.82898246	-2.08896146	1.60491325		
3	1.54886800	-6.13941874			
4	-6.13542375				

$\underline{e^*}_{ij}$

j \ i	0	1	2	3	4
0	2	0	-3	-6	-9
1	2	0	-3	-7	
2	1	-1	-4		
3	2	-2			
4	1				

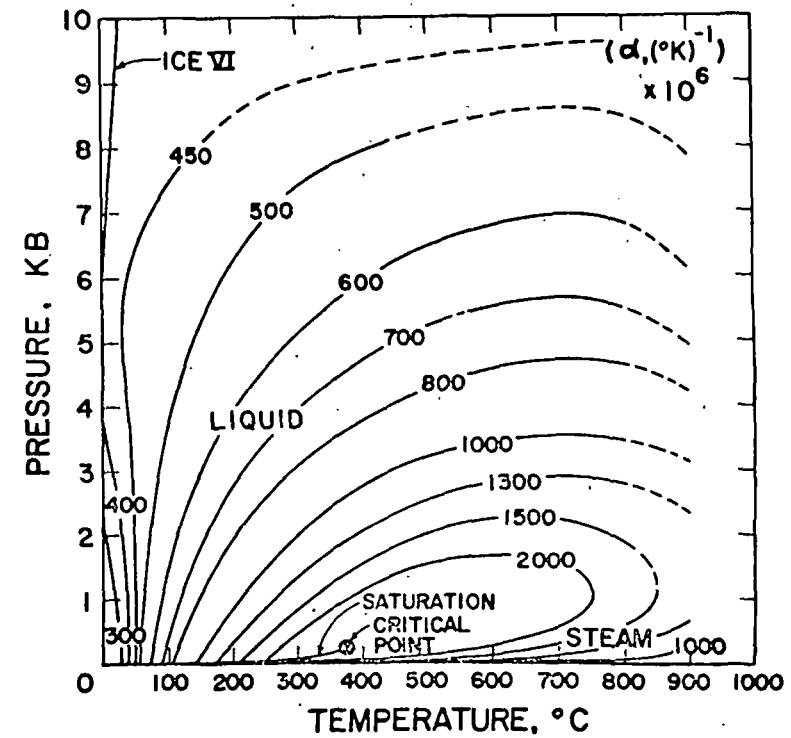

Fig. 16. Isopleths of α (labeled in $(°K)^{-1}$) as a function of pressure and temperature (table 7 and figs. 5 and 6).

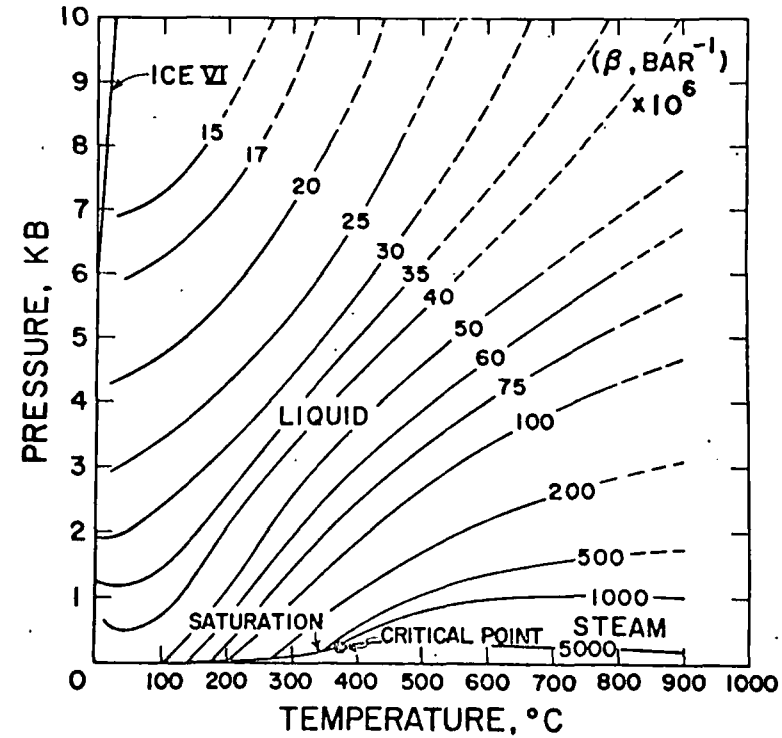

Fig. 17. Isopleths of β (labeled in bar^{-1}) as functions of pressure and temperature (table 8 and figs. 7 and 8).

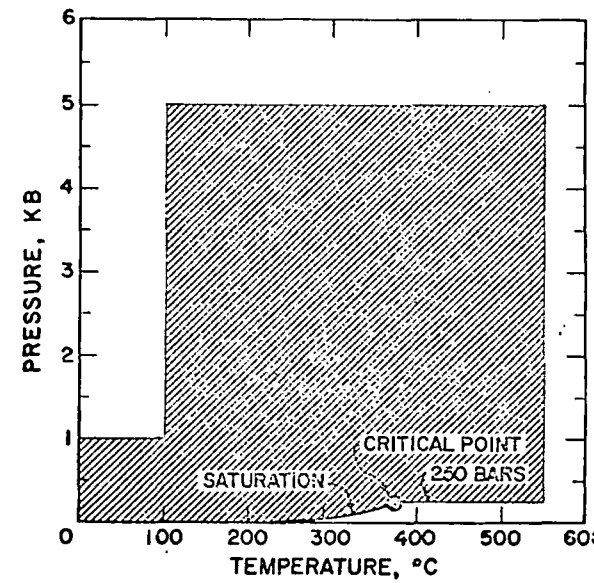

Fig. 18. Pressure-temperature region represented by dielectric constant data (Oshry, ms; Owen and others, 1961; Heger, ms) regressed with equation (44) to define the fit

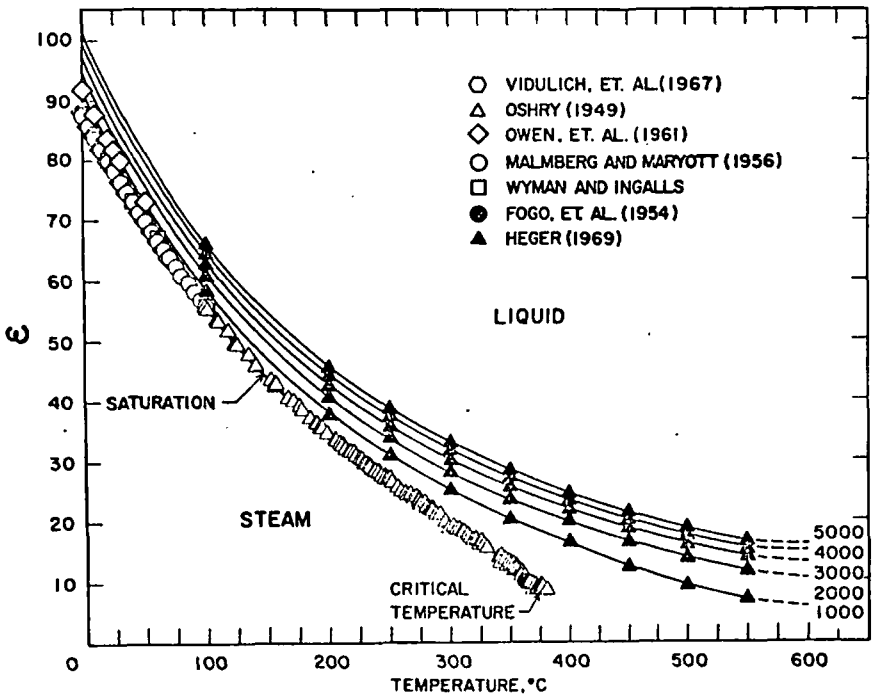

Fig. 19. Dielectric constant (table 15) as a function of temperature at constant pressure (labeled in bars) computed from equations (19) through (21) and (47) and coefficients in tables 4, 5, 6, and 14 (curves). The symbols represent values taken from the literature.

from 1 to 5 kb, and from 550°C to 600°C at pressures from 250 bars to 5 kb. However, such is not the case above 600°C, which precludes use of equation (47) and the fit coefficients in table 14 to compute extrapolated dielectric constants at higher temperatures.

It can be seen in figure 19 that the dielectric constant of H_2O decreases rapidly from values ranging from 88 to 100 at 0°C to < 20 at 600°C as temperature increases at constant pressure. In contrast, as pressure increases to 5 kb at constant temperature (fig. 20), the dielectric constant increases of the order of 10 to 15 units. Isopleths of the dielectric constant are shown in figure 21, where it can be deduced that $(\partial P/\partial T)_\epsilon$ changes from ~ 500 bar $(°K)^{-1}$ at 0°C to < 5 bar $(°K)^{-1}$ at high temperatures and low pressures.

The dashed curves in figures 19, 20, and 22 through 24 were drawn through interpolated values of the dielectric constant computed by Quist and Marshall (1965) at high temperatures and pressures; they do not represent extrapolations computed from equation (47) and the coefficients in table 14, which are inapplicable above 600°C. It can be seen that Quist and Marshall's values are reasonably consistent with Heger's data and the computed curves below 600°C. Nevertheless, owing to small discrepancies, composite regression of their values with those below 600°C

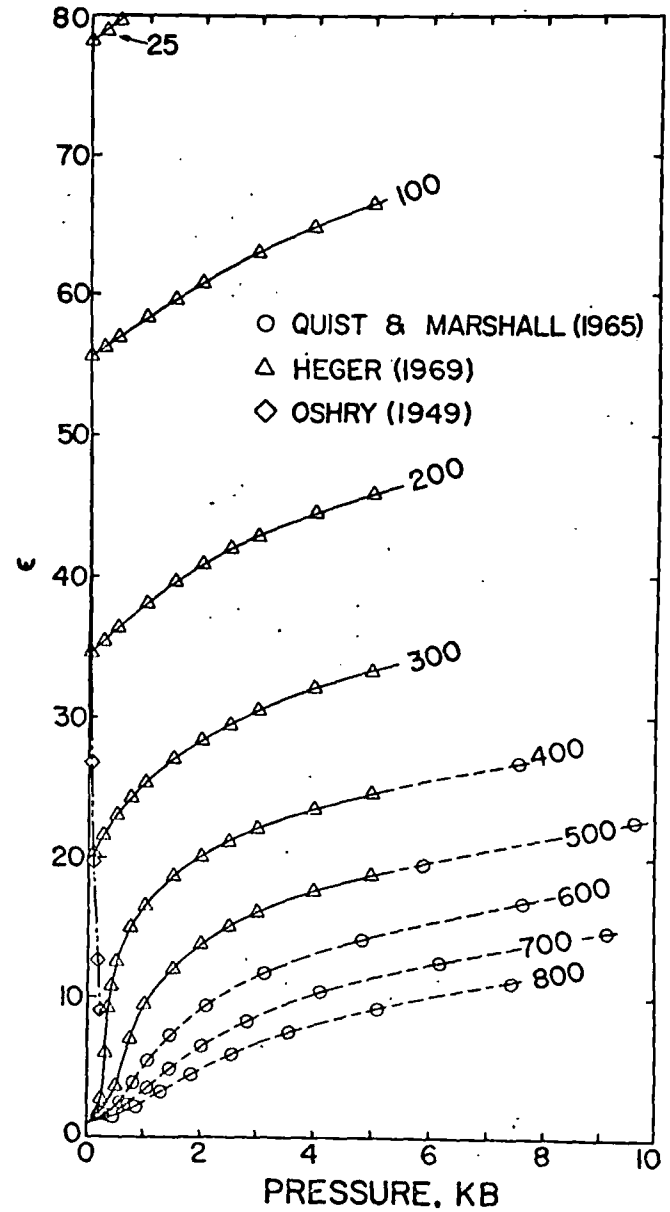

Fig. 20. Dielectric constant (table 15) as a function of pressure at constant temperature (labeled in °C) computed from equations (19) through (21) and (47) and coefficients in tables 4, 5, 6, and 14 (solid curves). The symbols correspond to values taken from the literature, and the dashed curves represent smooth graphic interpolation of Quist and Marshall's (1965) values for pressures > 5 kb and temperatures > 600°C.

yields an unacceptable fit of equation (47), and finite difference derivatives ($(\Delta\varepsilon/\Delta T)_P$ and $(\Delta\varepsilon/\Delta P)_T$) calculated from Quist and Marshall's values are not consistent with those computed from Heger's experimental data at lower temperatures. Partial derivatives obtained by differentiating the functions used by Quist and Marshall (eqs 44 through 46) are similarly inconsistent, but, in contrast, partial differentiation of equation (47) yields derivatives in close agreement with their finite difference counterparts below 550°C (see below).

The dependence of ln ε on temperature and pressure is depicted in figures 22 and 23. The solid curves in these figures were generated by equation (47), and the symbols represent experimental data (or computed values in the case of those taken from Quist and Marshall). It can be seen in figure 22 that the near linear dependence of ln ε on temperature at constant pressure below ~ 100°C (Gurney, 1953) becomes substantially nonlinear at higher temperatures. In contrast, ln ε as a function of pressure at constant temperature approaches linearity at high pressures and temperatures, but it is also nearly linear at low temperatures (fig. 23).

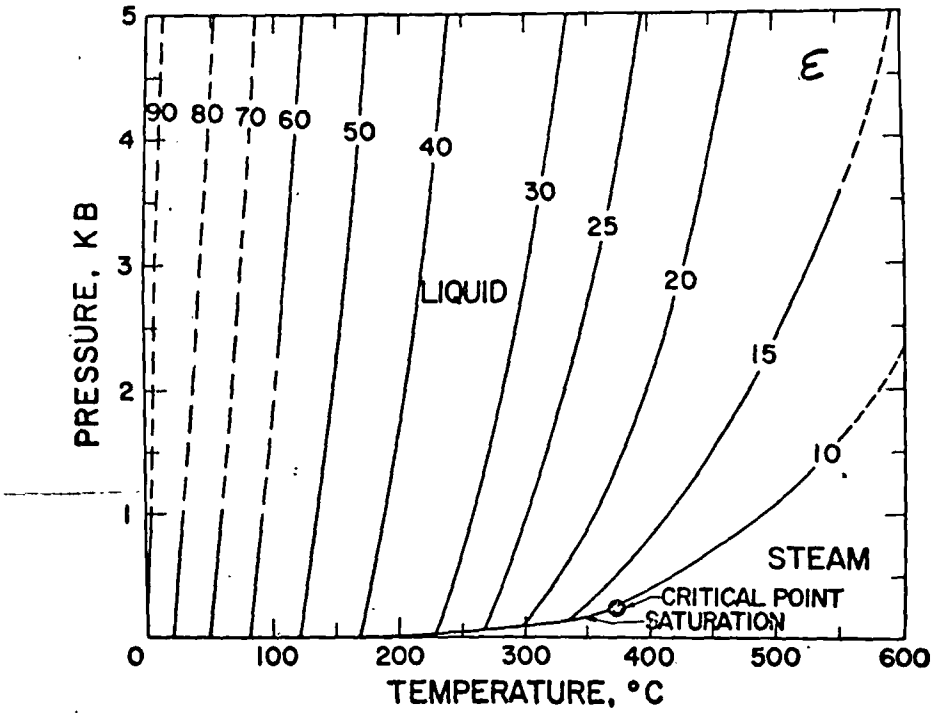

Fig. 21. Isopleths of ε (indicated by the labels on the curves) as a function of pressure and temperature (table 15 and figures 19 and 20).

Partial differentiation of equations (48) and (49) leads to

$$\left(\frac{\partial^2 \varepsilon}{\partial P^2}\right)_T = \varepsilon\left(\frac{\partial \ln \varepsilon}{\partial P}\right)_T \left(\frac{\partial \ln \beta}{\partial P}\right)_T + \beta^2 \sum_{i=0}^{4}\sum_{j=0}^{4-i} j^2 e_{ij} T^i \rho^j \quad (50)$$

and

$$\left(\frac{\partial^2 \varepsilon}{\partial T^2}\right)_P = \sum_{i=0}^{4}\sum_{j=0}^{4-i} e_{ij} \rho^j \left(j\alpha(j\alpha T^i - 2i\, T^{i-1}) + i(i-1)T^{i-2} - jT^i \left(\frac{\partial \alpha}{\partial T}\right)_P \right) \quad (51)$$

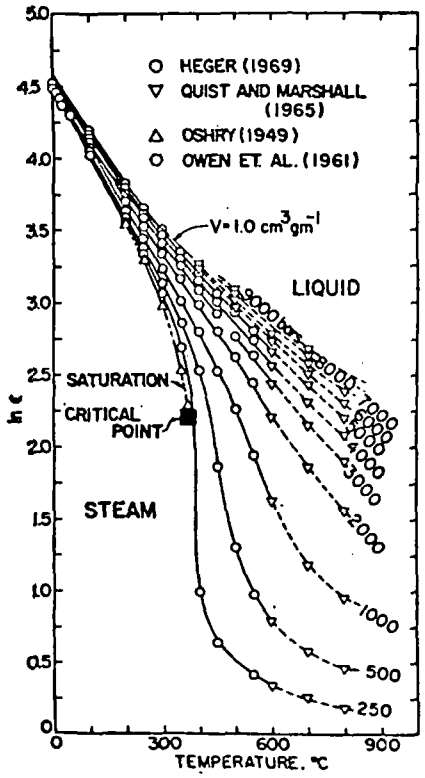

Fig. 22

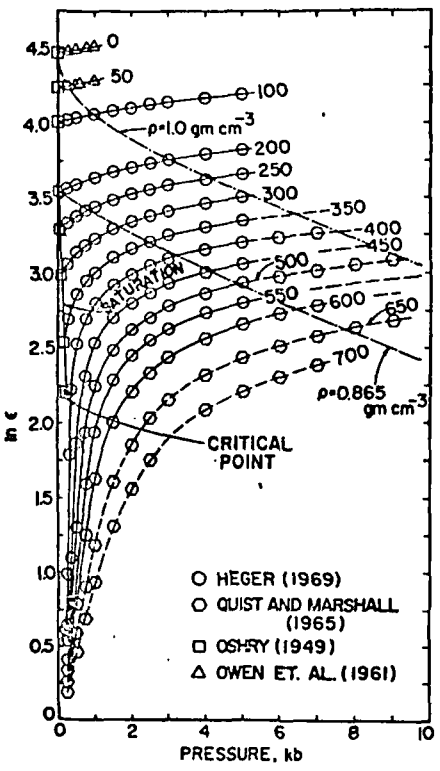

Fig. 23

Fig. 22. Logarithm of the dielectric constant (table 15) as a function of temperature at constant pressure (labeled in bars) computed from equations (19) through (21) and (47) and coefficients in tables 4, 5, 6, and 11 (solid curves). The symbols correspond to values taken from the literature and the dashed curves represent graphic interpolation of Quist and Marshall's (1965) values at pressures > 600 C.

Fig. 23. Logarithm of the dielectric constant (table 15) as a function of pressure at constant temperature (labeled in °C) computed from equations (19) through (21) and (47) and coefficients in tables 4, 5, 6, and 11 (solid curves). The symbols correspond to values taken from the literature, and the dashed curves represent graphic interpolation of Quist and Marshall's (1965) values at pressures > 5 kb and temperatures > 600 C.

The relation of the dielectric constant to specific volume is depicted in figure 24, where it can be seen that $(\partial \ln \varepsilon/\partial \ln V)_T$ is essentially independent of both density and temperature. Under these conditions $(\partial \ln \varepsilon/\partial P)_T$ is nearly proportional to the coefficient of isothermal compressibility.

The partial derivatives of equation (47) with respect to temperature and pressure can be written as

$$\left(\frac{\partial \dot{\varepsilon}}{\partial P}\right)_T = \varepsilon\left(\frac{\partial \ln \varepsilon}{\partial P}\right)_T = \beta \sum_{i=0}^{4}\sum_{j=0}^{4-i} j\, e_{ij} T^i \rho^j \quad (48)$$

$$\left(\frac{\partial \varepsilon}{\partial T}\right)_P = \varepsilon\left(\frac{\partial \ln \varepsilon}{\partial T}\right)_P = \sum_{i=0}^{4}\sum_{j=0}^{4-i} e_{ij} \rho^j (iT^{i-1} - j\alpha T^i) \quad (49)$$

where α and β again stand for the coefficients of isobaric thermal expansion and isothermal compressibility. Values of $(\partial \ln \varepsilon/\partial P)_T$ and $(\partial \ln \varepsilon/\partial T)_P$ computed from equations (48) and (4) using values of ε, β, and α given above are shown in tables 16 and 17 and plotted as curves in figures 25 through 28, where it can be seen that the predicted values are in close agreement with their finite difference counterparts ($(\Delta \ln \varepsilon/\Delta P)_T$ and $(\Delta \ln \varepsilon/\Delta T)_P$) calculated directly from the experimental data. Uncertainties in the values of $(\partial \ln \varepsilon/\partial T)_P$ and $(\partial \ln \varepsilon/\partial P)_T$ computed from equations (48) and (49) are of the order of a few percent or less, which corresponds to the uncertainties in the values of α and β employed in the calculations.

It can be seen in figure 26 that $(\partial \ln \varepsilon/\partial P)_T$ like β decreases dramatically and monotonically with increasing pressure at constant temperature $\geqq 200$°C, but unlike β, $(\partial \ln \varepsilon/\partial P)_T$ increases monotonically with increasing temperature at all (constant) pressures (fig. 25). At high pressures, $(\partial \ln \varepsilon/\partial P)_T \to (\partial^2 \ln \varepsilon/\partial P^2)_T \to 0$ as pressure increases at any given temperature (figs. 26 and 29). Similarly, as temperature decreases below ~ 100°C at all pressures, $(\partial \ln \varepsilon/\partial P)_T \to (\partial(\partial \ln \varepsilon/\partial P)_T/\partial T)_P \to 0$ (figs. 25 and 33).

The strong influence of the critical phenomenon on the temperature and pressure dependence of $(\partial \ln \varepsilon/\partial T)_P$ is apparent in figures 27 and 28. Note that the isobars for pressures $\leqq 2$ kb in the steam phase region pass through a minimum with increasing temperature, as do the isotherms for temperatures above the critical temperature. In the vicinity of the critical point, $(\partial \ln \varepsilon/\partial P)_T$ is large and positive and $(\partial \ln \varepsilon/\partial T)_P$ is large and negative. At the critical point, $(\partial \ln \varepsilon/\partial P)_T = -(\partial \ln \varepsilon/\partial T)_P = \infty$, but as the thermodynamic behavior of H_2O approaches ideality with decreasing pressure, $\varepsilon \to 1$.

which were used together with equations (47) through (49), values of V, α, β, $(\partial\alpha/\partial T)_P$, $(\partial\beta/\partial P)_T$, $(\partial \ln \varepsilon/\partial P)_T$, and $(\partial \ln \varepsilon/\partial T)_P$ given above, and the identities,

$$\left(\frac{\partial^2 \ln \varepsilon}{\partial P^2}\right)_T = \frac{1}{\varepsilon}\left(\frac{\partial^2 \varepsilon}{\partial P^2}\right)_T - \frac{1}{\varepsilon^2}\left(\frac{\partial \varepsilon}{\partial P}\right)_T^2 \qquad (52)$$

and

$$\left(\frac{\partial^2 \ln \varepsilon}{\partial T^2}\right)_P = \frac{1}{\varepsilon}\left(\frac{\partial^2 \varepsilon}{\partial T^2}\right)_P - \frac{1}{\varepsilon^2}\left(\frac{\partial \varepsilon}{\partial T}\right)_P^2 \qquad (53)$$

to compute the curves shown in figures 29 through 32 and the partial derivatives in tables 18 and 19. The close agreement of the values of $(\partial \ln \varepsilon/\partial P)_T$ and $(\partial \ln \varepsilon/\partial T)_P$ computed from equations (48) and (49) with their finite difference counterparts in figures 25 through 28 suggests that the partial derivatives computed from equations (50) through (53) are reasonably accurate representations of $(\partial^2 \ln \varepsilon/\partial P^2)_T$ and $(\partial^2 \ln \varepsilon/\partial T^2)_P$ within the fit region shown in figure 18. This conclusion is further substantiated below (fig. 33) by the agreement of computed values of $(\partial(\partial \ln \varepsilon/\partial P)_T/\partial T)_P$ with finite difference derivatives calculated directly from the curves in figures 25 and 28.

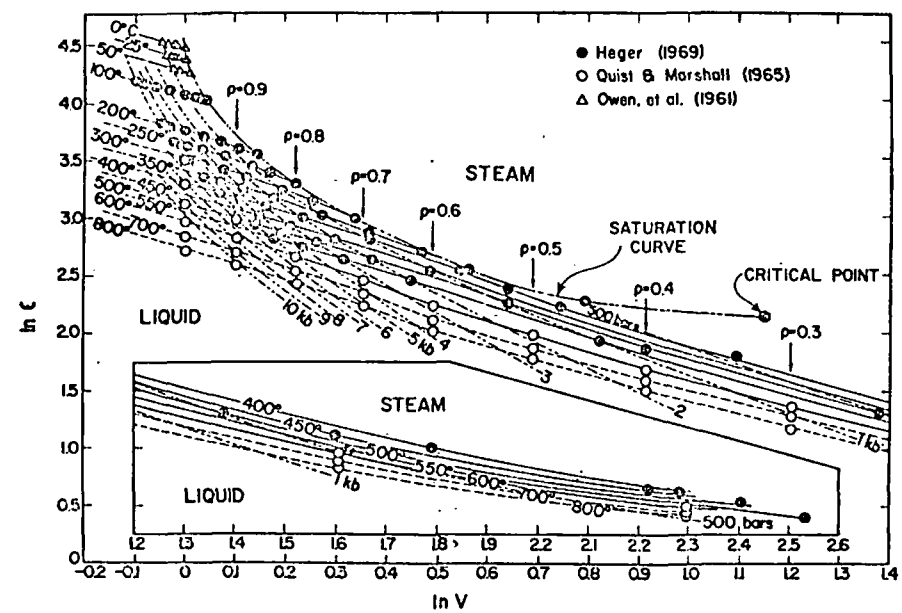

Fig. 24. Logarithm of the dielectric constant as a function of ln V at constant temperature (solid curves) and constant pressure (dashed curves) computed from equations (19) through (21) and (47) and coefficients in tables 4, 5, 6, and 14. The symbols correspond to values taken from the literature, and the dashed curves represent smooth graphic interpolation of Quist and Marshall's (1965) values at pressures > 5 kb and temperatures > 600°C.

It can be seen in figure 32 that a large discrepancy in $(\partial^2 \ln \varepsilon/\partial T^2)_T$ arises between 1 and 2 kb at 25°C, which is outside the fit region in figure 18. Similar discrepancies occur above ~ 500°C, which is near the upper limit of the fit region. Erroneous values of $(\partial^2 \ln \varepsilon/\partial T^2)_P$ and $(\partial^2 \ln \varepsilon/\partial P^2)_P$ may arise from errors in $(\partial\alpha/\partial T)_P$ and $(\partial\beta/\partial P)_T$, which is apparently the case at 25°C above a kilobar in figure 32. Although comparative calculations for pressures and temperatures within the fit region indicate that errors of the order of 5 to 20 percent in $(\partial\alpha/\partial T)_P$ and $(\partial\beta/\partial P)_T$ have a minor effect on $(\partial^2 \ln \varepsilon/\partial T^2)_P$ and $(\partial^2 \ln \varepsilon/\partial P^2)_T$, the second partial derivatives of ln ε are nevertheless highly uncertain near the boundaries of the fit region. For this reason, equations (52) and (53) as well as equations (56) and (57), which are derived below, should not be used for temperatures above ~ 500°C or pressures above ~ 500 bars at temperatures ≤ 100°C.

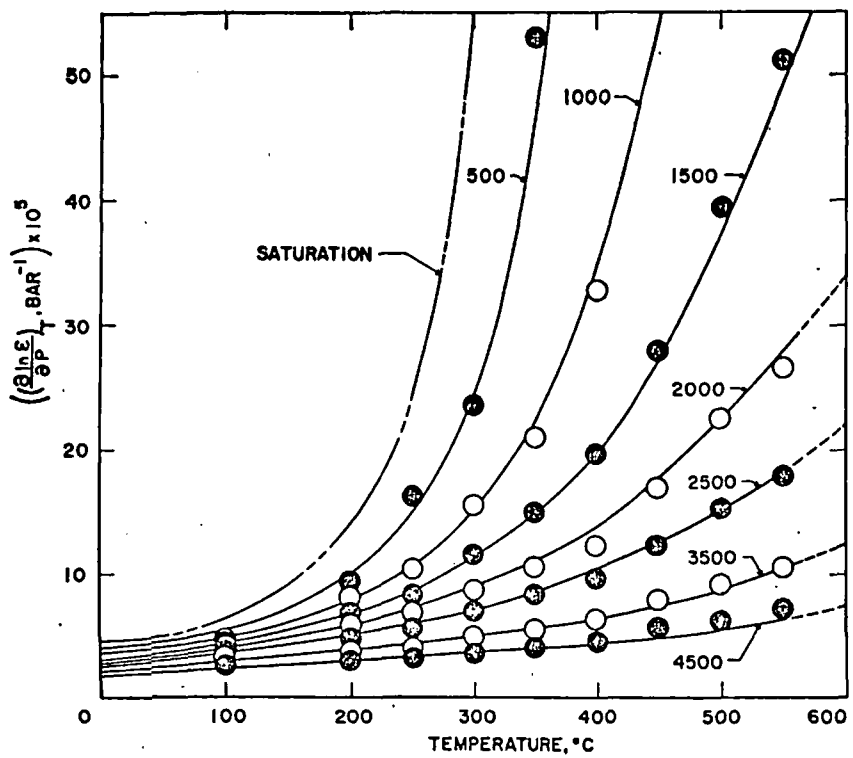

Fig. 25. Partial derivative of ln ε with respect to pressure at constant temperature (table 16) as a function of temperature at constant pressure (labeled in bars) computed from equations (19) through (22), (32), (38), (47), and (48) and coefficients in tables 4, 5, 6, 9, 10, and 14 (curves). The symbols represent corresponding finite difference derivatives computed from data given by Oshry (ms), Owen and others (1961), and/or Heger (ms).

TABLE 15

Dielectric constant (ε) computed from equation (47) and the values of V in table 3—see figures 19 through 21

t	PRESSURE, KB										
(°C)	SAT	0.5	1	1.5	2	2.5	3	3.5	4	4.5	5
25	78.47	80.20	81.78	(83.05)	(84.38)	(85.56)	(86.63)	(87.62)	(88.57)	(89.48)	(90.35)
50	69.96	71.59	73.09	(74.23)	(75.51)	(76.64)	(77.65)	(78.58)	(79.48)	(80.34)	(81.18)
75	62.30	63.91	65.38	(66.56)	(67.78)	(68.87)	(69.84)	(70.72)	(71.57)	(72.38)	(73.17)
100	55.47	57.10	58.55	59.78	60.98	62.06	63.00	63.85	64.65	65.43	66.17
125	49.37	51.05	52.53	53.76	54.97	56.04	56.98	57.82	58.60	59.34	60.05
150	43.91	45.68	47.19	48.42	49.64	50.73	51.68	52.52	53.28	54.00	54.68
175	39.02	40.90	42.46	43.69	44.92	46.03	47.00	47.85	48.61	49.31	49.96
200	34.60	36.63	38.27	39.51	40.75	41.88	42.87	43.73	44.48	45.17	45.81
225	30.58	32.79	34.54	35.82	37.06	38.20	39.21	40.07	40.83	41.51	42.13
250	26.87	29.31	31.20	32.55	33.79	34.94	35.95	36.83	37.58	38.25	38.86
275	23.38	26.12	28.20	29.63	30.88	32.03	33.04	33.92	34.67	35.33	35.92
300	19.99	23.15	25.46	27.00	28.27	29.41	30.43	31.30	32.05	32.70	33.27
325	16.58	20.32	22.94	24.61	25.90	27.05	28.05	28.92	29.66	30.29	30.85
350	12.87	17.57	20.58	22.40	23.74	24.88	25.88	26.74	27.47	28.09	28.63
375		14.86	18.37	20.35	21.74	22.89	23.89	24.74	25.45	26.06	26.58
400		(12.13)	16.27	18.42	19.88	21.06	22.05	22.88	23.59	24.18	24.68
425		(9.38)	14.30	16.63	18.16	19.35	20.34	21.17	21.86	22.44	22.92
450		(6.80)	12.46	14.95	16.56	17.78	18.77	19.59	20.27	20.84	21.31
475		(4.98)	10.78	13.41	15.08	16.33	17.34	18.16	18.83	19.39	19.85
500		(3.94)	9.27	12.01	13.75	15.03	16.05	16.88	17.56	18.11	18.56
525		(3.30)	7.97	10.78	12.57	13.90	14.94	15.78	16.46	17.02	17.48
550		(2.87)	6.89	9.74	11.58	12.95	14.03	14.90	15.59	16.16	16.63
575		(2.56)	(6.08)	(8.91)	(10.81)	(12.24)	(13.36)	(14.26)	(14.99)	(15.58)	(16.06)
600		(2.39)	(5.53)	(8.33)	(10.30)	(11.80)	(12.98)	(13.93)	(14.70)	(15.32)	(15.83)

TABLE 16

Partial derivative of the natural logarithm of the dielectric constant with respect to pressure at constant temperature in $bar^{-1} \times 10^5$ computed from equations (47) and (48) and the values of V and β in tables 3 and 8—see figures 25 and 26

t	PRESSURE, KB									
(°C)	SAT	0.5	1	2	2.5	3	3.5	4	4.5	5
25	4.67	4.1	3.8	(3.1)	(2.8)	(2.6)	(2.3)	(2.1)	(2.0)	(1.8)
50	4.94	4.3	4.0	(3.3)	(3.0)	(2.7)	(2.5)	(2.3)	(2.1)	(1.9)
75	5.50	4.8	4.3	(3.5)	(3.2)	(2.9)	(2.6)	(2.4)	(2.2)	(2.0)
100	6.34	5.4	4.8	3.8	3.4	3.1	2.8	2.6	2.4	(2.2)
125	7.48	6.1	5.3	4.2	3.7	3.3	3.0	2.7	2.5	(2.3)
150	9.02	7.1	6.0	4.6	4.0	3.6	3.2	2.9	2.7	(2.4)
175	11.10	8.4	6.8	5.1	4.4	3.9	3.5	3.1	2.8	(2.6)
200	14.00	10.0	7.8	5.7	4.9	4.2	3.7	3.3	3.0	(2.7)
225	18.20	12.1	9.0	6.4	5.4	4.6	4.0	3.5	3.2	(2.9)
250	24.66	14.9	10.6	7.1	5.9	5.0	4.3	3.8	3.3	(3.0)
275	35.40	18.8	12.5	8.0	6.5	5.4	4.6	4.0	3.5	(3.1)
300	55.52	24.5	15.0	8.9	7.2	5.9	4.9	4.2	3.7	(3.2)
325	101.95	33.0	18.3	10.0	7.9	6.4	5.3	4.5	3.8	(3.4)
350	274.99	46.4	22.5	11.1	8.6	6.9	5.6	4.7	4.0	(3.5)
375		69.1	28.0	12.5	9.5	7.4	6.0	5.0	4.2	(3.6)
400		111.5	34.9	14.0	10.4	8.0	6.4	5.2	4.4	(3.7)
425		197.2	43.5	15.7	11.4	8.7	6.8	5.5	4.6	(3.9)
450		319.6	54.0	17.7	12.6	9.4	7.3	5.9	4.8	(4.0)
475		349.5	66.5	20.1	14.0	10.3	7.9	6.3	5.1	(4.2)
500		309.1	80.5	22.8	15.5	11.2	8.5	6.7	5.4	(4.4)
525			(94.7)	(25.0)	(16.4)	(12.4)	(9.8)	(7.6)	(5.9)	(4.7)
550			(106.7)	(28.0)	(18.3)	(13.6)	(10.6)	(8.2)	(6.3)	(5.1)
575			(114.7)	(31.0)	(20.3)	(14.9)	(11.5)	(8.8)	(6.8)	(5.4)
600			(118.2)	(33.9)	(22.2)	(16.2)	(12.4)	(9.5)	(7.4)	(5.9)

TABLE 17

Partial derivative of the natural logarithm of the dielectric constant with respect to temperature at constant pressure in $(°K)^{-1} \times 10^3$ computed from equations (47) and (49) and the values of V and α in tables 3 and 7—see figures 27 and 28

t	PRESSURE, KB									
(°C)	SAT	0.5	1	2	2.5	3	3.5	4	4.5	5
25	-4.55	-4.5	-4.5	(-4.4)	(-4.4)	(-4.4)	(-4.4)	(-4.4)	(-4.3)	(-4.3)
50	-4.62	-4.5	-4.5	(-4.4)	(-4.3)	(-4.3)	(-4.3)	(-4.3)	(-4.2)	(-4.2)
75	-4.64	-4.5	-4.4	(-4.3)	(-4.2)	(-4.2)	(-4.2)	(-4.1)	(-4.1)	(-4.1)
100	-4.66	-4.5	-4.4	-4.2	-4.1	-4.1	-4.1	-4.0	-4.0	(-4.0)
125	-4.67	-4.5	-4.3	-4.1	-4.0	-4.0	-3.9	-3.9	-3.9	(-3.8)
150	-4.71	-4.4	-4.3	-4.0	-3.9	-3.9	-3.8	-3.8	-3.7	(-3.7)
175	-4.78	-4.4	-4.2	-3.9	-3.8	-3.7	-3.7	-3.6	-3.6	(-3.6)
200	-4.90	-4.4	-4.1	-3.8	-3.7	-3.6	-3.5	-3.5	-3.5	(-3.4)
225	-5.12	-4.4	-4.1	-3.7	-3.6	-3.5	-3.4	-3.4	-3.3	(-3.3)
250	-5.50	-4.5	-4.0	-3.6	-3.5	-3.4	-3.3	-3.3	-3.2	(-3.2)
275	-6.18	-4.7	-4.1	-3.6	-3.4	-3.3	-3.2	-3.2	-3.1	(-3.1)
300	-7.42	-5.0	-4.1	-3.5	-3.4	-3.2	-3.2	-3.1	-3.1	(-3.0)
325	-10.02	-5.5	-4.2	-3.5	-3.3	-3.2	-3.1	-3.1	-3.0	(-3.0)
350	-18.24	-6.2	-4.4	-3.5	-3.3	-3.2	-3.1	-3.0	-3.0	(-3.0)
375		-7.3	-4.7	-3.5	-3.3	-3.2	-3.1	-3.0	-3.0	(-3.0)
400		-9.0	-5.0	-3.6	-3.3	-3.2	-3.1	-3.0	-3.0	(-2.9)
425		-11.7	-5.3	-3.6	-3.4	-3.2	-3.1	-3.0	-3.0	(-2.9)
450		-13.5	-5.7	-3.7	-3.4	-3.2	-3.1	-3.0	-2.9	(-2.9)
475		-11.0	-5.9	-3.7	-3.3	-3.1	-3.0	-2.9	-2.8	(-2.8)
500		-8.0	-6.1	-3.6	-3.2	-3.0	-2.8	-2.7	-2.6	(-2.6)
525			(-6.0)	(-3.5)	(-3.0)	(-2.7)	(-2.5)	(-2.4)	(-2.3)	(-2.2)
550			(-5.5)	(-3.1)	(-2.6)	(-2.3)	(-2.1)	(-1.9)	(-1.8)	(-1.7)
575			(-4.5)	(-2.4)	(-1.9)	(-1.6)	(-1.4)	(-1.2)	(-1.1)	(-1.0)
600			(-2.9)	(-1.4)	(-1.0)	(-0.7	(-0.5)	(-0.3)	(-0.2)	(-0.1)

TABLE 18

Partial derivative of $(\partial \ln \varepsilon/\partial P)_T$ with respect to pressure at constant temperature in $bar^{-2} \times 10^9$ computed from equation (50) and the values of V, β, $(\partial\beta/\partial P)_T$, ε, and $(\partial \ln \varepsilon/\partial P)_T$ in tables 3, 8, 11, 15, and 16—see figures 29 and 30

t	PRESSURE, KB									
(°C)	SAT	0.5	1	2	2.5	3	3.5	4	4.5	5
25	-15.42	-8.4								
50	-16.66	-8.6								
75	-20.10	-10.8								
100	-26.41	-14.7	(-10.0)	(-8.8)	(-7.5)	(-6.4)	(-5.5)	(-4.7)	(-4.0)	(-3.5)
125	-36.64	-20.3	-14.1	-10.3	-8.6	-7.2	-6.1	-5.2	-4.4	(-3.8)
150	-52.94	-28.3	-19.2	-12.3	-10.0	-8.2	-6.9	-5.8	-4.9	(-4.2)
175	-79.55	-39.7	-25.8	-15.0	-11.8	-9.5	-7.8	-6.5	-5.5	(-4.7)
200	-125.21	-56.5	-34.6	-18.4	-14.1	-11.1	-8.9	-7.4	-6.2	(-5.2)
225	-209.40	-81.9	-46.5	-22.7	-17.0	-13.0	-10.3	-8.3	-6.9	(-5.8)
250	-380.92	-122.2	-63.0	-28.1	-20.4	-15.2	-11.8	-9.4	-7.7	(-6.4)
275	-783.27	-189.3	-86.4	-34.7	-24.6	-17.9	-13.6	-10.7	-8.6	(-7.1)
300	-1953.83	-307.7	-119.9	-42.8	-29.4	-20.9	-15.5	-12.0	-9.6	(-7.9)
325	-6917.75	-532.3	-168.4	-52.6	-35.1	-24.4	-17.8	-13.5	-10.7	(-8.7)
350	-57594.10	-1000.3	-238.5	-64.5	-41.7	-28.3	-20.2	-15.2	-11.9	(-9.6)
375		-2108.2	-339.1	-79.0	-49.4	-32.8	-23.0	-17.0	-13.2	(-10.5)
400		-5157.3	-482.0	-96.6	-58.3	-37.8	-26.1	-19.0	-14.6	(-11.6)
425			(-682.7)	-117.9	-68.7	-43.5	-29.5	-21.3	-16.1	(-12.7)
450			(-958.4)	-143.6	-80.7	-49.9	-33.3	-23.7	-17.8	(-14.0)
475			(-1311.9)	(-174.2)	(-94.8)	(-57.2)	(-37.5)	(-26.4)	(-19.7)	(-15.4)
500			(-1695.6)	(-210.1)	(-111.0)	(-65.5)	(-42.3)	(-29.4)	(-21.7)	(-16.9)

It can be seen in figure 30 that $(\partial^2 \ln \varepsilon/\partial P^2)_T$ increases rapidly with increasing pressure $\leq$ 2 kb at all (constant) temperatures $\geq$ 200°C, but like $(\partial\beta/\partial P)_T$ in figure 10, its isobaric dependence on temperature is characterized by minima in the low pressure isobars. Note also that $(\partial^2 \ln \varepsilon/\partial T^2)_P$ minimizes as an isothermal function of pressure at high temperatures and low pressures (fig. 32). In contrast, the isobaric temperature dependence of $(\partial^2 \ln \varepsilon/\partial T^2)_P$ depicted in figure 31 exhibits an extremum in the vicinity of 75° to 150°C, which is flanked by a minimum on either side at pressures < 2 kb; as pressure increases, the low-temperature minimum disappears and at high temperatures, $(\partial^2 \ln$

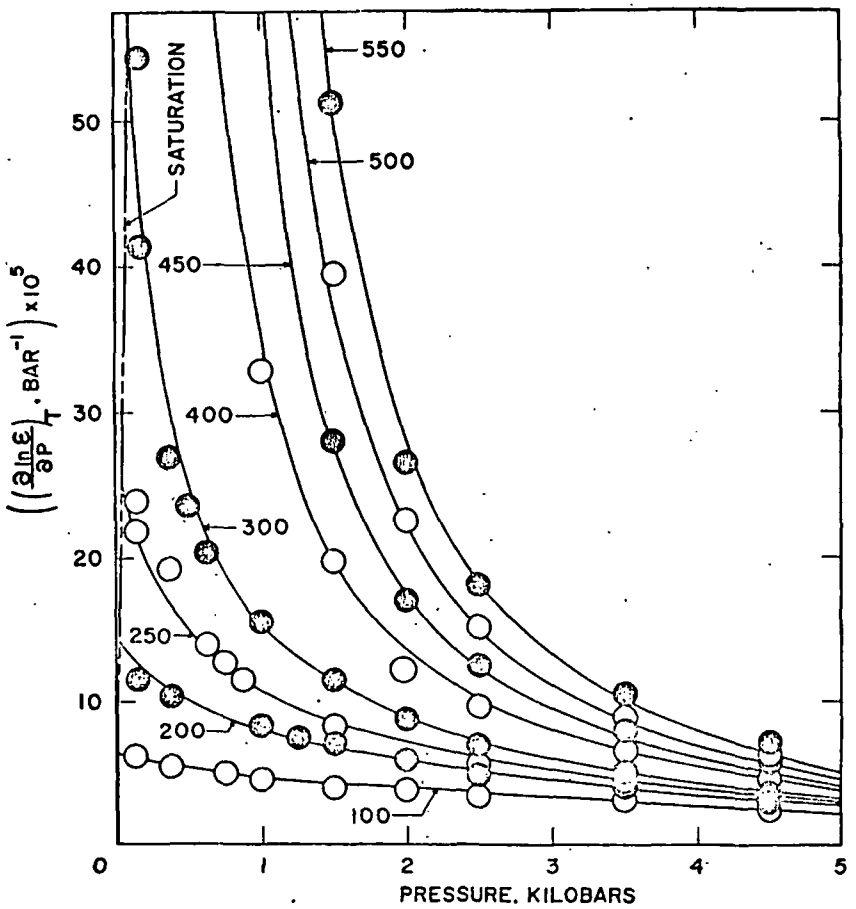

Fig. 26. Partial derivative of ln ε with respect to pressure at constant temperature (table 16) as a function of pressure at constant temperature (labeled in °C) computed from equations (19) through (22), (32), (38), (47), and (48) and coefficients in tables 4, 5, 6, 9, 10, and 14 (curves). The symbols represent corresponding finite difference derivatives computed from data given by Oshry (ms), Owen and others (1961), and/or Heger (ms).

$\varepsilon/\partial T^2)_P$ increases dramatically with increasing temperature at constant pressure. Note that $(\partial^2 \ln \varepsilon/\partial T^2)_P$ is negative at low pressures and positive at high pressures. As a consequence of the relations depicted in figure 24, the behavior of $(\partial^2 \ln \varepsilon/\partial P^2)_T$ in figures 29 and 30 is similar to that exhibited by $(\partial\beta/\partial P)_T$ in figures 10 and 11, respectively.

Because

$$\left(\frac{\partial\left(\frac{\partial \varepsilon}{\partial T}\right)_P}{\partial P}\right)_T = \left(\frac{\partial\left(\frac{\partial \varepsilon}{\partial P}\right)_T}{\partial T}\right)_P \tag{54}$$

and

$$\left(\frac{\partial\left(\frac{\partial \ln \varepsilon}{\partial T}\right)_P}{\partial P}\right)_T = \left(\frac{\partial\left(\frac{\partial \ln \varepsilon}{\partial P}\right)_T}{\partial T}\right)_P \tag{55}$$

it follows that the partial derivative of equation (48) with respect to temperature at constant pressure is equivalent to that of equation (49)

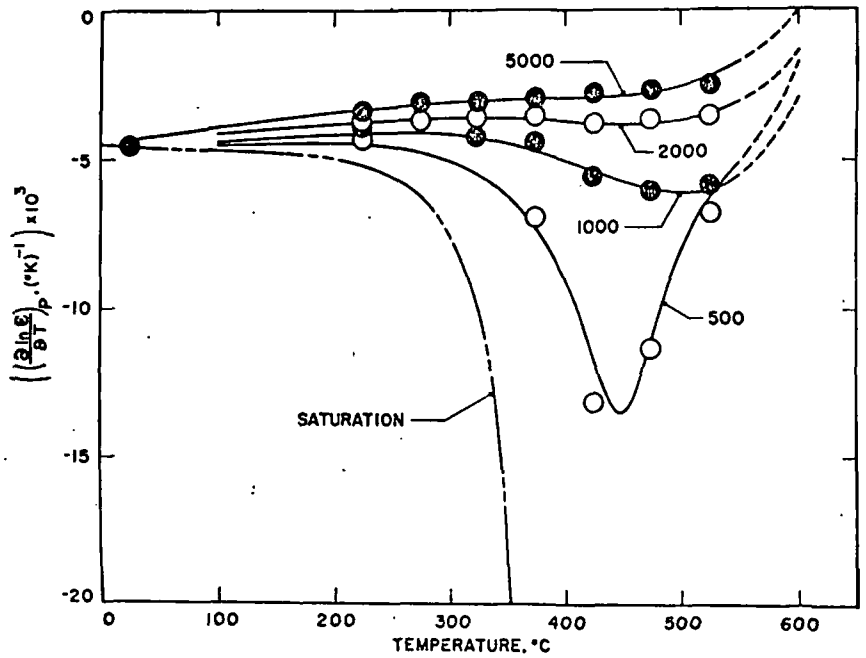

Fig. 27. Partial derivative of ln ε with respect to temperature at constant pressure (table 17) as a function of temperature at constant pressure (labeled in bars) computed from equations (19) through (21), (25), (33), (39), (47), and (49) and coefficients in tables 4, 5, 6, 9, 10, and 14 (curves). The symbols represent corresponding finite difference derivatives computed from data given by Oshry (ms), Owen and others (1961), and/or Heger (ms).

TABLE 19

Partial derivative of $(\partial \ln \varepsilon/\partial T)_P$ with respect to temperature at constant pressure in $(°K)^{-2} \times 10^6$ computed from equation (51) and the values of V, α, $(\partial\alpha/\partial T)_P$, ε, and $(\partial \ln \varepsilon/\partial T)_P$ in tables 3, 7, 13, 15, and 17—see figures 31 and 32

t (°C)	PRESSURE, KB									
	SAT	0.5	1	2	2.5	3	3.5	4	4.5	5
25	-4.09	-1.3								
50	-1.57	0.3								
75	-9.57	1.2								
100	-0.55	1.3	(2.5)	(3.8)	(4.2)	(4.5)	(4.7)	(4.9)	(5.0)	(5.1)
125	-1.08	1.2	2.5	4.1	4.5	4.8	5.0	5.2	5.3	(5.3)
150	-2.09	0.9	2.5	4.3	4.7	5.0	5.2	5.3	5.4	(5.4)
175	-3.84	0.5	2.5	4.2	4.7	5.0	5.1	5.2	5.3	(5.3)
200	-6.93	-0.5	2.3	4.0	4.5	4.8	4.9	5.0	5.0	(5.0)
225	-12.41	-2.1	1.6	3.5	4.1	4.4	4.5	4.6	4.6	(4.6)
250	-22.30	-4.9	0.5	2.9	3.5	3.8	3.9	3.9	3.9	(3.9)
275	-41.38	-9.0	-1.2	2.1	2.7	3.0	3.1	3.2	3.2	(3.1)
300	-84.56	-15.0	-3.5	1.2	1.8	2.2	2.3	2.3	2.3	(2.3)
325	-222.63	-23.4	-6.2	0.2	0.9	1.3	1.4	1.5	1.5	(1.5)
350	-1232.61	-35.5	-9.1	-0.7	0.1	0.5	0.7	0.8	0.8	(0.8)
375		-54.4	-11.6	-1.5	-0.6	-0.1	0.2	0.3	0.4	(0.4)
400		-87.1	-13.2	-2.1	-0.9	-0.3	0.1	0.3	0.4	(0.6)
425			(-13.5)	-2.0	-0.7	0.1	0.6	0.9	1.2	(1.3)
450			(-12.4)	-1.2	0.4	1.4	2.0	2.5	2.8	(3.1)
475			(-9.0)	(0.9)	(2.8)	(4.0)	(4.7)	(5.3)	(5.7)	(6.1)
500			(-1.9)	(4.8)	(6.9)	(8.2)	(9.0)	(9.6)	(10.1)	(10.6)

TABLE 20

Partial derivative of $(\partial \ln \varepsilon/\partial P)_T$ with respect to temperature at constant pressure in bar^{-1} $(°K)^{-1} \times 10^4$ computed from equation (56) and the values of V, α, β, $(\partial\beta/\partial T)_P$, ε, $(\partial \ln \varepsilon/\partial P)_T$, and $(\partial \ln \varepsilon/\partial T)_P$ in tables 3, 7, 8, 12, and 15 through 17—see figure 33

t (°C)	PRESSURE, KB									
	SAT	0.5	1	2	2.5	3	3.5	4	4.5	5
25	0.39	0.4								
50	1.69	1.3								
75	2.80	2.0								
100	3.94	2.7	(1.9)	(1.3)	(1.1)	(0.9)	(0.8)	(0.7)	(0.6)	(0.5)
125	5.32	3.5	2.4	1.5	1.2	1.0	0.9	0.8	0.7	(0.6)
150	7.17	4.4	3.0	1.8	1.4	1.2	1.0	0.8	0.7	(0.6)
175	9.89	5.6	3.6	2.1	1.6	1.3	1.0	0.9	0.7	(0.6)
200	14.17	7.3	4.4	2.4	1.8	1.4	1.1	0.9	0.7	(0.6)
225	21.45	9.7	5.5	2.8	2.0	1.5	1.1	0.9	0.7	(0.6)
250	35.00	13.2	6.9	3.2	2.2	1.6	1.2	0.9	0.7	(0.5)
275	63.63	18.7	8.8	3.6	2.4	1.7	1.2	0.9	0.7	(0.5)
300	137.25	27.4	11.4	4.0	2.6	1.8	1.3	0.9	0.7	(0.5)
325	407.74	41.9	14.8	4.5	2.9	1.9	1.3	0.9	0.7	(0.5)
350	2716.07	68.0	19.2	5.0	3.1	2.0	1.4	1.0	0.7	(0.4)
375		119.8	24.6	5.7	3.5	2.2	1.5	1.0	0.7	(0.5)
400		235.9	31.0	6.4	3.8	2.4	1.6	1.1	0.7	(0.5)
425			(38.2)	7.3	4.3	2.7	1.8	1.2	0.8	(0.5)
450			(46.0)	8.5	4.9	3.1	2.0	1.4	0.9	(0.6)
475			(53.5)	(9.8)	(5.6)	(3.5)	(2.3)	(1.6)	(1.1)	(0.8)
500			(57.6)	(11.3)	(6.4)	(4.0)	(2.6)	(1.8)	(1.3)	(1.0)

TABLE 21

Finite difference partial derivative of $(\partial(\partial \ln \varepsilon/\partial P)_T/\partial T)_P$ with respect to temperature at constant pressure in $bar^{-1}(°K)^{-2} \times 10^9$

t (°C)	PRESSURE, KB									
	SAT	0.5	1	2	2.5	3	3.5	4	4.5	5
25	5.85	4.8								
50	4.65	3.0								
75	4.35	2.7								
100	4.91	2.8	(1.8)	(0.9)	(0.7)	(0.5)	(0.4)	(0.3)	(0.2)	(0.2)
125	6.31	3.3	2.0	1.0	0.7	0.5	0.3	0.2	0.2	(0.1)
150	8.92	4.2	2.4	1.1	0.7	0.5	0.3	0.2	0.1	(0.1)
175	13.66	5.6	2.9	1.3	0.8	0.5	0.3	0.1	0.1	(0.0)
200	22.60	7.9	3.7	1.4	0.8	0.4	0.2	0.1	0.0	(-0.1)
225	40.78	11.5	4.9	1.5	0.8	0.4	0.2	0.1	0.0	(-0.1)
250	82.44	17.3	6.5	1.6	0.8	0.4	0.2	0.0	-0.1	(-0.1)
275	196.55	27.1	8.8	1.7	0.9	0.4	0.2	0.0	-0.1	(-0.1)
300	612.38	44.1	11.9	1.8	0.9	0.4	0.2	0.0	-0.1	(-0.1)
325	3149.17	75.7	15.6	2.0	1.0	0.5	0.2	0.1	0.0	(-0.1)
350	22725.69	141.3	19.6	2.3	1.1	0.6	0.3	0.1	0.0	(-0.0)
375			(23.6)	2.8	1.4	0.8	0.4	0.3	0.1	(0.1)
400			(27.1)	3.3	1.7	1.0	0.6	0.4	0.3	(0.2)
425			(30.4)	4.1	2.1	1.2	0.8	0.6	0.4	(0.3)
450			(31.9)	4.9	2.6	1.6	1.0	0.8	0.6	(0.5)
475			(25.7)	(5.7)	(3.0)	(1.8)	(1.3)	(1.0)	(0.8)	(0.7)
500			(1.5)	(3.6)	(4.6)	(1.8)	(1.3)	(1.4)	(1.4)	(0.9)

TABLE 22

Y (eq 65) in $(°K)^{-1} \times 10^5$ computed from values of ε and $(\partial \ln \varepsilon/\partial T)_P$ in tables 15 and 17—see figure 34

t (°C)	PRESSURE, KB									
	SAT	0.5	1	2	2.5	3	3.5	4	4.5	5
25	-5.80	-5.65	(-5.51)	(-5.27)	(-5.17)	(-5.07)	(-4.99)	(-4.91)	(-4.84)	(-4.77)
50	-6.60	-6.35	(-6.13)	(-5.80)	(-5.66)	(-5.55)	(-5.45)	(-5.35)	(-5.26)	(-5.18)
75	-7.45	-7.08	(-6.79)	(-6.34)	(-6.17)	(-6.03)	(-5.90)	(-5.79)	(-5.69)	(-5.59)
100	-8.39	-7.87	-7.48	-6.89	-6.68	-6.51	-6.36	-6.23	-6.11	(-5.99)
125	-9.47	-8.74	-8.22	-7.46	-7.20	-6.98	-6.81	-6.65	-6.51	(-6.38)
150	-10.73	-9.71	-9.01	-8.06	-7.73	-7.46	-7.25	-7.07	-6.91	(-6.76)
175	-12.25	-10.80	-9.87	-8.68	-8.26	-7.94	-7.68	-7.47	-7.29	(-7.13)
200	-14.17	-12.05	-10.79	-9.33	-8.82	-8.42	-8.12	-7.87	-7.67	(-7.49)
225	-16.75	-13.56	-11.81	-10.01	-9.39	-8.92	-8.56	-8.28	-8.05	(-7.85)
250	-20.48	-15.46	-12.99	-10.75	-10.01	-9.45	-9.03	-8.71	-8.45	(-8.24)
275	-26.42	-17.99	-14.40	-11.56	-10.68	-10.03	-9.55	-9.18	-8.90	(-8.67)
300	-37.09	-21.59	-16.18	-12.48	-11.44	-10.69	-10.13	-9.72	-9.41	(-9.16)
325	-60.43	-26.93	-18.48	-13.54	-12.32	-11.44	-10.81	-10.34	-9.99	(-9.72)
350	-141.66	-35.28	-21.53	-14.80	-13.34	-12.32	-11.60	-11.07	-10.68	(-10.38)
375		-49.15	-25.54	-16.29	-14.54	-13.34	-12.50	-11.90	-11.46	(-11.13)
400		-74.46	-30.74	-18.04	-15.91	-14.49	-13.51	-12.82	-12.32	(-11.94)
425		-124.64	-37.33	-20.05	-17.43	-15.74	-14.58	-13.77	-13.19	(-12.76)
450		-197.96	-45.46	-22.26	-19.01	-16.97	-15.61	-14.66	-13.98	(-13.48)
475		-220.61	-55.10	-24.51	-20.47	-18.02	-16.40	-15.28	-14.49	(-13.91)
500		-203.18	-65.64	-26.43	-21.47	-18.55	-16.65	-15.36	-14.44	(-13.78)
525			(-75.14)	(-27.55)	(-21.55)	(-18.14)	(-16.00)	(-14.56)	(-13.53)	(-12.78)
550			(-79.80)	(-26.53)	(-19.90)	(-16.16)	(-13.84)	(-12.28)	(-11.18)	(-10.37)
575			(-74.23)	(-22.35)	(-15.71)	(-11.98)	(-9.68)	(-8.16)	(-7.09)	(-6.30)
600			(-53.20)	(-13.98)	(-8.38)	(-5.23)	(-3.33)	(-2.07)	(-1.19)	(-0.54)

$$+\beta\sum_{i=0}^{4}\sum_{j=0}^{4-i} j\,e_{ij}\,\rho^j\left(\,j\alpha(j\alpha T^i - 2iT^{i-1}) + \right.$$

$$\left. -i(i-1)T^{i-2} - jT^i\left(\frac{\partial\alpha}{\partial T}\right)_P\,\right) \qquad (57)$$

It can be seen in figure 33 that the values of $(\partial(\partial \ln \varepsilon/\partial P)_T/\partial T)_P$ in table 20, which were computed from equation (56) and values of V, α, β, $(\partial\beta/\partial T)_P$, $(\partial \ln \varepsilon/\partial T)_P$, and $(\partial \ln \varepsilon/\partial P)_T$ given above, are in close agreement with finite difference derivatives calculated from the values of $(\partial \ln \varepsilon/\partial P)_T$ and $(\partial \ln \varepsilon/\partial T)_P$ in figures 25 and 28. However (as noted above), for temperatures $\geq$ 500°C and pressures $\geq$ 500 bars at temperatures $\leq$ 100°C, the proximity of the fit region boundary in figure 18 introduces inconsistencies in the values of $(\partial(\partial \ln \varepsilon/\partial P)_T/\partial T)_P$ computed from the values of V, α, β, $(\partial\beta/\partial T)_P$, ε, $(\partial \ln \varepsilon/\partial T)_P$, and $(\partial \ln \varepsilon/\partial P)_T$ in tables 3, 7, 8, 12, and 15 through 17. For this reason, equations (56) and (57) should not be used to calculate values of $(\partial(\partial \ln \varepsilon/\partial P)_T/\partial T)_P$ and $(\partial^2(\partial \ln \varepsilon/\partial P)_T/\partial T^2)_P$ for T > 500°C or P > 500 bars at T < 100°C. Because

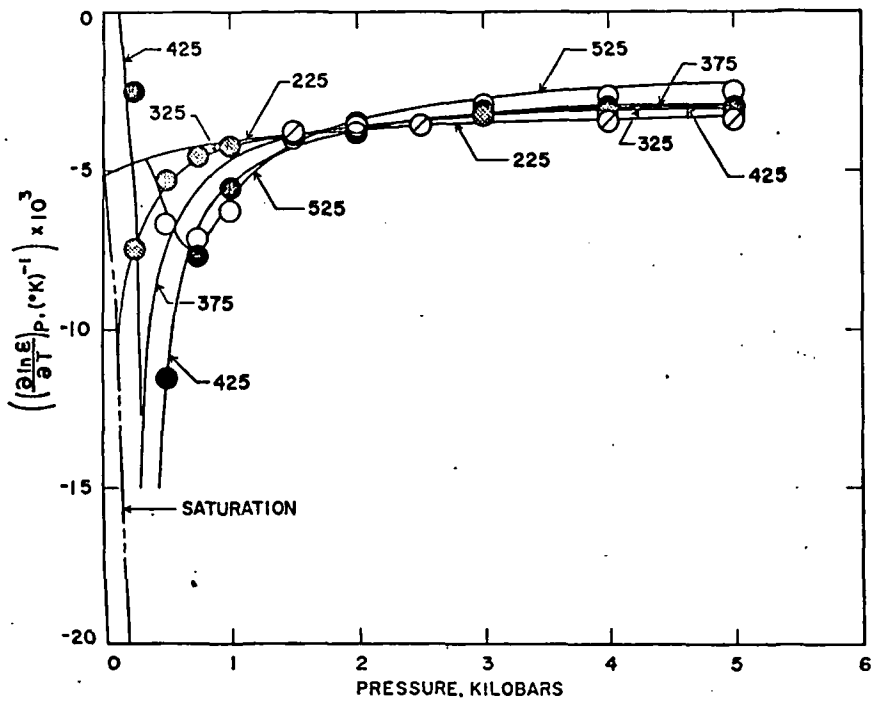

Fig. 28. Partial derivative of ln ε with respect to temperature at constant pressure (table 17) as a function of pressure at constant temperature (labeled in °C) computed from equations (19) through (21), (25), (33), (39), (47), and (49) and coefficients in tables 4, 5, 6, 9, 10, and 14. The symbols represent corresponding finite difference derivatives computed from data given by Oshry (ms), Owen and others (1961), and/or Heger (ms).

with respect to pressure at constant temperature. Hence,

$$\left(\frac{\partial\left(\frac{\partial\varepsilon}{\partial P}\right)_T}{\partial T}\right)_P = \left(\frac{\partial\left(\frac{\partial\varepsilon}{\partial T}\right)_P}{\partial P}\right)_T$$

$$= \varepsilon\left(\left(\frac{\partial\left(\frac{\partial \ln \varepsilon}{\partial P}\right)_T}{\partial T}\right)_P + \left(\frac{\partial \ln \varepsilon}{\partial T}\right)_P\left(\frac{\partial \ln \varepsilon}{\partial P}\right)_T\right)$$

$$= \left(\frac{\partial\varepsilon}{\partial P}\right)_T\left(\frac{\partial \ln \beta}{\partial T}\right)_P + \beta\sum_{i=0}^{4}\sum_{j=0}^{4-i} j\,e_{ij}\,\rho^j(iT^{i-1} - j\alpha T^i) \qquad (56)$$

from which it follows that

$$\left(\frac{\partial^2\left(\frac{\partial\varepsilon}{\partial P}\right)_T}{\partial T^2}\right)_P = \varepsilon\left(\left(\frac{\partial^2\left(\frac{\partial \ln \varepsilon}{\partial P}\right)_T}{\partial T^2}\right)_P + 2\left(\frac{\partial \ln \varepsilon}{\partial T}\right)_P\left(\frac{\partial\left(\frac{\partial \ln \varepsilon}{\partial P}\right)_T}{\partial T}\right)_P + \left(\frac{\partial^2 \ln \varepsilon}{\partial T^2}\right)_P\left(\frac{\partial \ln \varepsilon}{\partial P}\right)_T + \left(\frac{\partial \ln \varepsilon}{\partial T}\right)_P^2\left(\frac{\partial \ln \varepsilon}{\partial P}\right)_T\right) = \left(\frac{\partial\varepsilon}{\partial P}\right)_T\left(\frac{\partial^2 \ln \beta}{\partial T^2}\right)_P + 2\left(\frac{\partial\left(\frac{\partial\varepsilon}{\partial P}\right)_T}{\partial T}\right)_P\left(\frac{\partial \ln \beta}{\partial T}\right)_P + \left(\frac{\partial\varepsilon}{\partial P}\right)_T\left(\frac{\partial \ln \beta}{\partial T}\right)_P^2 +$$

to the change in Gibbs free energy attending its transfer from a vacuum to a medium of dielectric constant ε, can be written as

$$\Delta G_{e,j} = \omega_j \left(\frac{1}{\varepsilon} - 1 \right) \qquad (58)$$

where

$$\omega_j = \frac{N^\circ Z_j^2 e^2}{2 r_{e,j}} \quad , \qquad (59)$$

$\Delta G_{e,j}$ denotes the molal Gibbs free energy of transfer for the jth ion, N° stands for Avogadro's number (6.02252×10^{23} mole^{-1}), e represents the

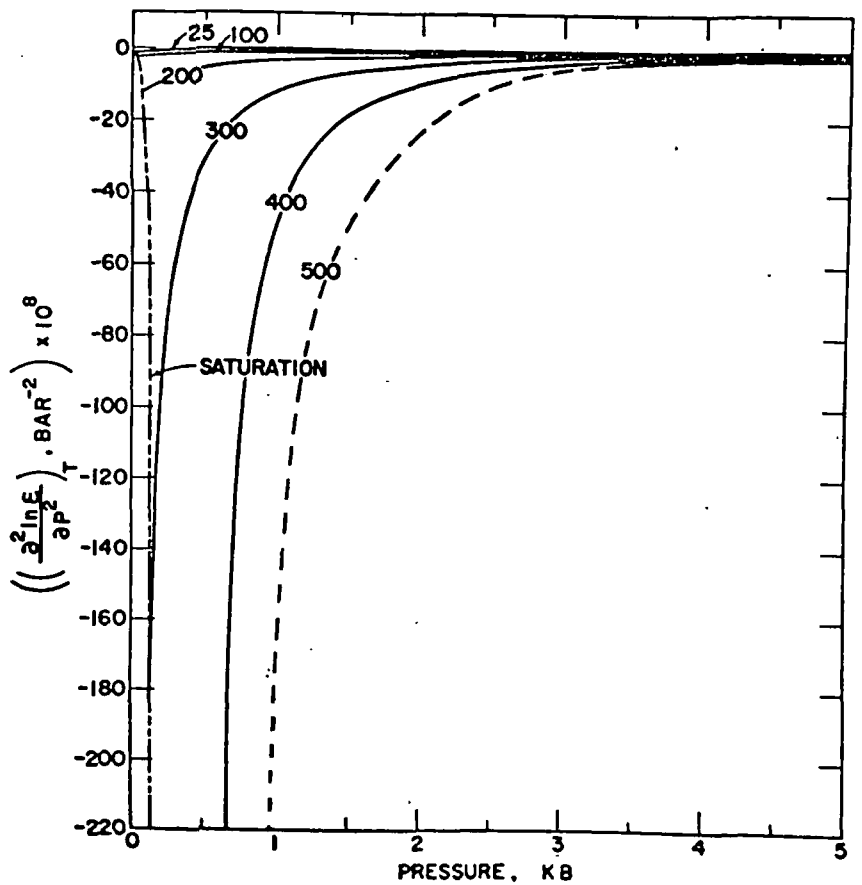

Fig. 30. Partial derivative of $(\partial \ln \varepsilon/\partial P)_T$ with respect to pressure at constan temperature (table 18) as a function of pressure at constant temperature (labeled i °C) computed from equations (19) through (23), (32), (35), (38), (41), (47), (48), an (50) and coefficients in tables 4, 5, 6, 9, 10, and 14.

evaluation of equation (57) requires values of $(\partial^2 \ln \beta/\partial T^2)_P$, which cannot be computed with confidence from the partial derivatives of equations (36) and (42), the values of $(\partial^2(\partial \ln \varepsilon/\partial P)_T/\partial T^2)_P$ given in table 21 correspond to finite difference derivatives calculated from the values of $(\partial(\partial \ln \varepsilon/\partial P)_T/\partial T)_P$ in figure 33.

BORN FUNCTIONS

Continuum theories of liquid H_2O and electrostatic models of ion solvation in aqueous solution require values for the partial derivatives of ε^{-1} with respect to temperature and pressure. Because ε^{-1} and its partial derivatives, which are designated here as Born functions, are used extensively in solution chemistry, they are tabulated and plotted below as functions of pressure and temperature.

The Born equation (Born, 1920), which relates the effective electrostatic radius of an incompressible ion (with spherical charge symmetry)

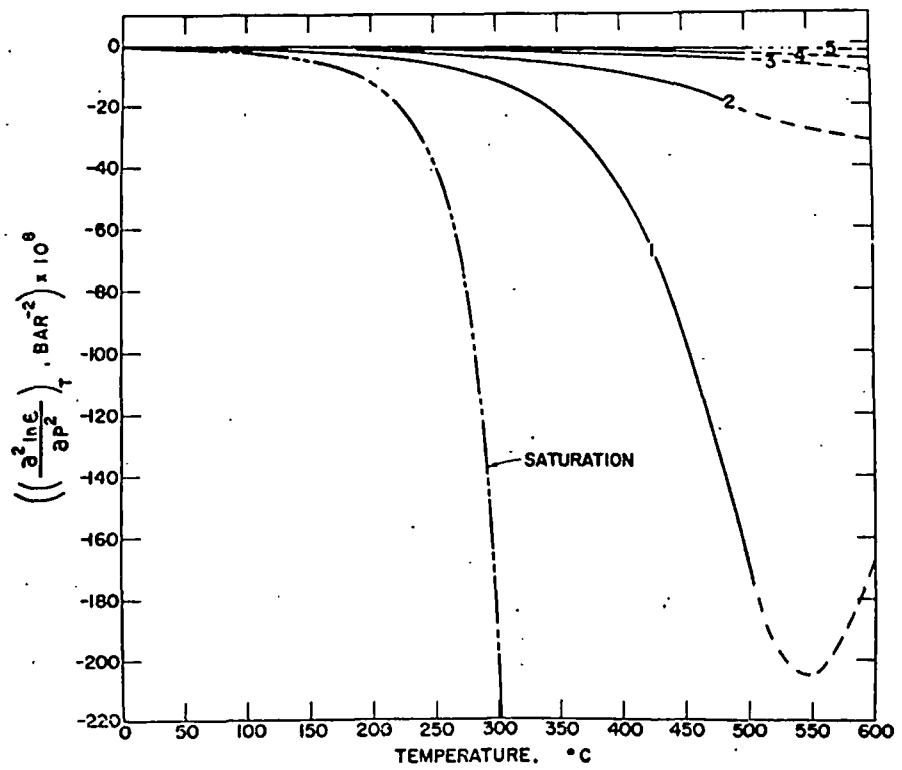

Fig. 29. Partial derivative of $(\partial \ln \varepsilon/\partial P)_T$ with respect to pressure at constant temperature (table 18) as a function of temperature at constant pressure (labeled in kb) computed from equations (19) through (23), (32), (35), (38), (41), (47), (48), and (50) and coefficients in tables 4, 5, 6, 9, 10, and 14.

TABLE 23

X (eq 66) in $(°K)^{-2} \times 10^7$ computed from values of ϵ, $(\partial \ln \epsilon/\partial T)_P$, and $(\partial^2 \ln \epsilon/\partial T^2)_P$ in tables 15, 17, and 19—see figure 34

t	PRESSURE, KB									
(°C)	SAT	0.5	1	2	2.5	3.	3.5	4	4.5	5
25	-3.16	-2.7								
50	-3.28	-2.8								
75	-3.55	-3.0								
100	-4.01	-3.3	(-2.8)	(-2.3)	(-2.1)	(-1.9)	(-1.8)	(-1.7)	(-1.7)	(-1.6)
125	-4.65	-3.7	-3.1	-2.3	-2.1	-1.9	-1.8	-1.7	-1.6	(-1.6)
150	-5.53	-4.1	-3.3	-2.4	-2.1	-1.9	-1.8	-1.7	-1.6	(-1.5)
175	-6.84	-4.7	-3.5	-2.4	-2.1	-1.9	-1.7	-1.6	-1.5	(-1.5)
200	-8.95	-5.4	-3.9	-2.6	-2.2	-1.9	-1.8	-1.6	-1.5	(-1.5)
225	-12.63	-6.7	-4.3	-2.8	-2.3	-2.0	-1.8	-1.7	-1.6	(-1.5)
250	-19.57	-8.7	-5.1	-3.0	-2.5	-2.2	-1.9	-1.8	-1.7	(-1.6)
275	-34.02	-11.9	-6.3	-3.4	-2.8	-2.4	-2.2	-2.0	-1.9	(-1.8)
300	-69.80	-17.3	-8.0	-4.0	-3.2	-2.8	-2.5	-2.3	-2.2	(-2.1)
325	-194.82	-26.3	-10.6	-4.7	-3.8	-3.2	-2.9	-2.7	-2.5	(-2.4)
350	-1215.87	-42.0	-14.0	-5.5	-4.4	-3.7	-3.3	-3.1	-2.9	(-2.8)
375		-72.5	-18.3	-6.5	-5.1	-4.3	-3.8	-3.5	-3.3	(-3.1)
400		-139.1	-23.5	-7.5	-5.8	-4.8	-4.1	-3.7	-3.5	(-3.3)
425			(-29.4)	(-8.4)	(-6.2)	(-5.0)	(-4.2)	(-3.7)	(-3.4)	(-3.1)
450			(-35.7)	(-8.9)	(-6.2)	(-4.7)	(-3.7)	(-3.1)	(-2.7)	(-2.4)
475			(-41.1)	(-8.4)	(-5.1)	(-3.3)	(-2.3)	(-1.6)	(-1.1)	(-0.8
500			(-42.0)	(-6.1)	(-2.3)	(-0.4)	(0.6)	(1.3)	(1.8)	(2.2)

TABLE 24

$\hat{Q}$ (eq 67) in $\text{bar}^{-1} \times 10^6$ computed from values of ϵ and $(\partial \ln \epsilon/\partial P)_T$ in tables 15 and 16—see figure 35

t	PRESSURE, KB									
(°C)	SAT	0.5	1	2	2.5	3	3.5	4	4.5	5
25	0.60	0.51	0.46	(0.36)	(0.33)	(0.30)	(0.27)	(0.24)	(0.22)	(0.20)
50	0.71	0.61	0.55	(0.43)	(0.39)	(0.35)	(0.32)	(0.29)	(0.26)	(0.24)
75	0.88	0.75	0.66	(0.52)	(0.46)	(0.41)	(0.37)	(0.34)	(0.31)	(0.28)
100	1.14	0.94	0.81	0.62	0.55	0.49	0.44	0.40	0.36	(0.33)
125	1.52	1.20	1.01	0.76	0.66	0.58	0.52	0.47	0.42	(0.38)
150	2.05	1.56	1.26	0.92	0.79	0.69	0.61	0.55	0.49	(0.45)
175	2.85	2.05	1.60	1.14	0.96	0.83	0.72	0.64	0.57	(0.52)
200	4.05	2.72	2.03	1.40	1.16	0.98	0.85	0.75	0.66	(0.59)
225	5.95	3.68	2.61	1.72	1.41	1.17	1.00	0.87	0.76	(0.68)
250	9.18	5.09	3.39	2.12	1.70	1.39	1.17	1.00	0.87	(0.77)
275	15.14	7.22	4.44	2.59	2.04	1.64	1.36	1.15	0.99	(0.87)
300	27.77	10.59	5.90	3.16	2.44	1.93	1.57	1.32	1.12	(0.97)
325	61.49	16.25	7.97	3.85	2.91	2.27	1.82	1.50	1.27	(1.09)
350	213.62	26.41	10.94	4.69	3.47	2.66	2.10	1.71	1.43	(1.21)
375		46.50	15.23	5.73	4.14	3.11	2.42	1.95	1.61	(1.35)
400		91.93	21.45	7.03	4.94	3.64	2.80	2.22	1.81	(1.51)
425		210.24	30.44	8.66	5.91	4.28	3.23	2.53	2.04	(1.68)
450		469.90	43.37	10.72	7.10	5.03	3.75	2.90	2.31	(1.88)
475		702.10	61.73	13.32	8.55	5.93	4.35	3.33	2.62	(2.12)
500		785.14	86.87	16.57	10.30	7.00	5.06	3.82	2.99	(2.39)
525			(118.81)	(19.90)	(11.82)	(8.32)	(6.19)	(4.61)	(3.46)	(2.70)
550			(154.72)	(24.20)	(14.13)	(9.71)	(7.10)	(5.24)	(3.92)	(3.04)
575			(188.81)	(28.71)	(16.57)	(11.15)	(8.04)	(5.89)	(4.38)	(3.38)
600			(213.77)	(32.87)	(18.84)	(12.48)	(8.89)	(6.47)	(4.80)	(3.70)

TABLE 25

U (eq 68) in bar^{-1} $(°K)^{-1} \times 10^9$ computed from values of ϵ, $(\partial \ln \epsilon/\partial P)_T$, $(\partial \ln \epsilon/\partial T)_P$, and $(\partial(\partial \ln \epsilon/\partial P)_T)/\partial T)_P$ in tables 15 through 17 and 20—see figure 35

t	PRESSURE, KB									
(°C)	SAT	0.5	1	2	2.5	3	3.5	4	4.5	5
25	3.20	2.9								
50	5.68	4.6								
75	8.59	6.6								
100	12.42	9.0	(6.8)	(4.7)	(4.0)	(3.5)	(3.0)	(2.7)	(2.4)	(2.1)
125	17.86	12.2	8.9	5.9	4.9	4.1	3.6	3.1	2.7	(2.4)
150	26.01	16.6	11.6	7.3	5.9	4.9	4.2	3.6	3.1	(2.7)
175	38.95	22.8	15.2	9.1	7.1	5.8	4.8	4.1	3.5	(3.0)
200	60.80	32.0	20.0	11.3	8.6	6.8	5.5	4.6	3.9	(3.3)
225	100.62	46.0	26.6	13.9	10.3	7.9	6.3	5.1	4.3	(3.6)
250	180.75	68.1	35.9	17.1	12.3	9.2	7.1	5.7	4.7	(3.9)
275	365.68	105.4	49.3	20.8	14.5	10.6	8.0	6.3	5.1	(4.1)
300	892.43	171.2	69.1	25.3	17.2	12.2	9.0	7.0	5.5	(4.4)
325	3075.19	295.2	98.4	30.8	20.4	14.1	10.2	7.7	6.0	(4.8)
350	24995.05	550.5	141.8	37.6	24.2	16.4	11.7	8.7	6.6	(5.2)
375		1146.1	205.5	46.3	28.9	19.2	13.4	9.8	7.4	(5.7)
400		2774.6	297.6	57.5	34.8	22.7	15.6	11.2	8.4	(6.4)
425			(429.4)	(71.9)	(42.2)	(27.0)	(18.4)	(13.1)	(9.7)	(7.3)
450			(615.1)	(90.6)	(51.5)	(32.3)	(21.7)	(15.4)	(11.2)	(8.5)
475			(863.2)	(114.1)	(62.8)	(38.6)	(25.6)	(18.0)	(13.1)	(9.8)
500			(1149.6)	(142.3)	(75.8)	(45.6)	(29.8)	(20.8)	(15.1)	(11.3)

TABLE 26

N (eq 69) in $\text{bar}^{-2} \times 10^{10}$ computed from values of ϵ, $(\partial \ln \epsilon/\partial P)_T$, and $(\partial^2 \ln \epsilon/\partial P^2)_T$ in tables 15, 16, and 18—see figure 36

t	PRESSURE, KB									
(°C)	SAT	0.5	1	2	2.5	3	3.5	4	4.5	5
25	-2.24	-1.2								
50	-2.73	-1.5								
75	-3.71	-2.0								
100	-5.49	-3.1	(-2.1)	(-1.7)	(-1.4)	(-1.2)	(-1.0)	(-0.8)	(-0.7)	(-0.6)
125	-8.56	-4.7	-3.2	-2.1	-1.8	-1.5	-1.2	-1.0	-0.9	(-0.7)
150	-13.91	-7.3	-4.8	-2.9	-2.2	-1.8	-1.5	-1.2	-1.0	(-0.9)
175	-23.55	-11.4	-7.2	-3.9	-3.0	-2.3	-1.9	-1.5	-1.3	(-1.1)
200	-41.85	-18.1	-10.6	-5.3	-3.9	-3.0	-2.4	-1.9	-1.6	(-1.3)
225	-79.30	-29.4	-15.8	-7.2	-5.2	-3.9	-3.0	-2.3	-1.9	(-1.6)
250	-164.37	-49.3	-23.8	-9.8	-6.9	-4.9	-3.7	-2.9	-2.3	(-1.9)
275	-388.63	-86.1	-36.1	-13.3	-9.0	-6.3	-4.6	-3.5	-2.8	(-2.3)
300	-1131.44	-158.9	-56.0	-18.0	-11.7	-8.0	-5.7	-4.3	-3.4	(-2.7)
325	-4798.85	-315.6	-88.0	-24.2	-15.3	-10.1	-7.1	-5.2	-4.0	(-3.1)
350	-50615.56	-691.9	-140.5	-32.4	-19.8	-12.8	-8.7	-6.3	-4.8	(-3.8)
375		-1740.3	-227.3	-43.5	-25.5	-16.0	-10.8	-7.7	-5.7	(-4.5)
400		-5276.1	-371.1	-58.4	-32.8	-20.1	-13.2	-9.2	-6.8	(-5.3)
425			(-610.0)	(-78.6)	(-42.3)	(-25.1)	(-16.1)	(-11.1)	(-8.1)	(-6.2)
450			(-1003.5)	(-105.8)	(-54.4)	(-31.3)	(-19.7)	(-13.4)	(-9.7)	(-7.3)
475			(-1627.9)	(-142.3)	(-69.9)	(-39.1)	(-24.1)	(-16.1)	(-11.5)	(-8.6)
500			(-2528.7)	(-190.6)	(-89.8)	(-48.7)	(-29.3)	(-19.3)	(-13.6)	(-10.1)

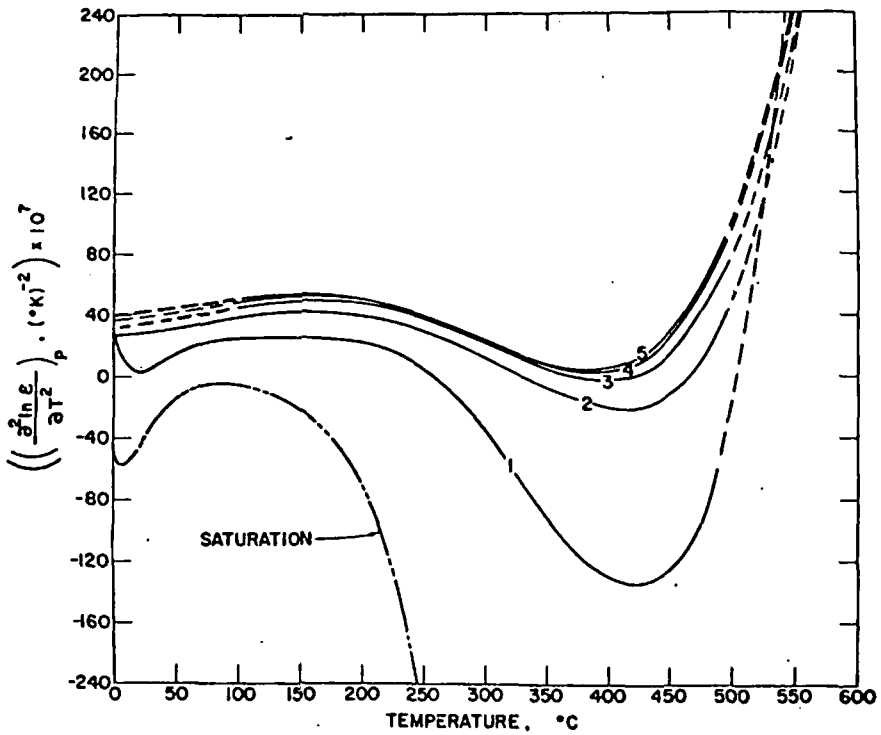

Fig. 31. Partial derivative of $(\partial \ln \varepsilon/\partial T)_P$ with respect to temperature at constant pressure (table 19) as a function of temperature at constant pressure (labeled in kb) computed from equations (19) through (21), (25), (27), (33), (37), (39), (43), (47), (49), and (51) and coefficients in tables 4, 5, 6, 9, 10, and 14.

Values of Y, X, $\hat{Q}$, U, and N computed from equations (65) through (69) and values of $(\partial \ln \varepsilon/\partial T)_P$, $(\partial^2 \ln \varepsilon/\partial T^2)_P$, $(\partial \ln \varepsilon/\partial P)_T$, $(\partial(\partial \ln \varepsilon/\partial P)_T/\partial T)_P$, $(\partial \ln \varepsilon/\partial T)_P$, and $(\partial^2 \ln \varepsilon/\partial P^2)_T$ given above are shown in tables 22 through 26 and plotted in figures 34 through 36. Owing to the high sensitivity of X, U, and N to small errors in the partial derivatives of ε and V, values of these variables are not given in tables 23, 25, and 26 for temperatures > 500°C or pressures > 500 bars at temperatures < 100°C.

It can be seen in figure 34 that the isobars for both Y and X exhibit minima at high temperatures. In contrast, $\hat{Q}$ and U increase and N decreases monotonically with increasing temperature at constant pressure (figs. 35 and 36). Because each of the Born functions depends on the expansibility and/or compressibility of H_2O, $-Y$, $-X$, $\hat{Q}$, U, and $-N$ all approach ∞ at the critical point of H_2O. As a consequence, the standard thermodynamic partial molal properties of aqueous electrolytes also approach positive or negative infinity at the critical point of H_2O (Helgeson and Kirkham, 1974c).

electronic charge (4.80298 esu), and Z_j and $r_{e,j}$ refer to the charge and effective electrostatic radius of the subscripted ion. If $r_{e,j}$ is independent of temperature and pressure, it follows from equation (58) that the change in the molal entropy ($\Delta S_{s,j}$), heat capacity ($\Delta C_{P,s,j}$), volume ($\Delta V_{s,j}$), expansibility ($\Delta E_{x,s,j}$), and compressibility ($\Delta \kappa_{s,j}$) for the transfer process can be expressed as

$$\Delta S_{s,j} = \omega_j Y \,, \tag{60}$$

$$\Delta C_{P,s,j} = T\left(\frac{\partial \Delta S_{s,j}}{\partial T}\right)_P = \left(\frac{\partial \Delta H_{s,j}}{\partial T}\right)_P = \omega_j T X \,, \tag{61}$$

$$\Delta V_{s,j} = -\omega_j \hat{Q} \,, \tag{62}$$

$$\Delta E_{x,s,j} = \left(\frac{\partial \Delta V_{s,j}}{\partial T}\right)_P = -\omega_j U \,, \tag{63}$$

and

$$-\Delta \kappa_{s,j} = \left(\frac{\partial \Delta V_{s,j}}{\partial P}\right)_T = -\omega_j N \,, \tag{64}$$

where $\Delta H_{s,j}$ is the molal enthalpy change for the transfer process, and Y, X, $\hat{Q}$, U, and N stand for various Born functions given by

$$Y = \frac{1}{\varepsilon}\left(\frac{\partial \ln \varepsilon}{\partial T}\right)_P \,, \tag{65}$$

$$X = \frac{1}{\varepsilon}\left(\left(\frac{\partial^2 \ln \varepsilon}{\partial T^2}\right)_P - \left(\frac{\partial \ln \varepsilon}{\partial T}\right)_P^2\right), \tag{66}$$

$$\hat{Q} = \frac{1}{\varepsilon}\left(\frac{\partial \ln \varepsilon}{\partial P}\right)_T \,, \tag{67}$$

$$U = \frac{1}{\varepsilon}\left(\left(\frac{\partial\left(\frac{\partial \ln \varepsilon}{\partial P}\right)_T}{\partial T}\right)_P - \left(\frac{\partial \ln \varepsilon}{\partial T}\right)_P \left(\frac{\partial \ln \varepsilon}{\partial P}\right)_T\right) \tag{68}$$

and

$$N = \frac{1}{\varepsilon}\left(\left(\frac{\partial^2 \ln \varepsilon}{\partial P^2}\right)_T - \left(\frac{\partial \ln \varepsilon}{\partial P}\right)_T^2\right). \tag{69}$$

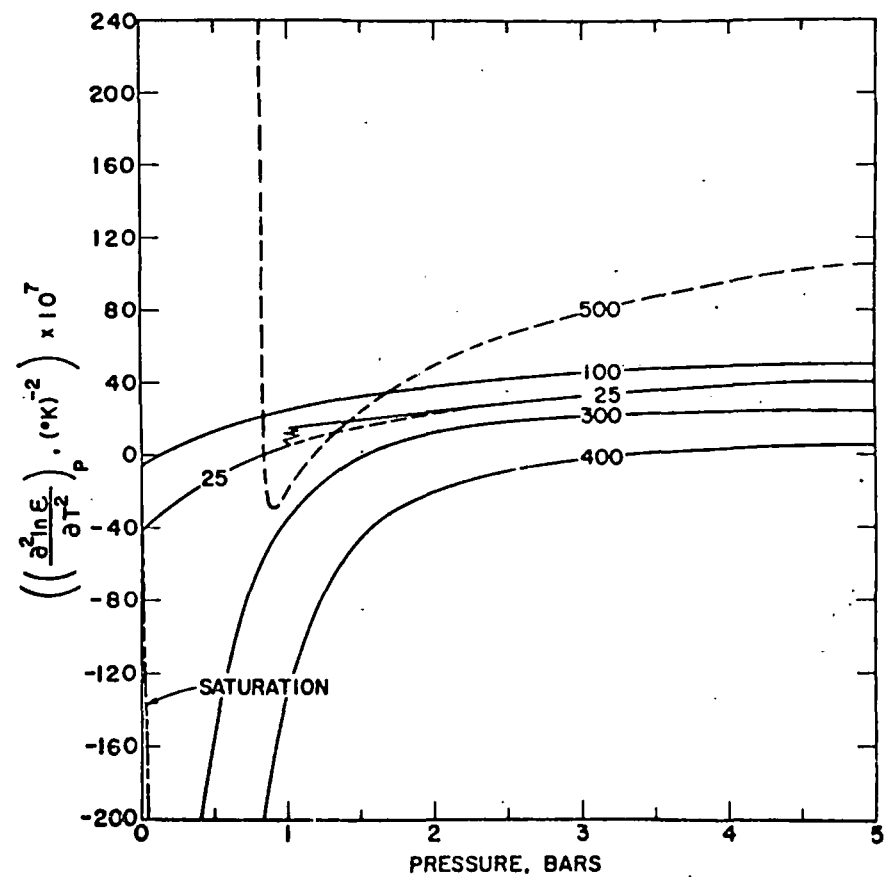

Fig. 32. Partial derivatives of $(\partial \ln \epsilon/\partial T)_\rho$ with respect to temperature at constant pressure (table 19) as a function of pressure at constant temperature (labeled in °C) computed from equations (19) through (21), (25), (27), (33), (37), (39), (43), (47), (49), and (51) and coefficients in tables 4, 5, 6, 9, 10, and 14.

ENTROPY

Computed values of the third law molal entropy of H_2O are given in table 27 and plotted in figures 37 and 38. Entropies for pressures ≤ a kilobar were obtained by first evaluating the combined partial derivatives of equations (14) through (17) with respect to temperature at constant density; that is,

$$-\left(\frac{\partial \psi}{\partial T}\right)_\rho = -\left(\frac{\partial A}{\partial T}\right)_\rho - S_{triple} = S - S_{triple}$$

$$= -\left(\frac{\partial \psi^\circ}{\partial T}\right)_\rho - R(\ln \rho + \rho Q) - RT\rho\left(\frac{\partial Q}{\partial T}\right)_\rho \qquad (70)$$

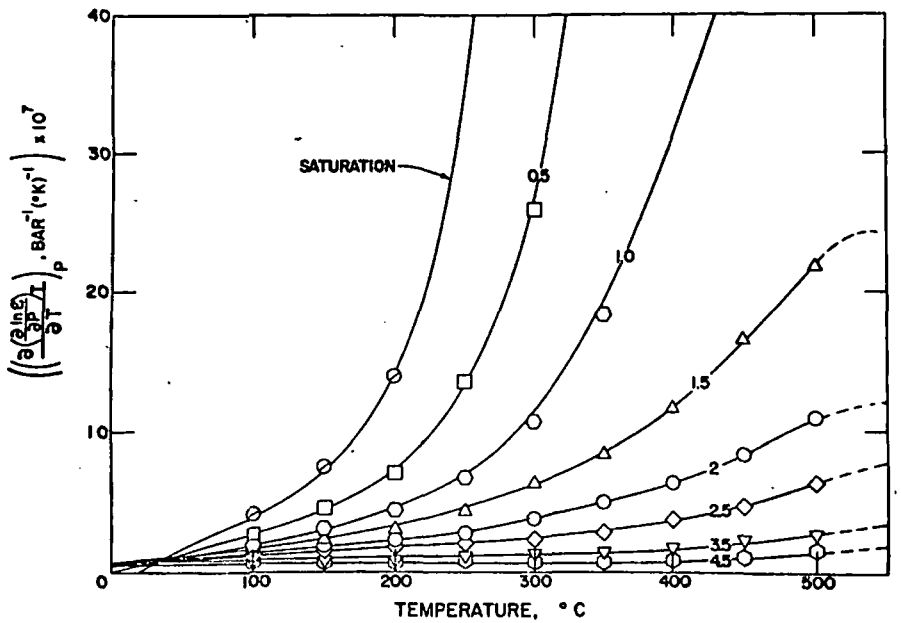

Fig. 33. Partial derivative of $(\partial \ln \epsilon/\partial P)_T$ with respect to temperature at constant pressure (table 20) as a function of temperature at constant pressure (labeled in kb) computed from equations (19) through (22), (24), (25), (32), (33), (36), (38), (39), (42), (47), (48), (49), (50) through (53), and (56) and coefficients in tables 4, 5, 6, 9, 10, and 14 (curves). The symbols represent corresponding finite difference derivatives computed from the finite difference derivatives of ln ϵ plotted in figure 25.

where S_{triple} refers to the third law molal entropy of liquid H_2O at the triple point in joules g^{-1} (table 2), and $(\partial Q/\partial T)_\rho$ and $(\partial \psi^\circ/\partial T)_\rho$ represent partial derivatives of equations (15) and (16) given in the appendix (eqs A-43 and A-48, respectively). Entropies above a kilobar were computed from

$$S_{P,T} = S_{P=1000,T} - \left(\int_{P=1000}^{P} V\alpha dP\right)_T \qquad (71)$$

where $S_{P,T}$ stands for the third law molal entropy at the pressure and temperature of interest, $S_{P=1000,T}$ refers to the corresponding entropy at 1 kb, and V and α represent the molal volume and coefficient of isobaric thermal expansion as a function of pressure at the temperature of interest. The integral in equation (71) for region A in figure 9 was evaluated numerically using equations (21), (33), and (39) together with an equal-interval integration routine adapted from Arden and Astill (1970).

For temperatures > 550°C in region B of figure 9, equation (71) was combined with the pressure integral of equation (39) to give

$$S_{P,T} = S_{P=1000,T} - \sum_{i=0}^{5}\sum_{j=0}^{6-i} i\,\dot{D}_{ij}\,T^{i-1}\,((1800)^{j+1} - (1000)^{j+1})/(j+1)$$
$$- \sum_{i=0}^{9}\sum_{j=0}^{9-i} i\,D_{ij}\,T^{i-1}\,(P^{j+1} - (1800)^{j+1})/(j+1) \qquad (72)$$

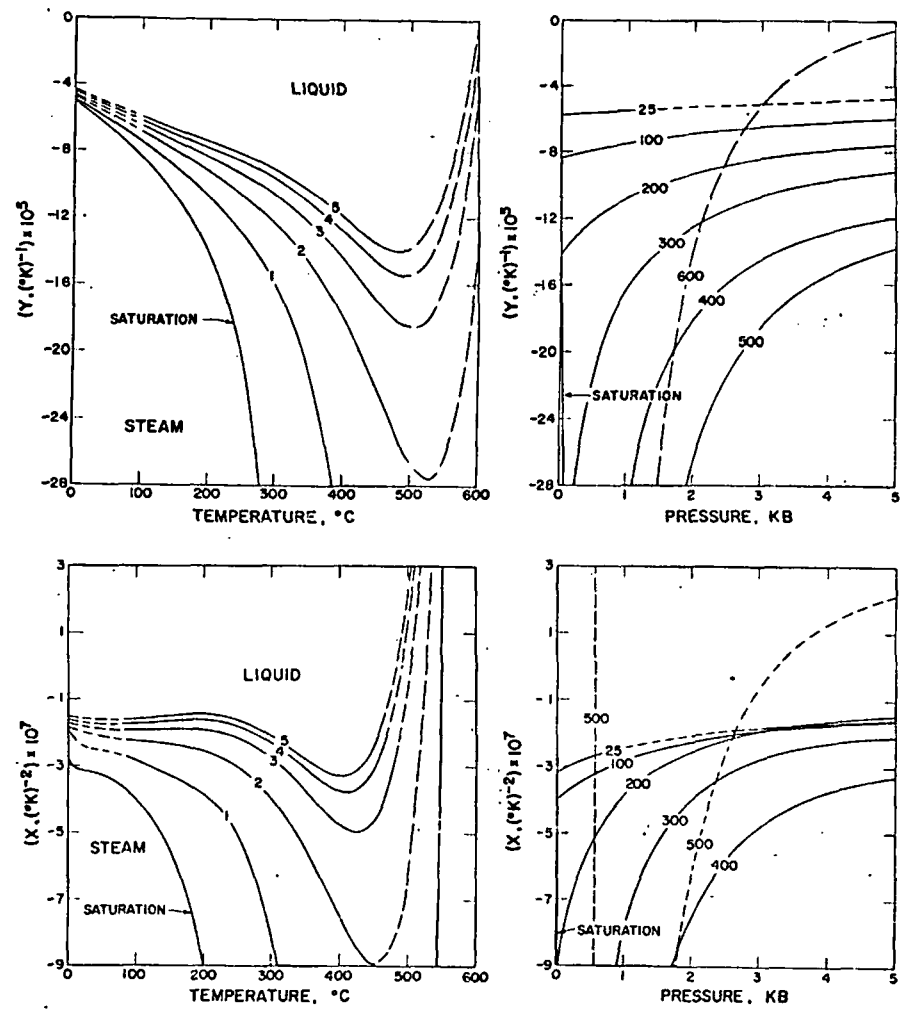

Fig. 34. Dependence of Y (table 22) and X (table 23) on temperature at constant pressure (labeled in kb) and pressure at constant temperature (labeled in °C) computed from equations (65) and (66) and values of ε, $(\partial \ln \varepsilon/\partial T)_P$, and $(\partial^2 \ln \varepsilon/\partial T^2)_P$ in tables 15, 17, and 19.

where D_{ij} and $\dot{D}_{ij}$ represent the arrays of fit coefficients for regions B and C, respectively, in table 10. For temperatures ≤ 550°C in region B, $\dot{D}_{ij}$ in equation (72) is set to zero, and $S_{P=1000,T}$ is replaced by $S_{P=1800,T}$ in region A. Similarly, for temperatures and pressures in region C, D_{ij} in equation (72) is set to zero, and (1800) is replaced by P.

The entropies computed in this study for pressures above a kilobar are generally in close agreement with those calculated by Burnham, Holloway, and Davis (1969b); those for pressures below a kilobar are identical (except for the unit conversion and difference in conventions) to those given by Keenan and others (1969). Estimated uncertainties in the entropies given in table 26 for pressures above a kilobar are of the order of 0.5 percent or less.

It can be seen in figure 37 that the entropy of H_2O in the liquid phase region decreases only slightly and exhibits a near-linear dependence

TABLE 27

Third law molal entropy (S) in cal mole^{-1} (°K)$^{-1}$ computed from equations (70) through (72), values of V and α in tables 3 and 7, and data in table 2—see figures 37 through 39

t	PRESSURE, KB									
(°C)	SAT	0.5	1	2	3	4	5	6	7	8
25	16.71	16.65	16.58	16.4	16.2	16.1	15.9	15.8	15.6	(15.5)
50	18.16	18.06	17.97	17.8	17.6	17.4	17.2	17.1	16.9	(16.8)
75	19.50	19.38	19.26	19.0	18.8	18.6	18.5	18.3	18.1	(17.9)
100	20.76	20.60	20.46	20.2	20.0	19.8	19.6	19.4	19.2	(19.0)
125	21.94	21.75	21.59	21.3	21.1	20.8	20.6	20.4	20.2	(20.1)
150	23.06	22.84	22.66	22.3	22.1	21.8	21.6	21.4	21.2	(21.0)
175	24.14	23.88	23.67	23.3	23.0	22.8	22.5	22.3	22.1	(21.9)
200	25.17	24.88	24.64	24.2	23.9	23.7	23.4	23.2	23.0	(22.8)
225	26.17	25.84	25.56	25.1	24.8	24.5	24.2	24.0	23.8	(23.6)
250	27.16	26.76	26.45	26.0	25.6	25.3	25.0	24.8	24.6	(24.4)
275	28.14	27.67	27.31	26.8	26.4	26.1	25.8	25.6	25.3	(25.1)
300	29.14	28.57	28.14	27.6	27.1	26.8	26.5	26.3	26.1	(25.8)
325	30.20	29.46	28.95	28.3	27.9	27.5	27.2	27.0	26.7	(26.5)
350	31.40	30.38	29.75	29.0	28.6	28.2	27.9	27.6	27.4	(27.2)
375		31.34	30.54	29.7	29.2	28.8	28.5	28.2	28.0	(27.8)
400		32.37	31.33	30.4	29.9	29.5	29.1	28.9	28.6	(28.4)
425		33.53	32.11	31.1	30.5	30.1	29.7	29.4	29.2	(29.0)
450		34.89	32.90	31.7	31.1	30.7	30.3	30.0	29.7	(29.5)
475		36.27	33.67	32.4	31.7	31.2	30.8	30.5	30.2	(30.0)
500		37.40	34.44	33.0	32.2	31.7	31.3	31.0	30.7	(30.5)
525		38.30	35.20	33.5	32.8	32.2	31.8	31.5	31.2	(30.9)
550		39.02	35.94	34.1	33.3	32.7	32.3	32.0	31.7	(31.4)
575		39.64	36.65	34.6	33.7	33.1	32.7	32.3	32.0	(31.8)
600		40.18	37.31	35.2	34.2	33.6	33.2	32.8	32.5	(32.3)
625		40.67	37.93	35.7	34.7	34.1	33.7	33.3	33.0	(32.7)
650		41.11	38.50	36.2	35.2	34.6	34.1	33.8	33.4	(33.2)
675		41.53	39.03	36.8	35.7	35.1	34.6	34.2	33.9	(33.6)
700		41.91	39.52	37.2	36.2	35.5	35.0	34.6	34.3	(34.0)
725		42.27	39.98	(37.7)	(36.6)	(35.9)	(35.4)	(35.0)	(34.7)	(34.4)
750		42.61	40.41	(38.1)	(37.0)	(36.3)	(35.8)	(35.4)	(35.1)	(34.8)
775		42.94	40.81	(38.5)	(37.4)	(36.7)	(36.2)	(35.8)	(35.4)	(35.1)
800		43.24	41.18	(38.9)	(37.8)	(37.1)	(36.5)	(36.1)	(35.8)	(35.5)
825		43.54	41.54							
850		43.82	41.87							
875		44.10	42.19							
900		44.36	42.50							

on pressure as pressure increases isothermally from 0.001 to 10 kb. In the steam phase region the entropy of H_2O increases rapidly and asymptotically with decreasing pressure at constant temperature. With increasing pressure above ~ 2 kb, the effect of the critical phenomenon on the entropy of H_2O diminishes and disappears (fig. 38). Isentropes are plotted in figure 39, where it can be seen that $(\partial P/\partial T)_S$ (which is equal to $C_P/TV\alpha$) at 25°C decreases from ~ 550 bar $(°K)^{-1}$ at low pressures to ~ 330 bar $(°K)^{-1}$ at 5 kb, and then increases to ~ 380 bar $(°K)^{-1}$ at 10 kb.

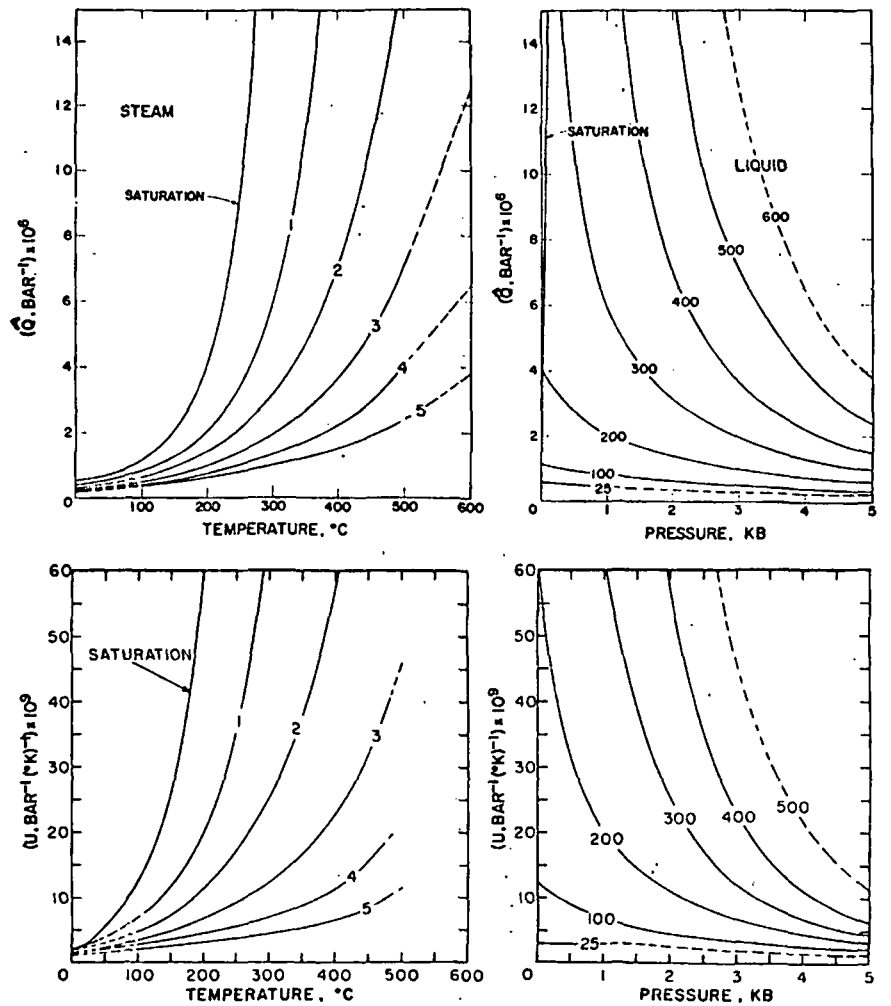

Fig. 35. Dependence of $\hat{Q}$ (table 24) and U (table 25) on temperature at constant pressure (labeled in kb) and pressure at constant temperature (labeled in °C) computed from equations (67) and (68) and values of ϵ, $(\partial \ln \epsilon/\partial P)_T$, $(\partial \ln \epsilon/\partial T)_P$, and $(\partial(\partial \ln \epsilon/\partial P)_T/\partial T)_P$ in tables 15 through 17 and 20.

As entropy and temperature increase at a given pressure, $(\partial P/\partial T)_S$ decreases asymptotically, reaching values < 1 bar $(°K)^{-1}$ in the steam phase region.

HELMHOLTZ AND GIBBS FREE ENERGIES

The values of the apparent molal Helmholtz free energy of formation (ΔA) of H_2O for pressures ≤ a kilobar in table 28 and figures 40 and 41 were computed from equations (9) and (14) through (17) using data given in table 2. Corresponding apparent molal Gibbs free energies of formation (table 29 and figs. 42 and 43) were then calculated from equations (3) and (8) using data in table 2, values of $A - A_{triple}$ computed from equations (14) through (17), and specific volumes calculated from equation (19). For pressures greater than a kilobar, apparent molal Gibbs free energies of formation were computed from

$$\Delta G_{P,T} = \Delta G_{P=1000,T} + \left(\int_{P=1000}^{P} VdP \right)_T \tag{73}$$

with the aid of equation (21), which can be integrated for region 1 in figure 3 to give

$$\left(\int_{P=1000}^{P} VdP \right)_T = \sum_{i=0}^{8} \left(\mathring{a}_{i0}\, t^i \ln (P^*/1000) - \sum_{j=1}^{8-i} \mathring{a}_{ij}\, t^i (P^{*-j} - (1000)^{-j}/j \right)$$

$$+ \sum_{i=0}^{9} \left(a_{i0}\, t^i \ln (P/P^*) + \sum_{j=1}^{9-i} a_{ij}\, t^i (P^j - P^{*j})/j \right) \tag{74}$$

where a_{ij} designates the array of fit coefficients for region 1 (table 5), $\mathring{a}_{ij}$ stands for the array of fit coefficients for region 2 (designated as a_{ij} in table 6), and $P^* = 1000$ bars for temperatures ≤ 410°C but corresponds to the upper pressure limit of region 2 in figure 3 for 410°C ≤ t < 800°C where $P^* = 1300 + 1.2249\,(t - 410)$. For pressures and temperature in region 2 of figure 3, a_{ij} in equation (74) is set to zero and P^* is replaced by P. Values of ΔA at pressures above a kilobar were computed from

$$\Delta A_{P,T} = \Delta A_{P=1000,T} + (\Delta G_{P,T} - \Delta G_{P=1000,T}) - PV_{P,T} + 1000V_{P=1000,T} \tag{75}$$

The results of the free energy calculations are summarized in tables 28 and 29 and figures 40 through 45. Estimated uncertainties in the values given in tables 28 and 29 for pressures > a kilobar are of the order of 0.1 percent or less.

As indicated above, the Gibbs free energies of H_2O calculated by Burnham, Holloway, and Davis (1969b) are not consistent with those computed in this study, which also differ from those reported by Pistorius and Sharp (1960, 1961). The latter authors referred their values to the internal energy of an ideal gas at absolute zero. Burnham, Holloway, and Davis used equation (4) to calculate Gibbs free energies for pressures below a kilobar from values of H and S given by Bain (1964), which are actually equal to $H-H_{triple}$ and $S-S_{triple}$, respectively. The Gibbs free energy values reported by Burnham, Holloway, and Davis thus contravene the third law properties of H_2O in other compilations by requiring

$$G - G_{triple} = H - H_{triple} - T(S - S_{triple}) \quad . \qquad (76)$$

Equation (76) is valid only if temperature is held constant or $S_{triple} = 0$, which is the convention ($S_{triple} = G_{triple} = 0$) adopted by Bain in accord

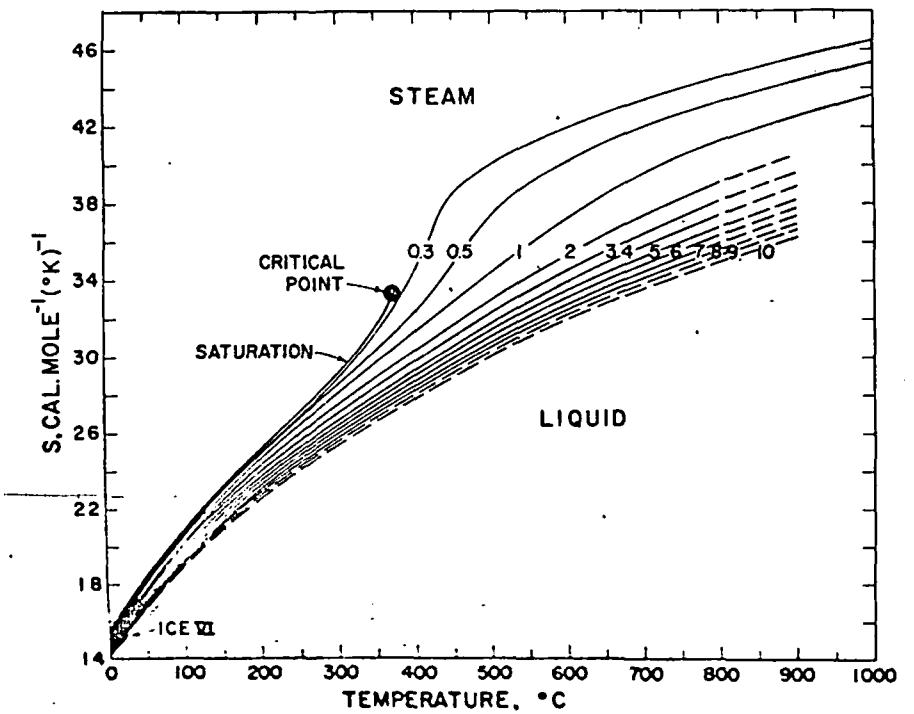

Fig. 38. Third law molal entropy (table 27) as a function of temperature at constant pressure (labeled in kb) computed from equations (19) through (21), (25), (33), and (70) through (72), data in table 2, and coefficients in tables 4, 5, 6, 9, and 10.

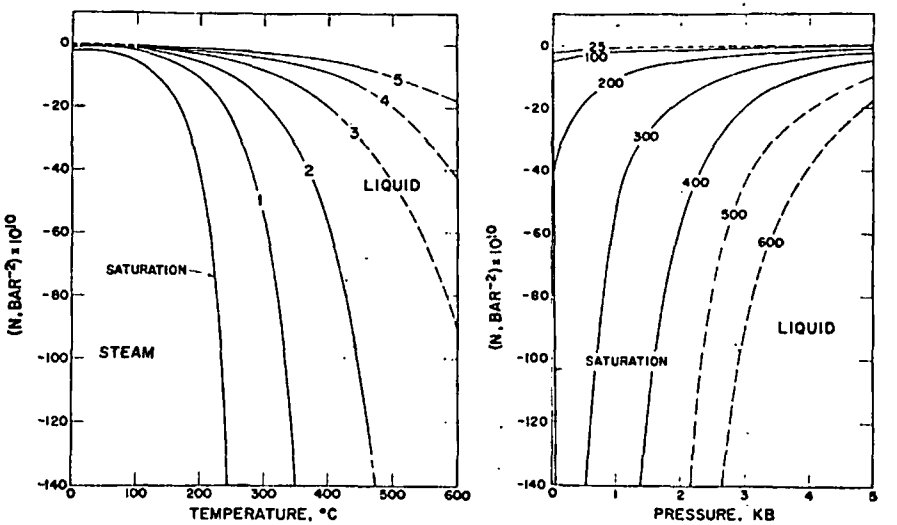

Fig. 36. Dependence of N (table 26) on temperature at constant pressure (labeled in kb) and pressure at constant temperature (labeled in °C) computed from equation (69) and values of ε, $(\partial \ln \varepsilon/\partial P)_T$ and $(\partial^2 \ln \varepsilon/\partial P^2)_T$ in tables 15, 16, and 18.

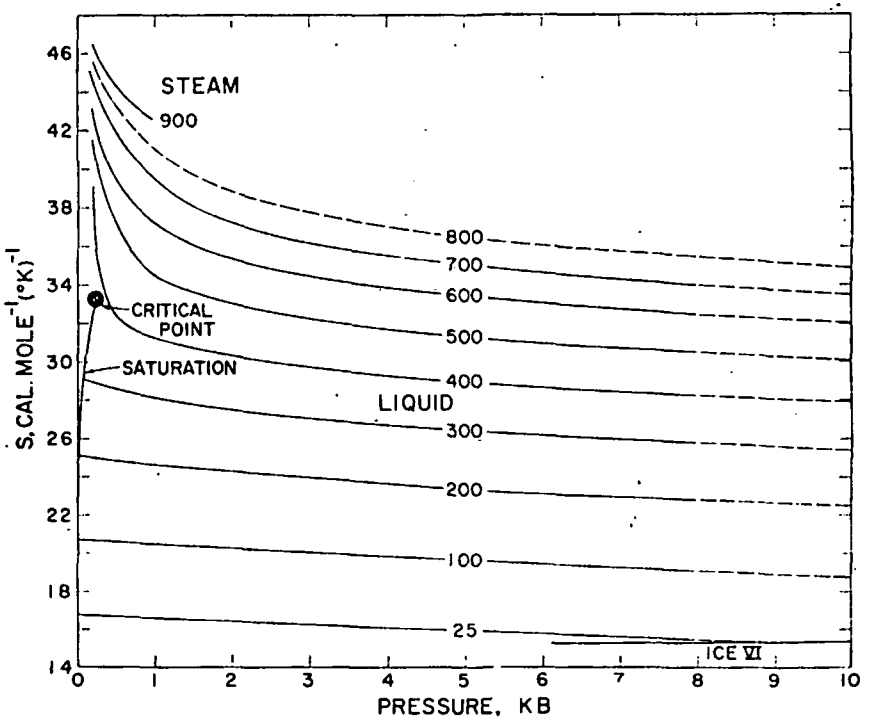

Fig. 37. Third law molal entropy (table 27) as a function of pressure at constant temperature (labeled in °C) computed from equations (19) through (21), (25), (33), and (70) through (72), data in table 2, and coefficients in tables 4, 5, 6, 9, and 10.

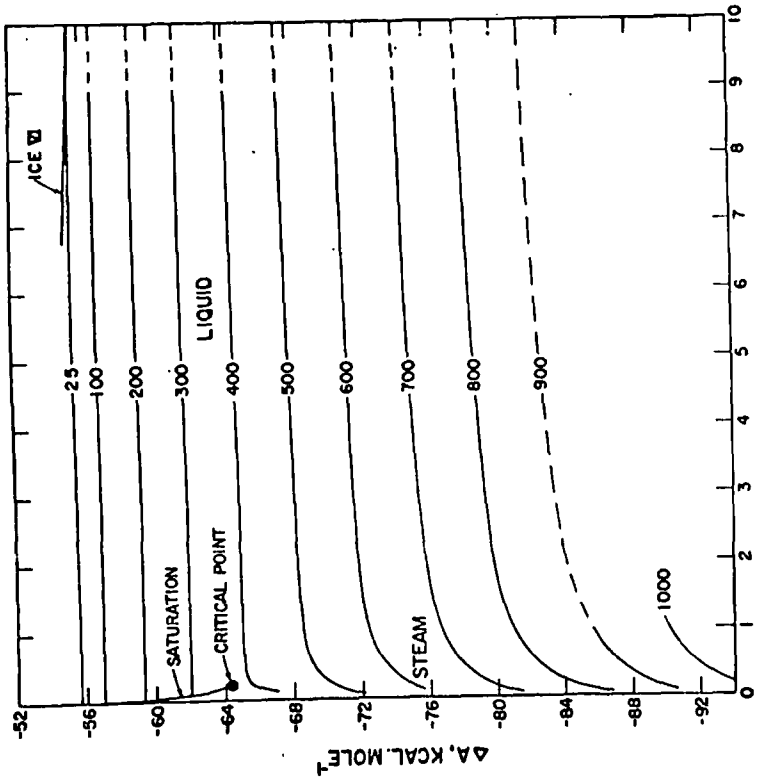

Fig. 40. Apparent molal Helmholtz free energy of formation (table 28) as a function of pressure at constant temperature (labeled in °C) computed from equations (3), (8), (9), (14) through (17), (19), (20), and (73) through (75), data in table 2, and coefficients in tables 4, 5, and 6.

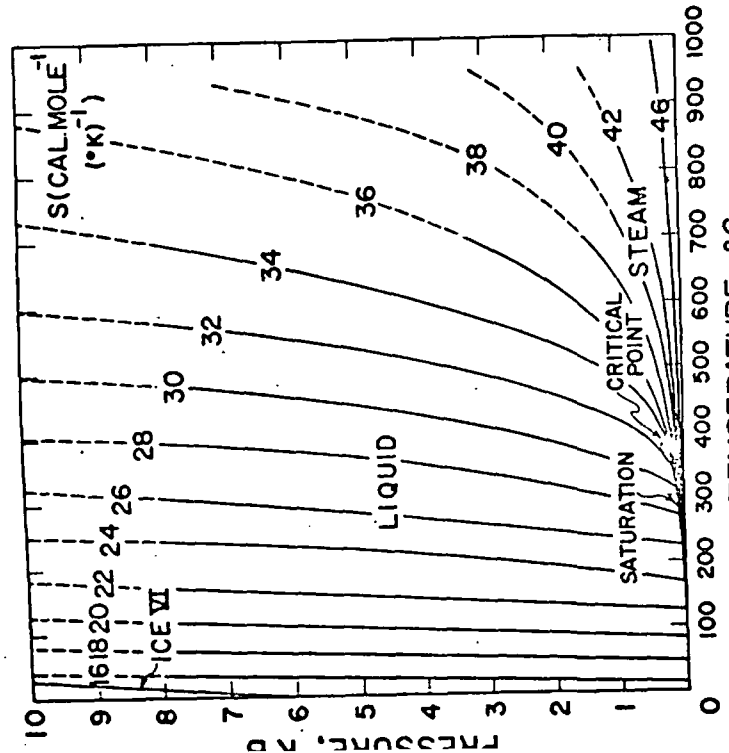

Fig. 39. Isentropes (labeled in cal mole^{-1} (°K)$^{-1}$) as a function of temperature and pressure (table 27 and figs. 37 and 38).

with the 5th International Conference on the Properties of Steam. Burnham, Holloway, and Davis then used equation (73) to compute Gibbs free energies of H_2O at higher pressures. The Gibbs free energies computed in this study differ from those given by Burnham, Holloway, and Davis by $\Delta G_{triple} - S_{triple}(T - T_{tr})$.

It can be seen in figure 40 that the apparent molal Helmholtz free energy of formation of H_2O is relatively insensitive to isothermal changes in pressure compared to its Gibbs counterpart (fig. 42), except in the steam phase region where the two variables decrease rapidly with decreasing pressure and approach each other at low pressures. At high pressures, both ΔG and ΔA approach linear functions of pressure at constant temperature, but as temperature increases at constant pressure, ΔA becomes increasingly more sensitive to pressure than ΔG (figs. 41 and 43). At 900°C, an increase in pressure from 1 to 10 kb causes a change of more than 7 kcal mole^{-1} in ΔG compared to <5 kcal mole^{-1} in ΔA; in contrast, at 30°C the same pressure change results in ~ 3.5 kcal mole^{-1} of change in ΔG but < 0.5 kcal mole^{-1} in ΔA. Isopleths for these two functions are shown in figures 44 and 45 where $(\partial P/\partial T)_A$ (which is equal to $(S + PV\alpha)/PV\beta$) can be compared with $(\partial P/\partial T)_G$ (that is, S/V), which is considerably more positive throughout the pressure-temperature range considered.

ACTIVITY AND FUGACITY

The activity (a) of H_2O is defined as

$$a = f/f^\circ \tag{77}$$

where f° stands for the fugacity of H_2O in the standard state (which is specified at 1 bar). The fugacity of H_2O is related to its pressure by

$$f = \chi P \tag{78}$$

where χ is the fugacity coefficient. Taking account of the relation,

$$\ln a = \frac{G - G^\circ}{RT} \tag{79}$$

it follows that

$$\left(\frac{\partial \ln a}{\partial P}\right)_T = \left(\frac{\partial \ln f}{\partial P}\right)_T = \frac{V}{RT} \tag{80}$$

and we can write

$$\left(\frac{\partial \ln \chi}{\partial P}\right)_T = \frac{V}{RT} - \frac{1}{P} \tag{81}$$

Hence, for a given temperature,

$$\ln \chi = \int_0^P \left(\frac{V}{RT} - \frac{1}{P}\right) dP = \int_0^P (z-1)\, d\ln P \qquad (82)$$

where z is the compressibility factor defined by

$$z = PV/RT \qquad (83)$$

For pressures $\leq$ a kilobar, the fugacity coefficient of H_2O can be computed by first rearranging equation (19) as

$$z - 1 = \rho Q + \rho^2 \left(\frac{\partial Q}{\partial \rho}\right)_T \qquad (84)$$

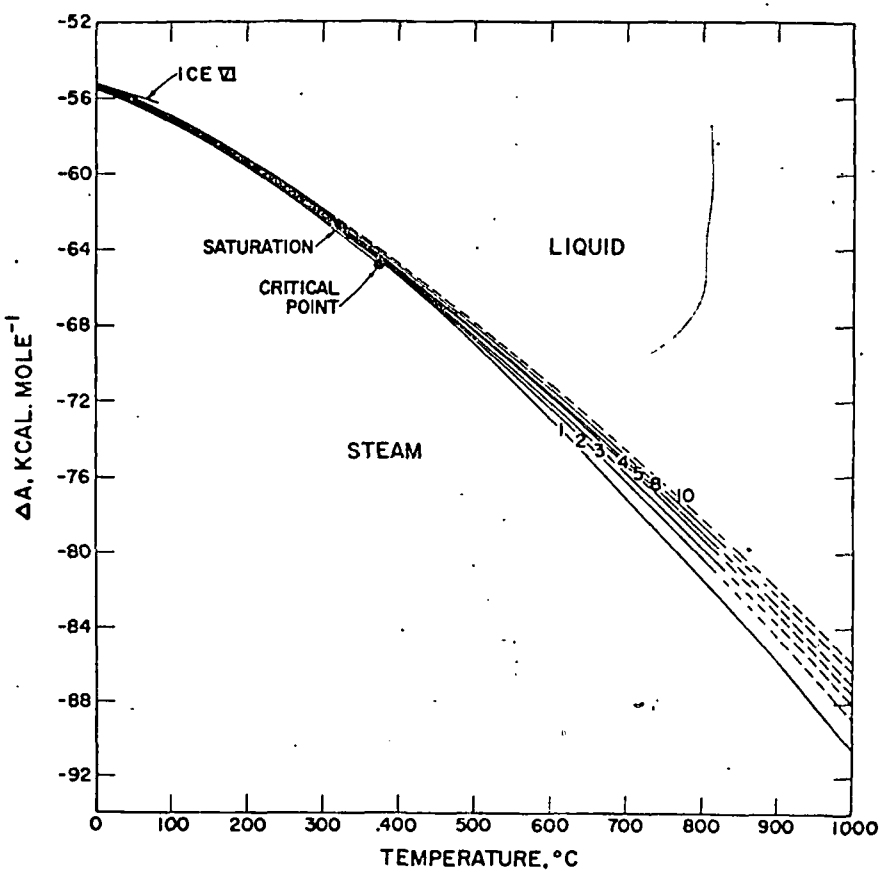

Fig. 41. Apparent molal Helmholtz free energy of formation (table 28) as a function of temperature at constant pressure (labeled in kb) computed from equations (3), (8), (9), (14) through (17), (19), 20), and (73) through (75), data in table 2, and coefficients in tables 4, 5, and 6.

TABLE 28

Apparent molal Helmholtz free energy of formation (ΔA) in kcal mole^{-1} computed from equations (3), (8), (9), (14) through (17), and (73) through (75), data in table 2, and values of V in table 3—see figures 40, 41, and 44

t	PRESSURE, KB										
(°C)	SAT	0.5	1	2	3	4	5	6	7	8	9
25	-55.812	-55.809	-55.804	-55.78	-55.76	-55.73	-55.69	-55.66	-55.62	-55.58	-55.54
50	-56.248	-56.246	-56.240	-56.22	-56.19	-56.16	-56.13	-56.09	-56.06	-56.02	-55.98
75	-56.719	-56.717	-56.711	-56.69	-56.66	-56.63	-56.60	-56.56	-56.52	-56.48	-56.44
100	-57.222	-57.220	-57.213	-57.19	-57.17	-57.13	-57.10	-57.06	-57.02	-56.98	-56.94
125	-57.756	-57.754	-57.747	-57.72	-57.69	-57.66	-57.63	-57.59	-57.54	-57.50	-57.46
150	-58.319	-58.316	-58.308	-58.28	-58.25	-58.22	-58.18	-58.14	-58.09	-58.05	-58.01
175	-58.909	-58.905	-58.897	-58.87	-58.83	-58.80	-58.76	-58.71	-58.67	-58.62	-58.58
200	-59.526	-59.521	-59.511	-59.48	-59.44	-59.40	-59.36	-59.31	-59.26	-59.22	-59.17
225	-60.168	-60.162	-60.150	-60.12	-60.07	-60.03	-59.98	-59.93	-59.88	-59.83	-59.78
250	-60.835	-60.828	-60.814	-60.78	-60.73	-60.68	-60.63	-60.58	-60.52	-60.47	-60.42
275	-61.528	-61.518	-61.500	-61.46	-61.40	-61.35	-61.29	-61.24	-61.18	-61.13	-61.07
300	-62.246	-62.233	-62.210	-62.16	-62.10	-62.04	-61.98	-61.92	-61.86	-61.81	-61.74
325	-62.994	-62.973	-62.943	-62.88	-62.82	-62.75	-62.69	-62.62	-62.56	-62.50	-62.44
350	-63.776	-63.740	-63.699	-63.63	-63.55	-63.48	-63.41	-63.34	-63.28	-63.21	-63.14
375		-64.537	-64.479	-64.39	-64.31	-64.23	-64.15	-64.08	-64.01	-63.94	-63.87
400		-65.370	-65.283	-65.17	-65.08	-64.99	-64.91	-64.83	-64.75	-64.68	-64.60
425		-66.253	-66.112	-65.98	-65.87	-65.77	-65.68	-65.58	-65.52	-65.44	-65.36
450		-67.211	-66.969	-66.80	-66.68	-66.57	-66.47	-66.38	-66.30	-66.21	-66.13
475		-68.249	-67.853	-67.64	-67.50	-67.38	-67.28	-67.18	-67.09	-67.00	-66.91
500		-69.325	-68.766	-68.50	-68.35	-68.21	-68.10	-67.99	-67.90	-67.80	-67.70
525		-70.411	-69.708	-69.38	-69.20	-69.06	-68.93	-68.82	-68.72	-68.61	-68.51
550		-71.502	-70.679	-70.28	-70.08	-69.92	-69.78	-69.66	-69.55	-69.44	-69.33
575		-72.597	-71.676	-71.20	-70.97	-70.79	-70.65	-70.52	-70.40	-70.28	-70.17
600		-73.697	-72.694	-72.14	-71.87	-71.68	-71.52	-71.39	-71.26	-71.14	-71.02
625		-74.803	-73.731	-73.08	-72.79	-72.58	-72.41	-72.27	-72.13	-72.00	-71.87
650		-75.914	-74.781	-74.05	-73.72	-73.49	-73.31	-73.16	-73.01	-72.88	-72.74
675		-77.031	-75.845	-75.03	-74.67	-74.42	-74.22	-74.06	-73.91	-73.76	-73.62
700		-78.154	-76.918	-76.03	-75.63	-75.36	-75.15	-74.97	-74.81	-74.66	-74.51
725		-79.283	-78.001	-77.04	-76.60	-76.30	-76.08	-75.90	-75.73	-75.57	-75.41
750		-80.418	-79.092	-78.06	-77.58	-77.27	-77.03	-76.83	-76.65	-76.49	-76.32
775		-81.558	-80.191	-79.09	-78.57	-78.24	-77.99	-77.78	-77.59	-77.41	-77.24
800		-82.705	-81.298	-80.13	-79.58	-79.22	-78.95	-78.73	-78.54	-78.35	-78.17
825		-83.857	-82.411								
850		-85.014	-83.530								
875		-86.177	-84.656								
900		-87.346	-85.788								

which can be combined with equation (82) to give

$$\ln \chi_{P,T} = \int_0^P \left(\rho Q + \rho^2 \left(\frac{\partial Q}{\partial \rho}\right)_T \right) d\ln P \qquad (85)$$

The integral on the right side of equation (85) differs insignificantly from the corresponding integral for P = 0.001 to P = 1, which yields the values of $\chi_{1\ bar}$ shown in table 25. Below 100°C, the values of $\chi_{1\ bar}$ in table 30 correspond to those of metastable steam.

For the standard state adopted in this study, the fugacity coefficient of H_2O at 1 bar is related to the apparent molal Gibbs free energy of H_2O in the standard state (ΔG°) by[3]

$$\Delta G^\circ = \Delta G_{1\ bar} - RT \ln \chi_{1\ bar} \qquad (86)$$

[3] The values of $\Delta G_{1\ bar}$ and $\chi_{1\ bar}$ in tables 25 and 31, respectively, are consistent with $\Delta G^\circ_{f,\ 298.15^\circ K} = -56{,}687$ cal mole^{-1}, which corresponds to the standard Gibbs free energy of formation of H_2O_{liq} from its elements in their stable form at 25°C and 1 bar. The value of $\Delta G^\circ_{f,\ 298.15^\circ K}$ computed in this study compares favorably with that given by Wagman and others (1968), who report -56,690 cal mole^{-1}.

which permits calculation of the fugacity and fugacity coefficient of H_2O at higher pressures from equations (78) and (79). Values of f and χ computed in this manner (tables 30 and 31) are in close agreement with corresponding values given by Burnham, Holloway, and Davis (1969b), Haas (1970), and Anderson (1964, 1967). Estimated uncertainties in the values of f and χ given in tables 30 and 31 are of the order of 1 percent or less.

The fugacity of H_2O is plotted in figures 46 and 47, where it can be seen that H_2O exhibits relatively large negative departures from ideality at low temperatures and pressures which diminish with increasing pressure and temperature toward line A′ in figure 48. At pressures and temperatures along this line, H_2O behaves as an ideal supercritical phase, but at higher pressures and temperatures it exhibits positive departures from ideality which increase with increasing pressure and temperature. Although not shown in figure 48, line A′ reverses its trend at higher temperatures and swings back toward the steam phase region at low pressures and high temperatures, where H_2O behaves as an ideal gas.

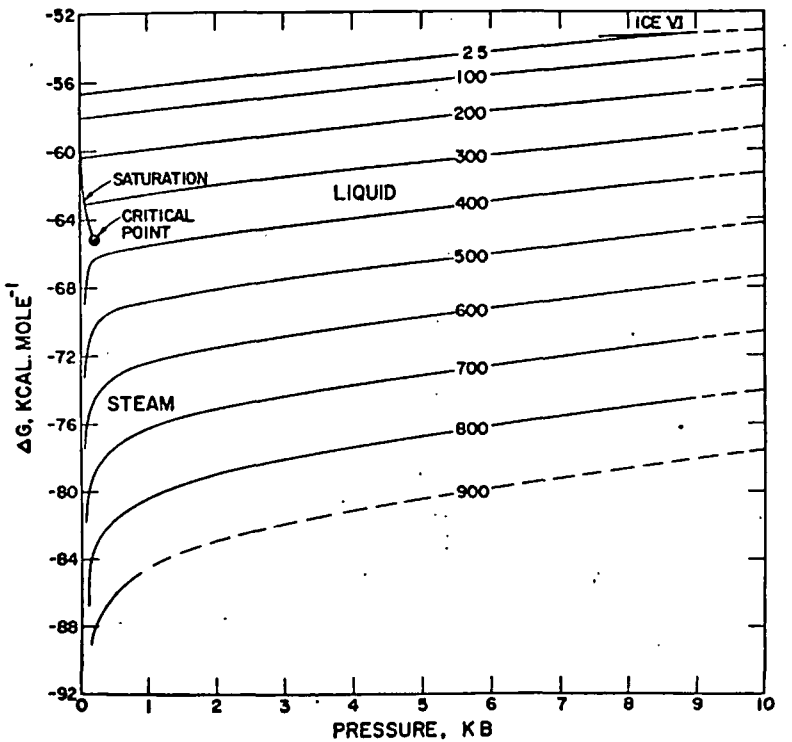

Fig. 42. Apparent molal Gibbs free energy of formation (table 29) as a function of pressure at constant temperature (labeled in °C) computed from equations (3), (8), (9), (14) through (17), (19), (20), (73), and (74), data in table 2, and coefficients in tables 4, 5, and 6.

INTERNAL ENERGY AND ENTHALPY

The apparent molal internal energies of formation of H_2O (ΔE) given in table 32 and plotted in figures 49 and 50 were computed from

$$\Delta E = \Delta E_{triple} + (\Delta A - \Delta A_{triple}) + TS - T_{tr} S_{triple} \quad (87)$$

using data in table 2 and the values of S and ΔA computed above. Corresponding values of the apparent molal enthalpy of formation of H_2O (table 33) were then calculated in a similar manner from

$$\Delta H = \Delta H_{triple} + (\Delta E - \Delta E_{triple}) + PV - P_{tr} V_{triple} \quad (88)$$

It can be seen in figure 49 that $(\partial \Delta E/\partial P)_T$ is negative throughout the pressure-temperature region considered ($(\partial \Delta E/\partial P)_T = V(P\beta - T\alpha)$), which

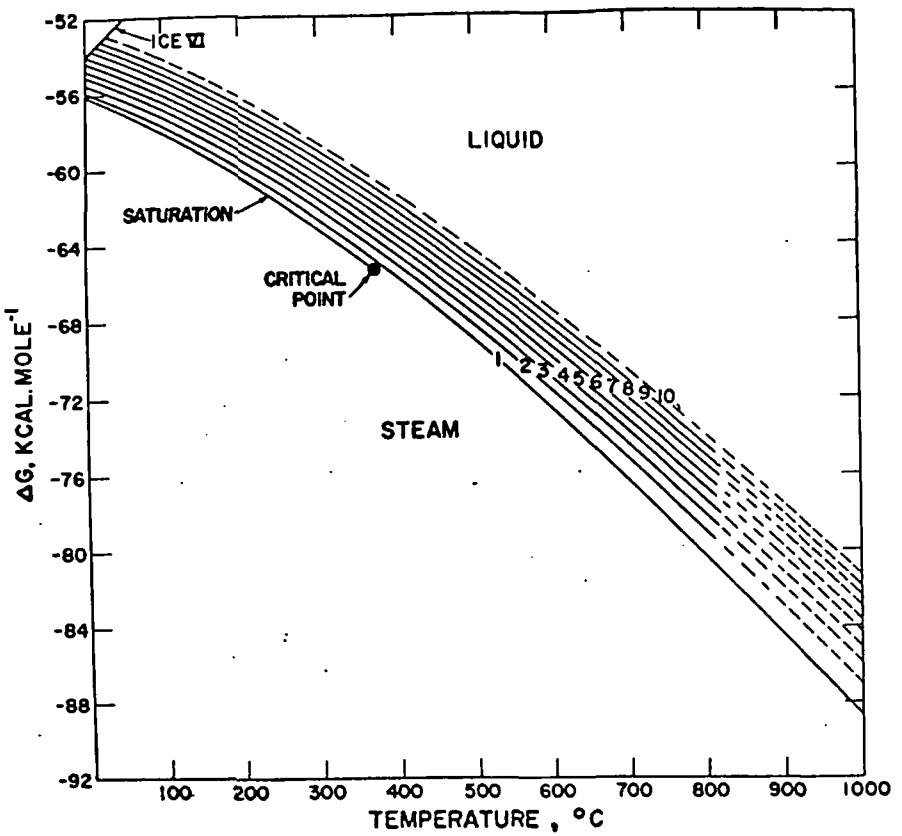

Fig. 43. Apparent molal Gibbs free energy of formation (table 29) as a function of temperature at constant pressure (labeled in kb) computed from equations (3), (8), (9), (14) through (17), (19), (20), (73), and (74), data in table 2, and coefficients in tables 4, 5, and 6.

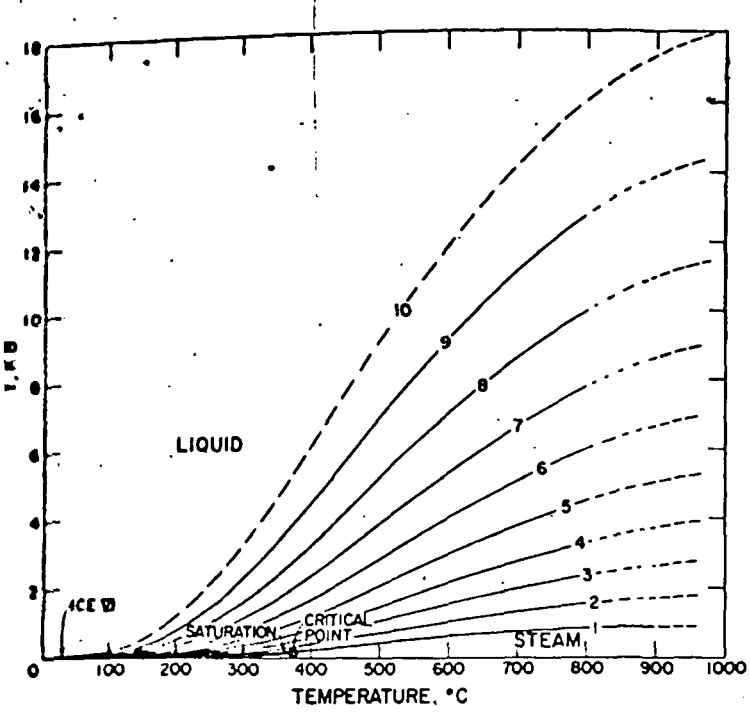

Fig. 46. Fugacity (table 31) as a function of temperature at constant pressure (labeled in kb) computed from equation (78) and the fugacity coefficients in table 30.

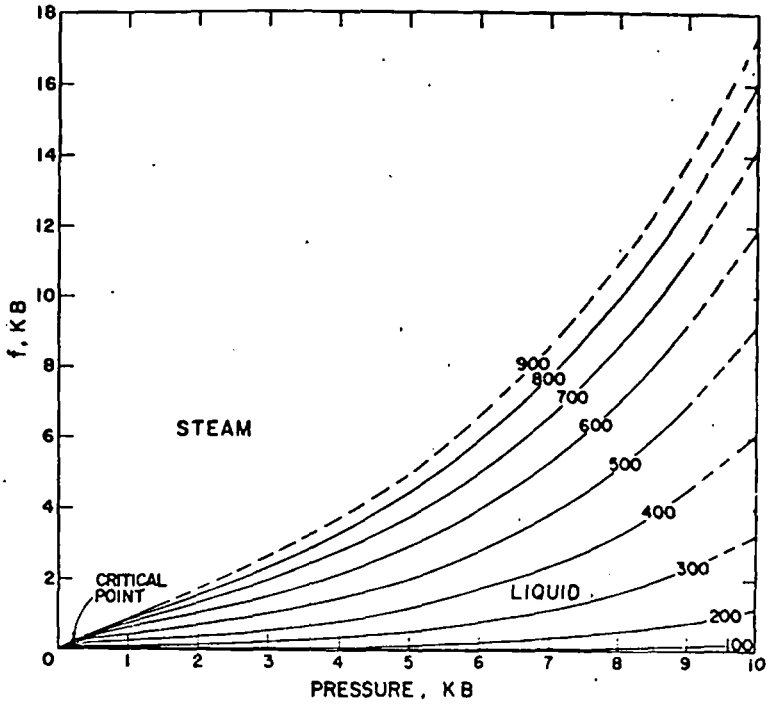

Fig. 47. Fugacity (table 31) as a function of pressure at constant temperature (labeled in kb) computed from equation (78) and the fugacity coefficients in table 30.

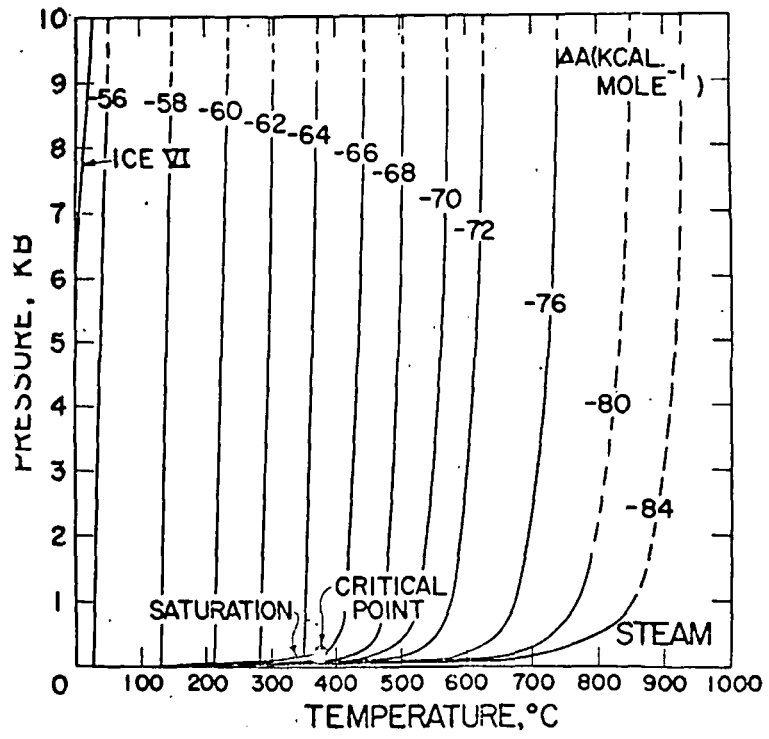

Fig. 44. Isopleths of the apparent molal Helmholtz free energy of formation (labeled in kcal mole^{-1}) as a function of temperature and pressure (table 28 and figs. 40 and 41).

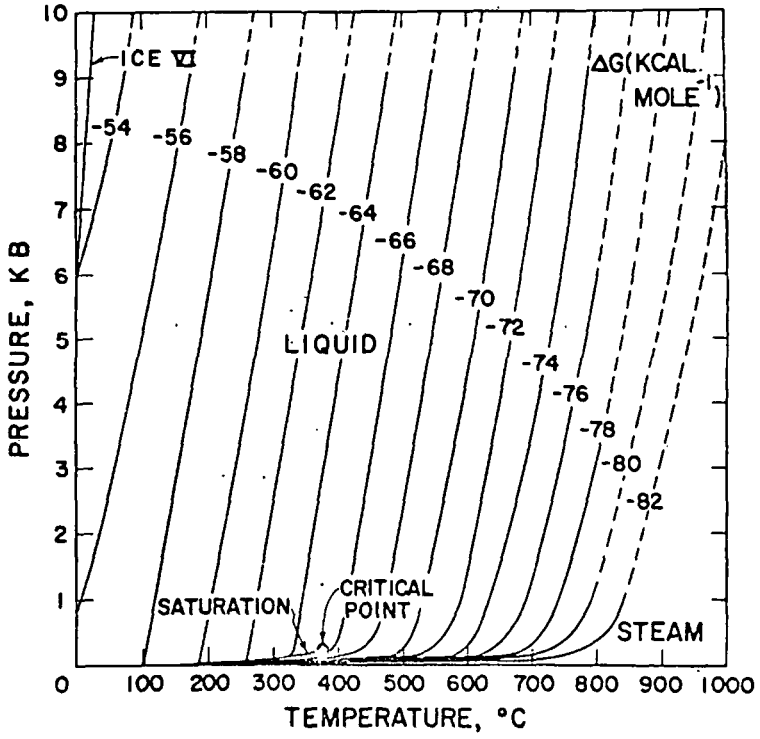

Fig. 45. Isopleths of the apparent molal Gibbs free energy of formation (labeled in kcal mole^{-1}) as a function of temperature and pressure (table 29 and figs. 42 and 43).

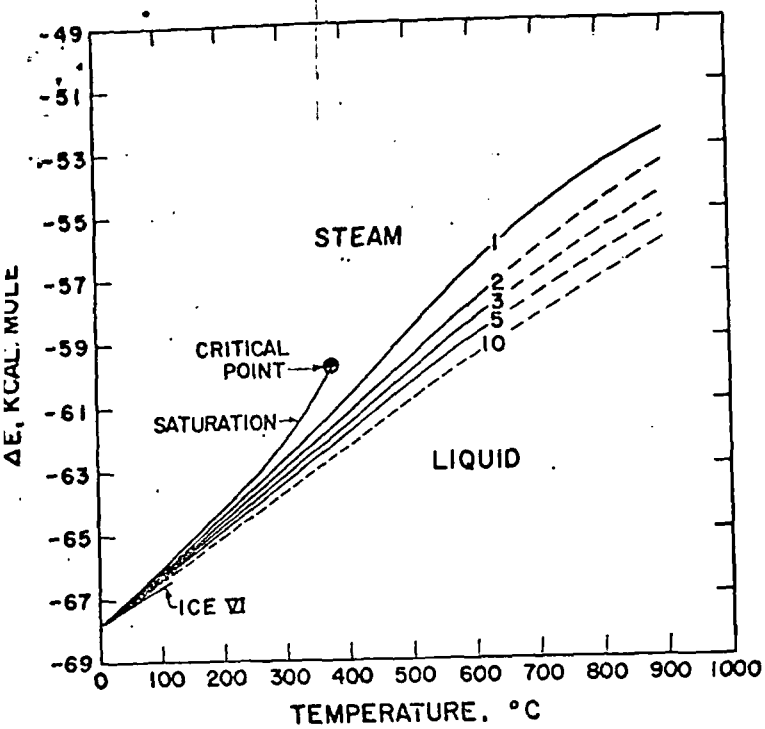

Fig. 50. Apparent molal internal energy of formation (table 32) as a function of temperature at constant pressure (labeled in kb) computed from equation (87), data in table 2, and the values of S and ΔA in tables 27 and 28 and figures 37, 38, 40, and 41.

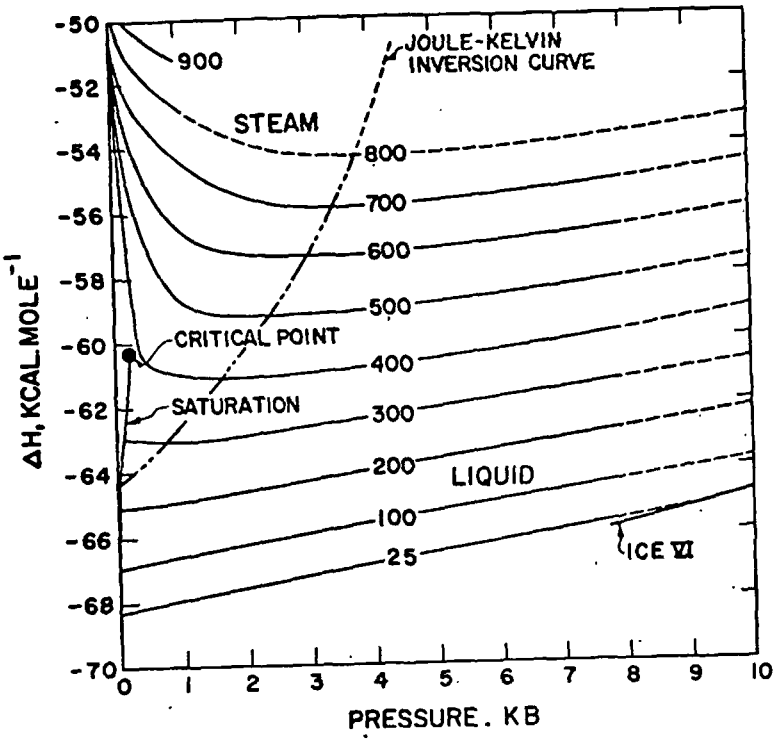

Fig. 51. Apparent molal enthalpy of formation (table 33) as a function of pressure at constant temperature (labeled in °C) computed from equation (88), data in table 2, and the values of V and ΔE in tables 3 and 32 and figures 1, 2, 49, and 50.

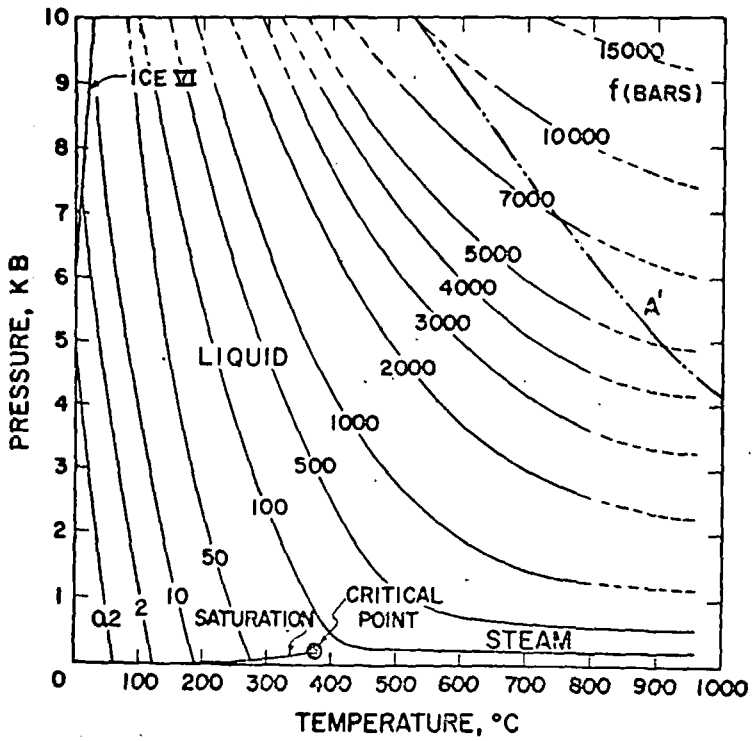

Fig. 48. Isopleths of fugacity (labeled in bars) as a function of temperature and pressure (table 31 and figs. 46 and 47).

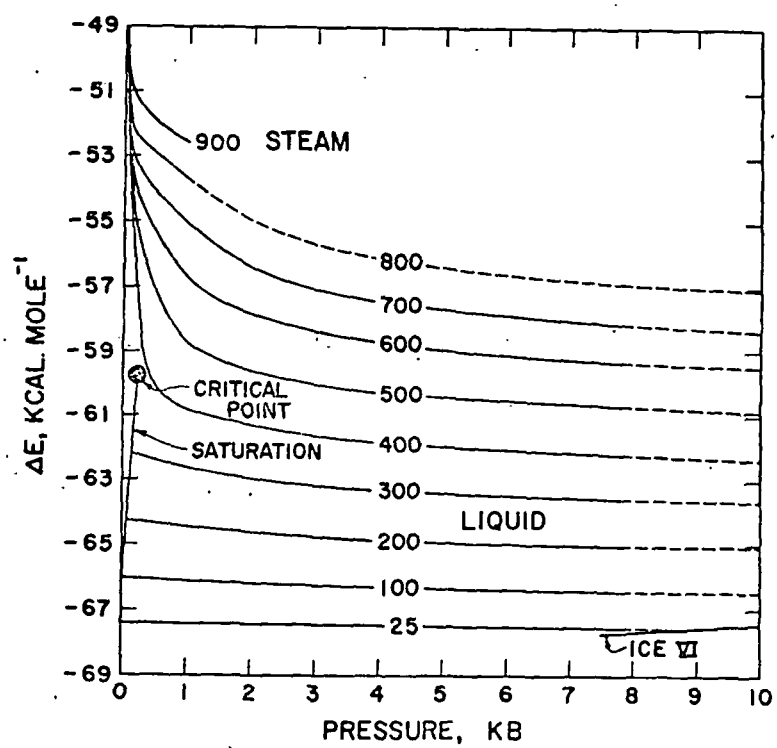

Fig. 49. Apparent molal internal energy of formation (table 32) as a function of pressure at constant temperature (labeled in °C) computed from equation (87), data in table 2, and the values of S and ΔA in tables 27 and 28 and figures 37, 38, 40, and 41.

contrasts with $(\partial\Delta H/\partial P)_T$. The latter function (which is equal to $V(1 - T\alpha)$) is negative in the steam phase region as well as in the liquid phase region above ~ 300°C at pressures less than ~ 1 to 3 kb (depending on the temperature) but positive at high pressures and all temperatures (fig. 51). The minima in the isotherms in figure 51 dampen with decreasing temperature and disappear below ~ 300°C, where $(\partial\Delta H/\partial P)_T$ for liquid H_2O is positive at all pressures.

The isobaric temperature dependence of ΔE is shown in figure 50, where it can be seen that the family of isobars fans out to an increasing degree with increasing temperature. At high temperatures, $(\partial\Delta E/\partial T)_P$ (which is equal to $C_P - PV\alpha$) decreases with increasing temperature at constant pressure. In contrast, $(\partial\Delta E/\partial T)_P$ increases as temperature increases isobarically below ~ 400° to 500°C. Similar behavior is evident in figure 52, where the isobars for the apparent molal enthalpy of formation exhibit a sigmoid curvature which dampens and disappears with increasing pressure. As a consequence, the slopes of the isenthalps in figure 54, which are defined by the reciprocal of the Joule-Kelvin coefficient $((TV\alpha - V)/C_P)$, change from positive to negative values as pressure increases across the Joule-Kelvin inversion curve (figs. 51 and 54).

TABLE 29

Apparent molal Gibbs free energy of formation (ΔG) in kcal mole^{-1} computed from equations (3), (8), (9), (14) through (17), (73) and (74), data in table 2, and values of V in table 3—see figures 42, 43, and 45

t (°C)	PRESSURE, KB											
	SAT	0.001	0.5	1	2	3	4	5	6	7	8	9
25	-56.687	-56.687	-56.473	-56.263	-55.85	-55.46	-55.07	-54.69	-54.32	-53.95	-53.59	-53.23
50	-57.122	-57.122	-56.907	-56.695	-56.28	-55.88	-55.49	-55.10	-54.73	-54.36	-53.99	-53.63
75	-57.593	-57.593	-57.375	-57.161	-56.74	-56.34	-55.94	-55.55	-55.17	-54.80	-54.43	-54.06
100	-58.096	-58.105	-57.875	-57.657	-57.23	-56.82	-56.42	-56.03	-55.64	-55.26	-54.89	-54.52
125	-58.630	-59.283	-58.404	-58.183	-57.75	-57.34	-56.93	-56.53	-56.14	-55.76	-55.38	-55.01
150	-59.191	-60.475	-58.962	-58.736	-58.30	-57.87	-57.46	-57.06	-56.66	-56.28	-55.89	-55.52
175	-59.779	-61.679	-59.546	-59.316	-58.87	-58.44	-58.02	-57.61	-57.21	-56.82	-56.43	-56.05
200	-60.392	-62.894	-60.156	-59.919	-59.46	-59.02	-58.60	-58.19	-57.78	-57.38	-56.99	-56.61
225	-61.029	-64.122	-60.790	-60.547	-60.08	-59.63	-59.20	-58.78	-58.37	-57.97	-57.57	-57.18
250	-61.688	-65.359	-61.447	-61.197	-60.72	-60.26	-59.82	-59.40	-58.98	-58.57	-58.17	-57.78
275	-62.369	-66.608	-62.128	-61.869	-61.38	-60.91	-60.47	-60.03	-59.61	-59.20	-58.79	-58.40
300	-63.069	-67.865	-62.831	-62.562	-62.06	-61.58	-61.13	-60.69	-60.26	-59.84	-59.43	-59.03
325	-63.789	-69.133	-63.556	-63.276	-62.76	-62.27	-61.81	-61.36	-60.92	-60.50	-60.09	-59.68
350	-64.527	-70.409	-64.304	-64.010	-63.47	-62.98	-62.50	-62.05	-61.61	-61.18	-60.76	-60.34
375		-71.694	-65.076	-64.764	-64.21	-63.70	-63.22	-62.75	-62.30	-61.87	-61.44	-61.03
400		-72.988	-65.872	-65.537	-64.96	-64.44	-63.94	-63.47	-63.02	-62.58	-62.14	-61.72
425		-74.290	-66.695	-66.330	-65.73	-65.19	-64.69	-64.21	-63.75	-63.30	-62.86	-62.43
450		-75.600	-67.550	-67.143	-66.51	-65.96	-65.45	-64.96	-64.49	-64.03	-63.59	-63.16
475		-76.918	-68.440	-67.975	-67.32	-66.74	-66.22	-65.72	-65.24	-64.78	-64.33	-63.89
500		-78.244	-69.361	-68.827	-68.13	-67.54	-67.00	-66.50	-66.01	-65.54	-65.09	-64.64
525		-79.577	-70.308	-69.697	-68.96	-68.35	-67.80	-67.28	-66.79	-66.31	-65.85	-65.40
550		-80.917	-71.275	-70.587	-69.81	-69.18	-68.61	-68.09	-67.58	-67.10	-66.63	-66.18
575		-82.264	-72.258	-71.494	-70.67	-70.02	-69.44	-68.90	-68.39	-67.90	-67.42	-66.96
600		-83.618	-73.256	-72.419	-71.54	-70.87	-70.28	-69.73	-69.21	-68.71	-68.23	-67.76
625		-84.979	-74.267	-73.359	-72.43	-71.73	-71.13	-70.56	-70.03	-69.53	-69.04	-68.57
650		-86.347	-75.289	-74.315	-73.33	-72.61	-71.99	-71.41	-70.87	-70.36	-69.86	-69.39
675		-87.721	-76.322	-75.284	-74.24	-73.50	-72.86	-72.27	-71.72	-71.20	-70.70	-70.22
700		-89.102	-77.365	-76.266	-75.17	-74.40	-73.74	-73.14	-72.58	-72.05	-71.54	-71.06
725		-90.488	-78.417	-77.260	-76.11	-75.31	-74.63	-74.02	-73.46	-72.92	-72.40	-71.90
750		-91.881	-79.479	-78.264	-77.05	-76.23	-75.54	-74.91	-74.34	-73.79	-73.27	-72.76
775		-93.280	-80.548	-79.280	-78.01	-77.16	-76.45	-75.81	-75.23	-74.67	-74.14	-73.63
800		-94.685	-81.625	-80.304	-78.98	-78.10	-77.37	-76.72	-76.12	-75.56	-75.02	-74.51
825		-96.096	-82.710	-81.338								
850		-97.513	-83.802	-82.381								
875		-98.935	-84.901	-83.432								
900		-100.363	-86.007	-84.491								

In contrast, the analogous curves for ΔE in figure 53 have positive slopes $((\partial P/\partial T)_E = -(C_P - PV\alpha)/(PV\beta - TV\alpha))$ at all the pressures and temperatures considered. Taking account of the difference in units and conventions, the values of ΔH and ΔE computed in this study are closely consistent with the enthalpies and internal energies reported by Keenan and others (1969) and Burnham, Holloway, and Davis (1969b). Estimated uncertainties in the values of ΔH and ΔE given in tables 32 and 33 for pressures > a kilobar are of the order of 0.2 percent or less.

HEAT CAPACITY

The heat capacity of H_2O at constant volume (C_V) or pressure (C_P) can be computed by first taking the partial derivative of equation (70) with respect to temperature at constant density, which leads to

$$C_V = \left(\frac{\partial \Delta E}{\partial T}\right)_\rho = T\left(\frac{\partial S}{\partial T}\right)_\rho = -T\left(\frac{\partial^2 \psi}{\partial T^2}\right)_\rho$$

$$= -T\left(\frac{\partial^2 \psi_\circ}{\partial T^2}\right)_\rho - 2RT\rho\left(\frac{\partial Q}{\partial T}\right)_\rho - RT^2\rho\left(\frac{\partial^2 Q}{\partial T^2}\right)_\rho \qquad (89)$$

where $(\partial Q/\partial T)_\rho$, $(\partial^2 Q/\partial T^2)_\rho$, and $(\partial^2 \psi_\circ/\partial T^2)$ refer to the partial derivatives of equations (15) and (16) numbered (A-43), (A-44), and (A-49) in the appendix. The heat capacity at constant volume is related to the heat capacity at constant pressure by

$$C_P = \left(\frac{\partial \Delta H}{\partial T}\right)_P = T\left(\frac{\partial S}{\partial T}\right)_P = C_V + \frac{\alpha^2 VT}{\beta}, \qquad (90)$$

which was used together with equation (89) and the values of V, α, and β computed above to calculate the heat capacities given in tables 34 and 35 and those plotted in figures 55 and 56 for pressures ≦ a kilobar. The values of C_P in the tables and diagrams for pressures above a kilobar were computed from

$$C_{P,T} = C_{P=1000,T} - T\left(\int_{P=1000}^{P} \left(\frac{\partial^2 V}{\partial T^2}\right)_P dP\right)_T$$

$$= C_{P=1000,T} - T\left(\int_{P=1000}^{P} V\left(\alpha^2 + \left(\frac{\partial \alpha}{\partial T}\right)_P\right) dP\right)_T \qquad (91)$$

which follows by partial differentiation of equation (80). The integral on the right side of equation (91) was evaluated for region A in figure 9 with the aid of equations (21), (33), and (37) and an equal-interval numerical integration routine adapted from Arden and Astill (1970). Corresponding calculations for regions B and C were carried out by first

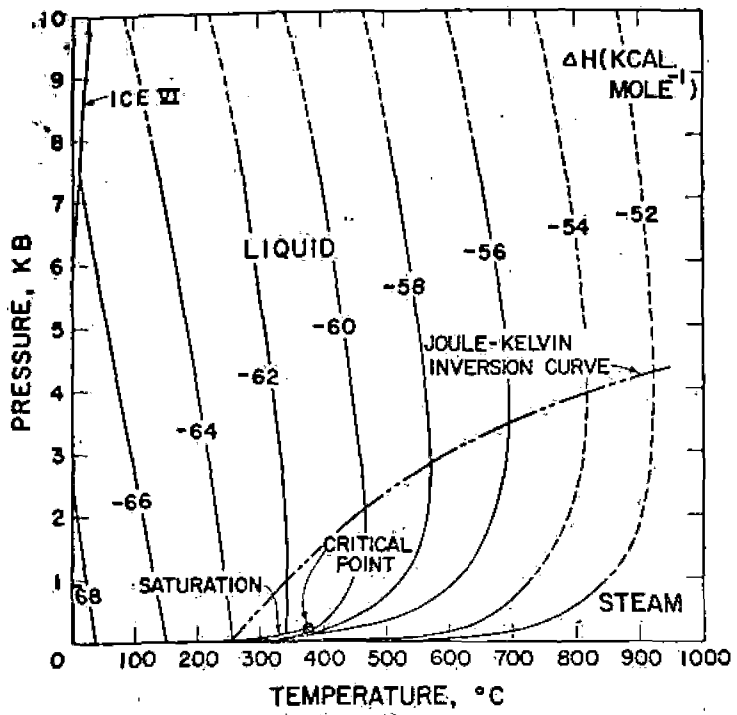

Fig. 54. Isenthalps (labeled in kcal mole^{-1}) as a function of pressure and temperature (table 33 and figs. 51 and 52).

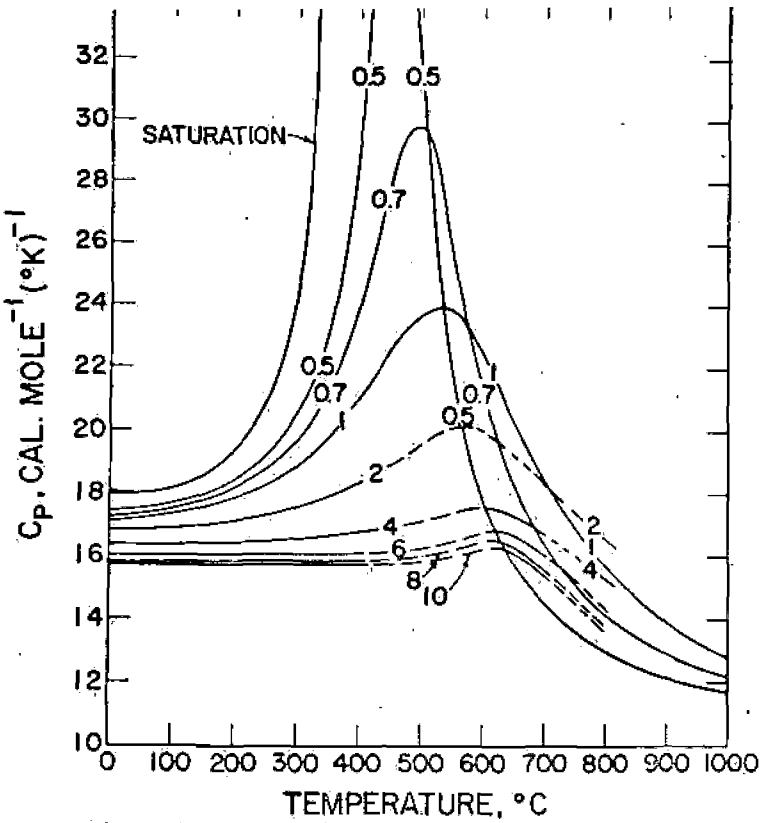

Fig. 55. Isobaric molal heat capacity (table 34) as a function of temperature at constant pressure (labeled in kilobars) computed from equations (19) through (21), (25), (27), (33), (37), (43), and (89) through (93) and coefficients in tables 4, 5, 6, 9, and 10 (solid curves). The dashed curves from 400° to 600°C represent graphic interpolation across the boundary between regions A and B in figure 9 (see text).

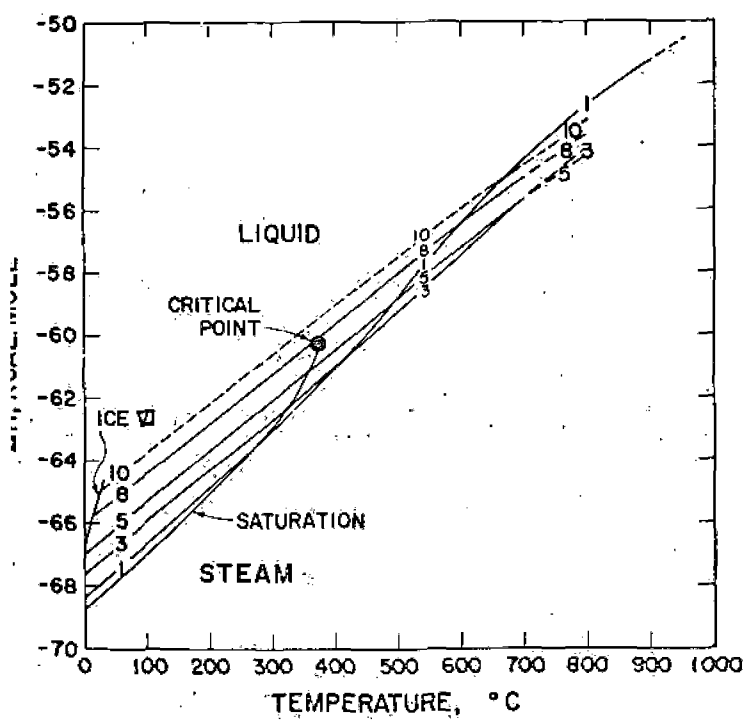

Fig. 52. Apparent molal enthalpy of formation (table 33) as a function of temperature at constant pressure (labeled in kb) computed from equation (88), data in table 2, and the values of V and ΔE in tables 3 and 32 and figures 1, 2, 49, and 50.

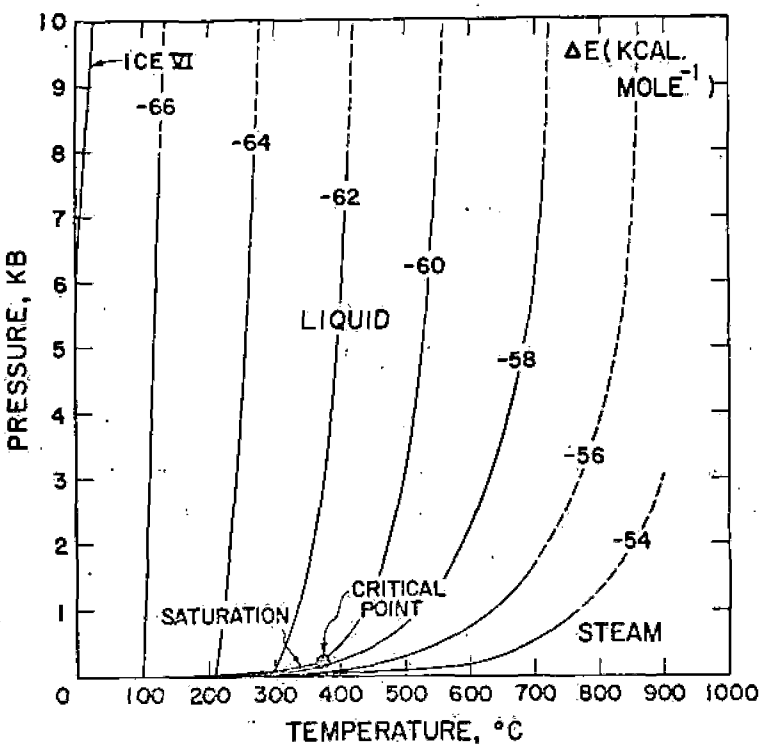

Fig. 53. Isopleths of the apparent molal internal energy of formation (labeled in kcal mole^{-1}) as a function of pressure and temperature (table 32 and figs. 49 and 50).

differentiating equation (39) with respect to temperature at constant pressure, which leads to

$$\left(\frac{\partial^2 V}{\partial T^2}\right)_P = \sum_{i=0}^{\hat{i}} \sum_{j=0}^{\hat{i}+k-i} i(i-1)D_{ij}\, T^{i-2}\, P^j \qquad (92)$$

Hence, for temperatures > 550°C in region B of figure 9,

$$\left(\int_{P=1000}^{P} \left(\frac{\partial^2 V}{\partial T^2}\right)_P dP\right)_T = \sum_{i=0}^{5} \sum_{j=0}^{6-i} i(i-1)\mathring{D}_{ij}\, T^{i-2} \left((1800)^{j+1} - (1000)^{j+1}\right)/(j+1)$$

$$+ \sum_{i=0}^{9} \sum_{j=0}^{9-i} i(i-1)D_{ij}\, T^{i-2} \left(P^{j+1} - (1800)^{j+1}\right)/(j+1) \qquad (93)$$

TABLE 30

Fugacity coefficient (χ) computed from equations (77) through (79), (82), (85), and (86) and values of V and ΔG in tables 3 and 29

t	PRESSURE, KB											
(°C)	SAT	0.001	0.5	1	2	3	4	5	6	7	8	9
25	0.9995	0.0331	0.0001	0.0001	0.000	0.000	0.000	0.000	0.000	0.000	0.001	0.001
50	0.9968	0.1270	0.0003	0.0002	0.000	0.000	0.000	0.001	0.001	0.001	0.002	0.003
75	0.9925	0.3912	0.0010	0.0007	0.001	0.001	0.001	0.001	0.002	0.003	0.005	0.007
100	0.9838	0.9851	0.0027	0.0018	0.002	0.002	0.002	0.003	0.004	0.006	0.009	0.014
125	0.9732	0.9888	0.0060	0.0040	0.003	0.004	0.005	0.006	0.009	0.012	0.017	0.024
150	0.9587	0.9915	0.0120	0.0078	0.007	0.007	0.009	0.011	0.015	0.021	0.029	0.040
175	0.9397	0.9934	0.0218	0.0141	0.012	0.013	0.015	0.019	0.025	0.033	0.045	0.061
200	0.9165	0.9950	0.0366	0.0236	0.019	0.020	0.024	0.030	0.038	0.050	0.066	0.089
225	0.8889	0.9960	0.0577	0.0369	0.029	0.031	0.036	0.044	0.055	0.071	0.093	0.122
250	0.8572	0.9966	0.0859	0.0546	0.043	0.045	0.051	0.062	0.077	0.097	0.125	0.162
275	0.8221	0.9971	0.1219	0.0773	0.061	0.062	0.070	0.083	0.102	0.128	0.163	0.208
300	0.7840	0.9975	0.1659	0.1050	0.082	0.083	0.092	0.109	0.132	0.163	0.205	0.259
325	0.7431	0.9978	0.2176	0.1377	0.106	0.107	0.118	0.138	0.166	0.203	0.252	0.315
350	0.6990	0.9982	0.2763	0.1752	0.135	0.135	0.148	0.171	0.203	0.246	0.303	0.375
375		0.9984	0.3406	0.2169	0.167	0.165	0.180	0.207	0.244	0.293	0.357	0.439
400		0.9987	0.4083	0.2622	0.202	0.199	0.216	0.245	0.287	0.343	0.414	0.504
425		0.9989	0.4766	0.3100	0.239	0.235	0.253	0.286	0.333	0.394	0.473	0.571
450		0.9991	0.5416	0.3594	0.278	0.273	0.293	0.329	0.380	0.447	0.533	0.640
475		0.9992	0.5990	0.4094	0.319	0.312	0.334	0.373	0.429	0.501	0.593	0.708
500		0.9993	0.6481	0.4589	0.361	0.353	0.376	0.418	0.478	0.556	0.654	0.776
525		0.9994	0.6899	0.5070	0.403	0.394	0.418	0.464	0.528	0.611	0.715	0.843
550		0.9995	0.7259	0.5528	0.445	0.435	0.461	0.510	0.577	0.665	0.775	0.909
575		1.0000	0.7575	0.5960	0.486	0.476	0.504	0.555	0.627	0.719	0.833	0.973
600		1.0000	0.7848	0.6358	0.527	0.517	0.546	0.600	0.675	0.771	0.890	1.034
625		1.0000	0.8087	0.6724	0.566	0.557	0.587	0.644	0.722	0.821	0.945	1.093
650		1.0000	0.8297	0.7057	0.603	0.595	0.628	0.686	0.767	0.870	0.997	1.150
675		1.0000	0.8482	0.7359	0.639	0.632	0.667	0.727	0.811	0.917	1.047	1.203
700		1.0000	0.8646	0.7633	0.673	0.668	0.704	0.767	0.853	0.962	1.095	1.254
725		1.0000	0.8791	0.7880	0.705	0.703	0.740	0.805	0.894	1.005	1.142	1.302
750		1.0000	0.8920	0.8103	0.735	0.735	0.775	0.842	0.932	1.046	1.184	1.347
775		1.0000	0.9034	0.8305	0.763	0.766	0.808	0.877	0.969	1.085	1.225	1.390
800		1.0000	0.9132	0.8487	0.789	0.795	0.839	0.910	1.004	1.122	1.263	1.429
825		1.0000	0.9218	0.8651								
850		1.0000	0.9311	0.8799								
875		1.0000	0.9385	0.8934								
900		1.0000	0.9452	0.9056								

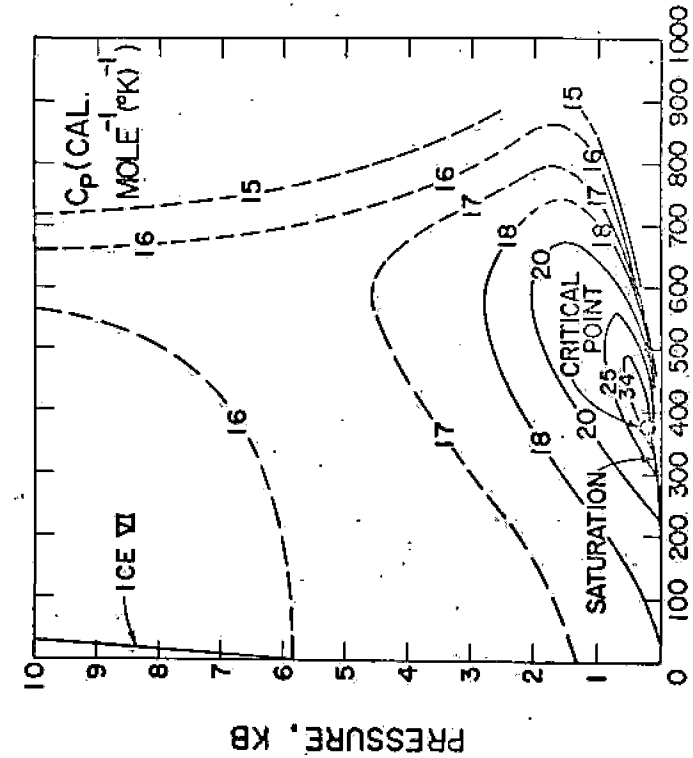

Fig. 57. Isopleths of the isobaric molal heat capacity (labeled in cal mole^{-1} (°K)$^{-1}$) as a function of pressure and temperature (table 34 and figs. 55 and 56).

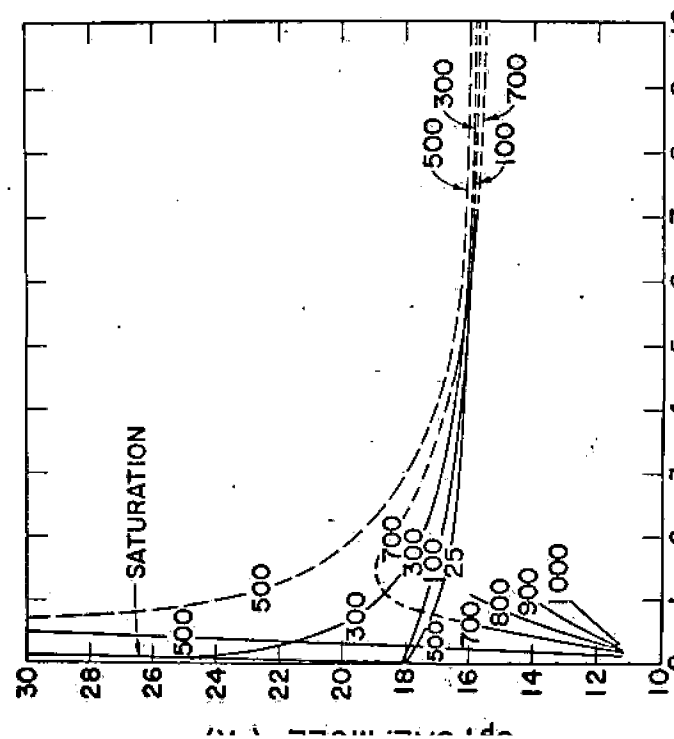

Fig. 56. Isobaric molal heat capacity (table 34) as a function of pressure at constant temperature (labeled in °C) computed from equations (19) through (21), (25), (27), (33), (37), (43), and (89) through (93) and coefficients in tables 4, 5, 6, 9, and 10 (solid curves). The dashed curve for 500°C represents graphic interpolation across the boundary between regions A and B in figure 9 (see text).

where D_{ij} and $\mathring{D}_{ij}$ again stand for the arrays of fit coefficients for regions B and C, respectively, in table 10. For temperatures $\leq$ 550°C in region B, $\mathring{D}_{ij}$ in equation (93) is set to zero, and $C_{P=1000,T}$ in equation (91) is replaced by $C_{P=1500,T}$ in region A. For temperatures and pressures in region C, D_{ij} in equation (93) is set to zero, and (1800) is replaced by P.

The heat capacities computed in this study for pressures $\leq$ a kilobar are in close agreement with those given by Schmidt (1969) and (graphically) by Keenan and others (1969). Estimated uncertainties in the values of C_P shown in table 34 for pressures $>$ a kilobar are of the order of 2 percent or less. Values of C_V at pressures $>$ a kilobar are not given in table 35 owing to the high sensitivity of C_V to small errors in α and β. Errors of a few percent in these coefficients may lead to errors $>$ 10 percent in C_V. Because the uncertainty in the values of α and β computed above are of this order of magnitude, the values of C_V computed for pressures $>$ a kilobar exhibit inconsistencies with those for pressures below a kilobar. Accurate values of C_P above 700°C and a kilobar cannot be computed from equations (91) and (93) owing to the relatively high

TABLE 31

Fugacity (f) in bars computed from equation (78) and the fugacity coefficients in table 30—see figures 46 through 48

t	PRESSURE, KB											
(°C)	SAT	0.001	0.5	1	2	3	4	5	6	7	8	9
25	0.0317	0.0331	0.045	0.064	0	0	0	1	2	3	6	11
50	0.1231	0.1270	0.172	0.239	0	1	2	3	5	9	16	28
75	0.3829	0.3912	0.524	0.715	1	2	4	7	13	22	37	63
100	0.9970	0.9851	1.344	1.802	3	6	10	16	27	45	75	124
125	2.2584	0.9888	3.002	3.971	7	12	19	32	52	85	137	219
150	4.5615	0.9915	5.991	7.835	13	22	36	58	92	146	230	359
175	8.3819	0.9934	10.889	14.109	23	38	60	96	150	233	359	550
200	14.2406	0.9950	18.315	23.551	38	61	96	149	229	350	530	797
225	22.6454	0.9960	28.840	36.859	59	93	143	219	332	499	743	1101
250	34.0550	0.9966	42.938	54.620	86	134	205	308	460	681	1001	1461
275	48.8462	0.9971	60.931	77.255	121	186	280	417	614	897	1301	1875
300	67.2733	0.9975	82.930	104.962	163	248	370	544	793	1145	1640	2336
325	89.4572	0.9978	108.801	137.696	213	321	474	690	995	1422	2016	2840
350	115.4150	0.9982	138.163	175.201	270	404	592	854	1220	1726	2423	3380
375		0.9984	170.279	216.911	334	496	722	1033	1463	2052	2856	3948
400		0.9987	204.161	262.155	403	597	863	1227	1724	2399	3311	4539
425		0.9989	238.320	309.994	478	705	1013	1431	1997	2759	3781	5144
450		0.9991	270.780	359.448	556	818	1171	1645	2281	3131	4261	5756
475		0.9992	299.522	409.424	638	936	1334	1865	2572	3510	4746	6371
500		0.9993	324.041	458.917	721	1058	1502	2091	2869	3893	5234	6983
525		0.9994	344.953	506.973	805	1181	1673	2319	3167	4276	5719	7588
550		0.9995	362.965	552.790	889	1305	1845	2548	3465	4656	6197	8180
575		1.0000	378.758	596.026	973	1429	2016	2776	3761	5032	6667	8758
600		1.0000	392.388	635.828	1053	1551	2185	2999	4049	5397	7120	9311
625		1.0000	404.336	672.363	1131	1670	2350	3218	4330	5751	7557	9841
650		1.0000	414.844	705.680	1206	1786	2510	3431	4603	6093	7976	10347
675		1.0000	424.108	735.925	1278	1898	2666	3637	4867	6421	8378	10829
700		1.0000	432.296	763.300	1346	2005	2817	3836	5120	6737	8762	11286
725		1.0000	439.548	788.030	1410	2108	2961	4026	5363	7038	9126	11718
750		1.0000	445.988	810.349	1470	2206	3099	4209	5595	7324	9471	12124
775		1.0000	451.720	830.486	1526	2298	3231	4383	5816	7596	9797	12506
800		1.0000	456.837	848.661	1578	2386	3356	4549	6026	7854	10105	12865
825		1.0000	461.418	865.082								
850		1.0000	465.533	879.938								
875		1.0000	469.241	893.407								
900		1.0000	472.597	905.646								

sensitivity of C_P to errors in $(\partial\alpha/\partial T)_P$ calculated from equation (37). Inter-regional discrepancies in the computed values of this derivative at the boundary separating regions A and B in figure 9 also preclude calculation of accurate values of C_P in the temperature interval ~ 450° to 550°C above a kilobar. The values of C_P given for this interval in table 29 were obtained by graphic interpolation of the dashed segments of the curves in figure 55. The heat capacities computed in this study for pressures $>$ a kilobar compare favorably with those reported by Jâza, Kmoníček, and Šifner (1966) and Tödheide (1972).

Owing to the drastic effect of the critical phenomenon on the heat capacity of H_2O, the isobars in figure 55 exhibit extrema that dampen progressively and shift to higher temperatures as pressure increases from the critical point (where $C_P = \infty$). The amplitude of the extrema in the isobars for pressures $>$ 5 kb is $<$ 1 cal mole^{-1} (°K)$^{-1}$ (fig. 55), but at high temperatures C_P decreases rapidly with increasing temperature at all (constant) pressures. It is apparent in figure 56 that the high-temperature

TABLE 32

Apparent molal internal energy of formation (ΔE) in kcal mole^{-1} computed from equation (87), data in table 2, and values of ΔA in table 28—see figures 49, 50, and 53

t	PRESSURE, KB									
(°C)	SAT	0.5	1	2	3	4	5	6	7	8
25	-67.436	-67.452	-67.466	-67.5	-67.5	-67.5	-67.5	-67.6	-67.6	(-67.6)
50	-66.986	-67.016	-67.041	-67.1	-67.1	-67.1	-67.2	-67.2	-67.2	(-67.2)
75	-66.536	-66.579	-66.614	-66.7	-66.7	-66.8	-66.8	-66.8	-66.8	(-66.8)
100	-66.084	-66.140	-66.186	-66.3	-66.3	-66.3	-66.4	-66.4	-66.5	(-66.5)
125	-65.628	-65.700	-65.758	-65.8	-65.9	-66.0	-66.0	-66.1	-66.1	(-66.1)
150	-65.168	-65.257	-65.329	-65.4	-65.5	-65.6	-65.6	-65.7	-65.7	(-65.8)
175	-64.701	-64.810	-64.897	-65.0	-65.1	-65.2	-65.3	-65.3	-65.4	(-65.4)
200	-64.225	-64.358	-64.463	-64.6	-64.7	-64.8	-64.9	-64.9	-65.0	(-65.0)
225	-63.738	-63.900	-64.025	-64.2	-64.3	-64.4	-64.5	-64.6	-64.6	(-64.7)
250	-63.236	-63.435	-63.584	-63.8	-63.9	-64.0	-64.1	-64.2	-64.3	(-64.3)
275	-62.711	-62.959	-63.138	-63.4	-63.5	-63.7	-63.8	-63.8	-63.9	(-64.0)
300	-62.152	-62.468	-62.688	-63.0	-63.1	-63.3	-63.4	-63.5	-63.5	(-63.6)
325	-61.539	-61.956	-62.231	-62.6	-62.8	-62.9	-63.0	-63.1	-63.2	(-63.2)
350	-60.818	-61.415	-61.766	-62.1	-62.4	-62.5	-62.7	-62.7	-62.8	(-62.9)
375		-60.832	-61.289	-61.7	-62.0	-62.1	-62.3	-62.4	-62.5	(-62.5)
400		-60.189	-60.800	-61.3	-61.6	-61.8	-61.9	-62.0	-62.1	(-62.2)
425		-59.450	-60.300	-60.9	-61.2	-61.4	-61.5	-61.7	-61.8	(-61.8)
450		-58.589	-59.788	-60.5	-60.8	-61.0	-61.2	-61.3	-61.4	(-61.5)
475		-57.724	-59.268	-60.0	-60.4	-60.6	-60.8	-61.0	-61.1	(-61.2)
500		-57.013	-58.743	-59.6	-60.0	-60.3	-60.5	-60.6	-60.7	(-60.8)
525		-56.453	-58.218	-59.2	-59.7	-59.9	-60.1	-60.3	-60.4	(-60.5)
550		-55.988	-57.702	-58.8	-59.3	-59.6	-59.8	-59.9	-60.1	(-60.2)
575		-55.584	-57.201	-58.5	-59.0	-59.3	-59.5	-59.7	-59.8	(-59.9)
600		-55.220	-56.724	-58.0	-58.6	-58.9	-59.1	-59.3	-59.4	(-59.6)
625		-54.884	-56.273	-57.6	-58.2	-58.5	-58.8	-58.9	-59.1	(-59.2)
650		-54.567	-55.848	-57.2	-57.8	-58.1	-58.4	-58.6	-58.7	(-58.9)
675		-54.266	-55.446	-56.8	-57.4	-57.8	-58.0	-58.2	-58.4	(-58.5)
700		-53.978	-55.066	-56.4	-57.0	-57.4	-57.7	-57.9	-58.0	(-58.2)
725		-53.698	-54.704	(-56.0)	(-56.7)	(-57.0)	(-57.3)	(-57.5)	(-57.7)	(-57.8)
750		-53.427	-54.359	(-55.6)	(-56.3)	(-56.7)	(-57.0)	(-57.2)	(-57.4)	(-57.5)
775		-53.163	-54.029	(-55.3)	(-55.9)	(-56.4)	(-56.7)	(-56.9	(-57.0)	(-57.2)
800		-52.904	-53.711	(-54.9)	(-55.6)	(-56.0)	(-56.3)	(-56.5)	(-56.8)	(-56.9)
825		-52.650	-53.405							
850		-52.401	-53.108							
875		-52.155	-52.820							
900		-51.912	-52.541							

isotherms maximize between 1 and 2 kb. The relations shown in figures 55 and 56 lead to the configuration of isopleths depicted in figure 57, where it can be seen that the isopleths ring the "infinite peak" of the critical point in an elongated pattern.

SUMMARY OF THE PROPERTIES OF H_2O_{liquid} AT SATURATION

The thermodynamic and electrostatic properties of steam-saturated liquid H_2O at closely spaced intervals from 0° to 350°C are given in tables 36 through 40. The numerical data in these tables were computed in the manner described above. The values of P, V, ΔE, ΔH, and S correspond (after unit and convention conversion) to those given by Keenan and others (1969). The fugacities and fugacity coefficients shown in the tables are in close agreement with those computed by Haas (1970), as are the values of α and β with those calculated for 1 atm by Kell (1967). The heat capacities are in accord with Schmidt's (1969) tabulation, and the values of the dielectric constant are consistent with those given by Oshry

TABLE 33

Apparent molal enthalpy of formation (ΔH) in kcal mole^{-1} computed from equation (88), data in table 2, and values of ΔE in table 32—see figures 51, 52, and 54

t	PRESSURE, KB									
(°C)	SAT	0.5	1	2	3	4	5	6	7	8
25	-68.315	-68.119	-67.930	-67.6	-67.2	-66.9	-66.5	-66.2	-65.9	(-65.6)
50	-67.865	-67.681	-67.501	-67.1	-66.8	-66.5	-66.1	-65.8	-65.5	(-65.2)
75	-67.415	-67.241	-67.069	-66.7	-66.4	-66.1	-65.7	-65.4	-65.1	(-64.8)
100	-66.962	-66.799	-66.635	-66.3	-66.0	-65.7	-65.3	-65.0	-64.7	(-64.4)
125	-66.506	-66.355	-66.139	-65.9	-65.6	-65.2	-64.9	-64.6	-64.3	(-64.0)
150	-66.044	-65.907	-65.761	-65.5	-65.1	-64.8	-64.5	-64.2	-63.9	(-63.6)
175	-65.575	-65.455	-65.320	-65.0	-64.7	-64.4	-64.1	-63.8	-63.5	(-63.2)
200	-65.096	-64.997	-64.875	-64.6	-64.3	-64.0	-63.7	-63.4	-63.1	(-62.8)
225	-64.604	-64.532	-64.423	-64.2	-63.9	-63.6	-63.3	-63.0	-62.7	(-62.4)
250	-64.093	-64.058	-63.971	-63.7	-63.5	-63.2	-62.9	-62.6	-62.3	(-62.0)
275	-63.556	-63.572	-63.512	-63.3	-63.1	-62.8	-62.5	-62.2	-61.9	(-61.6)
300	-62.979	-63.070	-63.045	-62.9	-62.6	-62.4	-62.1	-61.8	-61.5	(-61.2)
325	-62.338	-62.544	-62.569	-62.4	-62.2	-62.0	-61.7	-61.4	-61.1	(-60.8)
350	-61.573	-61.984	-62.081	-62.0	-61.8	-61.5	-61.3	-61.0	-60.7	(-60.4)
375		-61.375	-61.579	-61.5	-61.4	-61.1	-60.9	-60.6	-60.3	(-60.0)
400		-60.695	-61.059	-61.1	-60.9	-60.7	-60.5	-60.2	-59.9	(-59.6)
425		-59.896	-60.522	-60.6	-60.5	-60.3	-60.1	-59.8	-59.5	(-59.3)
450		-58.932	-59.966	-60.2	-60.1	-59.9	-59.7	-59.4	-59.1	(-58.9)
475		-57.919	-59.394	-59.7	-59.7	-59.5	-59.3	-59.0	-58.8	(-58.5)
500		-57.054	-58.808	-59.3	-59.2	-59.1	-58.9	-58.6	-58.4	(-58.1)
525		-56.354	-58.211	-58.8	-58.8	-58.7	-58.5	-58.3	-58.0	(-57.8)
550		-55.765	-57.613	-58.3	-58.4	-58.3	-58.1	-57.9	-57.6	(-57.4)
575		-55.249	-57.024	-57.9	-58.0	-58.0	-57.8	-57.6	-57.3	(-57.1)
600		-54.783	-56.453	-57.5	-57.6	-57.5	-57.3	-57.1	-56.9	(-56.8)
625		-54.352	-55.906	-57.0	-57.1	-57.1	-57.0	-56.7	-56.5	(-56.3)
650		-53.947	-55.385	-56.5	-56.7	-56.6	-56.5	-56.3	-56.1	(-55.9)
675		-53.562	-54.890	-56.0	-56.2	-56.2	-56.1	-55.9	-55.7	(-55.4)
700		-53.193	-54.418	-55.5	-55.8	-55.8	-55.7	-55.5	-55.3	(-55.0)
725		-52.837	-53.967	(-55.1)	(-55.4)	(-55.4)	(-55.3)	(-55.1)	(-54.9)	(-54.7)
750		-52.492	-53.536	(-54.6)	(-54.9)	(-55.0)	(-54.9)	(-54.7)	(-54.5)	(-54.3)
757		-52.157	-53.121	(-54.2)	(-54.5)	(-54.6)	(-54.5)	(-54.3)	(-54.2)	(-53.9)
800		-51.829	-52.722	(-53.8)	(-54.1)	(-54.2)	(-54.1)	(-54.0)	(-53.8)	(-53.6)
825		-51.508	-52.337							
850		-51.193	-51.963							
875		-50.883	-51.601							
900		-50.577	-51.248							

(ms) and Owen and others (1961). In contrast, the logarithmic partial derivatives of ε in table 36 differ from those computed for 1 atm by Owen and others, who derived their values by regressing dielectric constant data from 0° to 70°C and 1 to 1000 bars with a quadratic power function of temperature-and pressure. The partial derivatives of ln ε in table 36 also differ somewhat from the estimates computed by Sen and Cobble (1974).

CONCLUDING REMARKS

The equations presented above permit calculation of a large number of thermodynamic/electrostatic properties of H_2O in addition to those discussed in the foregoing pages. Owing to space limitations, many of these could not be included in this summary, but some are the subject of the following communication (Helgeson and Kirkham, 1974a). The calculations make it possible to predict the consequences of geochemical

TABLE 34

Isobaric molal heat capacity (C_P) in cal mole^{-1} (°K)$^{-1}$ computed from equations (89) through (93) and values of V, α, β, and $(\partial\alpha/\partial T)_P$ in tables 3, 7, 8, and 13—see figures 55 through 57

t	PRESSURE, KB									
(°C)	SAT	0.5	1	2	3	4	5	6	7	8
25	18.01	17.46	17.09	16.7	16.5	16.3	16.2	16.2	16.2	(16.2)
50	17.99	17.56	17.24	16.8	16.5	16.3	16.2	16.1	16.1	(16.0)
75	18.05	17.65	17.35	16.9	16.6	16.4	16.2	16.1	16.0	(15.9)
100	18.15	17.72	17.39	16.9	16.6	16.3	16.1	16.0	15.9	(15.8)
125	18.32	17.83	17.46	16.9	16.6	16.3	16.1	16.0	15.9	(15.8)
150	18.57	17.99	17.57	17.0	16.6	16.3	16.1	16.0	15.9	(15.8)
175	18.90	18.20	17.72	17.1	16.7	16.4	16.2	16.0	15.9	(15.8)
200	19.35	18.45	17.89	17.1	16.7	16.4	16.2	16.0	15.9	(15.8)
225	19.97	18.76	18.07	17.2	16.7	16.4	16.2	16.1	15.9	(15.9)
250	20.89	19.16	18.27	17.3	16.8	16.4	16.2	16.1	16.0	(15.9)
275	22.34	19.72	18.52	17.4	16.8	16.5	16.2	16.1	15.9	(15.9)
300	24.78	20.51	18.84	17.5	16.9	16.5	16.2	16.1	15.9	(15.9)
325	29.52	21.65	19.26	17.7	17.0	16.5	16.3	16.1	16.0	(15.9)
350	43.45	23.25	19.79	17.9	17.1	16.6	16.3	16.1	16.0	(15.9)
375		25.57	20.43	18.1	17.2	16.7	16.4	16.1	16.0	(15.9)
400		29.18	21.13	18.3	17.3	16.7	16.3	16.1	15.9	(15.8)
425		35.15	21.86	(18.6)	(17.6)	(16.8)	(16.4)	(16.1)	(16.0)	(15.8)
450		41.20	22.56	(18.9)	(17.8)	(16.9)	(16.4)	(16.1)	(16.0)	(15.9)
475		38.26	23.19	(19.2)	(18.0)	(17.0)	(16.5)	(16.2)	(16.1)	(15.9)
500		30.58	23.70	(19.6)	(18.2)	(17.1)	(16.6)	(16.2)	(16.1)	(16.0)
525		25.46	23.96	(19.9)	(18.5)	(17.2)	(16.8)	(16.3)	(16.2)	(16.1)
550		21.89	23.83	(20.1)	(18.8)	(17.4)	(17.0)	(16.4)	(16.3)	(16.2)
575		19.52	23.26	(20.2)	(19.0)	(17.5)	(17.1)	(16.5)	(16.4)	(16.3)
600		17.88	22.38	(19.7)	(18.2)	(17.5)	(17.1)	(16.8)	(16.6)	(16.5)
625		16.68	21.36	(19.6)	(18.2)	(17.5)	(17.1)	(16.8)	(16.6)	(16.5)
650		15.77	20.32	(19.3)	(18.0)	(17.3)	(16.9)	(16.7)	(16.5)	(16.4)
675		15.05	19.33	(18.8)	(17.7)	(17.1)	(16.7)	(16.4)	(16.2)	(16.1)
700		14.47	18.43	(18.3)	(17.4)	(16.8)	(16.4)	(16.1)	(15.8)	(15.6)
725		14.00	17.63							
750		13.60	16.90							
775		13.26	16.26							
800		12.97	15.69							
825		12.72	15.17							
850		12.50	14.71							
875		12.32	14.30							
900		12.16	13.93							

reactions among minerals and aqueous electrolyte solutions at high pressures and temperatures (Helgeson and Kirkham, 1975a and b). The tables afford numerical values for such predictions, and the diagrams facilitate correlation of the thermodynamic/electrostatic behavior of H_2O with geologic observations and theoretical models of geochemical processes.

ACKNOWLEDGMENTS

During the course of this study, many people contributed helpful suggestions, discussion, programming expertise, and critical comment, but we are especially indebted to Philippe Lehot. We are also grateful to Professor J. H. Keenan and his colleagues for permission to program and publish calculations based on equation (14), to C. W. Burnham and A. J. Ellis for critical reviews of the manuscript, and to Scott Cornelius, Robin Reid, John Dalton, Yoshi Hidaka, Richard Weiss, David Bice, Robert

TABLE 35

Isochoric molal heat capacity (C_v) in cal mole^{-1} (°K)$^{-1}$ computed from equation (89) and the values of V in table 3

t (°C)	PRESSURE, KB										
	SAT	100	200	300	400	500	600	700	800	900	1000
25	17.83	17.67	17.53	17.40	17.27	17.16	17.05	16.95	16.69	16.77	16.86
50	17.31	17.20	17.09	17.00	16.90	16.82	16.74	16.66	16.46	16.52	16.59
75	16.78	16.70	16.62	16.55	16.48	16.41	16.35	16.29	16.13	16.18	16.24
100	16.25	16.18	16.12	16.06	16.00	15.95	15.90	15.85	15.70	15.75	15.80
125	15.74	15.67	15.62	15.56	15.51	15.46	15.42	15.37	15.23	15.28	15.33
150	15.25	15.19	15.14	15.09	15.04	15.00	14.96	14.91	14.78	14.83	14.87
175	14.80	14.74	14.69	14.65	14.61	14.57	14.53	14.49	14.37	14.41	14.45
200	14.39	14.34	14.29	14.25	14.21	14.18	14.15	14.12	14.01	14.05	14.08
225	14.04	13.99	13.93	13.89	13.86	13.83	13.81	13.78	13.70	13.73	13.76
250	13.73	13.68	13.62	13.57	13.54	13.52	13.50	13.49	13.44	13.45	13.47
275	13.50	13.44	13.35	13.29	13.26	13.24	13.23	13.22	13.20	13.21	13.21
300	13.35	13.32	13.14	13.05	13.01	12.98	12.98	12.98	12.99	12.99	12.98
325	13.39	13.53	13.06	12.87	12.78	12.75	12.74	12.75	12.80	12.78	12.76
350	13.82	10.00	13.34	12.80	12.61	12.54	12.52	12.53	12.61	12.58	12.55
375		9.12	14.65	13.06	12.54	12.37	12.32	12.32	12.43	12.39	12.35
400		8.61	11.62	14.85	12.66	12.26	12.14	12.12	12.24	12.19	12.15
425		8.30	10.25	12.91	13.04	12.23	11.99	11.93	12.06	11.99	11.95
450		8.12	9.50	11.17	12.43	12.16	11.85	11.75	11.87	11.80	11.75
475		8.02	9.07	10.24	11.31	11.74	11.65	11.56	11.68	11.61	11.56
500		7.96	8.80	9.70	10.55	11.13	11.33	11.35	11.50	11.43	11.37
525		7.94	8.65	9.37	10.07	10.63	10.96	11.11	11.33	11.25	11.18
550		7.93	8.55	9.17	9.77	10.28	10.65	10.87	11.18	11.09	10.99
575		7.94	8.49	9.04	9.57	10.04	10.40	10.66	11.03	10.94	10.82
600		7.96	8.46	8.96	9.43	9.86	10.22	10.48	10.90	10.80	10.67
625		7.99	8.44	8.89	9.33	9.73	10.07	10.34	10.78	10.67	10.53
650		8.02	8.43	8.85	9.25	9.63	9.95	10.21	10.66	10.55	10.40
675		8.05	8.43	8.81	9.19	9.54	9.84	10.09	10.55	10.43	10.28
700		8.09	8.43	8.79	9.13	9.45	9.74	9.98	10.43	10.31	10.17
725		8.13	8.44	8.76	9.08	9.38	9.64	9.87	10.30	10.19	10.05
750		8.18	8.45	8.75	9.03	9.31	9.55	9.76	10.17	10.07	9.93
775		8.22	8.47	8.73	8.99	9.24	9.46	9.66	10.04	9.94	9.81
800		8.27	8.49	8.72	8.96	9.18	9.38	9.55	9.91	9.82	9.70
825		8.32	8.51	8.71	8.92	9.12	9.30	9.46	9.78	9.69	9.59
850		8.37	8.53	8.71	8.89	9.07	9.22	9.36	9.64	9.57	9.48
875		8.42	8.56	8.71	8.87	9.02	9.15	9.27	9.52	9.45	9.37
900		8.47	8.59	8.72	8.85	8.97	9.09	9.19	9.39	9.34	9.27

TABLE 36

Summary of the electrostatic properties of steam-saturated H_2O_{liquid}

[a] t	[b] P	[c] V	[d] $\alpha \times 10^5$	[e] $\beta \times 10^6$	[f] $(\partial\beta/\partial P)_T \times 10^9$	[g] $(\partial\beta/\partial T)_P \times 10^9$	[h] $(\partial\alpha/\partial T)_P \times 10^8$
0	0.006	18.0194	-5.46	50.67	-11.93	-247.17	1320.85
5	0.009	18.0175	1.30	49.48	-14.48	-252.51	1362.61
10	0.012	18.0217	8.01	48.26	-15.57	-230.02	1310.78
15	0.017	18.0318	14.35	47.19	-15.89	-196.16	1219.72
20	0.023	18.0474	20.19	46.33	-15.87	-159.55	1118.08
25	0.032	18.0681	25.53	45.60	-15.66	-123.83	1019.58
30	0.042	18.0934	30.40	45.06	-15.44	-90.81	930.14
35	0.056	18.1230	34.85	44.69	-15.27	-60.85	851.81
40	0.074	18.1564	38.94	44.46	-15.16	-33.73	784.79
45	0.096	18.1935	42.72	44.35	-15.12	-9.13	728.42
50	0.123	18.2340	46.24	44.36	-15.17	13.32	681.71
55	0.158	18.2777	49.55	44.48	-15.30	34.02	643.55
60	0.199	18.3245	52.69	44.69	-15.52	53.28	612.84
65	0.250	18.3742	55.69	45.01	-15.82	71.42	588.57
70	0.312	18.4267	58.58	45.41	-16.20	88.68	569.80
75	0.386	18.4820	61.39	45.89	-16.66	105.28	555.69
80	0.474	18.5400	64.14	46.46	-17.20	121.40	545.51
85	0.578	18.6008	66.85	47.10	-17.83	137.22	538.64
90	0.701	18.6642	69.53	47.82	-18.53	152.90	534.53
95	0.845	18.7303	72.20	48.62	-19.32	168.57	532.73
00	1.013	18.7991	74.86	49.50	-20.20	184.37	532.88
05	1.208	18.8707	77.52	50.46	-21.18	200.44	534.66
10	1.433	18.9450	80.20	51.50	-22.26	216.90	537.87
15	1.691	19.0222	82.89	52.62	-23.44	233.88	542.32
20	1.985	19.1022	85.61	53.83	-24.75	251.51	547.92
25	2.321	19.1851	88.36	55.12	-26.18	269.95	554.60
30	2.701	19.2710	91.14	56.51	-27.75	289.32	562.35
35	3.130	19.3599	93.96	57.99	-29.47	309.78	571.21
40	3.613	19.4519	96.82	59.58	-31.36	331.52	581.25
45	4.154	19.5470	99.74	61.28	-33.43	354.70	592.59
50	4.758	19.6455	102.71	63.09	-35.71	379.53	605.37
55	5.431	19.7473	105.75	65.03	-38.22	406.23	619.76
60	6.178	19.8525	108.85	67.10	-40.99	435.06	635.97
65	7.004	19.9613	112.04	69.32	-44.05	466.28	654.25
70	7.916	20.0738	115.32	71.69	-47.43	500.22	674.86
75	8.920	20.1901	118.70	74.24	-51.18	537.23	698.09
80	10.021	20.3104	122.19	76.96	-55.35	577.72	724.30
85	11.226	20.4347	125.81	79.89	-60.00	622.15	753.84
90	12.543	20.5634	129.58	83.04	-65.19	671.06	787.13
95	13.978	20.6966	133.51	86.43	-71.02	725.08	824.63
00	15.537	20.8344	137.62	90.09	-77.56	784.91	866.87
25	25.476	21.6039	161.75	113.48	-126.08	1206.73	1172.77
50	39.728	22.5416	195.13	149.96	-225.07	1996.44	1736.78
75	59.415	23.7224	245.37	211.54	-458.96	3681.11	2854.08
00	85.805	25.2858	329.48	329.06	-1149.55	8089.35	5470.84
25	120.387	27.5307	499.05	607.65	-4157.99	24748.10	14159.30
50	165.125	31.3508	1038.30	1698:85	-36533.97	174219.75	80781.59

[a] °C. [b] bar. [c] cm^3 mole^{-1}. [d] (°K)$^{-1}$. [e] bar^{-1}. [f] bar^{-2}. [g] bar^{-1}(°K)$^{-1}$. [h] (°K)$^{-2}$

TABLE 37

Summary of thermodynamic properties of steam-saturated H_2O_{liquid}

t[a]	P[b]	S[c]	ΔA[d]	ΔG[d]	ΔE[d]	ΔH[d]
0	0.006	15.13	-55.413	-56.288	-67.888	-68.766
5	0.009	15.46	-55.490	-56.364	-67.797	-68.676
10	0.012	15.78	-55.568	-56.442	-67.707	-68.585
15	0.017	16.10	-55.648	-56.522	-67.616	-68.495
20	0.023	16.41	-55.729	-56.603	-67.526	-68.405
25	0.032	16.71	-55.812	-56.686	-67.436	-68.315
30	0.042	17.01	-55.896	-56.770	-67.346	-68.225
35	0.056	17.31	-55.982	-56.856	-67.256	-68.135
40	0.074	17.60	-56.069	-56.944	-67.166	-68.045
45	0.096	17.88	-56.158	-57.032	-67.076	-67.955
50	0.123	18.16	-56.248	-57.122	-66.986	-67.865
55	0.158	18.44	-56.339	-57.214	-66.896	-67.775
60	0.199	18.71	-56.432	-57.307	-66.806	-67.685
65	0.250	18.98	-56.526	-57.401	-66.716	-67.595
70	0.312	19.24	-56.622	-57.496	-66.626	-67.505
75	0.386	19.50	-56.719	-57.593	-66.536	-67.415
80	0.474	19.76	-56.817	-57.691	-66.446	-67.324
85	0.578	20.02	-56.917	-57.791	-66.355	-67.234
90	0.701	20.27	-57.017	-57.891	-66.265	-67.143
95	0.845	20.51	-57.119	-57.993	-66.174	-67.053
100	1.013	20.76	-57.222	-58.096	-66.084	-66.962
105	1.208	21.00	-57.327	-58.201	-65.993	-66.871
110	1.433	21.24	-57.432	-58.306	-65.902	-66.780
115	1.691	21.48	-57.539	-58.413	-65.811	-66.689
120	1.985	21.71	-57.647	-58.521	-65.720	-66.598
125	2.321	21.94	-57.756	-58.630	-65.628	-66.506
130	2.701	22.17	-57.867	-58.740	-65.537	-66.414
135	3.130	22.40	-57.978	-58.851	-65.445	-66.322
140	3.613	22.62	-58.091	-58.963	-65.353	-66.230
145	4.154	22.84	-58.204	-59.077	-65.260	-66.137
150	4.758	23.06	-58.319	-59.191	-65.168	-66.044
155	5.431	23.28	-58.435	-59.307	-65.075	-65.951
160	6.178	23.50	-58.552	-59.423	-64.982	-65.858
165	7.004	23.71	-58.670	-59.541	-64.888	-65.764
170	7.916	23.92	-58.789	-59.660	-64.795	-65.670
175	8.920	24.14	-58.909	-59.779	-64.701	-65.575
180	10.021	24.34	-59.030	-59.900	-64.606	-65.480
185	11.226	24.55	-59.153	-60.022	-64.511	-65.385
190	12.543	24.76	-59.276	-60.144	-64.416	-65.289
195	13.978	24.96	-59.400	-60.268	-64.321	-65.193
200	15.537	25.17	-59.526	-60.392	-64.225	-65.096
225	25.476	26.17	-60.168	-61.029	-63.738	-64.604
250	39.728	27.16	-60.835	-61.688	-63.236	-64.093
275	59.415	28.14	-61.528	-62.369	-62.711	-63.556
300	85.805	29.14	-62.246	-63.069	-62.152	-62.979
325	120.387	30.20	-62.994	-63.789	-61.539	-62.338
350	165.125	31.40	-63.776	-64.527	-60.818	-61.573

[a] °C. [b] bar. [c] cal mole^{-1} (°K)$^{-1}$. [d] kcal mole^{-1}.

TABLE 38

Summary of thermodynamic properties of steam-saturated H_2O_{liquid}

t[a]	P[b]	ρ[c]	C_P[d]	C_V[d]	χ	f[b]
0	0.006	0.9998	18.08	18.08	0.9996	0.0061
5	0.009	0.9999	18.10	18.10	1.0004	0.0087
10	0.012	0.9996	18.09	18.07	1.0000	0.0123
15	0.017	0.9991	18.06	18.01	1.0003	0.0171
20	0.023	0.9982	18.03	17.92	0.9995	0.0234
25	0.032	0.9971	18.01	17.83	0.9995	0.0317
30	0.042	0.9957	17.99	17.72	0.9986	0.0424
35	0.056	0.9941	17.98	17.62	0.9985	0.0562
40	0.074	0.9922	17.98	17.52	0.9977	0.0737
45	0.096	0.9902	17.98	17.41	0.9976	0.0957
50	0.123	0.9880	17.99	17.31	0.9968	0.1231
55	0.158	0.9856	17.99	17.20	0.9954	0.1568
60	0.199	0.9831	18.00	17.10	0.9948	0.1984
65	0.250	0.9805	18.02	16.99	0.9937	0.2487
70	0.312	0.9777	18.03	16.89	0.9934	0.3098
75	0.386	0.9747	18.05	16.78	0.9925	0.3829
80	0.474	0.9717	18.06	16.68	0.9911	0.4697
85	0.578	0.9685	18.08	16.57	0.9893	0.5721
90	0.701	0.9652	18.10	16.47	0.9883	0.6932
95	0.845	0.9618	18.13	16.36	0.9869	0.8344
100	1.013	0.9583	18.15	16.25	0.9838	0.9970
105	1.208	0.9547	18.18	16.15	0.9821	1.1865
110	1.433	0.9509	18.21	16.04	0.9801	1.4041
115	1.691	0.9471	18.25	15.94	0.9780	1.6533
120	1.985	0.9431	18.28	15.84	0.9758	1.9371
125	2.321	0.9390	18.32	15.74	0.9732	2.2584
130	2.701	0.9348	18.36	15.64	0.9707	2.6216
135	3.130	0.9305	18.41	15.54	0.9679	3.0295
140	3.613	0.9261	18.46	15.44	0.9650	3.4861
145	4.154	0.9216	18.51	15.34	0.9619	3.9955
150	4.758	0.9170	18.57	15.25	0.9587	4.5615
155	5.431	0.9123	18.63	15.15	0.9552	5.1878
160	6.178	0.9075	18.69	15.06	0.9516	5.8788
165	7.004	0.9025	18.76	14.97	0.9478	6.6388
170	7.916	0.8975	18.83	14.88	0.9439	7.4720
175	8.920	0.8923	18.90	14.80	0.9397	8.3819
180	10.021	0.8870	18.98	14.71	0.9355	9.3742
185	11.226	0.8816	19.06	14.63	0.9310	10.4516
190	12.543	0.8761	19.15	14.55	0.9263	11.6189
195	13.978	0.8704	19.25	14.47	0.9215	12.8806
200	15.537	0.8647	19.35	14.39	0.9165	14.2406
225	25.476	0.8339	19.97	14.04	0.8889	22.6454
250	39.728	0.7992	20.89	13.73	0.8572	34.0550
275	59.415	0.7594	22.34	13.50	0.8221	48.8462
300	85.805	0.7125	24.78	13.35	0.7840	67.2733
325	120.387	0.6544	29.52	13.39	0.7431	89.4572
350	165.125	0.5746	43.45	13.82	0.6990	115.4150

[a] °C. [b] bar. [c] g cm^{-3}. [d] cal mole^{-1} (°K)$^{-1}$.

Turner, Joachim Hampel, David Pitou, and Joan Delany, who assisted at various times with plotting, drafting, and preparation of the manuscript. The work reported here was supported in part by NSF grants GA 25314, GA 36023, and GA 35888 in addition to funds received from the University of California Research Committee, the Anaconda Company, and the Kennecott Copper Corporation. Acknowledgment is also made with thanks to the donors of the Petroleum Research Fund, administered by the American Chemical Society, for support of this research under PRF #5356-AC2. Finally, we would like to express our appreciation to Debbie Aoki for contributing her expert talents in typing and retyping the manuscript.

TABLE 39

Summary of thermodynamic properties of steam-saturated H_2O_{liquid}

t[a]	P[b]	ε	$\left(\frac{\partial \ln \varepsilon}{\partial P}\right)_T$[c] × 10^5	$\left(\frac{\partial \ln \varepsilon}{\partial T}\right)_P$[d] × 10^3	$\left(\frac{\partial^2 \ln \varepsilon}{\partial P^2}\right)_T$[e] × 10^9	$\left(\frac{\partial^2 \ln \varepsilon}{\partial T^2}\right)_P$[f] × 10^6	$\left(\frac{\partial(\partial \ln \varepsilon/\partial P)_T}{\partial T}\right)_P$[g] × 10^7	$\left(\frac{\partial^2(\partial \ln \varepsilon/\partial P)_T}{\partial T^2}\right)_P$[h] × 10^8
0	0.006	87.79	4.72	-4.42	-9.8	-4.79	-0.35	
5	0.009	85.86	4.70	-4.45	-12.6	-5.73	-0.52	-0.13
10	0.012	83.97	4.68	-4.48	-14.1	-5.75	-0.42	3.64
15	0.017	82.10	4.66	-4.50	-14.8	-5.34	-0.19	5.30
20	0.023	80.27	4.66	-4.53	-15.2	-4.74	0.09	5.84
25	0.032	78.47	4.67	-4.55	-15.4	-4.09	0.33	5.85
30	0.042	76.70	4.70	-4.57	-15.6	-3.47	0.67	5.63
35	0.056	74.96	4.74	-4.59	-15.7	-2.89	0.95	5.35
40	0.074	73.26	4.79	-4.60	-16.0	-2.38	1.21	5.08
45	0.096	71.59	4.86	-4.61	-16.3	-1.94	1.46	4.84
50	0.123	69.96	4.94	-4.62	-16.7	-1.57	1.69	4.65
55	0.158	68.36	5.03	-4.63	-17.2	-1.26	1.92	4.51
60	0.199	66.79	5.13	-4.63	-17.7	-1.02	2.15	4.41
65	0.250	65.26	5.24	-4.64	-18.4	-0.82	2.36	4.36
70	0.312	63.77	5.37	-4.64	-19.2	-0.67	2.58	4.34
75	0.386	62.30	5.50	-4.64	-20.1	-0.57	2.80	4.35
80	0.474	60.87	5.64	-4.65	-21.1	-0.51	3.02	4.41
85	0.578	59.48	5.80	-4.65	-22.2	-0.48	3.24	4.49
90	0.701	58.11	5.97	-4.65	-23.5	-0.47	3.47	4.60
95	0.845	56.77	6.15	-4.65	-24.9	-0.50	3.70	4.74
100	1.013	55.47	6.34	-4.66	-26.4	-0.55	3.94	4.91
105	1.208	54.19	6.54	-4.66	-28.1	-0.62	4.19	5.12
110	1.433	52.94	6.75	-4.66	-30.0	-0.71	4.45	5.36
115	1.691	51.73	6.98	-4.67	-32.0	-0.82	4.72	5.63
120	1.985	50.53	7.23	-4.67	-34.2	-0.94	5.01	5.95
125	2.321	49.37	7.48	-4.67	-36.6	-1.08	5.32	6.31
130	2.701	48.23	7.76	-4.68	-39.3	-1.24	5.64	6.72
135	3.130	47.11	8.04	-4.69	-42.3	-1.42	5.98	7.17
140	3.613	46.02	8.35	-4.69	-45.5	-1.62	6.35	7.69
145	4.154	44.96	8.68	-4.70	-49.0	-1.84	6.75	8.27
150	4.758	43.91	9.02	-4.71	-52.9	-2.09	7.17	8.92
155	5.431	42.89	9.39	-4.72	-57.2	-2.37	7.63	9.66
160	6.178	41.89	9.78	-4.73	-62.0	-2.68	8.13	10.48
165	7.004	40.91	10.19	-4.75	-67.3	-3.02	8.66	11.42
170	7.916	39.96	10.63	-4.76	-73.1	-3.41	9.25	12.47
175	8.920	39.02	11.10	-4.78	-79.6	-3.84	9.89	13.66
180	10.021	38.10	11.60	-4.80	-86.8	-4.33	10.59	15.01
185	11.226	37.20	12.14	-4.82	-94.8	-4.87	11.36	16.55
190	12.543	36.32	12.72	-4.85	-103.8	-5.48	12.20	18.30
195	13.978	35.45	13.33	-4.87	-113.9	-6.16	13.14	20.30
200	15.537	34.60	14.00	-4.90	-125.2	-6.	14.17	22.60
225	25.476	30.58	18.20	-5.12	-209.4	-12.41	21.45	40.78
250	39.729	26.87	24.66	-5.50	-380.9	-22.30	35.00	82.44
275	59.415	23.38	35.40	-6.18	-783.3	-41.38	63.63	196.55
300	85.805	19.99	55.52	-7.42	-1953.8	-84.56	137.25	612.38
325	120.387	16.58	101.95	-10.02	-6917.8	-222.63	407.75	3149.17
350	165.125	12.87	274.99	-18.24	-57594.1	-1232.61	2716.03	45593.00

[a] °C. [b] bar. [c] $(°K)^{-1}$. [d] $(°K)^{-2}$. [e] bar^{-1} [f] bar^{-1} $(°K)^{-1}$. [g] bar^{-2}. [h] bar^{-1} $(°K)^{-2}$.

TABLE 40

Summary of Born functions (eqs 65 through 69) for steam-saturated H_2O_{liquid}

t[a]	P[b]	Y[c] × 10^5	X[d] × 10^7	Q[e] × 10^6	U[f] × 10^9	N[g] × 10^{10}
0.00	.006	-5.04	-2.77	0.54	1.98	-1.37
5.00	.009	-5.18	-2.97	0.55	1.83	-1.73
10.00	.012	-5.33	-3.07	0.56	1.99	-1.94
15.00	.017	-5.49	-3.12	0.57	2.33	-2.07
20.00	.023	-5.64	-3.15	0.58	2.75	-2.17
25.00	.032	-5.80	-3.16	0.60	3.20	-2.24
30.00	.042	-5.96	-3.18	0.61	3.68	-2.32
35.00	.056	-6.12	-3.19	0.63	4.17	-2.40
40.00	.074	-6.28	-3.21	0.65	4.66	-2.49
45.00	.096	-6.44	-3.24	0.68	5.16	-2.60
50.00	.123	-6.60	-3.28	0.71	5.68	-2.73
55.00	.158	-6.77	-3.32	0.74	6.22	-2.88
60.00	.199	-6.94	-3.37	0.77	6.77	-3.05
65.00	.250	-7.11	-3.42	0.80	7.35	-3.24
70.00	.312	-7.28	-3.48	0.84	7.95	-3.46
75.00	.386	-7.45	-3.55	0.88	8.59	-3.71
80.00	.474	-7.63	-3.63	0.93	9.27	-3.99
85.00	.578	-7.82	-3.71	0.98	9.98	-4.31
90.00	.701	-8.00	-3.81	1.03	10.74	-4.66
95.00	.845	-8.20	-3.90	1.08	11.55	-5.05
100.00	1.013	-8.39	-4.01	1.14	12.42	-5.49
105.00	1.208	-8.60	-4.12	1.21	13.35	-5.98
110.00	1.433	-8.81	-4.24	1.28	14.36	-6.52
115.00	1.691	-9.02	-4.37	1.35	15.43	-7.13
120.00	1.985	-9.24	-4.50	1.43	16.60	-7.80
125.00	2.321	-9.47	-4.65	1.52	17.86	-8.56
130.00	2.701	-9.71	-4.80	1.61	19.22	-9.40
135.00	3.130	-9.95	-4.97	1.71	20.71	-10.34
140.00	3.613	-10.20	-5.14	1.81	22.32	-11.40
145.00	4.154	-10.46	-5.33	1.93	24.09	-12.58
150.00	4.758	-10.73	-5.53	2.05	26.01	-13.91
155.00	5.431	-11.01	-5.75	2.19	28.13	-15.40
160.00	6.178	-11.30	-5.99	2.33	30.45	-17.08
165.00	7.004	-11.61	-6.25	2.49	33.01	-18.98
170.00	7.916	-11.92	-6.53	2.66	35.83	-21.12
175.00	8.920	-12.25	-6.84	2.85	38.95	-23.55
180.00	10.021	-12.60	-7.18	3.05	42.42	-26.31
185.00	11.226	-12.96	-7.56	3.26	46.27	-29.45
190.00	12.543	-13.34	-7.98	3.50	50.58	-33.03
195.00	13.978	-13.75	-8.44	3.76	55.39	-37.13
200.00	15.537	-14.17	-8.95	4.05	60.80	-41.85
225.00	25.476	-16.75	-12.63	5.95	100.62	-79.30
250.00	39.728	-20.48	-19.57	9.18	180.75	-164.37
275.00	59.415	-26.42	-34.02	15.14	365.68	-388.63
300.00	85.805	-37.09	-69.80	27.77	892.43	-1131.44
325.00	120.387	-60.43	-194.82	61.49	3075.19	-4798.85
350.00	165.125	-141.66	-1215.87	213.62	24995.05	-50615.56

[a] °C. [b] bar. [c] $(°K)^{-1}$. [d] $(°K)^{-2}$. [e] bar^{-1} [f] bar^{-1} $(°K)^{-1}$. [g] bar^{-2}.

APPENDIX

The partial derivatives of equation (16) can be expressed in simple notation by first writing

$$Q = \underline{x} \sum_{\underline{j}=1}^{7} \underline{Y}_{\underline{j}} \underline{z}_{\underline{j}} \tag{A-1}$$

where

$$\underline{x} = \tau - \tau_{\underline{c}} \,, \tag{A-2}$$

$$\underline{Y}_{\underline{j}} = (\tau - \tau_{\underline{a}\underline{j}})^{\underline{j}-2} \,, \tag{A-3}$$

and

$$\underline{z}_{\underline{j}} = \underline{u}_{\underline{j}} + \underline{v}\underline{w}_{\underline{j}} \,, \tag{A-4}$$

where

$$\underline{u}_{\underline{j}} = \sum_{\underline{i}=1}^{8} \underline{A}_{\underline{i}\underline{j}} (\rho - \rho_{\underline{a}\underline{j}})^{\underline{i}-1} \,, \tag{A-5}$$

$$\underline{v} = e^{-4.8\rho} \,, \tag{A-6}$$

and

$$\underline{w}_{\underline{j}} = \sum_{\underline{i}=9}^{10} \underline{A}_{\underline{i}\underline{j}} \rho^{\underline{i}-9} \,. \tag{A-7}$$

It then follows that

$$\left(\frac{\partial Q}{\partial \tau}\right)_P = \frac{Q}{\underline{x}}\left(\frac{\partial \underline{x}}{\partial \tau}\right)_P + \underline{x} \sum_{\underline{j}=1}^{7} \left(\underline{Y}_{\underline{j}} \left(\frac{\partial \underline{z}_{\underline{j}}}{\partial \tau}\right)_P + \underline{z}_{\underline{j}} \left(\frac{\partial \underline{Y}_{\underline{j}}}{\partial \tau}\right)_P\right) \tag{A-8}$$

and

$$\left(\frac{\partial^2 Q}{\partial \tau^2}\right)_P = \frac{Q}{\underline{x}}\left(\frac{\partial^2 \underline{x}}{\partial \tau^2}\right)_P + \frac{2}{\underline{x}}\left(\frac{\partial \underline{x}}{\partial \tau}\right)_P \left(\left(\frac{\partial Q}{\partial \tau}\right)_P - \frac{Q}{\underline{x}}\left(\frac{\partial \underline{x}}{\partial \tau}\right)_P\right)$$

$$+ \underline{x} \sum_{\underline{j}=1}^{7} \left(\underline{Y}_{\underline{j}} \left(\frac{\partial^2 \underline{z}_{\underline{j}}}{\partial \tau^2}\right)_P + 2\left(\frac{\partial \underline{Y}_{\underline{j}}}{\partial \tau}\right)_P \left(\frac{\partial \underline{z}_{\underline{j}}}{\partial \tau}\right)_P + \underline{z}_{\underline{j}} \left(\frac{\partial^2 \underline{Y}_{\underline{j}}}{\partial \tau^2}\right)_P\right) \tag{A-9}$$

where

$$\left(\frac{\partial \underline{x}}{\partial \tau}\right)_P = -\frac{\tau}{\underline{x}} \,, \tag{A-10}$$

$$\left(\frac{\partial^2 \underline{x}}{\partial \tau^2}\right)_P = \frac{2\tau}{\underline{x}^2} \,, \tag{A-11}$$

$$\left(\frac{\partial \underline{Y}_{\underline{j}}}{\partial \tau}\right)_P = -\frac{(\underline{j}-2)\tau \underline{Y}_{\underline{j}}}{\underline{x}(\tau - \tau_{\underline{a}\underline{j}})} \,, \tag{A-12}$$

$$\left(\frac{\partial^2 \underline{Y}_{\underline{j}}}{\partial \tau^2}\right)_P = \frac{1}{\underline{Y}_{\underline{j}}}\left(\frac{\partial \underline{Y}_{\underline{j}}}{\partial \tau}\right)_P^2 + \frac{\underline{Y}_{\underline{j}}(\underline{j}-2)\tau(\tau - 2\tau_{\underline{a}\underline{j}})}{\underline{x}^2(\tau - \tau_{\underline{a}\underline{j}})^2} \,, \tag{A-13}$$

$$\left(\frac{\partial \underline{z}_{\underline{j}}}{\partial \tau}\right)_P = \left(\frac{\partial \underline{u}_{\underline{j}}}{\partial \tau}\right)_P + \underline{v}\left(\frac{\partial \underline{w}_{\underline{j}}}{\partial \tau}\right)_P + \underline{w}_{\underline{j}}\left(\frac{\partial \underline{v}}{\partial \tau}\right)_P \,, \tag{A-14}$$

and

$$\left(\frac{\partial^2 \underline{z}_{\underline{j}}}{\partial \tau^2}\right)_P = \left(\frac{\partial^2 \underline{u}_{\underline{j}}}{\partial \tau^2}\right)_P + \underline{v}\left(\frac{\partial^2 \underline{w}_{\underline{j}}}{\partial \tau^2}\right)_P + 2\left(\frac{\partial \underline{v}}{\partial \tau}\right)_P \left(\frac{\partial \underline{w}_{\underline{j}}}{\partial \tau}\right)_P + \underline{w}_{\underline{j}}\left(\frac{\partial^2 \underline{v}}{\partial \tau^2}\right)_P \tag{A-15}$$

where

$$\left(\frac{\partial \underline{u}_{\underline{j}}}{\partial \tau}\right)_P = -\alpha\rho \sum_{\underline{i}=1}^{8} (\underline{i}-1)\, \underline{A}_{\underline{i}\underline{j}} (\rho - \rho_{\underline{a}\underline{j}})^{\underline{i}-2} \,, \tag{A-16}$$

$$\left(\frac{\partial^2 \underline{u}_{\underline{j}}}{\partial \tau^2}\right)_P = \frac{1}{\alpha}\left(\frac{\partial \underline{u}_{\underline{j}}}{\partial \tau}\right)_P \left(\left(\frac{\partial \alpha}{\partial \tau}\right)_P - \alpha^2\right)$$

$$+ \rho^2\alpha^2 \sum_{\underline{i}=1}^{8} (\underline{i}-1)(\underline{i}-2)\underline{A}_{\underline{i}\underline{j}} (\rho - \rho_{\underline{a}\underline{j}})^{\underline{i}-3} \,, \tag{A-17}$$

$$\left(\frac{\partial \underline{v}}{\partial \tau}\right)_P = 4.8\rho\alpha\underline{v} \,, \tag{A-18}$$

$$\left(\frac{\partial^2 \underline{v}}{\partial \tau^2}\right)_P = 4.8\left(\rho\alpha\left(\frac{\partial \underline{v}}{\partial \tau}\right)_P + \rho\underline{v}\left(\frac{\partial \alpha}{\partial \tau}\right)_P - \rho\underline{v}\alpha^2\right) \,, \tag{A-19}$$

$$\left(\frac{\partial \underline{w}_{\underline{j}}}{\partial \tau}\right)_P = -\rho\alpha\underline{A}_{10\underline{j}} \tag{A-20}$$

and

$$\left(\frac{\partial^2 \underline{w}_j}{\partial T^2}\right)_P = \rho \underline{A}_{10j} \left(\alpha^2 - \left(\frac{\partial \alpha}{\partial T}\right)_P\right) \tag{A-21}$$

Similarly, we can write

$$\left(\frac{\partial Q}{\partial \rho}\right)_T = \underline{x} \sum_{j=1}^{7} \underline{Y}_j \left(\frac{\partial \underline{z}_j}{\partial \rho}\right)_T , \tag{A-22}$$

$$\left(\frac{\partial^2 Q}{\partial \rho^2}\right)_T = \underline{x} \sum_{j=1}^{7} \underline{Y}_j \left(\frac{\partial^2 \underline{z}_j}{\partial \rho^2}\right)_T \tag{A-23}$$

and

$$\left(\frac{\partial^3 Q}{\partial \rho^3}\right)_T = \underline{x} \sum_{j=1}^{7} \underline{Y}_j \left(\frac{\partial^3 \underline{z}_j}{\partial \rho^3}\right)_T \tag{A-24}$$

where

$$\left(\frac{\partial \underline{z}_j}{\partial \rho}\right)_T = \left(\frac{\partial \underline{u}_j}{\partial \rho}\right)_T + \underline{v} \left(\frac{\partial \underline{w}_j}{\partial \rho}\right)_T + \underline{w}_j \left(\frac{\partial \underline{v}}{\partial \rho}\right)_T , \tag{A-25}$$

$$\left(\frac{\partial^2 \underline{z}_j}{\partial \rho^2}\right)_T = \left(\frac{\partial^2 \underline{u}_j}{\partial \rho^2}\right)_T + 2\left(\frac{\partial \underline{v}}{\partial \rho}\right)_T \left(\frac{\partial \underline{w}_j}{\partial \rho}\right)_T + \underline{w}_j \left(\frac{\partial^2 \underline{v}}{\partial \rho^2}\right)_T \tag{A-26}$$

and

$$\left(\frac{\partial^3 \underline{z}_j}{\partial \rho^3}\right)_T = \left(\frac{\partial^3 \underline{u}_j}{\partial \rho^3}\right)_T + 3\left(\frac{\partial^2 \underline{v}}{\partial \rho^2}\right)_T \left(\frac{\partial \underline{w}_j}{\partial \rho}\right)_T + \underline{w}_j \left(\frac{\partial^3 \underline{v}}{\partial \rho^3}\right)_T \tag{A-27}$$

where

$$\left(\frac{\partial \underline{u}_j}{\partial \rho}\right)_T = -\frac{1}{\rho \alpha} \left(\frac{\partial \underline{u}_j}{\partial T}\right)_P \tag{A-28}$$

$$\left(\frac{\partial^2 \underline{u}_j}{\partial \rho^2}\right)_T = \sum_{i=1}^{8} (\underline{i}-1)(\underline{i}-2)\, \underline{A}_{ij} (\rho - \rho_{\underline{a}j})^{\underline{i}-3} \tag{A-29}$$

$$\left(\frac{\partial^3 \underline{u}_j}{\partial \rho^3}\right)_T = \sum_{i=1}^{8} (\underline{i}-1)(\underline{i}-2)(\underline{i}-3)\, \underline{A}_{ij} (\rho - \rho_{\underline{a}j})^{\underline{i}-4} , \tag{A-30}$$

$$\left(\frac{\partial \underline{v}}{\partial \rho}\right)_T = -4.8\underline{v} , \tag{A-31}$$

$$\left(\frac{\partial^2 \underline{v}}{\partial \rho^2}\right)_T = -4.8\left(\frac{\partial \underline{v}}{\partial \rho}\right)_T , \tag{A-32}$$

$$\left(\frac{\partial^3 \underline{v}}{\partial \rho^3}\right)_T = -4.8\left(\frac{\partial^2 \underline{v}}{\partial \rho^2}\right)_T , \tag{A-33}$$

and

$$\left(\frac{\partial \underline{w}_j}{\partial \rho}\right)_T = \underline{A}_{10j} . \tag{A-34}$$

By cross partial differentiation it also follows that

$$\left(\frac{\partial\left(\frac{\partial Q}{\partial \rho}\right)_T}{\partial T}\right)_P = \frac{1}{\underline{x}} \left(\frac{\partial Q}{\partial \rho}\right)_T \left(\frac{\partial \underline{x}}{\partial T}\right)_P + \underline{x} \sum_{j=1}^{7} \left(\frac{\partial \underline{Y}_j}{\partial T}\right)_P \left(\frac{\partial \underline{z}_j}{\partial \rho}\right)_T + \underline{Y}_j \left(\frac{\partial\left(\frac{\partial \underline{z}_j}{\partial \rho}\right)_T}{\partial T}\right)_P \tag{A-35}$$

where

$$\left(\frac{\partial\left(\frac{\partial \underline{z}_j}{\partial \rho}\right)_T}{\partial T}\right)_P = \left(\frac{\partial\left(\frac{\partial \underline{u}_j}{\partial \rho}\right)_T}{\partial T}\right)_P + \underline{w}_j \left(\frac{\partial\left(\frac{\partial \underline{v}}{\partial \rho}\right)_T}{\partial T}\right)_P + 2\left(\frac{\partial \underline{w}_j}{\partial \rho}\right)_T \left(\frac{\partial \underline{v}}{\partial T}\right)_P \tag{A-36}$$

in which

$$\left(\frac{\partial\left(\frac{\partial \underline{u}_j}{\partial \rho}\right)_T}{\partial T}\right)_P = -\rho\alpha \left(\frac{\partial^2 \underline{u}_j}{\partial \rho^2}\right)_T \tag{A-37}$$

and

$$\left(\frac{\partial\left(\frac{\partial \underline{v}}{\partial \rho}\right)_T}{\partial T}\right)_P = -4.8\left(\frac{\partial \underline{v}}{\partial T}\right)_P \tag{A-38}$$

Also,

$$\left(\frac{\partial\left(\frac{\partial^2 Q}{\partial \rho^2}\right)_T}{\partial T}\right)_P = \frac{1}{\underline{x}} \left(\frac{\partial^2 Q}{\partial \rho^2}\right)_T \left(\frac{\partial \underline{x}}{\partial T}\right)_P + \underline{x} \sum_{j=1}^{7} \left(\underline{Y}_j \left(\frac{\partial\left(\frac{\partial^2 \underline{z}_j}{\partial \rho^2}\right)_T}{\partial T}\right)_P + \left(\frac{\partial \underline{Y}_j}{\partial T}\right)_P \left(\frac{\partial^2 \underline{z}_j}{\partial \rho^2}\right)_T\right) \tag{A-39}$$

where

$$\left(\frac{\partial\left(\frac{\partial^2 z_j}{\partial\rho^2}_T\right)}{\partial T}\right)_P = \left(\frac{\partial\left(\frac{\partial^2 u_j}{\partial\rho^2}_T\right)}{\partial T}\right)_P + 2\left(\frac{\partial\left(\frac{\partial v}{\partial\rho}\right)_T}{\partial T}\right)_P \left(\frac{\partial w_j}{\partial\rho}\right)_T + w_j\left(\frac{\partial\left(\frac{\partial^2 v}{\partial\rho^2}_T\right)}{\partial T}\right)_P + \left(\frac{\partial w_j}{\partial T}\right)_P \left(\frac{\partial^2 v}{\partial\rho^2}\right)_T \quad \text{(A-40)}$$

in which

$$\left(\frac{\partial\left(\frac{\partial^2 u_j}{\partial\rho^2}_T\right)}{\partial T}\right)_P = -\rho o\left(\frac{\partial^3 u_j}{\partial\rho^3}\right)_T \quad \text{(A-41)}$$

and

$$\left(\frac{\partial\left(\frac{\partial^2 v}{\partial\rho^2}\right)_T}{\partial T}\right)_P = -4.8\left(\frac{\partial\left(\frac{\partial v}{\partial\rho}\right)_T}{\partial T}\right)_P \quad \text{(A-42)}$$

The first and second isochoric partial derivatives of equation (16) can be written as

$$\left(\frac{\partial Q}{\partial T}\right)_\rho = \left(\frac{\partial Q}{\partial T}\right)_P - x\sum_{j=1}^{7} Y_j\left(\frac{\partial z_j}{\partial T}\right)_P \quad \text{(A-43)}$$

and

$$\left(\frac{\partial^2 Q}{\partial T^2}\right)_\rho = \frac{Q}{x}\left(\frac{\partial^2 x}{\partial T^2}\right)_P + \frac{2}{x}\left(\frac{\partial x}{\partial T}\right)_P\left(\left(\frac{\partial Q}{\partial T}\right)_\rho - \frac{Q}{x}\left(\frac{\partial x}{\partial T}\right)_P\right) + x\sum_{j=1}^{7} z_j\left(\frac{\partial^2 Y_j}{\partial T^2}\right)_P \quad \text{(A-44)}$$

Further,

$$\left(\frac{\partial\left(\frac{\partial Q}{\partial T}\right)_\rho}{\partial T}\right)_P = \left(\frac{\partial^2 Q}{\partial T^2}\right)_P + \frac{1}{x}\left(\frac{\partial x}{\partial T}\right)_P\left(\left(\frac{\partial Q}{\partial T}\right)_\rho - \left(\frac{\partial Q}{\partial T}\right)_P\right) - x\sum_{j=1}^{7}\left(Y_j\left(\frac{\partial^2 z_j}{\partial T^2}\right)_P + \left(\frac{\partial Y_j}{\partial T}\right)_P\left(\frac{\partial z_j}{\partial T}\right)_P\right) \quad \text{(A-45)}$$

and

$$\left(\frac{\partial\left(\frac{\partial Q}{\partial\rho}\right)_T}{\partial T}\right)_\rho = \frac{1}{x}\left(\frac{\partial Q}{\partial\rho}\right)_T\left(\frac{\partial x}{\partial T}\right)_P + x\sum_{j=1}^{7}\left(\frac{\partial Y_j}{\partial T}\right)_P\left(\frac{\partial z_j}{\partial\rho}\right)_T . \quad \text{(A-46)}$$

from which it follows that

$$\left(\frac{\partial\left(\frac{\partial\left(\frac{\partial Q}{\partial\rho}\right)_T}{\partial T}\right)_\rho}{\partial T}\right)_P = -\frac{1}{x}\left(\frac{\partial Q}{\partial\rho}\right)_T\left(\frac{\partial^2 x}{\partial T^2}\right)_P + \frac{1}{x}\left(\frac{\partial x}{\partial T}\right)_P\left(\left(\frac{\partial\left(\frac{\partial Q}{\partial\rho}\right)_T}{\partial T}\right)_P + \left(\frac{\partial\left(\frac{\partial Q}{\partial\rho}\right)_T}{\partial T}\right)_\rho - \frac{2}{x}\left(\frac{\partial x}{\partial T}\right)_P\left(\frac{\partial Q}{\partial\rho}\right)_T\right) + x\sum_{j=1}^{7}\left(\left(\frac{\partial Y_j}{\partial T}\right)_P\left(\frac{\partial\left(\frac{\partial z_j}{\partial\rho}\right)_T}{\partial T}\right)_P + \left(\frac{\partial z_j}{\partial\rho}\right)_T\left(\frac{\partial^2 Y_j}{\partial T^2}\right)_P\right) . \quad \text{(A-47)}$$

The first and second partial derivatives of equation (15) with respect to temperature can be written as

$$\left(\frac{\partial\psi^\circ}{\partial T}\right)_\rho = \sum_{j=1}^{6}\left((1-1)\,c_j/(T\tau^{(j-1)})\right) + (c_7 + 2c_8)/T \quad \text{(A-48)}$$

and

$$\left(\frac{\partial^2\psi^\circ}{\partial T^2}\right)_\rho = \sum_{j=1}^{6}\left((j-1)(j-2)\,c_j/(T^2\tau^{(j-1)})\right) - (c_7 + 2c_8)/T^2 . \quad \text{(A-49)}$$

References

Adams, L. H., 1931, Equilibrium in binary systems under pressure. I. An experimental and thermodynamic investigation of the system NaCl–H_2O at 25°: Am Chem. Soc. Jour., v. 53, p. 3769-3813.

Akerlof, G. C., 1932, Dielectric constants of some organic solvent-water mixtures at various temperatures: Am. Chem. Soc. Jour., v. 54, p. 4125-4139.

Akerlof, G. C., and Oshry, H. I., 1950, The dielectric constant of water at high temperatures and in equilibrium with its vapor: Am. Chem. Soc. Jour., v. 72, p. 2844-2847.

Al'tshuler, L. V., Bakanova, A. A., and Trunin, R. F., 1958, Phase transformations of of water compressed by strong shock waves: Soviet Physics Doklady, v. 3, p. 761-763.

Amagat, E. N., 1893, Elasticite et dilatibilite des fluids: Annales de Chimie et Physique, ser. 6, v. 29, p. 68-136; 505-574.

Anderson, G. M., 1964, The calculated fugacity of water to 1000°C and 10,000 bars: Geochim. et Cosmochim. Acta, v. 28, p. 713-715.

———— 1967, Specific volumes and fugacities of water, *in* Barnes, H. L., ed., Geochemistry of hydrothermal ore deposits: San Francisco, Calif., Holt, Rinehart and Wilson, p. 632-635.

Arden, B. W., and Astill, K. N., 1970, Numerical algorithms: origins and applications: Menlo Park, Calif., Addison-Wesley, 308 p.

Bain, R. W., ed., 1964, Steam Tables 1964: Edinburgh, Her Majesty's Stationery Office, Natl. Eng. Lab., Dept. Sci. Indus. Research, 147 p.

Barker, J. A., and Henderson, D., 1972, The structure and properties of water and aqueous solutions: Washington, D.C., Dept. Interior, Office of Saline Water, Resources and Devel. Prog. Rept. No. 773, 41 p.

Benson, S. W., 1968, Thermochemical Kinetics: New York, John Wiley and Sons, 223 p.

Born, M., 1920, Volumen und Hydratationswärme der Ionen: Zeitschr. Physik, v. 1, p. 45-48.

Bridgeman, P. W., 1913, The thermodynamic properties of liquid water to 80°C and 12,000 KGM: Am. Acad. Arts and Sci. Proc., v. 48, p. 307-362.

———— 1931, The volume of 18 liquids as a function of pressure: Am. Acad. Arts and Sci. Proc., v. 66, p. 185-233.

———— 1935, The pressure-volume-temperature relations of the liquid and the phase diagram of heavy water: *Jour Chem Physics*, v. 3, p. 597-605.

Burnham, C. W., Holloway, J. R., and Davis, N. F., 1969a, The specific volume of water in the range 1000 to 8900 bars, 20° to 900° C: Am. Jour. Sci., v. 267-A, Schairer, p. 70-95.

———— 1969b, Thermodynamic properties of water to 1,000°C and 10,000 bars: Geol. Soc. America Spec. Paper 132, 96 p.

Callendar, G. S., and Egerton, A. C., 1944, The 1939 Callendar steam tables: London, 1973 p.

———— 1958, Tables of total heat of steam: Leatherhead, Surrey, Elec. Research Assoc., ERA Rept. J/T 173, 72 p.

Carnot, S., 1824, Reflexions sur la puissance motrice du feu: Paris, Chez Bachelier Libraire.

Cole, R. H., 1960, Dielectric polarization and loss: Ann. Rev. Physics Chemistry, v. 11, p. 149-168.

David, H. D., and Hamann, S. D., 1959, The chemical effects of pressure, Part 5.—The electrical conductivity of water at high shock pressures: Faraday Soc. Trans., v. 55, p. 72-77.

———— 1960, The chemical effects of pressure, Part 6.—The electrical conductivity of several liquids at high shock pressures: Faraday Soc. Trans., v. 56, p. 1043-1050.

Dorsey, N. E., 1940, Properties of ordinary water substance: New York, Reinhold Publishing Corp., 673 p.

Dudziak, K. H., and Franck, E. U., 1966, Messungen der Viskosität des Wassers bis 560°C und 3500 bar: Ber. Bunsengesellschaft für phys. Chemie, v. 70, p. 1120-1128.

Dzung, L. S., and Rohrbach, U. W., 1955, Enthalpie-Entropie Diagramme für Wasserdampf und Wasser: Berlin, Springer.

Fine, R. A., and Millero, F. J., 1973, Compressibility of water as a function of temperature and pressure: Jour. Chem. Physics, v. 59, p. 5529-5536.

Fisher, J. R., and Barnes, H. L., 1972, The ion-product constant of water to 350°: Jour. Phys. Chemistry, v. 76, p. 90-99.

Fogo, J. K., Benson, S. W., and Copeland, C. S., 1954, The electrical conductivity of supercritical solutions of sodium chloride and water: Jour. Chem. Physics, v. 22, p. 212-217.

Franck, E. U., 1956, Hochverdichteter Wasserdampf II. Ionendissoziation von KCl in H_2O bis 750°C: Zeitschr. Phys. Chemie, v. 8, p. 107-126.

———— 1961, Überkritisches Wasser als electrolytisches Lösungsmittel: Angew. Chemie, v. 73, p. 309-322.

———— 1969, Ions in aqueous solutions at high temperatures and pressures: Jour. Chem. Physics, p. 9-18.

Franks, F., ed., 1972, Water Volume I, The physics and chemistry of water: New York, Plenum Press, 596 p.

Gier, T. E., and Young, H. S., 1963, private communication cited by Lawson, A. W., and Hughes, A. J., "High pressure properties of water", *in* Bradley, R. S., ed., High pressure physics and chemistry, v. 1: New York, Acad. Press, p. 207-225.

Gildseth, W., Habenschuss, A., and Spedding, F. H., 1972, Precision measurements of densities and thermal dilation of water between 5° and 80°C: Jour. Chem. Eng. Data, v. 17, p. 402-409.

Goranson, R. W., 1938, Silicate-water systems; phase equilibrium in the $NaAlSi_3O_8$–H_2O and $KAlSi_3O_8$–H_2O systems at high temperatures and pressures: Am. Jour. Sci., 5th ser., v. 35-A, p. 71-91.

———— 1942, Temperature-pressure-volume and phase relations of water, *in* Birch, F., ed., Handbook of Physical Constants: Geol. Soc. America Spec. Paper 36, p. 203-212.

Greene, F. T., Beachey, J., Milne, T. A., 1972, An experimental study of the structure, thermodynamics and kinetic behavior of water: Washington, D.C., Dept. Interior, Office of Saline Water, Resources Devel. Prog. Rept. 772, 33 p.

Grindley, T., and Lind, J. E., Jr., 1971, PVT Properties of water and mercury: Jour. Chem. Physics, v. 54, p. 3983-3989.

Gurney, R. W., 1953, Ions in solution: Dover, N.Y., McGraw-Hill, 206 p.

Haas, J. L., Jr., 1970, Fugacity of H_2O from 0° to 350°C at the liquid-vapor equilibrium and at 1 atmosphere: Geochim. et Cosmochim. Acta, v. 34, p. 929-932.

Harris, F. E., Haycock E. W., and Alder, B. J., 1953, Dielectric polarization and structure of polar liquids under pressure: Jour Chem. Physics, v. 21, p. 1943-1948.

Hasted, J. B., 1961, The dielectric properties of water, *in* Birks, J. B., and Hard, J., eds., Progress in dielectrics, v. 3: London, Heywood and Co., p. 101-147.

———— 1972, Liquid water: dielectric properties, *in* Franks, F., ed., Water, v. I, The Physics and chemistry of water: New York, Plenum, p. 255-309.

Heger, K., ms, 1969, Die statische Dielektrizitätskonstante von Wasser und Methylalkohol im überkritischen Temperatur-und Druckbereich: Ph.D. dissert., Univ. Karlsruhe, Karlsruhe, West Germany, 59 p.

Helgeson, H. C., and Kirkham, D. H., 1974, Theoretical prediction of the thermodynamic behavior of aqueous electrolytes at high pressures and temperatures: II: Debye-Hückel parameters for activity coefficients and relative partial molal properties of the solute: Am. Jour. Sci., v. 274, p. 1199-1261.

———— 1975a, Theoretical prediction of the thermodynamic behavior of aqueous electrolytes at high pressures and temperatures. III. Equation of state for aqueous species at infinite dilution: Am. Jour. Sci., v. 275.

———— 1975b, Theretical prediction of the thermodynamic behavior of aqueous electrolytes at high pressures and temperatures. IV. Calculation of the thermodynamic properties of aqueous species and electrolyte solutions to 5 kb and 600°C: Am. Jour. Sci., v. 275.

Holloway, J. R., Eggler, D. H., and Davis, N. F., 1971, Analytical expression for calculating the fugacity and free energy of H_2O to 10,000 bars and 1,300°C: Geol. Soc. America Bull., v. 82, p. 2639-2642.

Holser, W. T., 1954, Fugacity of water at high temperatures and pressures: Jour. Phys. Chemistry, v. 58, p. 316-317.

Holser, W. T., and Kennedy, G. C., 1958, Properties of water. Part IV. Pressure-volume-temperature relations of water in the range 100-400°C and 100-1400 bars: Am. Jour. Sci., v. 256, p. 744-753.

———— 1959, Properties of water. Part V. Pressure-volume-temperature relations of water in the range 400-1000°C and 100-1400 bars: Am. Jour. Sci., v. 257, p. 71-77.

Holzapfel, W., and Franck, E. U., 1966, Leitfähigkeit und Ionendissoziation des Wassers bis 1000°C und 100 kbar: Ber. Bunsengeselschaft für phys. Chemie, v. 70, p. 1105-1112.

Horne, R. A., 1969, Marine chemistry: New York, John Wiley & Sons, 568 p.

———— ed., 1972, Water and aqueous solutions: New York, John Wiley & Sons, 837 p.

Howard J. C., 1961, Thermodynamic Data for Water: Washington, D.C., U.S. Dept. Commerce, Office Tech. Services, 15 p.

International Formulation Committee, 1967, The 1968 IFC formulation for Industrial use: Düsseldorf, Germany, IFC Secretariat, Ver. Deutscher Ingenieure.

———— 1968, The 1968 IFC formulation for scientific and general use: New York, Am. Soc. Mechanical Engineers, Secretariat, Internat. Conf. Properties of Steam.

Jansoone, V. M., and Franck, E. U., 1972, The dielectric constant of water to high temperatures and pressures from the mean spherical model in the wertheim solution: Ber. der Bunsengesellschaft für phys. Chemie, v. 76, p. 945.

Juza, J., Kmoníček, V., and Šifner, O., 1966, An equation of state for water and steam: Prague, Československé Akad. VED, Acad. Nakladatelstvi, p. 131-142.

Kay, R. L., Vidulich, G. A., and Pribadi, K. S., 1969, A reinvestigation of the dielectric constant of water and its temperature coefficient: Jour. Phys. Chemistry, v. 73, p. 445.

Keenan, J. H., 1930, Steam tables and Mollier diagram: New York, Am. Soc. Mechanical Eng.

Keenan, J. H., and Keyes, F. G., 1936, Thermodynamic Properties of Steam: New York, N.Y., John Wiley and Sons, Inc., 89 p.

Keenan, J. H., Keyes, F. G., Hill, P. G., and Moore, J. G., 1969, Steam Tables: New York, John Wiley and Sons, Inc., 162 p.

Kell, G. S., 1967, Precise representation of the volume properties of water at 1 atmosphere: Jour. Chem. Eng. Data, v. 12, no. 1, p. 66-70.

———— 1972, Thermodynamic and transport properties of fluid water, *in* Franks, F., ed., Water, Vol. 1, The physics and chemistry of water: New York, Plenum Press, p. 363-412.

Kell, G. S., McLaurin, G. E., and Whalley, E., 1968, Properties of water. II. Virial coefficients in the range 150° to 450°C without independent measurement of vapor volumes: Jour. Chem. Physics, v. 48, p. 3805-3813.

Kell, G. S., and Whalley, E., 1965, The PVT properties of water. I. Liquid water in the temperature range 0 to 150°C and at pressures up to 1 kb: Royal Soc. London Philos. Trans., ser. A, Math. Phys. Sci., v. 258, p. 565-617.

Kennedy, G. C., 1950, Pressure-volume-temperature relations in water at elevated temperatures and pressures: Am. Jour. Sci., v. 248, p. 540-564.

———— 1957, Properties of water Part I. Pressure-volume-temperature relations in steam to 100°C and 100 bars pressure: Am. Jour. Sci., v. 255, p. 724-730.

Kennedy, G. C., Knight, W. L., and Holser, W. T., 1958, Properties of Water. Part III. Specific volume of liquid water to 100°C and 1400 bars: Am. Jour. Sci., v. 256, p. 590-595.

Keyes, F. G., Smith, L.B., and Gerry, H. T., 1936, The specific volume of steam in the saturated and superheated condition together with derived values of the enthalpy, heat capacity, and Joule-Thompson coefficients: Part IV, Steam research program: Am. Acad. Arts and Sci. Proc., v. 70, p. 319-364.

Kirkwood, J. G., 1939, The dielectric polarization of polar liquids: Jour. Chem. Physics, v. 7, p. 911-919.

Knoblauch, O., Raisch, E., Hansen, H., and Koch, W., 1932, Tabellen und Diagramme für Wasserdampf: Munich and Berlin.

Köster, H., and Franck, E. U., 1969, Das spezifische Volumen des Wassers bei hohen Drücken bis 600°C und 10 kbar: Ber. der Bunsengesellschaft für phys. Chemie, v. 73, p. 716-722.

Kyropoulos, S., 1926, Die Druckabhängigkeit der Dielektrizitätskonstante einiger Flussigkeiten bis zu 3000 kg/cm²: Zeitschr. Physik., v. 40, p. 507-515.

Latimer, W. M., 1952, The oxidation states of the elements and their potentials in aqueous solutions: Englewood Cliffs, N.J., Prentice Hall, 392 p.

Lees, W. L., ms, 1949, Dielectric constants, as functions of pressure and temperature, of water and three alkyl halides: Ph.D. dissert., Harvard Univ., Dept. Physics, Cambridge, Mass.

Maier, S., and Franck, E. U., 1966, Die dichte des wassers von 200 bis 850°C und von 1000 bis 6000 bar: Ber. der Bunsengesellschaft für phys. Chemie, v. 70, p. 639-645.

Malmberg, C. G., and Maryott, A. A., 1956, Dielectric constant of water from 0° to 100°C: Natl. Bur. Standards Jour. Research, Research Paper 2641, v. 56, p. 1-8.

Meyer, C. A., McClintock, R. B., Silvestri, G. J., and Spencer, R. C., Jr., eds., 1967, Thermodynamic and Transport Properties of Steam: New York, Am. Soc. Mechanical Eng., 328 p.

Millero, F. J., Curry, R. W., and Drost-Hansen, W., 1969, Isothermal compressibility of water at various temperatures: Jour. Chem. Eng. Data, v. 14, p. 422-425.

Millero, F. J., Hoff, E. V., and Kahn, L., 1972, The effect of pressure on the ionization of water at various temperatures from molal-volume data: Jour. Solution Chemistry, v. 1, p. 309-327.

Millero, F. J., Knox, J. H., and Emmet, R. T., 1972, A high-precision, variable-pressure magnetic float densimeter: Jour. Solution Chemistry, v. 1, p. 173-186.

Mollier, R., 1932, Neue Tabellen und Diagramme für Wasserdampf: Berlin.

Nowak, E. S., and Grosh, R. J., 1961, An analyses of specific heat data for water and water vapor in the critical region: Argonne Natl. Lab. Tech. Rept. 8, 79 p.

Oshry, H. I., ms, 1949, The dielectric constant of saturated water from the boiling point to the critical point: Ph.D. dissert., Univ. Pittsburgh, Pittsburgh, Penn., 13 p.

Oster G., and Kirkwood, J. G., 1943, The influence of hindered molecular rotation on the dielectric constants of water, alcohols, and other polar liquids: Jour. Chem. Physics, v. 11, p. 175-178.

Owen, B. B., Miller, R. C., Milner, C. E., and Cogan, H. L., 1961, The dielectric constant of water as a function of temperature and pressure: Jour. Phys. Chemistry, v. 65, p. 2065-2070.

Owen, B. B., White, J. R., and Smith, J. S., 1956, An evaluation of the density of water at 5° intervals between 45 and 85°: Am. Chem. Soc. Jour., v. 78, p. 3561-3564.

Papetti, R. A., and Fujisaki, M. C., 1971, Equation of state of water at high temperatures and pressures: U.S. Natl. Tech. Inf. Service, AD Rept. 729757, 77 p.

Parker, V. B., Wagman, D. D., and Evans, W. H., 1971, Selected values of chemical thermodynamic properties, Part 6: Natl. Bur. Standards Tech. Note 270-6, 119 p.

Pistorius, C. W. F. T., and Sharp, W. E., 1960, Properties of water. Pt. VI, Entropy and Gibbs free energy of water in the range 10-1000°C and 1-250,000 bars: Am. Jour. Sci., v. 258, p. 757-768.

———— 1961, Erratum—Properties of water. Pt. VI, Entropy and Gibbs free energy of water in the range 10-1000°C and 1-250,000 bars, a clarification: Am. Jour. Sci., v. 259, p. 397-398.

Quist, A. S., 1970, The ionization constant of water to 800° and 4000 bars: Jour. Phys. Chemistry, v. 74, p. 3396-3402.

Quist, A. S., and Marshall, W. L., 1965, Estimation of the dielectric constant of water to 800°: Jour. Phys. Chemistry, v. 69, p. 3165-3167.

Rice, M. H., and Walsh, J. M., 1957, Equation of state of water to 250 kilobars: Jour. Chem. Physics, v. 26, p. 824-830.

Robie, R. A., and Waldbaum, D. R., 1968, Thermodynamic properties of minerals and related substances at 298.15°K (25°C) and one atmosphere (1.013 bars) pressure and at higher temperatures: U.S. Geol. Survey Bull. 1259, 256 p.

Rowe, A. M., Jr., and Chou, J. C. S., 1970, Pressure-volume-temperature-concentration relation of aqueous NaCl solutions: Jour. Chem. Eng. Data, v. 15, p. 61-66.

Scaife, B. K. P., 1955, Isothermal pressure dependence of the dielectric properties of eugenol, glycerol, and water: Physics. Soc. (London) Proc., v. B 68, p. 790-799.

Schall, R., 1950, Die zustandsgleichung des Wassers bei hohen Drucken nach Röntgenblitzaufnahmen intensiver Stosswellen: Zeitschr. angew. Physics, v. 2, p. 252-254.

Schmidt, E., 1969, Properties of water and steam in SI units: New York, Springer-Verlag, 205 p.

Sen, U., and Cobble, J. W., ms, 1974, A unified approach to the theory of electrolytes in water (in preparation).

Sengers, J. M. H., and Greer, S. C., 1972, Thermodynamic anomalies near the critical point of steam: Jour. Heat and Mass Transfer, v. 15, p. 1865-1886.

Sharp, W. E., 1952, The thermodynamic functions for water in the range −10 to 1000°C and 1 to 250,000 bars: Livermore, Calif., Univ. California Lawrence Radiation Lab., UCRL 7118, 51 p.

Thermal Stability of Chloritoid at High Pressure and relatively High Oxygen Fugacity[1]

by J. GANGULY *and* R. C. NEWTON

Department of Geological Sciences, Yale University and Department of the Geophysical Sciences, University of Chicago

ABSTRACT

The equilibrium conditions for the oxidation reaction of chloritoid to staurolite, magnetite, quartz, and vapor have been determined experimentally in the pressure range 10–25 kb using the hematite–magnetite buffer. At 10 kb total pressure the reaction is in equilibrium at 575° C. At 5 kb a value of 544° C was obtained by extrapolation of the high pressure results with an adjustment for the changing thermodynamic properties of water in the low pressure range.

At oxygen fugacities along the nickel–nickel oxide buffer, the thermal stability of chloritoid is promoted by 50–60° C above the hematite–magnetite values. Here the breakdown products staurolite, almandine, and magnetite are probably more stable.

The recently produced petrographic evidence for the oxidation breakdown of chloritoid and the relative lack of sensitivity of the reaction to moderate changes in total pressure and oxygen fugacity indicate that it may have potential as an important indicator on the temperature scale of progressive metamorphism. Several independent temperature estimates of the chloritoid breakdown event by workers in the field agree very well with the present value of about 550° C for the oxidation reaction of chloritoid to staurolite, magnetite, quartz, and vapor at the hematite–magnetite buffer in the pressure range 5–10 kb.

INTRODUCTION

CHLORITOID, $H_2FeAl_2SiO_7$, has long been recognized as an important marker mineral in the low and middle grades of metamorphism (Winkler, 1965, p. 78). It is found principally in pelitic schists and has interesting genetic and reaction relationships with other important iron-bearing silicate minerals, as deduced from petrographic evidence. It occurs in either a triclinic or monoclinic structure type. The two structures are closely related (Halferdahl, 1961), with probably only a small energy difference between them. Many occurrences are a mixture of the two polymorphs.

The present knowledge of the stability relations of chloritoid lags behind that concerning many other important rock-forming minerals largely because of the tardy recognition that oxygen fugacity plays a major role in determining which of the many proposed chloritoid reactions are stable. Experimental techniques for controlling oxygen fugacity in iron-bearing systems have been developed only in the last few years. Only one other extensive experimental investigation involving chloritoid has made use of oxygen-fugacity buffers, that of Richardson (1968).

[1] Research supported by National Science Foundation Grant GA573.

[Journal of Petrology, Vol. 9, Part 3, pp. 444–66, 1968]

GANGULY & N

In the review of so
that follows, the foll
(Chd)—$H_2FeAl_2SiO_7$
(Náray-Szabó & Sas
(Her)—$FeAl_2O_4$; alm

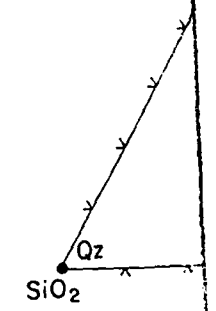

FIG. 1. Ternary diagram s
phases involved in the
cordierite, Alm = almand
h

(And), or sillimanite (
Fe_3O_4; hematite (Hem
alumina-rich low-tempe
(Kerrick, 1968) need no
reactions at elevated te
for staurolite has been
Schreyer & Chinner, 196
more water and less sil
Sasvári: there may be se
& Chinner, 1966). This
posed reactions involvin

Consideration of oxida
of various possible brea
anhydrous molecular

In the review of some of the proposed simple chloritoid breakdown reactions that follows, the following mineral formulae will be adhered to: chloritoid (Chd)—$H_2FeAl_2SiO_7$ (Halferdahl, 1961); staurolite (St)—$HFe_2Al_9Si_4O_{24}$ (Náray-Szabó & Sasvári, 1958); cordierite (Crd)—$Fe_2Al_4Si_5O_{18}$; hercynite (Her)—$FeAl_2O_4$; almandine (Alm)—$Fe_3Al_2Si_3O_{12}$; kyanite (Ky), andalusite

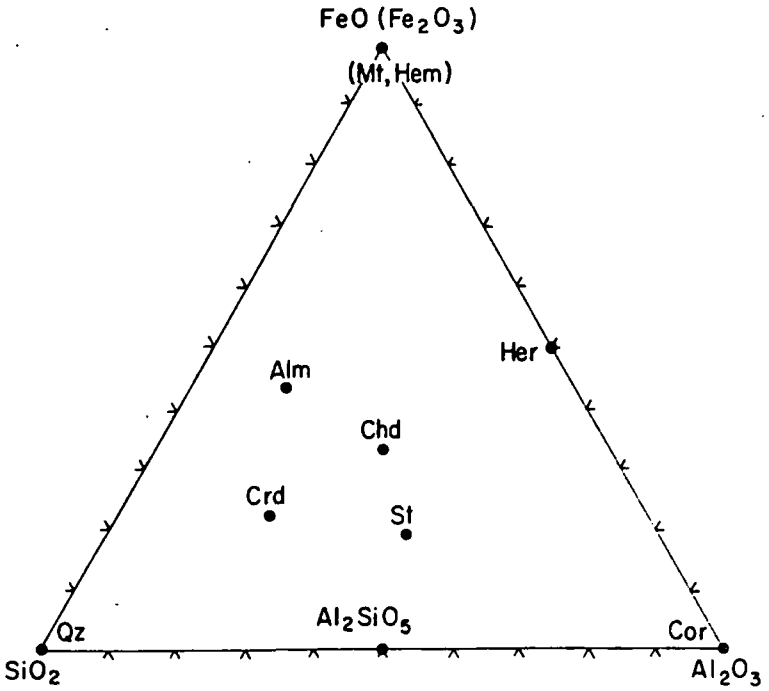

FIG. 1. Ternary diagram showing anhydrous molecular compositions of the major crystalline phases involved in the discussion of equilibrium relations. Chd = chloritoid, Crd = cordierite, Alm = almandine, St = staurolite, Mt = magnetite, Hem = hematite, Her = hercynite, Cor = corundum, Qz = quartz.

(And), or sillimanite (Sil)—Al_2SiO_5; quartz (Qz)—SiO_2; magnetite (Mt)—Fe_3O_4; hematite (Hem)—Fe_2O_3; and corundum (Cor)—Al_2O_3. Hydrous alumina-rich low-temperature phases such as kaolin, diaspore, and pyrophyllite (Kerrick, 1968) need not be considered in a discussion of chloritoid breakdown reactions at elevated temperatures and pressures. The formula $HFe_2Al_9Si_4O_{24}$ for staurolite has been criticized by several recent workers (Juurinen, 1956; Schreyer & Chinner, 1966; Richardson, 1966). Many analyses show somewhat more water and less silica than implied by the formula of Náray-Szabó & Sasvári: there may be some solid solution of protons for silicon atoms (Schreyer & Chinner, 1966). This reservation must be kept in mind in terms of the proposed reactions involving staurolite.

Consideration of oxidation state is crucial in discussing the stability relations of various possible breakdown products of chloritoid. Fig. 1 shows the ideal anhydrous molecular compositions of the important phases in the triangle

FeO–Al_2O_3–SiO_2. An axis of increasing oxygen fugacity may be imagined extending perpendicularly into the page. Progressively more oxidized assemblages are favored as f_{O_2} increases. Certain amounts of Fe_2O_3 may be incorporated into the structures of Chd, Crd, St, Her, and, to a lesser extent, Alm. Major amounts of ferric iron are present when Mt and Hem become stable. The most reduced possible assemblage corresponding to Chd composition is Alm–Cor. The assemblages Crd–Her and Alm–St–Her may contain some ferric iron. It is not evident which of these can be the more oxidized. At greater oxygen fugacity magnetite appears, and the sequence of possible assemblages is, with increasing f_{O_2} Alm–St–Mt, Crd–St–Mt, St–Mt–Qz, and Ky (And, Sil)–Mt. The relative oxidation order among the magnetite-bearing assemblages is determined by the amount of magnetite in the assemblage. The most oxidized possible assemblage is Ky (And, Sil)–Hem.

A few experimental investigations of chloritoid stability have been undertaken previously. Halferdahl (1961) experimentally deduced the reaction:

1. $5Chd = Crd + 3Her + 5H_2O$

in the pressure range 1–7 kb total pressure and the reaction:

2. $31Chd = 4St + 5Alm + 8Her + 29H_2O$

in the pressure range 7–30 kb. Halferdahl's experiments were made with metastable starting materials such as siderite and γ-alumina and, in a few runs, natural chloritoid. Chloritoid was found to break down according to reaction 1 in the range 570–700° C and at 700° nearly independently of pressure according to reaction 2. The breakdown reactions were not reversed.

Ganguly (1968) approximately located the reaction:

3. $23Chd + 8Qz = 5Alm + 4St + 21H_2O$

at 600° C and 10 kb total pressure using a Ni–NiO buffer. He considered, on theoretical grounds, that the equilibrium would not show much dependence on oxygen fugacity but that it should become metastable with respect to reactions involving magnetite at f_{O_2} somewhat higher than the Ni–NiO buffer. Hoschek (1967) experimentally determined the P–T curve of the reaction:

4. $4Chd + 5And = 2St + Qz + 3H_2O$

in the water-pressure range 4–8 kb. The curve he presented lies at about 545° C independently of the pressure. Although oxygen fugacity buffers were not used the f_{O_2} may have been nearly stable throughout the long (up to 120 days) duration of the runs by virtue of a buffering action of the metal pressure vessel. The reaction was reversed using synthetic crystalline starting materials. Very recently, Richardson (1968) has investigated the same reaction (with sillimanite as the Al_2SiO_5 polymorph) using oxygen fugacities controlled by fayalite+magnetite+quartz buffers. His result, based on reversals of the reaction using synthetic crystalline starting materials, is very similar to that of Hoschek. Richardson also undertook a reconnaissance of chloritoid reactions involving Crd. An important finding was that breakdown reactions of Chd involving Crd are stable only at low pressures, below 3·5 kb.

None of the previous experimental studies has considered oxidation breakdown of chloritoid. Several recent workers have indicated, however, that in some geological situations chloritoid may have yielded magnetite as a breakdown product (Card, 1964; Schreyer & Chinner, 1966; Hoschek, 1967). For instance, Schreyer & Chinner found staurolite pseudomorphous after chloritoid in quartzite lenses containing magnetite at Big Rock, Rio Arriba Co., New Mexico. They considered oxidation breakdown as a possibility. The reaction can be written:

5. $54\text{Chd}+5\text{O}_2 = 12\text{St}+10\text{Mt}+6\text{Qz}+48\text{H}_2\text{O}$

(Hoschek, 1967). This reaction would presumably take place under conditions of f_{O_2} somewhat higher than in the case of the non-oxidation reactions. Instability of the assemblage almandine plus H_2O at the more elevated f_{O_2} conditions is implied in reaction 5, the alternative assemblage being staurolite, magnetite, and quartz. At still higher oxygen fugacities the assemblage staurolite and quartz also should become unstable, and should be superseded by magnetite or hematite and kyanite, which event would probably take place only at f_{O_2} closely approaching or greater than that defined at a given temperature and total pressure by the magnetite–hematite buffer. The breakdown reaction of chloritoid then becomes:

6. $6\text{Chd}+\text{O}_2$ (or $\frac{2}{3}\text{O}_2$) $= 6\text{Ky}+2\text{Mt}$ (or 3Hem)$+6\text{H}_2\text{O}$.

The chloritoid breakdown reactions involving magnetite are considered in the present study. Cordierite may be eliminated from consideration in the phase relations because its appearance is confined to the low-pressure limits of geological interest. Thus, the breakdown reactions of interest are 3, 5, and 6. In addition, a breakdown of chloritoid to yield almandine, staurolite, and magnetite should be considered:

7. $19\text{Chd}+\frac{4}{3}\text{O}_2 = 4\text{St}+\text{Alm}+\frac{8}{3}\text{Mt}+17\text{H}_2\text{O}$.

The probable disposition of these equilibria in the oxygen fugacity versus temperature plane at a constant total pressure of 10 kb has been analyzed by Ganguly (1968), largely on theoretical grounds. The detailed arguments need not be repeated here. Fig. 2 shows the expected relations.

The present experimental study was undertaken to determine accurately the upper temperature limits of stability of chloritoid according to reaction 5 under conditions of controlled oxygen fugacity at high total pressure, with the hope of capitalizing on the fact that reactions among silicates often run with relatively great rapidity at very high water pressures. If a long base-line of experimental brackets of the dehydration of chloritoid at high pressures can be produced, a short extrapolation to probable pressures of deep-seated metamorphism (5–10 kb) is warranted. The magnetite–hematite (HM) buffer was used for most of the high-pressure, high-temperature runs. The question of whether reaction 5 is more stable than reaction 6 at the HM buffer is not really germane to the present issue: reaction 5 was found to proceed quite reversibly starting from synthetic crystalline materials, whether metastably or not. If the effect of

decreasing f_{O_2} on the dehydration temperature can be determined, the petrologic usefulness of a determination of reaction 5 on the HM buffer is not limited by experimental determination in a possibly metastable region.

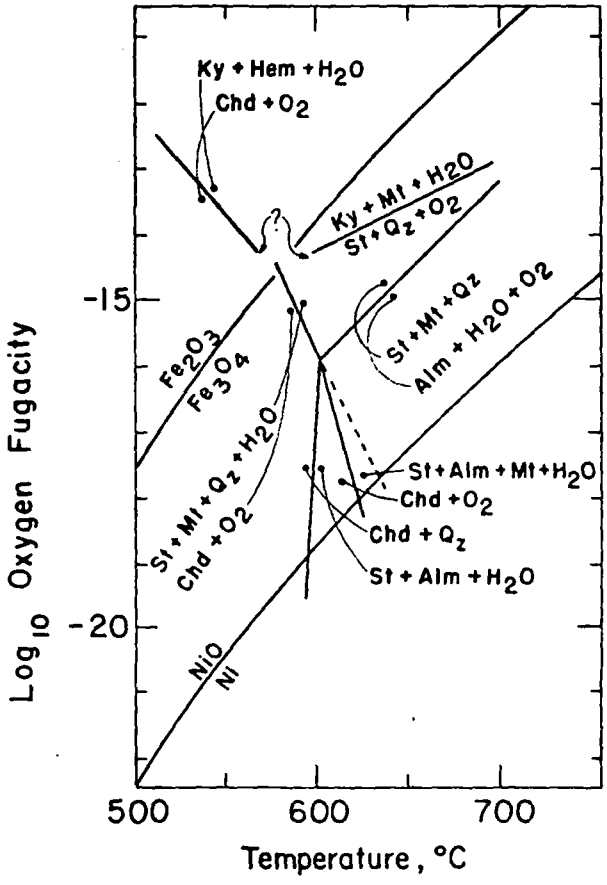

FIG. 2. Logf_{O_2} vs. T diagram at 10 kb for part of the system FeO–Al_2O_3–SiO_2–H_2O–O_2 showing probable range of reaction of chloritoid and oxygen to staurolite, magnetite, and quartz. Taken from Ganguly (1968).

EXPERIMENTAL METHODS

Apparatus and sample geometry

All experiments in the present study were performed in the piston-cylinder apparatus (Boyd & England, 1960), using a 1-in. diameter pressure vessel, talc pressure medium, and graphite-tube resistance furnace. The runs were made with an oxygen-fugacity buffer arrangement, prepared in the following way. Approximately 10 mg of starting material were sealed with water into a length of platinum tube about 0·35 in. long, $\frac{1}{16}$ in. diameter, and 0·005 in. wall thickness. The thin-walled platinum tube is very permeable to hydrogen at the conditions of

the runs and so served as the osmotic membrane. The flattened, empty portion of the capsule, about half its length, was folded over. The platinum capsule was packed with about 200 mg of the buffer mixture into a length of gold tube of $\frac{1}{8}$ in. diameter and 0·005 in. wall thickness. Excess water was added. Care was taken to keep the top surface of the platinum capsule clean so that there was no thickness of buffer mix between the platinum capsule and the thermocouple. The flattened

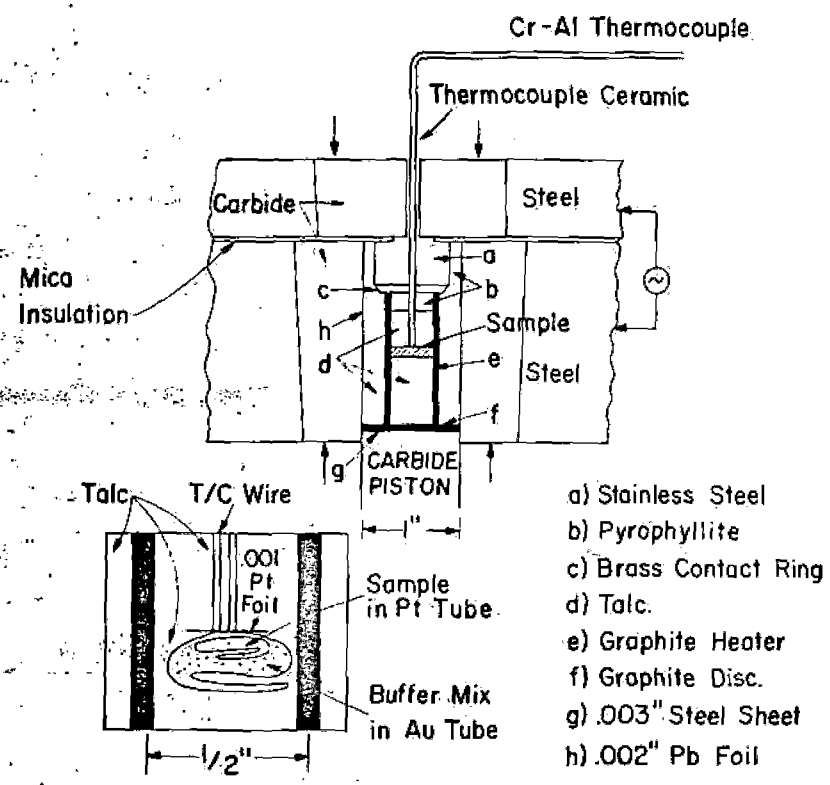

FIG. 3. Diagram of high-pressure, high-temperature buffer-capsule experimental arrangement.

lip of the gold capsule was sealed with a direct current arc-welder and then checked for pin-hole leaks by pinching with pliers. The buffer capsule was smothered in powdered talc and loaded into the high-pressure assembly. A 0·001 in.-thick platinum foil was placed on top of the gold capsule, at the point where the thermocouple makes contact, to provide an extra measure of protection against puncturing. Only those runs in which both the gold buffer capsule and the platinum sample capsule contained water when cut open after the run were considered valid runs. The high-pressure buffer technique described here and shown in Fig. 3 was developed by J. Ganguly while doing studies for the Ph.D. degree at the University of Chicago.

Temperature measurement and control

Chromel–alumel thermocouples were used in all of the present runs. The thermocouple juncture was in intimate touch contact with the gold and platinum

capsules, as revealed by the presence of a dent in both made by the thermocouple tip, which fact insures that temperatures were accurately measured. The small dimensions of the platinum capsule rule out the possibility of large temperature gradients. The Pt–Rh foil does not contaminate the Cr–Al thermocouple at temperatures below 750° C in run durations of a few days (Newton, 1965). The temperatures quoted in Table 3 are believed to be accurate to $\pm 5°$ C. No correction was made for the effect of pressure on the e.m.f. of the thermocouples. Temperatures were controlled to $\pm 1°$ C automatically. At the completion of a run, the sample was quenched to below 100° C in a few seconds by turning off the furnace current.

Pressure measurement

Determination of the sample pressure in the piston–cylinder apparatus is always a difficult problem. It is not sufficient merely to quote a 'friction correction', which is usually given as a percentage subtracted from the nominal pressure to give the sample pressure. Many qualifying statements must be made, because most experimenters have different techniques of loading and heating the sample. In the present runs the same 1-in. diameter chamber was used throughout. The carbide core had an inner hard steel liner 0·060 in. thick. The liner was shiny-smooth and had no cracks. Dry molybdenum sulfide powder was sprayed out of a squeeze-bottle on to the liner wall as a solid lubricant coating. A 0·002-in. lead foil anti-friction liner surrounded the talc cylinder. Only talc surrounded the buffer capsule: there were no hard internal parts and the temperatures were far below the firing temperature of talc. A 0·020-in. thick graphite disk was placed at the bottom of the assembly, with a 0·005-in. thick steel sheet between it and the face of the piston. Hot graphite at high pressure was found to be injurious to the tungsten carbide.

The assembly was pressed at room temperature to the final desired nominal pressure. For instance, if the final desired pressure was 10 kb, the gauge pressure was 100 bars (the ram had an effective diameter of 10 in.). The gauge pressure was read on a 350-bar Bourdon tube Heise gauge. The sample was then heated to the desired temperature by supplying high electrical current to the internal graphite heater sleeve. The gauge pressure always rose immediately in response to thermal expansion of the furnace assembly. For runs in the range 600–700° C the gauge pressure increase always levelled off at about 15 bars, or a nominal increase of 1·5 kb. It was necessary to use the method of press first and then heat, rather than the reverse procedure, which produces true 'piston-in' conditions, because it was found that further pressing of the hot gold capsule often resulted in ripping it. If the pressure conditions had been truly 'piston-in', a friction correction of about −10 per cent would have been applied and the sample pressure (quite hydrostatic because of the water in the two capsules) would have been known to within $\pm 0·4$ kb (Newton & Smith, 1967). In the present case, however, thermal expansion of the furnace assembly tends to

offset the frictional pressure loss. It developed that the nominal-pressure increase upon heating was always very nearly the amount which would be subtracted in a friction correction, or about 10 per cent of the nominal pressure before heating. It was therefore assumed that the pressure increase of the furnace assembly in the neighborhood of the sample capsule upon heating nearly compensated for the frictional loss, and no correction was made. This is the point of view taken by Boyd *et al.* (1966). In view of the lack of adequate pressure calibration, a generous estimate of pressure uncertainty must be made. It is thought that the pressure uncertainty in the present runs could not be any greater than $\pm 1{\cdot}0$ kb under any conceivable set of hypotheses. The large magnitude of the pressure uncertainty did not hamper the present investigation, however, because of the steep dP/dT slope of the equilibrium in question.

Preparation and properties of the starting material

All runs determining the equilibrium of reaction 5 were made on a starting mixture of synthetic chloritoid, synthetic staurolite, synthetic magnetite, and natural quartz. The chloritoid was synthesized from ferrous oxalate, silicic acid, and aluminum hydroxide, mixed in $FeAl_2SiO_6$ proportions and sealed with excess water in a $\frac{1}{8}$-in. diameter gold tube, at 20 kb and 625° C for 24 h. The only product was chloritoid, in small, ragged clots and clusters of crystals too fine grained for accurate optical measurements. The mean index of refraction was found to be $1{\cdot}72 \pm 0{\cdot}01$ by the oil immersion method. No unknown lines could be found in the Debye–Scherrer photograph. The chloritoid was mostly or all the triclinic polymorph. Halferdahl (1961) synthesized a mixture of the triclinic and monoclinic polymorphs in his runs. The powder X-ray photographs of his quenched charges showed many lines due to undetermined phases. The X-ray powder data of the present chloritoid is given in Table 1. The evidence supports the preponderance or entirety of the material being triclinic. The unit-cell constants were refined using the IBM 7090 least-square cell edge program written by Burnham (1963). The unit-cell constants of the chloritoid from the oxalate synthesis closely matched those of a sample of natural triclinic chloritoid from Chibougamau, Quebec, given by Halferdahl (1961). As a further check, a Debye–Scherrer photograph made with filtered iron radiation was very similar to the photograph of the Chibougamau chloritoid given by Halferdahl (1961, fig. 6, p. 80) and quite different from the monoclinic chloritoid shown in Halferdahl's fig. 6.

To test the effect of oxidation condition during the synthesis, a run was made on wüstite, aluminum hydroxide, silicic acid, and excess water in a sealed platinum capsule inside a hematite–magnetite buffer. The synthesis was made at 600° C and 20 kb total pressure for 24 h. Again the only discernible product was triclinic chloritoid. The unit-cell constants seemed to be significantly different from those of the product of the oxalate synthesis. The unit-cell constants are shown in Table 2. A higher content of Fe_2O_3 in the HM chloritoid

might account for the slightly different cell constants. The structural reasons for the deviation are not apparent. The index of refraction was also $1{\cdot}72 \pm 0{\cdot}01$.

The starting-mix staurolite was prepared from ferrous oxalate, aluminum hydroxide, and silicic acid according to the dry formula $Fe_2Al_9Si_4O_{23{\cdot}5}$. A trace of natural staurolite seed, and excess water were added and sealed into a gold

TABLE 1

Partial list of d-spacings of synthetic staurolite and chloritoid

Staurolite			*Chloritoid*		
hkl	*d*	*I*	*hkl*	*d*	*I*
150	3·056	W	†002	4·449	10
†221	3·015	7	$1\bar{1}2$, $\bar{1}12$	3·251	W*
†002	2·831	4	†003	2·965	9
†060	2·771	7	†021, $3\bar{1}1$	2·696	7
†151	2·693	9	310	2·661	W*
†132	2·401	10	†022, $3\bar{1}2$	2·456	5
311	2·354	5	†311	2·399	4
260	2·265	2	†40$\bar{1}$, 22$\bar{1}$	2·369	4
†171	2·109	5	$2\bar{2}1$, 203, 221, 113	2·301	W*
062	1·9770	4	†401, 221, 023, $3\bar{1}3$	2·139	4
400	1·9683	W	†33$\bar{1}$, 025, 225	1·5804	4
402	1·6156	2			
460	1·6057	W			
004	1·4151	1			
†462	1·3968	5			
†0 12 0	1·3849	3			

* Listed by Halferdahl (1961) as unique to triclinic polymorph.
† Used in unit-cell refinement.

tube. The synthesis runs were made at 725° C and 15 kb for 24 h. The result was 100 per cent staurolite, in crystals of average 10 μ size, with marked yellow pleochroism and abundant cruciform twins. The highest index of refraction found was 1·750. The d-spacings of major reflecting planes are given in Table 1. Table 2 gives the unit-cell constants resulting from a computer least-squares refinement. The unit cell volume is slightly but significantly larger than that of the staurolite from Pizzo Forno, Switzerland, used by J. V. Smith in his structural redetermination (in preparation).

A staurolite synthesis was made with a hematite–magnetite buffer to test the effect of high oxidizing conditions on the kind of staurolite formed. The starting material was wüstite, aluminum hydroxide, silicic acid, and a small amount of natural staurolite seed. Otherwise the conditions were the same as in the oxalate synthesis. The result was a very pleochroic staurolite with somewhat larger

crystals than before. The mean index of refraction may have been a shade higher than for the oxalate synthesis. The unit-cell volume was slightly larger than that of the oxalate synthesis (Table 2). The unit-cell constants of both synthetic staurolites fall well within the range of values for natural staurolite (Juurinen, 1956).

A starting mixture of the crystalline phases was prepared according to reaction 5, with about equal amounts of products and reactants, as determined by X-ray diffraction peak heights. Variations of the peak height ratios of the starting material were tested for by multiple scans and scans of mounts sprinkled

TABLE 2

Unit-cell constants of synthetic and natural chloritoid and staurolite

Material	*a* (Å)	*b* (Å)	*c* (Å)	α (*deg.*)	β (*deg.*)	γ (*deg.*)	V (Å³)
Staurolite	7·888	16·618	5·661				742·13
(Oxalate synthesis)	±0·002	±0·002	±0·001				±0·16
Staurolite	7·896	16·623	5·661				743·03
(HM synthesis)	±0·003	±0·003	±0·003				±0·30
Staurolite	7·871	16·620	5·656				739·94
(Pizzo Forno, Switz.)	±0·002	±0·003	±0·001				±0·23
(J. V. Smith)							
Chloritoid	9·493	5·480	9·165	96·47	102·27	89·94	462·76
(Oxalate synthesis)	±0·009	±0·019	±0·013	±0·37	±0·15	±0·26	±2·38
Chloritoid	9·552	5·440	9·153	97·34	101·57	89·45	462·05
(HM synthesis)	±0·027	±0·010	±0·005	±0·07	±0·07	±0·07	±0·77
Chloritoid	9·50	5·48	9·16	96° 53′	101° 49′	90° 2′	462·99
(Chibougamau, Que.)							
(Halferdahl, 1961)							

upon a thin layer of petroleum jelly. There was some effect of preferred orientation apparent on the relative intensity of the 002 reflection of chloritoid, which is the only reflection strong enough to use as an amount indicator with any confidence. Because of this the technique of comparing peak height ratios of starting material and quenched charges to determine the direction of reaction could not be applied with as much sensitivity as is possible in other systems.

Detection of reaction

The direction of the reaction was detected by the changes in relative X-ray spectral intensities of the phases involved. A 30–40 per cent change in the relative amounts of the phases was probably necessary to be certain of the direction of the reaction. The reaction was fast enough to make an unambiguous decision in runs of no more than 2 days duration at temperatures above 600° C. Fig. 4 shows X-ray spectrometer charts of the starting material and runs in which chloritoid grew and chloritoid broke down.

Problem of buffer effectiveness

Equilibration of the oxygen fugacity of the buffer with that of the charge is necessary for unambiguous interpretation of the results of experiments. That

hydrogen diffusion equilibrium was swift compared to the reaction rates was indicated in several ways. The most decisive indication was the fact that there was found to be a very large effect on the dehydration temperature of chloritoid

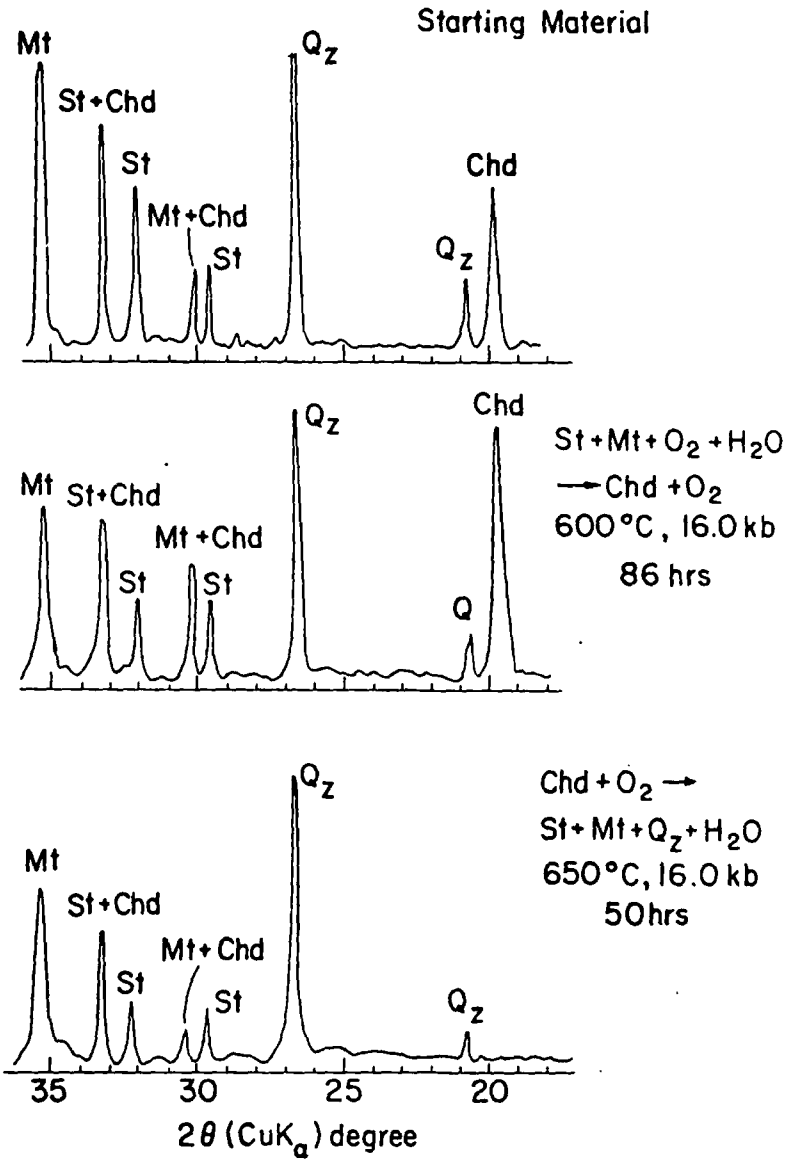

FIG. 4. Portions of X-ray diffraction spectrograms of starting material and products of high-temperature, high-pressure runs in which chloritoid grew and broke down.

in going from the HM buffer to the NNO buffer: the breakdown boundary was raised by about 60° C. Preliminary runs in this range made without a buffer, on the other hand, never yielded clear evidence of chloritoid growth or decline. Another indication was the growth of large, thin platelets of hematite inside

the platinum in all runs with the HM buffer. This phenomenon occurred even though the hematite–magnetite mixture of the buffer was strongly reduced. Originally the buffer was 90 per cent hematite, but after the runs the buffer had typically reduced to about 70 per cent magnetite, in very large shiny crystals. Since platinum is much more permeable to hydrogen than gold, there is no alternative but to suppose that the sample charge was well buffered. The nickel–nickel oxide buffers, originally containing 50 per cent of each substance, were slightly oxidized in the longest runs, and hematite never developed inside the platinum capsule. Finally, a special buffer check run was made at 700° C and 15 kb for 24 h, in which a platinum sample capsule containing hematite, magnetite, and water was placed inside an HM buffer capsule. The charge showed no evidence of reaction, even though the buffer mix underwent strong reduction. The foregoing evidence strongly indicates that buffer equilibration is attained quite rapidly and that the condition of oxygen fugacity which develops spontaneously within a sealed gold capsule containing water and iron silicates is somewhat more oxidizing than the NNO buffer and much less oxidizing than the HM buffer.

A closely related problem is that of depletion of the iron in the charge by the platinum capsule. Absorption of a significant amount of iron in the system by a platinum buffer capsule at much more reducing conditions than those of the present experiments has been reported (Eugster & Wones, 1962). Increasingly oxidizing conditions will have a powerful effect in preventing iron loss to the capsule, however. Consider a simple alloying equilibrium such as

$$FeO = Fe(Pt.soln) + \tfrac{1}{2}O_2$$

The equilibrium relation is

$$\ln a_{Fe}^{Pt} = -\frac{\Delta G^\circ(T) + P\Delta V_s}{RT} - \tfrac{1}{2}\ln f_{O_2}$$

where ΔG° is the standard Gibbs energy change in the reaction at 1 atm. ΔV_s is the volume change of the solids involved in the reaction, a_{Fe}^{Pt} is the activity of Fe in solid solution with platinum, and f_{O_2} is the oxygen fugacity. Using the dilute solution approximation and the data compiled by Eugster & Wones (1962, p. 90),

$$\left.\frac{X_{Fe}^{Pt}(\text{HM buffer})}{X_{Fe}^{Pt}(\text{WI buffer})}\right|_{20\text{ kb},723^\circ\text{K}} = 10^{-4.7}$$

and

$$\left.\frac{X_{Fe}^{Pt}(\text{NNO buffer})}{X_{Fe}^{Pt}(\text{WI buffer})}\right|_{20\text{ kb},723^\circ\text{K}} = 10^{-2.4}$$

where X_{Fe}^{Pt} is the fractional amount of alloying of iron into the platinum. It is thus seen that the orders of magnitude increase in oxygen fugacity in going to more oxidizing buffers results in orders of magnitude reduction in the depleting power of the platinum capsule. Some staurolite synthesis experiments on mixtures of wüstite, $Al(OH)_3$ and silicic acid using iron–wüstite, NNO, and

HM buffers confirmed this expectation. The runs were made at 700° C and 15 kb for 36 h. The wüstite–iron run resulted in staurolite plus a considerable amount of kyanite and corundum, indicating some depletion of iron from the charge. The other runs yielded staurolite only. The starting mix and the wüstite–iron run charge were analyzed spectrochemically by N. Suhr. There was a

TABLE 3

Experimental conditions and results of runs at high pressure and high temperature using starting material composed of synthetic chloritoid, staurolite, magnetite, natural quartz, and water

Run no.	*Buffer*	*P (kb)*	*T (°C)*	*Time (h)*	*Result**
1	NNO	19·5	650	49	Chd only
2	NNO	19·5	665	48	Strong Chd growth; Alm present
3	NNO	19·5	680	43	Strong Chd breakdown; Alm strong; Mt weak; Qz absent
4	HM	25·0	620	72	Very strong Chd growth
5	HM	25·0	635	54	Strong Chd growth
6	HM	25·0	650	49½	Strong Chd breakdown; slight Alm present
7	HM	20·5	600	72	Strong Chd growth
8	HM	20·5	610	69	Strong Chd growth
9	HM	20·5	625	94	Chd breakdown
10	HM	20·5	675	67	St+Mt+Qz only
11	HM	18·2	605	71½	Strong Chd growth
12	HM	18·2	620	96	Chd breakdown; slight Alm present
13	HM	16·0	600	86	Strong Chd growth
14	HM	16·0	615	70	Chd breakdown
15	HM	16·0	625	67	Strong Chd breakdown
16	HM	16·0	650	50	St+Mt+Qz only
17	HM	13·5	570	92	No apparent reaction
18	HM	13·5	590	72	Slight Chd growth
19	HM	13·5	615	74	Strong Chd breakdown
20	HM	10·5	585	103	Weak Chd breakdown
21	HM	10·5	600	50	Strong Chd breakdown

* Hem present in small amounts in all HM runs.

depletion of FeO by 16 per cent of the amount originally present in the charge of the wüstite–iron run. According to the preceding calculation, the depletion in a similar run with the NNO buffer should be about 0·1 per cent of the amount present and about 0·002 per cent for the hematite–magnetite run. Thus iron depletion of the charge is not regarded as a serious problem in the present investigation.

EXPERIMENTAL RESULTS

The results of experiments are listed in Table 3 and shown in Fig. 5. The reaction of chloritoid to staurolite, magnetite, quartz, and vapor (reaction 5) was reversed over a narrow range of temperatures at several pressures with the

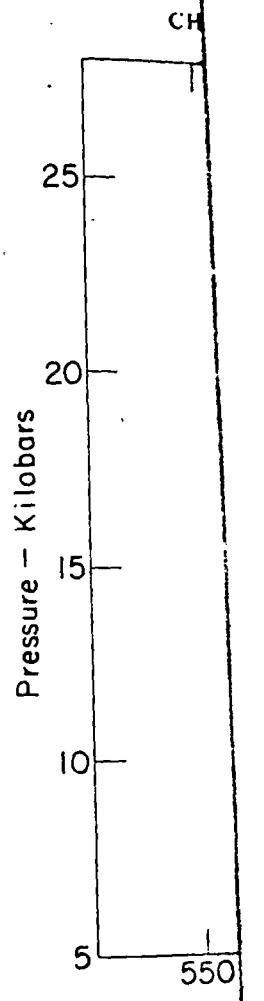

FIG. 5. Experimental data
circle denotes chloritoid gr
on HM buffer. Filled squ
denotes chloritoid breakd
in the run. Number one de
and pressure of runs is brac
(*a*) is 54Chd+5O$_2$ = 12St
mate location of the s

HM buffer. Below 600° C
fast to prove reversibility
in the range 10·5–25 kb
fugacity along the curve

log f_{O_2}

(Eugster & Wones, 1962.

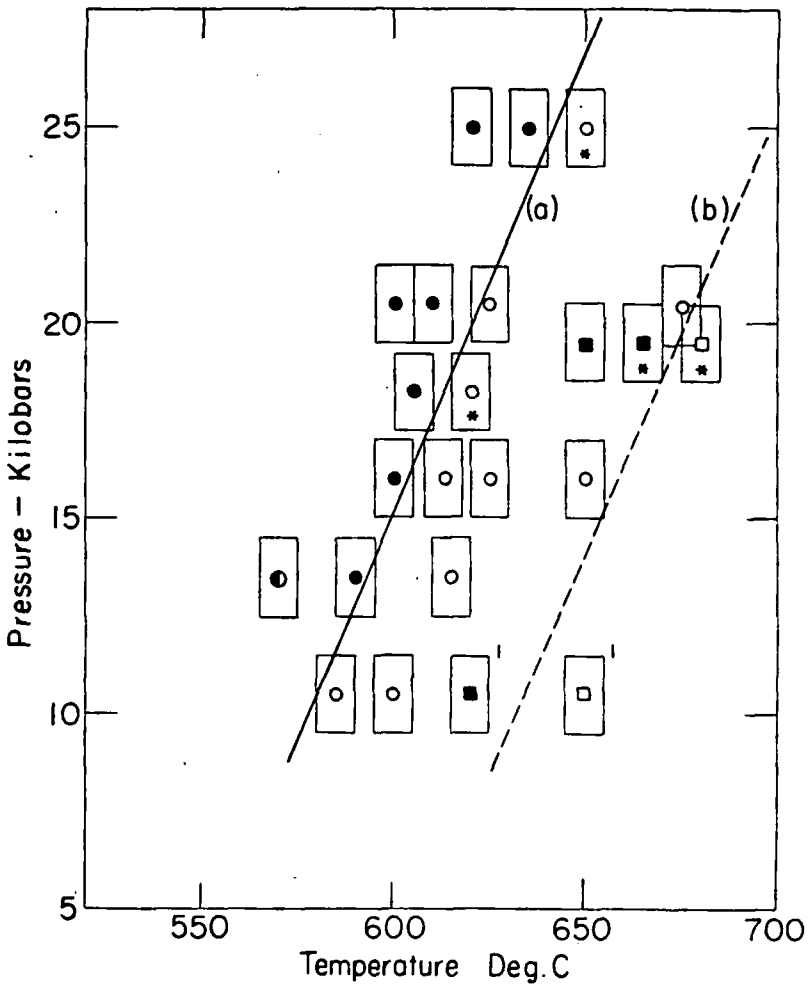

FIG. 5. Experimental data for oxidation breakdown of chloritoid at high pressures. Filled circle denotes chloritoid growth on HM buffer. Open circle denotes chloritoid breakdown on HM buffer. Filled square denotes chloritoid growth on NNO buffer. Open square denotes chloritoid breakdown on NNO buffer. Asterisk denotes that almandine appeared in the run. Number one denotes data from Ganguly (1968). Uncertainty in temperature and pressure of runs is bracketed by large rectangles surrounding experimental points. Line (*a*) is $54Chd + 5O_2 = 12St + Mt + 6Qz + 48H_2O$ (HM buffer, stable). Line (*b*) is the approximate location of the same equilibrium on the NNO buffer (metastable, see text).

HM buffer. Below 600° C and 16 kb the growth of chloritoid was not sufficiently fast to prove reversibility in runs of a few days duration. The best fit of the data in the range 10·5–25 kb yields an average slope of 233 bars/° C. The oxygen fugacity along the curve can be obtained from the equation

$$\log f_{O_2} = -\frac{24\,912}{T} + 14{\cdot}41 + \frac{0{\cdot}019(P-1)}{T}$$

(Eugster & Wones, 1962, p. 90), where T is in degrees Kelvin.

The only phase to appear in the HM buffer runs which was not among the starting materials was almandine. Almandine appeared in very slight amounts in the run at 18·2 kb and 625° C (Run no. 12, Table 3) and to a greater amount in the run at 25·0 kb and 650° C (Run no. 6, Table 3). The amount of almandine in the charge of the 18·2-kb run was on the lower limit of detectability with X-ray diffraction; the amount of almandine in the 25-kb run may have been about 10 per cent. Occasional small equant isotropic grains of high index of refraction were seen in the microscopic examination of these two charges. Both were runs in which chloritoid broke down. The appearance of almandine suggests that the very high pressures were suffice to stabilize it relative to staurolite, magnetite, and quartz, even at oxygen fugacities of the HM buffer. To determine if almandine is a stable breakdown product of chloritoid at a high f_{O_2} in the pressure range of geological interest, runs were made on mixtures of almandine, staurolite, magnetite, quartz, and water and 14·0 kb, 630° and 650° C and the HM buffer for 24 h. Almandine was greatly reduced in quantity relative to staurolite, magnetite, and quartz. Therefore, if almandine becomes a stable phase at high f_{O_2}, it must be above the pressure range of the metamorphic rocks. The runs of the present investigation above 14 kb may be metastable reversals of reaction 5. The very slight amount of almandine occurring in the two runs could not have significantly altered the essential univariant condition of the reaction. In any case, it is not probable that the breakdown of chloritoid according to reaction 7 takes place at a temperature far removed from that of reaction 5.

A reversal of reaction 5 on the NNO buffer was performed by Ganguly (1968) at 10·6 kb and 635±15° C. Additional runs with the starting mix for reaction 5 and with the NNO buffer were made in the present investigation in order to produce a dP/dT slope. A series of runs at 19·6 kb showed that the decrease of oxidation condition from the HM to the NNO buffer promoted the thermal stability by at least 50° C. Breakdown of chloritoid took place at 680° C and almandine appeared abundantly. Almandine also appeared in the run at 665° C, but chloritoid grew greatly in this run. It is strongly indicated but not proved by this result that reaction 7 is more stable with a NNO buffer than reaction 5. The explanation for the fact that reaction 5 could be reversed metastably at 10·6 kb and could not be reversed metastably at 19·5 kb lies in the faster kinetics at the higher temperature and pressure conditions, which made possible the nucleation of almandine. The metastable equilibrium curve for reaction 5 on the NNO buffer may lie at an even higher temperature than 680° C at 19·5 kb. Geometrical arguments indicate that the P–T curves for reaction 5 on the two buffers should be nearly parallel. The metastable reaction 1 in which hercynite was a product, should lie at still higher temperatures. A value of 700° C was found by Halferdahl (1961).

THERMODYNAMIC DISCUSSION

The enthalpy change, ΔH, for the reaction

$$54\text{Chd}+5\text{O}_2 = 12\text{St}+10\text{Mt}+6\text{Qz}+48\text{H}_2\text{O}$$

can be calculated at any total pressure by:

$$\Delta H = \left[\frac{\partial(\Delta G/T)}{\partial(1/T)_P}\right]$$

where ΔG is the Gibbs energy change of the reaction. An isobaric plot of $\Delta G/T$ versus $1/T$ thus yields ΔH as the tangent. ΔG at any (T, P) can be found by the relation

$$\Delta G(T, P) = \Delta G(T, P_{exp})+48[G^{H_2O}(T, P)-G^{H_2O}(T, P_{exp})]- -5RT\ln\left[\frac{f_{O_2}(T, P)}{f_{O_2}(T, P_{exp})}\right]+\Delta V_s(P-P_{exp}).$$

Here P_{exp} is the determined equilibrium pressure for the reaction, f_{O_2} is the fugacity of O_2 on the HM buffer and ΔV_s is the solid volume change of the reaction. Hence the first term to the right of the equals sign vanishes. The second term can be evaluated from tables for the Gibbs energy of water, such as that of Sharp (1962). The third term becomes $(-5)\,(R)\,(2{\cdot}303)\,(0{\cdot}019)\,(P-P_{exp})$ with P in bars (Eugster & Wones, 1962, p. 90). Using the molar volumes of chloritoid and staurolite given for the oxalate syntheses of Table 2 and the values from Robie (1962) for the other minerals, a ΔV_s of $-507{\cdot}0$ cm^3 is obtained. The fourth term then becomes

$$\frac{-507(P-P_{exp})}{41{\cdot}31},$$

with units of calories. It must be remembered that the coefficient of the second term depends strongly on the assumed amount of water in the staurolite formula and that the coefficient of the third term assumed that a negligible quantity of ferric iron is incorporated into the chloritoid and staurolite structures. The accuracy of the resulting values of ΔH will suffer from the uncertainties imposed by these considerations.

Plots of $-\Delta G/RT$ versus $1/T$ were prepared for nine different pressures including one atmosphere from the data for reaction 5, assuming a constant dP/dT slope of 233 bars/°C. Fig. 6 shows plots for four representative pressures. The curves are linear in their high temperature portions, which is to be expected, since their slopes, the $-\Delta H/R$ values, would not vary much over a 100° C temperature interval. Below about 560° C, however, the curves become curved over a short temperature interval. The only reasonable explanation of this fact is that the extrapolation of the constant 233 bars/°C slope of Fig. 5 is not warranted to pressures lower than about 7 kb, where the thermodynamic

properties of water begin to change drastically with decreasing pressure, and hence some curvature obtains in the line of reaction 5.

The ΔH values yielded by the straight-line portions of the plots of Fig. 6 are shown in Table 4. The values are smallest at about 3 kb, which is due to

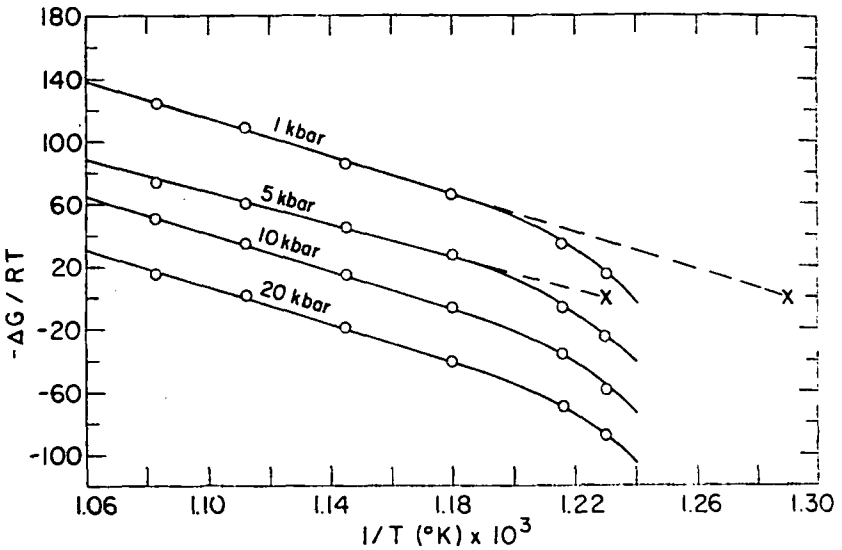

FIG. 6. Calculated values of $-\Delta G/RT$ for reaction 6 versus $1/T$ for various pressures. The zero-points of the extrapolations of the straight-line portions of the curves for the two lower pressures are marked X. They yield improved estimates of the equilibrium temperature for reaction 5.

TABLE 4

Thermodynamic data for the reaction $54Chd + 5O_2 = 12St + 10Mt + 6Qz + 48H_2O$

P bars	*T °C*	*ΔV cm³*	*ΔH cal*	$\frac{dP}{dT_{calc.}}\left(\frac{bar}{°C}\right)$	$\frac{dP}{dT_{meas.}}\left(\frac{bar}{°C}\right)$
1	296	122, 630	$1{\cdot}260\times10^6$	0·75	
1000	503	967	1·206	66·4	
2000	518	640	1·093	89·3	69
3000	523	512	1·016	101	97
5000	544	415	1·062	130	132
7000	562	338	1·105	162	159
10 000	575	276	1·193	209	189
16 000	607	201	1·107	259	250
20 000	621	170	1·206	327	264

the minimum of the enthalpy of water in this pressure range. The one atmosphere value for ΔH found in this calculation is $1{\cdot}260\times10^6$ cal for 54 moles of chloritoid, or 23·35 kcal per mole. Another calculation of $\Delta H°$ (at 1 atm) may be made by the method of Orville & Greenwood (1965). This method makes use of the expression:

$$\frac{\partial}{\partial(1/T)}\log_{10}K = \frac{-\Delta H°}{2{\cdot}303\,R} - \frac{\Delta V_s P_s}{2{\cdot}303\,R}$$

where P is some elevated solid pressure at which the plot of

$$\log_{10} K = \log_{10} \frac{f_{H_2O}^{48}}{f_{O_2}^{5}}$$

versus $1/T$ is prepared. The value of the fugacity of H_2O and O_2 are again taken from water tables and the Eugster & Wones (1962) expression, for points on the equilibrium curve at $P_S = P_T$. $\log_{10} K$ is modified by the addition:

$$\Delta \log_{10} K = -\frac{\Delta V_s (P_s - P_{exp})}{2{\cdot}303RT}$$

(Eugster & Wones, 1962). Fig. 7 shows a plot of $\log_{10} K^1 = \log_{10} K + \Delta \log_{10} K$ versus $1/T$ for $P_S = 20$ kb. The 1 atm value of ΔH by this method is $1{\cdot}086 \times 10^6$

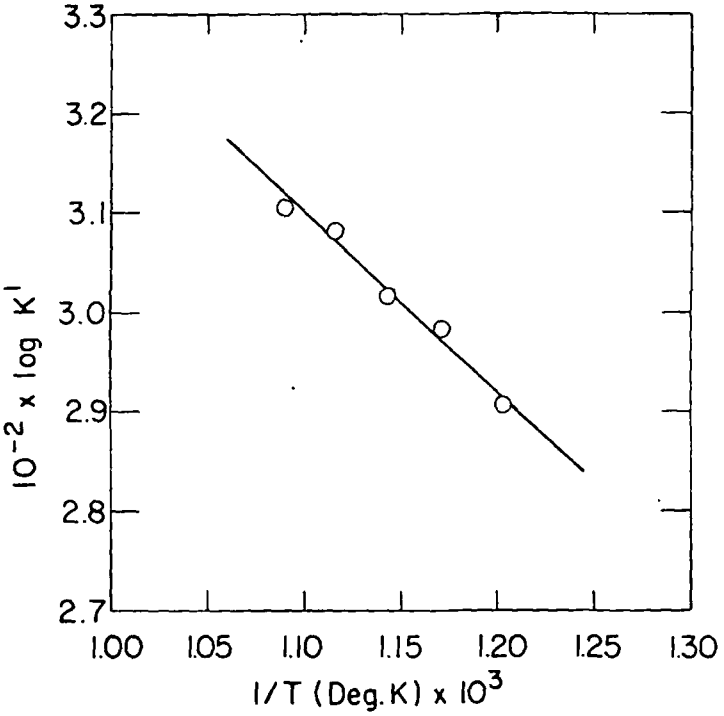

FIG. 7. 20-kb plot of ln K versus $1/T$ for reaction 6 which is used to calculate ΔH° for the reaction.

cal for 54 moles of chloritoid, which is reasonable agreement with the value of $1{\cdot}260 \times 10^6$ when the various sources of error such as difficulty in measuring the slopes accurately and the approximations of incompressible solids and ΔH independent of temperature are considered.

An estimate of the equilibrium curve of reaction 5 in the low temperature and pressure range may be made which is more reasonable than the straight-line extrapolation of the portion of the curve above 10 kb, by prolonging the straight-line portions of the $-\Delta G/RT$ versus $1/T$ curves to their zeros. This is

shown for the 1 and 5 kb curves in Fig. 6. Fig. 8 shows the low-temperature continuation of the chloritoid breakdown curve estimated in this way. At 1 kb the dehydration temperature is down to 503° C, and the one atmosphere value is 295° C. That this curvature in the low-pressure range is real and is necessitated by the properties of water may be shown by approximate calculations of the dP/dT slope of the reaction based on the Clausius–Clapeyron equation. The fluid volume change is difficult to evaluate exactly in the lack of data on the partial molal volumes of oxygen, but, to a first approximation

$$\Delta V_f = 48V^{H_2O} - 5V^{H_2O},$$

assuming that water and oxygen have the same volume per mole at a given P and T. The ΔH for the calculation was taken from the plots of $-\Delta G/RT$ versus $1/T$ for each pressure. Table 4 shows a comparison of the slopes so calculated with those measured graphically with a straight-edge from a carefully least-squared plot of the T value from Table 4 on a large sheet of millimeter paper. The general agreement of the measured and calculated slopes in the range 2–16 kb verifies that the curvature is a real effect.

GEOLOGICAL APPLICATIONS

Some occurrences of chloritoid and staurolite-bearing rocks may be interpreted in the light of the present experimental work, provided that the necessary amount of caution arising from uncertainty in total pressure, water pressure, oxygen fugacity, and effect of additional components in natural systems is applied.

Many occurrences of chloritoid involve kyanite as a companion mineral. This fact suggests that the range of total pressure to be considered is usually greater than 5 kb, based on the stability diagram of the Al_2SiO_5 polymorphs given by Fyfe (1967). Over this pressure range the reaction of chloritoid to yield staurolite, magnetite, quartz, and vapor varies from 540° C to 575° C in Fig. 8. Since the equilibrium considered here involves a restricted range of oxygen fugacities near the HM buffer, variation of oxygen fugacity during metamorphism would not have affected the breakdown temperature of chloritoid by more than a few tens of degrees as long as the breakdown products were staurolite, magnetite, quartz, and vapor. It is shown in the present investigation that decreasing oxygen fugacity promotes the thermal stability of chloritoid somewhat. The assumption that water pressure did not depart significantly from total pressure during progressive metamorphism of chloritoid schists is necessary to the interpretations that will be attempted.

Only MgO and MnO could have significant effects as 'impurity components' on the present equilibrium, because the phases chloritoid and staurolite are very restrictive to other components such as CaO. Moreover, available analyses suggest that Mg and Mn are not likely to be strongly partitioned between

staurolite and chloritoid (cf.
of MgO is not believed to ha
5. The tentative indication is
temperature scale of progres
uncertainties in total pressu
is likely to be minimal.

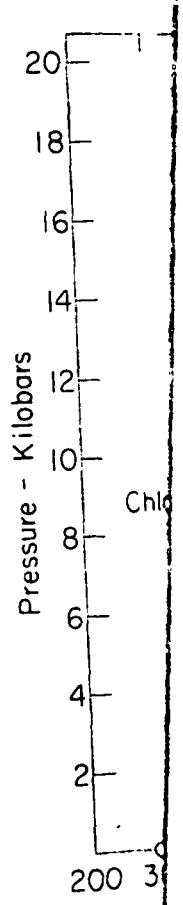

FIG. 8. An
54
prepared by setti

Schreyer & Chinner
bands of staurolite, qua
amounts of chloritoid,
Rock, New Mexico. The
recrystallization after
by Espanshade & Potte

staurolite and chloritoid (cf. Deer *et al.*, pp. 154, 165). Therefore the presence of MgO is not believed to have a large influence on the temperature of reaction 5. The tentative indication is that reaction 5 may provide a useful point on the temperature scale of progressive metamorphism, in that the total influence of uncertainties in total pressure, oxygen fugacity, and additional components is likely to be minimal.

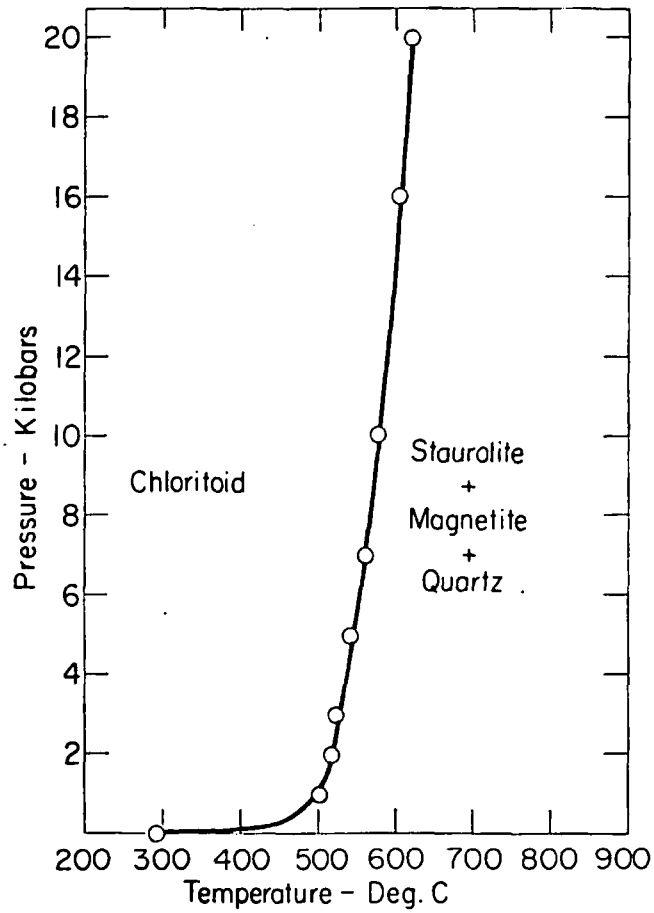

FIG. 8. An improved equilibrium diagram for the reaction

$$54Chd + 5O_2 = 12St + 10Mt + 6Qz + 48H_2O$$

prepared by setting the calculated ΔG values for the reaction equal to zero.

Schreyer & Chinner (1966) have described occurrences of thin concordant bands of staurolite, quartz, and magnetite (partially martitized) with accessory amounts of chloritoid, muscovite, apatite, and monazite in rocks from Big Rock, New Mexico. The staurolite shows radial sieve texture caused by mimetic recrystallization after chloritoid rosettes. Similar occurrences were described by Espanshade & Potter (1960, p. 75) from the Kings district, North and South

Carolina. In both occurrences kyanite is the only aluminum silicate polymorph developed regionally. Allowing the maximum uncertainty from all causes other than water pressure much less than total pressure, the limits of 540° and 570° C may be assigned on the assumption of oxidation breakdown of chloritoid, the basis of the present investigation. An alternative possibility, suggested by Schreyer & Chinner for the case of the Big Rock, New Mexico occurrence, is that the chloritoid reacted with a hypothetical pre-existing kyanite according to reaction 4 with Ky substituted for And. That the oxygen fugacities were close to those of the HM buffer is suggested by the absence of almandine from both deposits (see Fig. 2).

Naha (1956) described kyanite–chloritoid schists from South Dhalbhum and North-eastern Mayurbhanj, India, containing staurolite, muscovite, biotite, chlorite, and quartz. Thin sections of some of the rocks show staurolite, associated with granules of magnetite, in the process of incipient replacement by chloritoid. These observations suggest retrograde conversion of staurolite to chloritoid by reaction 5. The indication from the present experimental work is that temperatures in the range 530–570° C were recrossed before further retrograde reaction ceased.

Garlick & Epstein (1967, p. 208) suggested that some samples of regionally metamorphosed pelitic schists containing kyanite and staurolite have crystallized at temperatures in the range 520–600° C, on the basis of O^{18}/O^{16} ratios in coexisting magnetite and quartz. Interpretation of the minimum temperature for the coexistence of staurolite, magnetite, and quartz based on the present experimental work yields 540° C.

Card (1964, p. 1020) has suggested that, in the Agnew Lake area, Sudbury District, Ontario, the conversion of chloritoid to staurolite in some of the rocks involved the reaction $66Chd+8Qz+O_2 = 12St+12Alm+2Mt+60H_2O$. On the basis of the compositions of pyrrhotites which have supposedly equilibrated with pyrite during metamorphism, Card deduced 550° C as a likely temperature for the event. The reaction postulated by Card is in reality the combination of reactions 5 and 7 proceeding simultaneously. Fig. 2 and the present experimental work show that the composite reaction should define a temperature of about 560–580° C and an oxygen fugacity about midway between the HM and NNO buffer curves, if the pressures involved correspond to Miyashiro's estimate of the pressures of 5–10 kb for amphibolite facies rocks (1961, p. 285). The present experimental evidence is therefore in good agreement with the independent temperature estimate of Card.

Albee (1965) described kyanite-zone pelitic schists from Vermont containing chloritoid in association with garnet, magnetite, hematite, quartz, etc. The temperature of crystallization of these assemblages has been deduced to be 550° C on the basis of O^{18}/O^{16} ratio in coexisting quartz and magnetite and the compositions of coexisting Ca-free muscovite and paragonite (p. 297). Garlick & Epstein (1967) believe that the temperature of 550° C should fall in

the zone of stability
apparent inconsisten
of water prevailing a
mental work, howeve
chloritoid should be
550° C at pressures
curve.

The authors would
DC arc-welder, and
helpful discussions co
to Dr. S. Richardson
siderable changes in
from the National Sc

ALBEE, A. L., 1965. Phase
Mountain Quadrangle,
BOYD, F. R., & ENGLAND, J.
to 50 kilobars and tem
—— BELL, P. M., ENGLAN
apparatus. *Yb. Carnegi*
BURNHAM, C., 1962. Lattice
CARD, K. D., 1964. Metam
Bull. geol. Soc. Am. 75
DEER, W. A., HOWIE, R.,
Silicates. London, Lon
ESPANSHADE, G. H., & POTT
eastern States. *Prof. Pa*
EUGSTER, H. P., & WONE
J. Petrology, 3, 82–125.
FYFE, W. S., 1967. Stability
GANGULY, J., 1968. Analysi
system $FeO-Al_2O_3-SiO_2$
GARLICK, G. D., & EPSTEIN
metamorphosed rocks.
HALFERDAHL, L. B., 1961.
occurrence. *J. Petrology*
HOSCHEK, G., 1967. Untersu
Miner. Petrogr., 14, 123
JUURINEN, A., 1956. Compa
A-111 Geol.-Geog. 47.
KERRICK, D., 1968. Experim
kilobars water pressure.
NAHA, K. M., 1956. Kyanite
Q. Jl. geol. Min. metall.
NÁRAY-SZABÓ, I., & SASVÁRI,
11, 862–5.
NEWTON, R. C., 1965. The
—— & SMITH, J. V., 1967.
Ibid. 75, 268–86.

the zone of stability of staurolite, relative to chloritoid, and note that the apparent inconsistency might reflect 'differences in rock pressure or the activity of water prevailing at the time of metamorphism' (p. 207). The present experimental work, however, indicates that no abnormal situation is necessary, in that chloritoid should be stable relative to staurolite, magnetite, and quartz at 550° C at pressures above 6 kb and oxygen fugacities near the HM buffer curve.

ACKNOWLEDGEMENTS

The authors would like to thank Professor R. N. Clayton for the use of his DC arc-welder, and Professors R. F. Mueller and P. M. Orville for very helpful discussions concerning the theoretical aspects. Appreciation is expressed to Dr. S. Richardson for his many critical comments, which resulted in considerable changes in the manuscript. This research was supported by a grant from the National Science Foundation, no. GA573.

REFERENCES

ALBEE, A. L., 1965. Phase equilibria in three assemblages of kyanite-zone pelitic schists, Lincoln Mountain Quadrangle, Central Vermont. *J. Petrology*, **6**, 246–301.

BOYD, F. R., & ENGLAND, J. L., 1960. Apparatus for phase equilibrium measurements at pressures up to 50 kilobars and temperatures up to 1750° C. *J. geophys. Res.* **65**, 741–8.

—— BELL, P. M., ENGLAND, J. L., & GILBERT, M. C., 1966. Pressure measurement in single-stage apparatus. *Yb. Carnegie Instn. Wash.* **65**, 410–14.

BURNHAM, C., 1962. Lattice constant refinement. Ibid. **61**, 132–5.

CARD, K. D., 1964. Metamorphism in the Agnew Lake area, Sudbury District, Ontario, Canada. *Bull. geol. Soc. Am.* **75**, 1011–30.

DEER, W. A., HOWIE, H., & ZUSSMAN, J., 1962. *Rock-forming minerals*. Vol. 1, *Ortho- and Ring-Silicates*. London, Longmans.

ESPANSHADE, G. H., & POTTER, D. B., 1960. Kyanite, sillimanite and andalusite deposits of the Southeastern States. *Prof. Pap. U.S. geol. Surv.* **336**.

EUGSTER, H. P., & WONES, D. R., 1962. Stability relations of the ferruginous biotite, annite. *J. Petrology*, **3**, 82–125.

FYFE, W. S., 1967. Stability of Al_2SiO_5 polymorphs. *Chem. Geol.* **2**, 67–76.

GANGULY, J., 1968. Analysis of the stability of chloritoid and staurolite and some equilibria in the system FeO–Al_2O_3–SiO_2–H_2O–O_2. *Am. J. Sci.* **266**, 277–98.

GARLICK, G. D., & EPSTEIN, S., 1967. Oxygen isotope ratios in coexisting minerals of regionally metamorphosed rocks. *Geochim. cosmochim. Acta* **31**, 181–214.

HALFERDAHL, L. B., 1961. Chloritoid: its composition, X-ray and optical properties, stability and occurrence. *J. Petrology*, **2**, 49–135.

HOSCHEK, G., 1967. Untersuchungen zum Stabilitätsbereich von Chloritoid und Staurolith. *Beitr. Miner. Petrogr.*, **14**, 123–62.

JUURINEN, A., 1956. Composition and properties of staurolite. *Acad. Sci. Fennicae Annals.*, ser. A–III Geol.-Geog. **47**, 5–53.

KERRICK, D., 1968. Experiments on the upper stability limit of pyrophyllite at 1·8 kilobars and 3·9 kilobars water pressure. *Am. J. Sci.* **266**, 204–14.

NAHA, K. M., 1956. Kyanite-chloritoid schists from south Dhalbhum and northeastern Mayurbhanj. *Q. Jl. geol. Min. metall. Soc. India* **28**, 89–100.

NÁRAY-SZABÓ, I., & SASVÁRI, K., 1958. On the structure of staurolite, $HFe_2Al_9Si_4O_{24}$. *Acta crystallogr.* **11**, 862–5.

NEWTON, R. C., 1965. The thermal stability of zoisite. *J. Geol.* **73**, 431–41.

—— & SMITH, J. V., 1967. Investigations concerning the breakdown of albite at depth in the Earth. Ibid. **75**, 268–86.

ORVILLE, P. M., & GREENWOOD, H. J., 1965. Determination of ΔH of reaction from experimental pressure-temperature curves. *Am. J. Sci.* **263**, 678–83.
RICHARDSON, S. W., 1966. Staurolite. *Yb. Carnegie Instn. Wash.* **65**, 248–52.
—— (1968). Staurolite stability in a part of the system Fe–Al–Si–O–H. *J. Petrology*, **9**, 467–88.
ROBIE, R. A., 1962. Thermodynamic properties of minerals. *Rep. U.S. geol. Surv.* TEI-876, 31 pp.
SCHREYER, W., & CHINNER, G. A., 1966. Staurolite-quartzite bands in kyanite quartzite at Big Rock, Rio Arriba County, New Mexico. *Contr. Miner. Petrol.* **12**, 223–44.
WINKLER, H. G. F., 1965. *Die Genese der metamorphen Gesteine*. Springer Verlag.

Stauroli

Geophysical

The following reacti
extent of staurolite qua
have been determined i
tion ratio of the fluid
assemblage.

(I) Fe-staurolite
(II) Fe-staurolite
(III) Fe-chloritoid

In addition, two reactio
been investigated:

(IV) Fe-cordierite
(V) Fe-cordierite

The experimental infe
quartz and QFM-buffer
Fe-chloritoid, almandit
three mineral assemblag
ent fluid pressures. In o

(*a*) Above ~5 kb: sta
(*b*) Between ~1·5 an
narrower pressure
(*c*) Below ~3·5 kb:
quartz–fayalite–m

These phase assemblage
this must be proven in
priate composition and

BARROW (1893) rec
pelitic schists of the s
overlapping a kyanit
terrains throughout

However, staurolit
is commonly absent
rocks contain cordie
or sillimanite rather
adopt a classification

[1] Present address: G

Vapor Pressures of Water Over Aqueous Solutions of Strong Electrolytes

Charles L. Kusik[1]
Arthur D. Little, Inc., Cambridge, Mass. 02140

Herman P. Meissner
Chemical Engineering Department, MIT, Cambridge, Mass. 02139

Vapor pressures of water at any temperature and pressure over a solution of a single strong electrolyte involving ions 1 and 2 can be estimated by knowing at least one value of Γ_{12}^0, the reduced activity coefficient at some specified temperature and pressure. The quantity Γ_{12}^0 is defined as γ_{12}^{1/z_1z_2} where γ_{12} is the mean activity coefficient of this electrolyte and z_1 and z_2 are the charge numbers on the ions. For solutions of 1:1 electrolytes, water activities are presented graphically as a function of Γ^0 and the ionic strength. Values of water activities read from this figure can be easily corrected for higher electrolytes. It is shown that data on water vapor pressure lowering or boiling point rise can be used for estimating reduced activity coefficients for electrolytes at any desired temperature.

When we deal with aqueous solutions of strong electrolytes, it is often necessary to evaluate the vapor pressures (activities) of the water as well as the activities of the electrolytes present. The object here is to present a generalized procedure for estimating such vapor pressures, applicable when experimental data are not available.

Activity Coefficients of Strong Electrolytes

The magnitude of γ_{12}^0, the mean activity coefficient of a single strong electrolyte 12 composed of ions 1 and 2 in aqueous solution depends upon its molality m_{12} (moles per kilogram of water), upon the charges on the electrolyte's cation and anion, namely z_1 and z_2, respectively, and upon the temperature. Except at very low concentrations, activity coefficients for different electrolytes in their pure solutions at any given temperature and concentration are usually far from being equal. However, the general isothermal behavior of these activity coefficients at any temperature between 0 and 150°C is conveniently represented by the curves of Figure 1 showing the variation of the reduced activity coefficient Γ_{12}^0 [namely $(\gamma^0)^{1/z_1z_2}$] with the ionic strength μ (Meissner and Tester 1972). Each curve may be viewed as representing a solution of a different electrolyte. Inspection shows that all curves start at a value for Γ_{12}^0 of unity at zero concentration, and then diverge without crossover as concentration increases. Obviously, an entire isothermal curve for a particular electrolyte can be located on Figure 1, knowing a single value of γ_{12}^0 at an ionic strength of 2 or higher, and at the temperature of interest. Thus, when we know that log Γ_{12}^0 for $NaNO_3$ at a μ of 2 is -0.32 at 25°C, then its value at 25°C and a μ of 6 is determined from Figure 1 as -0.44 or Γ_{12}^0 is 0.363, compared to an experimental value of 0.371. For electrolytes on which no experimental data are available a method of predicting an approximate value for γ_{12}^0 at 25°C and an ionic strength of 2 has been proposed (Meissner and Tester 1972).

[1] To whom correspondence should be addressed.

Activity of Water in Electrolyte Solutions

As is customary, the activity of water $(a_w)_{z_1z_2}$ is expressed as p_w/p_w°, namely the ratio of the vapor pressures over the single electrolyte solution and over pure water, all at the temperature of interest. For a solution of a single strong electrolyte, the isothermal relationship between $(a_w)_{z_1z_2}$, γ_{12}^0, and concentration is expressed by the familiar Gibbs-Duhem equation, conveniently written as follows in standard texts (e.g., Pitzer and Brewer equation 22-27):

$$55.5\ d\ \ln\ (a_w)_{z_1z_2} = -\nu_{12}m_{12}\ d\ \ln\ m_{12} - \nu_{12}m_{12}\ d\ \ln\ \gamma_{12}^0 \quad (1)$$

Here ν_{12} represents the moles of ions formed upon dissociation of one mole of electrolyte. The ionic strength μ_{12} of a single electrolyte is related to its molality as follows:

$$\mu_{12} = 0.5\ z_1z_2\nu_{12}m_{12} \quad (2)$$

[Note: This equation is readily derived, in that μ equals $0.5\ m(\nu_1z_1^2 + \nu_2z_2^2)$, or $0.5\ m(\nu_1^2z_1^2/\nu_1 + \nu_2^2z_2^2/\nu_2)$. Since ν_1z_1 equals ν_2z_2, μ_{12} equals $0.5\ m_{12}\nu_1z_1\nu_2z_2(\nu_1 + \nu_2)/\nu_1\nu_2$. If we recognize that $(\nu_1 + \nu_2)$ equals ν_{12}, Equation 2 results upon canceling common terms in numerator and denominator.]

Substituting Γ^0 for $(\gamma^0)^{1/z_1z_2}$ in Equation 1, combining with Equation 2, and simplifying, we get

$$d\ \log\ (a_w)_{z_1z_2} = -\frac{d\mu_{12}}{(2.303)(27.75)z_1z_2} - \frac{\mu_{12}d\ \log\ \Gamma_{12}^0}{27.75} \quad (3)$$

Equation 3 can now be integrated between molality limits of zero and m, equivalent to limits for the ionic strength of zero and the final ionic strength of the solution μ_{12}; the corresponding limits for the reduced activity coefficient are unity and Γ_{12}^0. Performing the integration gives us

$$\log\ (a_w)_{z_1z_2} = -0.0156\ \mu_{12}/(z_1z_2) - (0.036)\int_0^{\Gamma_{12}^0} \mu d\ \log\ \Gamma_{12}^0 \quad (4)$$

When we know z_1, z_2, and μ_{12}, the first term on the right side of Equation 4 can be evaluated directly, while the second

Γ_{NaCl} is -0.06. When we correct for temperature by methods previously discussed, using Figure 1 and Equation 7, $(\log \Gamma)_{NaCl}$ at $\mu = 5$ and 25°C is -0.03. Thus, $\gamma = 0.94$ compared to a reported value of 0.874 (Robinson and Stokes, App. 8.10, 1959).

Obviously, the above procedure can be reversed to predict (by a trial and error procedure) the boiling point elevation from a known activity coefficient or water vapor pressure above the electrolyte at some other temperature.

Osmotic Coefficient

The osmotic coefficient is given for a single electrolyte, by Robinson and Stokes, p 29 (1959).

$$\phi_{12} = -\frac{55.5 \cdot 2.303}{\nu_{12} m_{12}} \log (a_w)_{z_1 z_2} \qquad (9)$$

which with Equations 2 and 6 can be transformed to

$$\phi_{12} = 1 - z_1 z_2 - [63.9\, z_1 z_2 \log (a_w{}^1)_{12}]/\mu_{12} \qquad (10)$$

Thus at a given ionic strength, ϕ_{12} can be easily derived from values of $\log a_w{}^1$ from Figure 2 and substituted in Equation 10.

Precision

Errors in estimating vapor pressure of water for various electrolyte solutions are generally within 20%. Further errors can be introduced when Γ values are predicted from vapor pressure lowering, extrapolated over large ranges of ionic strength in Figure 1 or large temperature ranges by Equation 7. Thus the relationships proposed here should be used only when direct experimental evidence is not available.

The extension of these developments to multicomponent solutions is to be the subject of a subsequent paper.

Nomenclature

a_w = activity of water
$(a_w)_{z_1 z_2}$ = activity of water in pure electrolyte 12
$(a_w{}^1)_{12}$ = activity of water in a pure 1:1 electrolyte
m_{12} = molal concentration of electrolyte (mol/kg of water)
m_1, m_2 = molal concentration of ions 1 and 2
z_+, z_- = cationic and anionic charge numbers

Greek Letters

$\gamma_{12}{}^0$ = mean activity coefficient in a solution containing pure electrolyte 12
$\Gamma_{12}{}^0$ = reduced activity coefficient $(\gamma^0)^{1/z_1 z_2}$
ϕ = osmotic coefficient (Equation 9)
μ_{12} = ionic strength of electrolyte 12 ($0.5\, m_1 z_1{}^2 + 0.5\, m_2 z_2{}^2$)
ν_1, ν_2, ν_{12} = number of ions 1, of ions 2, and ions 1 plus ions 2 found in dissolving 1 mole of electrolyte 12

Literature Cited

International Critical Tables, 1st ed., Vol. III, McGraw-Hill, New York, N.Y., 1928.
Meissner, H. P., et al., *AIChE J.*, 18(3), 661 (1972).
Meissner, H. P., Kusik, C. L., *ibid.*, (2), 294 (1972).
Meissner, H. P., Tester, J. W., *Ind. Eng. Chem. Process Des. Develop.*, 11, 128 (1972).
Pitzer, K. S., Brewer, L., "Thermodynamics," McGraw-Hill, New York, N.Y., 1961.
Robinson, R. A., Stokes, R. H., "Electrolyte Solutions," 2nd ed., Appendix 8.1, Academic Press, New York, N.Y., 1959.
Stokes, R. H., Robinson, R. A., *Ind. Eng. Chem.*, 41, 2013 (1949).
Smithsonian Physical Tables, Smithsonian Inst. Publ., pp 373–4, 9th rev. ed., Washington, D.C., 1954.

Received for review July 3, 1972
Accepted September 1, 1972